# Investigation of O-acetylserine sulfhydrylase enzymes from bacterial pathogens as potential drug targets

A thesis
submitted in fulfilment
of the requirements for the degree
of
**Doctor of Philosophy in Molecular and Cellular Biology**
at
**The University of Waikato**
by
**Jack McGarvie**


THE UNIVERSITY OF
WAIKATO
*Te Whare Wānanga o Waikato*

2025

# Abstract

Antimicrobial resistance (AMR) has emerged as a formidable global health crisis, necessitating the urgent development of novel antimicrobial strategies. Among the most concerning drug-resistant pathogens are *Neisseria gonorrhoeae* and *Staphylococcus aureus*, both of which lack a functional sulfate reduction pathway, rendering them reliant on alternative sulfur acquisition mechanisms. A key enzyme in the *de novo* biosynthesis of L-cysteine, O-acetylserine sulfhydrylase (CysK), represents a promising target for antimicrobial intervention due to its essential role in sulfur metabolism and bacterial survival. This thesis presents the first comprehensive biochemical and structural characterization of CysK from *N. gonorrhoeae* (NgCysK) and *S. aureus* (SaCysK), providing critical insights into their enzymatic function and potential for therapeutic targeting.

In this thesis, we present the structural characterisation of NgCysK and the model used for structure-based virtual inhibitor screening to identify potential NgCysK inhibitors. Virtual screening produced five hit compounds that were tested *in vitro,* giving compound 5 with inhibition in the mid micromolar range. Analysis of compound 5 docking indicates interactions with the NgCysK active site residues through hydrogen bonds and supporting hydrophobic interactions. This is the first reported inhibitor of NgCysK and provides a promising starting point for developing new antimicrobial adjuvants for treatment of gonorhoea infections.

Utilizing kinetic assays and small-angle X-ray scattering (SAXS), we elucidated the catalytic properties and structural dynamics of NgCysK and SaCysK, demonstrating their distinct substrate specificity. SAXS analysis indicates both enzymes are a single dimeric species in solution with no conformational changes during substrate binding. Combined with gel chromatography analysis, we showed the inability of *N. gonorrhoeae* to form the cysteine synthase complex by SAXS analysis.

Overall, this research underscores the significance of CysK as a viable antimicrobial target, contributing to the broader efforts of combatting AMR through metabolic pathway inhibition. By integrating structural biology, enzymology, and

computational drug discovery, this thesis advances our understanding of bacterial sulfur metabolism and lays the foundation for the rational design of next-generation antimicrobial therapies against drug-resistant *N. gonorrhoeae* and *S. aureus*.

# Acknowledgements

I would like to start by profoundly thanking my Chief Supervisor Dr. Joanna Hicks. Jo, you have helped and supported me through my whole journey as a scientific researcher thus far. Your generosity and understanding have helped me overcome any of the challenges thrown at me. I am immensely grateful for the countless opportunities you provided for me to present my research, and to take charge of my research journey, all of which have helped me grow as a researcher and develop a newfound resilience. I would also like to thank my Co-supervisor Dr. Erica Prentice for her guidance and support, whether it was an ear to vent to, help with analysis, or some much needed wisdom in the practice of enzyme kinetics, your calm and caring approach to assisting however and whenever possible was appreciated greatly.

Secondly, a thank you to Dr. Wanting Jiao. Thank you for your expertise in this project and your continually fantastic collaboration.

Thank you, Judith for being a legendary lab mum! Your consistent joy and pride in our lab family, the students, and academics alike, is infectious and is invaluable to us all. Even the roughest periods in our research are made lighter by you. Thank you for all the laughs and celebrations, and most importantly unwavering support over my time in the lab.

I would like to profusely thank my lab family, Emily, Keely, Carlin, Liz, Jolyn, and Meghan for helping me maintain my sanity, helping whenever I needed it and just making work feel fun! Since I started in the lab you have all always been there to support me and share in the joys and pains of research. A special thank you to Keely for all her help in teaching the witchcraft known as crystallography. Also, a special thank you to Meghan for reminding me how it works after a lengthy hiatus.

Special mention must go to Annmaree for my start in scientific research. I am forever grateful for your approach to training me when I first entered the lab, your patience and kindness is phenomenal.

Thank you to Emma and Stacy for being the gono gang's gonococcus experts and always being available for any queries.

Thank you to all the current and past students for making the lab a great place to work, from our lab excursions, coffee at the lake or our lab Christmas celebrations.

I would like to extend my thanks to The University of Waikato for funding the first three years of this thesis and my supervisor Dr. Joanna Hicks for the extra months I required.

To my family, thank you for always being there with a listening ear or a hug when I needed, for the constant care packages and sanity calls, and for always being interested in what I do. Your patience when my stress was at its highest is beyond commendable, so I apologise and thank you profusely, I could not have made it to where I am today without your unwavering love and support.

Finally, thank you Manuela for your incredible patience and support. This would have been a million times more difficult and stressful without you by my side, your willingness to move to New Zealand while I finish my studies is an incredibly brave move and one, I shall always cherish. Here's to the next adventure!

# Table of Contents

# List of Figures

# List of Tables

# Chapter One: Introduction

Antimicrobial resistance (AMR), often referred to as the "silent pandemic," is a growing global health crisis and is one of the top ten threats to public health. Antibiotic-resistant bacteria are responsible for a wide range of infections that compromise human health and challenge modern medicine. Among these pathogens, *Neisseria gonorrhoeae* and *Staphylococcus aureus* are of particular concern due to their increasing resistance to front-line antibiotics. Both, *N. gonorrhoeae*, the causative agent of gonorrhoea, and *S. aureus*, responsible for a wide range of infections, from skin and soft tissue infections to life-threatening conditions such as sepsis and pneumonia, are classified as high priority pathogens by the World Health Organisation (WHO, 2024). for the development of novel antimicrobial therapies. Increasing commonality of treatment failures due to extensively drug-resistant strains (Unemo et al., 2019) makes these two pathogens critical targets for new antimicrobial strategies.

One promising approach to developing new antimicrobials is targeting of bacterial metabolic pathways that are essential for survival and virulence. Among these, the *de novo* biosynthesis of L-cysteine has emerged as a promising target for antimicrobial intervention (Campanini et al., 2015; Hicks, Oldham, McGarvie, & Walker, 2022). L-cysteine is a vital amino acid required for the synthesis of several sulfur-containing biomolecules, including glutathione, thioredoxin, and iron-sulfur clusters, which are critical for oxidative stress resistance and bacterial survival (Abd El-Aleam, George, Georgey, & Abdel-Rahman, 2021; Brunner et al., 2016). Unlike humans, who obtain cysteine from dietary sources, many bacterial pathogens rely on endogenous L-cysteine biosynthesis, making this pathway an attractive target for selective antimicrobial development.

The cysteine biosynthesis pathway consists of two key enzymes: serine acetyltransferase (CysE), which catalyses the acetylation of L-serine to produce *O*-acetylserine, and *O*-acetylserine sulfhydrylase (CysK), which catalyses the final step of cysteine synthesis by condensing *O*-acetylserine with sulfide to produce L-cysteine (Becker & Tomkins, 1969). This pathway is regulated through L-cysteine feedback inhibition via L-cysteine binding to CysE (Benoni et al., 2017; Kredich & Tomkins, 1966). Research into the role of L-cysteine biosynthesis

pathways in bacteria has increased in recent years, with a particular focus on inhibiting this pathway for development of novel antimicrobials and adjuvants (Campanini et al., 2015; Hicks et al., 2022).

Elucidating the sulfur metabolism pathways in bacteria is of particular importance not only for development of novel antimicrobials or adjuvants but also for developments in biotechnology, engineering and other fields of research. In most bacteria, the reductive assimilation of sulfate to sulfide for the synthesis of cysteine is catalyzed by a suite of enzymes, often found in the sulfate reduction operon in bacteria. Not only, are *N. gonorrhoeae* and *S. aureus* high priority pathogens, but both are missing the sulfate reduction pathway (Hicks & Mullholland, 2018; Lithgow, Hayhurst, Cohen, Aharonowitz, & Foster, 2004). Both organisms are also capable of growing on thiosulfate as a sole sulfur source (Le Faou, 1984; Lithgow et al., 2004), however, *N. gonorrhoeae* is unable to recycle thiosulfate, and *S. aureus* is unable to import thiosulfate (Lensmire et al., 2023; Seib et al., 2006). Combined with their lack of sulfate reduction, intriguing questions regarding sulfur metabolism in these pathogens arise.

Sulfur acquisition and assimilation in *N. gonorrhoeae* is already being investigated by my Chief supervisor Dr. Joanna Hicks and other members of our research. Previous work by our group reviewed and analysed the *de novo* biosynthetic pathway in *Neisseria* species in extensive detail (Hicks & Mullholland, 2018), discovering the genetic disruption to the pathway and raising the question as to the role of NgCysK. Preliminary investigation conducted as a part of my Master's studies demonstrated that NgCysK has *O*-acetylserine sulfhydrylase activity comparable to other bacterial homologues, and can only utilise sulfide as a sulfur donor, being incapable of utilising thiosulfate (McGarvie, 2021). Based on NgCysE and NgCysK being functional enzymes, an alternative sulfurtransferase-dependent pathway for obtaining sulfide from thiosulfate and glutathione, previously characterised in *E. coli* (Kawano et al., 2017), is being investigated in *N. gonorrhoeae*, by PhD student Stacy van Niekerk. Initial characterisation of this pathway (van Niekerk, 2021) demonstrated that the *N. gonorrhoeae* sulfurtransferases were able to produce sulfide from thiosulfate. On the basis of our findings thus far, we propose that *N. gonorrhoeae* is capable of *de novo* L-cysteine biosynthesis. This research focuses on elucidating the role of CysK enzymes in pathogenic bacteria, their role in sulfur metabolism and how this can be explored

for antimicrobial development. This thesis follows on from preliminary characterisation work completed during my Master's studies. The work presented in this thesis details the first *in vitro* kinetic characterisation of NgCysK and SaCysK as well as the first structural characterisation of NgCysK. The first structural characterisation of SaCysK and NgCysK when the substrate OAS binds is also presented. The NgCysK crystal structure and homology generated model were used for structure-based virtual inhibitor screening to identify novel NgCysK inhibitors. Furthermore, this thesis provides an extensive review of antimicrobial targeting efforts of the *de novo* L-cystine biosynthetic pathway in bacterial pathogens. This thesis contains published articles, submitted manuscripts, and manuscripts prepared for submission. These articles are presented in thesis are a literature review and two manuscripts, followed by a Conclusion and Future Directions Chapter. The literature review is presented in Chapter Two. The citation for the review is as follows:

Hicks, J. L., Oldham, K. E. A., **McGarvie, J.**, & Walker, E. J. (2022). Combatting antimicrobial resistance via the cysteine biosynthesis pathway in bacterial pathogens. Bioscience reports, 42(10), BSR20220368. 10.1042/BSR20220368.

## 1.1 Thesis objectives

The overall aims of this thesis are to firstly; elucidate the role of *O*-acetylserine sulfhydrylase A (CysK) in the human pathogens *N. gonorrhoeae* and *S. aureus,* and to understand the utilisation of sulfur in these two pathogens with the same missing sulfate reduction pathway. To achieve this, the thesis objectives are as follows:

**Objective one:**

- To biochemically characterise the CysK enzymes from *N. gonorrhoeae* and *S. aureus* and their structural response to substrate binding.

This research is presented in Chapter Four as a manuscript prepared for submission:

**McGarvie, J.**, Oldham, K., Warrender, A., Prentice, E., & Hicks, J. (2025). Characterisation of O-acetylserine sulfhyrdrylase (CysK) enzymes from bacteria lacking a sulfate reduction pathway. *bioRxiv*, 2025.2003.2026.645513. 10.1101/2025.03.26.645513

**Objective two:**

- To identify and characterise novel inhibitors targeting CysK from *N. gonorrhoeae.*

This research is presented in Chapter Three as a manuscript prepared for submission:

**McGarvie, J.**, Warrender, A. K., Oldham, K. E. A., Jiao, W., & Hicks, J. L. (2025). Identification of inhibitors of *O*-acetylserine sulfhydrylase A from *Neisseria gonorrhoeae,*
(*ready for submission*)

## 1.2 Thesis outline

This thesis consists of five chapters titled; Introduction, Literature Review, Identification of inhibitors of *O*-acetylserine sulfhydrylase A from *Neisseria gonorrhoeae*, Characterisation of O-acetylserine sulfhydrylase (CysK) from bacteria lacking a sulfate reduction pathway. In several chapters, additional future direction sections have been included and are highlighted in blue text.

## 1.3 Acknowledgement of funding

I was funded by a Doctoral Scholarship from the University of Waikato. This research was funded by grants from the Waikato Medical Research Foundation and the Health Research Council (Grant number: 19-602) awarded to Chief Supervisor Dr. Joanna Hicks. Virtual inhibitor screening was funded by the Maurice Wilkins Centre. Access to the Australian Synchrotron macromolecular crystallography (MX) and small-angle X-ray scattering (SAXS) beamlines were funded through the New Zealand Synchrotron Group.

## 1.4 References


Abd El-Aleam, R. H., George, R. F., Georgey, H. H., & Abdel-Rahman, H. M. (2021). Bacterial virulence factors: a target for heterocyclic compounds to combat bacterial resistance. *RSC Advances, 11*(58), 36459-36482. 10.1039/d1ra06238g

Becker, M. A., & Tomkins, G. M. (1969). Pleiotropy in a Cysteine-requiring Mutant of *Salmonella typhimurium* Resulting from Altered Protein-Protein Interaction. *J. Biol. Chem., 244*(21), 6023-6030.

Benoni, R., De Bei, O., Paredi, G., Hayes, C. S., Franko, N., Mozzarelli, A., . . . Campanini, B. (2017). Modulation of Escherichia coli serine acetyltransferase catalytic activity in the cysteine synthase complex. *FEBS Letters, 591*(9), 1212-1224. 10.1002/1873-3468.12630

Brunner, K., Maric, S., Reshma, R. S., Almqvist, H., Seashore-Ludlow, B., Gustavsson, A.-L., . . . Schneider, G. (2016). Inhibitors of the Cysteine Synthase CysM with Antibacterial Potency against Dormant Mycobacterium tuberculosis. *Journal of Medicinal Chemistry, 59*(14), 6848-6859. 10.1021/acs.jmedchem.6b00674

Campanini, B., Pieroni, M., Raboni, S., Bettati, S., Benoni, R., Pecchini, C., . . . Mozzarelli, A. (2015). Inhibitors of the sulfur assimilation pathway in bacterial pathogens as enhancers of antibiotic therapy. *Curr Med Chem, 22*(2), 187-213. 10.2174/0929867321666141112122553

Hicks, J. L., & Mullholland, C. V. (2018). Cysteine biosynthesis in Neisseria species. *Microbiology, 164*(12), 1471-1480. 10.1099/mic.0.000728

Hicks, J. L., Oldham, K. E. A., McGarvie, J., & Walker, E. J. (2022). Combatting antimicrobial resistance via the cysteine biosynthesis pathway in bacterial pathogens. *Biosci Rep, 42*(10) 10.1042/bsr20220368

Kawano, Y., Onishi, F., Shiroyama, M., Miura, M., Tanaka, N., Oshiro, S., . . . Ohtsu, I. (2017). Improved fermentative l-cysteine overproduction by enhancing a newly identified thiosulfate assimilation pathway in Escherichia coli. *Applied Microbiology and Biotechnology, 101*(18), 6879-6889. 10.1007/s00253-017-8420-4

Kredich, N. M., & Tomkins, G. M. (1966). The Enzymic Synthesis of L-Cysteine in Escherichia coli and Salmonella typhimurium. *Journal of Biological Chemistry, 241*(21), 4955-4965. 10.1016/s0021-9258(18)99657-2

Le Faou, A. (1984). Sulphur nutrition and metabolism in various species of Neisseria. *Annales de l'Institut Pasteur / Microbiologie, 135*(1, Supplement B), 3-11. https://doi.org/10.1016/S0769-2609(84)80037-X

Lensmire, J. M., Wischer, M. R., Kraemer-Zimpel, C., Kies, P. J., Sosinski, L., Ensink, E., . . . Hammer, N. D. (2023). The glutathione import system satisfies the Staphylococcus aureus nutrient sulfur requirement and promotes interspecies competition. *PLOS Genetics, 19*(7), e1010834. 10.1371/journal.pgen.1010834

Lithgow, J. K., Hayhurst, E. J., Cohen, G., Aharonowitz, Y., & Foster, S. J. (2004). Role of a Cysteine Synthase in Staphylococcus aureus. *Journal of Bacteriology, 186*(6), 1579-1590. 10.1128/jb.186.6.1579-1590.2004

McGarvie, J. (2021). *Structural and biochemical characterisation of O-acetylserine sulphydrylase (CysK) from Neisseria gonorrhoeae* (Masters). The University of Waikato, Hamilton, New Zealand. Retrieved from https://hdl.handle.net/10289/14596

Seib, K. L., Wu, H.-J., Kidd, S. P., Apicella, M. A., Jennings, M. P., & McEwan, A. G. (2006). Defenses against Oxidative Stress in*Neisseria gonorrhoeae* a

System Tailored for a Challenging Environment. *Microbiology and Molecular Biology Reviews, 70*(2), 344-361. 10.1128/mmbr.00044-05

Unemo, M., Seifert, H. S., Hook, E. W., Hawkes, S., Ndowa, F., & Dillon, J.-A. R. (2019). Gonorrhoea. *Nature Reviews Disease Primers, 5*(1) 10.1038/s41572-019-0128-6

van Niekerk, S. L. (2021). *Alternative sulfur acquisition pathways in Neisseria gonorrhoeae* (Masters). The University of Waikato, Hamilton, New Zealand. Retrieved from https://researchcommons.waikato.ac.nz/entities/publication/b697ee92-66b6-415c-b562-6a34087536be

WHO. (2024). *WHO Bacterial Priority Pathogens List, 2024.* Retrieved from https://iris.who.int/bitstream/handle/10665/376776/9789240093461-eng.pdf?sequence=1

# Chapter Two: Literature Review

## 2.1 Preface

This chapter provides a comprehensive analysis of recent research on the development of antimicrobials and adjuvants that target key enzymes in the *de novo* L-cysteine biosynthesis pathway, namely, serine O-acetyltransferase (CysE) and O-acetylserine sulfhydrylase (CysK/OASS-A; CysM/OASS-B). This review highlights the significance of these enzymes as potential antimicrobial targets by emphasizing the essential role of cysteine biosynthesis in bacterial survival, particularly its involvement in pathogenesis, persistence, and antibiotic resistance. We specifically examine the detailed characterization of CysE and the bacterial isoforms of CysK and CysM, as well as current approaches used to identify and refine new inhibitors. Furthermore, we explore how these strategies are being implemented to develop novel antimicrobials and adjuvants, including those aimed at combating antimicrobial-resistant bacterial strains.

This review was commissioned based on the publication of our research groups previously published paper (Oldham, Prentice, Summers, & Hicks, 2022a) published as a peer-reviewed review article in *Bioscience Reports* (Portland Press). The content in this chapter follows the format of the published review. The citation for this publication is as follows:

Hicks, J. L., Oldham, K. E. A., **McGarvie, J.**, & Walker, E. J. (2022). Combatting antimicrobial resistance via the cysteine biosynthesis pathway in bacterial pathogens. *Bioscience reports, 42*(10), BSR20220368. 10.1042/BSR20220368.

## 2.2 Author contributions

Our research group investigate both CysE and CysK enzymes from *N. gonorrhoeae*, therefore the collation of literature and manuscript writing was conducted collaboratively between myself and co-authors Keely Oldham, Emma Walker and my Chief supervisor, Joanna Hicks. I wrote the sections pertaining to CysK and CysM (2.6), and part of the CysK inhibitor section (2.6.5) and created figures for these sections. Keely Oldham wrote the CysE section, and the Emma Walker wrote part of the CysK/CysM inhibitor section. Joanna Hicks wrote the introduction and

conclusion. All authors contributed equally to editing of the manuscript. Co-author contributions can be found in Appendix D.

# Combatting antimicrobial resistance via the cysteine biosynthesis pathway in bacterial pathogens.

Joanna L. Hicks[1], Keely E.A. Oldham[1,2], **Jack McGarvie[1]** and Emma J. Walker[1]

[1] *Te Huataki Waiora, School of Health, University of Waikato, Hamilton, New Zealand*

[2] *Te Aka Matuatua, School of Science, University of Waikato, Hamilton, New Zealand*

## 2.3 Abstract

Antibiotics are the cornerstone of modern medicine and agriculture, and rising antibiotic resistance is one the biggest threats to global health and food security. Identifying new and different druggable targets for the development of new antibiotics, is absolutely crucial to overcome resistance. Adjuvant strategies that either enhance the activity of existing antibiotics or improve clearance by the host immune system provide another mechanism to combat antibiotic resistance. Targeting a combination of essential and non-essential enzymes that play key roles in bacterial metabolism, is a promising strategy to develop new antimicrobials and adjuvants, respectively. The enzymatic synthesis of L-cysteine is one such strategy. Cysteine plays a key role in proteins and is crucial for the synthesis of many biomolecules important for defense against the host immune system. Cysteine synthesis is a two-step process, catalyzed by two enzymes. Serine acetyltransferase (CysE) catalyzes the first step to synthesize the pathway intermediate *O*-acetylserine, and *O*-acetylserine sulfhydrylase (CysK/CysM) catalyzes the second step using sulfide or thiosulfate to produce cysteine. Disruption of the cysteine biosynthesis pathway results in dysregulated sulfur metabolism, altering the redox state of the cell leading to decreased fitness, enhanced susceptibility to oxidative stress and increased sensitivity to antibiotics. In this review we summarize the structure and mechanism of characterized CysE and CysK/CysM enzymes from a variety of bacterial pathogens, and the evidence that supports targeting these enzymes for the development of new antimicrobials or antibiotic adjuvants. In

addition, we explore and compare compounds identified thus far that target these enzymes.

## 2.4 Introduction

Antibiotic resistance is a slow burning global pandemic that threatens not just human health and life expectancy but also food production. The discovery of antibiotics in the 1920s and 30s was a game changer for human health and agriculture. These drugs have saved millions of lives from previously fatal infections and massively reduced risk from surgical interventions. Within agriculture, antibiotics have been used for animal health and, in healthy food-producing animals to promote growth and prevent disease. Yet not 100 years after the 'golden era' of antibiotic discovery we are facing the problem of extensively drug resistant (XDR) and multi drug resistant (MDR) strains of bacterial pathogens. The rising emergence of antibiotic resistance and the lack of new antibiotic classes discovered over the past 60 years requires new strategies to overcome resistance and target bacterial pathogens. Identifying novel druggable targets different from those currently targeted by antimicrobials are crucial to overcoming antibiotic resistance. Along with this, adjuvant strategies targeting nonessential targets such as those important for bacterial virulence, persistence or host colonization are gaining interest (Becker et al., 2006; Bhave, Muse, & Carroll, 2007). Targeting these enzymes that are nonessential during the normal bacterial life cycle but become essential during infection and host invasion, could decrease the incidence of antimicrobial resistance (AMR), as inhibition of these nonessential targets would facilitate clearance by the immune system without stimulating resistance. Targeting nonessential enzymes often decreases bacterial fitness, thereby inhibitors of these enzymes could act as adjuvants to enhance the potency of existing antibiotics. Most pathogens spend at least part of their life cycle in an extremely challenging environment; infection and survival within the hostile host environment relies on a series of sulfur-containing molecules, including Fe-S clusters, thiamine, thioredoxin, glutathione and biotin which have detoxifying capabilities and reducing power (Fasnacht & Polacek, 2021; Roop, Gaines, Anderson, Caswell, & Martin, 2009).

Cysteine is absolutely crucial for the synthesis of sulfur-containing biomolecules, therefore inhibiting cysteine synthesis is a promising strategy for both potential new antimicrobials and antimicrobial adjuvants. Inhibition of cysteine biosynthesis has been proven to interfere with a pathogen's ability to fight oxidative stress, infect the host and establish long-term infection

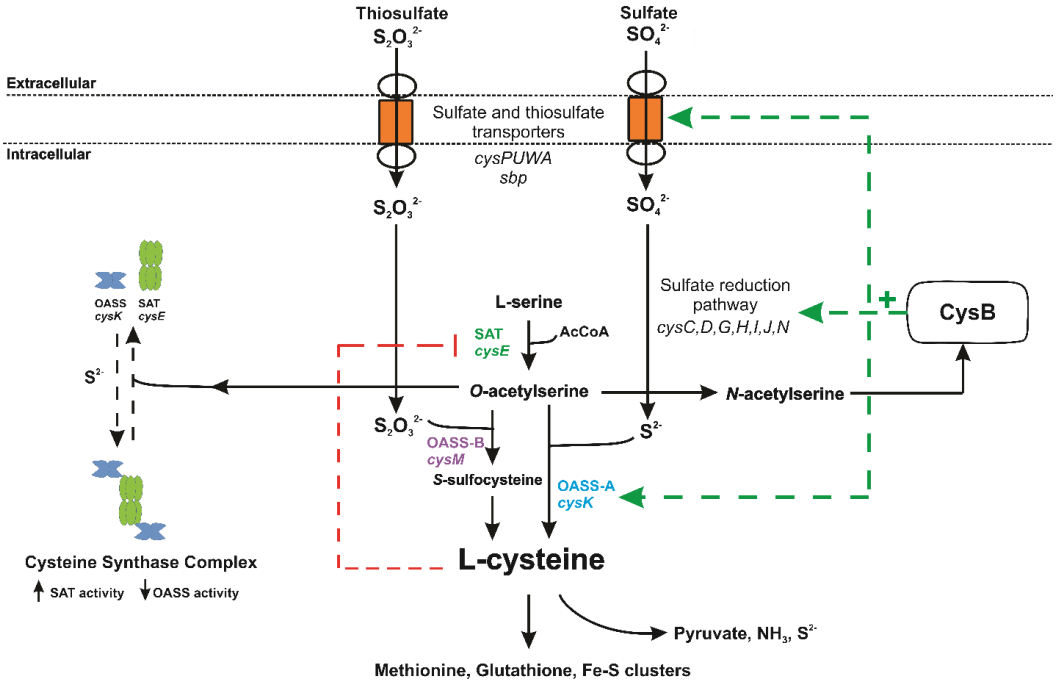


**Figure 2.1:** Overview of sulfur acquisition and assimilation pathways in bacteria. Inorganic sulfur uptake and assimilation pathways converge to be separately condensed with *O*-acetylserine to form cysteine. Transcriptional regulator, CysB, upregulates the sulfur uptake (*cysPUWA, sbp*) and sulfur reduction pathways (*cysC,D,G,H,I,J,N*), in the presence of the readily forming *O*-acetylserine isoform, *N*-acetylserine. Cysteine feeds into *de novo* synthesis of sulfur-containing metabolites, such as methionine, glutathione, thioredoxin and Fe-S clusters. Cysteine inhibits CysE via feedback inhibition. Cysteine can be catabolized by cysteine desulfhydrase to release pyruvate, ammonia and sulfide.

(Abd El-Aleam, George, Georgey, & Abdel-Rahman, 2021; Brunner et al., 2016; B. Campanini et al., 2015). For example, cysteine metabolism is a promising drug target in *Salmonella enterica* serovar Typhimurium (Becker & Tomkins, 1969; Turnbull & Surette, 2008, 2010) and *Mycobacterium tuberculosis* (Brunner et al., 2016; Brunner et al., 2017; Burns-Huang & Mundhra, 2019) where suppression or reduction of cysteine synthesis led to decreased fitness and infectivity. Inhibition of cysteine biosynthesis has also been associated with a dysregulated oxidative stress response, enhancing the antimicrobial activity of existing antibiotics (B. Campanini et al., 2015; Turnbull & Surette, 2008, 2010). Mammals lack the biosynthetic machinery for the *de novo* synthesis of cysteine from inorganic sulfur, relying on the reverse transulfuration of dietary methionine to obtain cysteine. Whereas

bacteria and plants have highly conserved enzymes for the assimilation of inorganic sulfur into cysteine (Stipanuk, Dominy, Lee, & Coloso, 2006).

The synthesis of cysteine is a two-step process, catalyzed by two enzymes, serine acetyltransferase (SAT;CysE) catalyzes the first step, requiring L-serine and acetyl coenzyme A (acetyl-CoA) to produce *O*-acetylserine (OAS). *O*-acetylserine sulfhydrylase A (OASS-A; CysK) combines *O*-acetylserine with sulfide to produce cysteine, whereas the OASS-B (CysM) isoform can utilize both sulfide and thiosulfate as the sulfur source for the synthesis of cysteine. The reductive assimilation of sulfate to sulfide for the synthesis of cysteine is catalyzed by a suite of enzymes, often found in the sulfate reduction operon in bacteria (Figure 2.1). Thiosulfate is an alternative sulfur source used directly to synthesize cysteine by the OASS-B isoform, CysM (Figure 2.1). The enzymes required for sulfate assimilation are also being explored as potential antimicrobial targets but are outside the scope of this review.

The pathways of sulfur acquisition converge at cysteine (Figure 2.1). Therefore, the regulation of cysteine synthesis acts to control sulfur flux within the cell. Regulation occurs at both the genetic and protein levels. At the genetic level, the transcription factor CysB, belonging to the LysR family of transcriptional regulators, controls expression of key transporters of sulfur containing molecules, the sulfate reduction operon, and enzymes involved in cysteine synthesis, with the exception of CysE which is not regulated by CysB (Figure 2.1) (Colyer & Kredich, 1996; Guédon & Martin-Verstraete, 2007; Hryniewicz & Kredich, 1994; Kredich, 1992; Lochowska, Iwanicka-Nowicka, Plochocka, & Hryniewicz, 2001). Whereas at the protein level, CysE which catalyzes the first step in the two-step reaction is inhibited by L-cysteine (Kredich & Tomkins, 1966) and also forms a complex with CysK, termed the cysteine synthase complex (CSC) (Figure 2.1). While part of the CSC, CysE activity is enhanced (Benoni et al., 2017), whereas CysK activity is inhibited due to the C-terminal peptide of CysE binding and occluding the active site of CysK (Benoni et al., 2017). Pathway intermediate *O*-acetylserine and its isomer *N*-acetylserine, along with sulfide, regulate formation of the CSC and act as inducers and anti-inducers of CysB, respectively.

In this review we briefly summarize the structural and mechanistic features of the CysE and CysK/CysM enzymes from bacterial pathogens and the evidence that supports targeting this pathway for the development of new antimicrobials. We provide a comparison of compounds identified thus far that inhibit the SAT and OASS enzymes and the methods used to identify these compounds.

## 2.5 Serine acetyltransferase (CysE)

CysE is a serine acetyltransferase that catalyzes the first committed step of the cysteine biosynthetic pathway (Figure 2.1), utilizing L-serine and acetyl-CoA to synthesize the pathway intermediate *O*-acetylserine. Not only does CysE catalyze the first committed step, it is subject to feedback inhibition by the pathway end product L-cysteine. CysE is nonessential in some bacterial pathogens, but curiously is essential in others, suggesting that CysE inhibition holds promise as a new antimicrobial target and/or as an antibacterial adjuvant.

### 2.5.1 Essentiality and Role of CysE During Infection

CysE is important not only for the *de novo* synthesis of cysteine, but also plays a key role in bacterial virulence. CysE is essential in the pathogens, *Staphylococcus aureus* (Chaudhuri et al., 2009), *Escherichia coli* O157:H7 strain (Warr et al., 2019), *Haemophilus influenzae* (Akerley et al., 2002) and the pathogenic *Neisseria* species; *Neisseria gonorrhoeae* (Remmele et al., 2014) and *Neisseria meningitidis* (Muir et al., 2020). Essentiality of *cysE* in these bacteria was elucidated using transposon mutagenesis screens, and requires further validation. Interestingly, all screens were performed in culture media containing cysteine and other organic sulfur compounds, indicating that these bacteria have a requirement for the *de novo* synthesis of cysteine, despite the availability of extracellular organic sulfur sources. Furthermore, some of these organisms have non-functional sulfate assimilation pathways, such as *N. gonorrhoeae* (Hicks & Mullholland, 2018) and *S. aureus* (Lithgow, Hayhurst, Cohen, Aharonowitz, & Foster, 2004), precluding the reduction of sulfate to sulfide as a source of sulfur for cysteine synthesis. While these organisms can grow on the alternative sulfur sources, thiosulfate and sulfide (Le Faou, 1984; Lithgow et al., 2004), the essentiality of *cysE* in cysteine rich media suggests capability for the *de novo* synthesis of cysteine. It is also possible that

CysE and/or the product *O*-acetylserine has an as yet unidentified function that makes it essential in these organisms.

In bacteria where CysE is nonessential and able to be deleted from the bacterial chromosome, growth defects and reduced virulence have been observed. For example, in the drug resistant pathogen *Klebsiella pneumoniae*, CysE is not essential, but when deleted the mutant exhibits decreased fitness in a mouse model of pneumonia, thereby playing an important role in lung infection (Bachman et al., 2015). Another key example is *M. tuberculosis*, where randomized transposon mutagenesis studies demonstrated profound effects for a number of sulfate reduction genes and *cysE* by gene disruption (Rengarajan, Bloom, & Rubin, 2005). Further investigation demonstrated attenuation of *M. tuberculosis cysE* deletion strains in *in vitro* models of dormancy (Sassetti & Rubin, 2003).

Furthermore, *cysE* deletion in the sheep pathogen *Brucella ovis* resulted in poor growth in rich media and an early entry into stationary phase (Varesio, Fiebig, & Crosson, 2021). *B. ovis ΔcysE* strains were more susceptible to oxidative stress, shown through increased sensitivity to hydrogen peroxide. Cell invasion assays revealed that deletion of *cysE* did not affect cell infection, but did significantly reduce replication within macrophages (Varesio et al., 2021). While the deletion of *cysE* is non-lethal, it imposes a fitness cost on *B. ovis* during intracellular growth, demonstrating the requirement for cysteine biosynthesis for survival within the host.

Deletion of *cysE* can also influence bacterial antibiotic resistance. For example, an *E. coli* K12 *cysE* deletion strain had increased tolerance to the antibiotic novobiocin (Rakonjac, Milic, & Savic, 1991). Conversely in the pathogen *S. typhimurium* loss of CysE function increased mecillinam sensitivity (Oppezzo & Antón, 1995). Supporting this increased antibiotic sensitivity phenotype, cysteine biosynthesis is crucial for swarm cell differentiation in *S. typhimurium*. Inactivation of cysteine biosynthetic genes resulting in cysteine auxotrophy led to increased antibiotic sensitivity in the swarm cell state (Turnbull & Surette, 2008), even though the swarm medium contained sufficient cysteine to support growth. There is a complex interplay between cysteine metabolism, oxidative stress and antibiotic resistance, under normal growth conditions. *S. typhimurium* cysteine auxotrophs are oxidatively stressed and supporting this, in wild-type cells oxidative stress induces

cysteine biosynthesis. *S. typhimurium cysE* deletion strains are incapable of synthesizing cysteine and have decreased concentrations of reduced thiols or decreased total glutathione, leading to increased susceptibility to oxidative stress (Turnbull & Surette, 2010). Differences seen between *E. coli* with increased tolerance to novobiocin and *S. typhimurium*, could be due to the mechanism of action of the antibiotic or the presence/absence of cysteine/cystine or inorganic sulfur compounds in the culture media used in experiments.

CysE from *E. coli* and *Providencia stuartii* impacts biofilm formation in these pathogens (Sturgill, Toutain, Komperda, O'Toole, & Rather, 2004). Deletion of *cysE* from *E. coli* and *P. stuartii*, enhanced biofilm formation. However, this could be reversed by supplementation with cysteine (100 μM) or *O*-acetylserine (10 mM), but not *N*-acetylserine (Sturgill et al., 2004). The high concentration of *O*-acetylserine required for biofilm reduction compared to cysteine, suggests cysteine itself negatively regulates biofilm formation in a yet to be determined role. Given that bacteria in biofilms are less sensitive to antibiotics, inhibiting their formation could provide a novel way for enhancing current antibiotics.

### 2.5.2 Structural Characteristics of CysE

CysE (EC 2.3.1.30) belongs to the acetyltransferase family of hexapeptide acyltransferases. Members of this family are defined by a six-peptide tandem repeat, [LIV]-[GAED]-$X_2$-[STAV]-X, which gives rise to a distinctive left-handed beta helix (LβH) (Raetz & Roderick, 1995). Structural characterization of CysE enzymes with and without substrates and cysteine (inhibitor) bound from a range of Gram-negative bacterial pathogens including *E. coli* (1T3D) (Pye, Tingey, Robson, & Moody, 2004), *H. influenzae* (1SSM, 1SSQ, 1SST) (Olsen, Huang, Vetting, & Roderick, 2004), *Yersinia pestis* (3GVD) (Kim, Zhou, Peterson, Anderson, & Joachimiak, 2009), *Brucella melitensis* (3MC4), *Vibrio cholerae* (4H7O), *Brucella abortus* (4HZC, 4HZD) (Kumar, Kumar, Alam, & Gourinath, 2014), *K. pneumoniae* (6JVU) (Verma et al., 2020), *N. gonorrhoeae* (6WYE, 7RA4) (Oldham, Prentice, Summers, & Hicks, 2022b) and *S. typhimurium* (7E3Y). These structures provide insight into active site architecture upon substrate and inhibitor binding, which can be used to inform inhibitor design.

The CysE monomer consists of an amino-terminus (N-terminus) alpha-helical domain and a carboxy terminus (C-terminus) LβH domain (Figure 2.2A). The monomers assemble to form a trimer, which in turn forms a functional hexamer through hydrophobic trimer-trimer interactions via the alpha helices of the N-terminal domains (Figure 2.2A) (Gorman & Shapiro, 2004; Oldham et al., 2022b; Olsen et al., 2004; Pye et al., 2004). There are six active sites in the hexamer, formed between adjacent monomers of the C-terminal LβH domain. There is one deviation from the hexapeptide repeat, producing a meandering loop which forms part of the active site (Pye et al., 2004).

The hexameric structure of CysE enzymes differs from other members of the acetyltransferase family, which are active trimers. The CysE hexamer forms the cysteine synthase complex (CSC) with the OASS-A/CysK enzyme. There are exceptions to this hexameric configuration, such as the CysE isoforms from the protozoan parasite *Entamoeba histolytica*, where CysE is an active trimer (Kumar, Raj, Nagpal, Subbarao, & Gourinath, 2011).

### 2.5.3 CysE Enzyme Mechanism

Inhibitor design also relies on a detailed understanding of the enzyme's kinetic mechanism as well as structural features. CysE catalyzes the acetyl-CoA dependent acetylation of the hydroxyl side chain of L-serine to form *O*-acetylserine. CysE represents a key regulatory mechanism for the cysteine biosynthetic pathway due to its feedback inhibition by L-cysteine (Kredich & Tomkins, 1966; Olsen et al., 2004). CysE is constitutively expressed, and is regulated post-translationally through formation of the CSC (Pye et al., 2004). Kinetic characterization of CysE enzymes shows a ternary mechanism, with a random order mechanism reported (Hindson & Shaw, 2003). During catalysis, a conserved catalytic histidine (His158; *E. coli* CysE numbering) acting as a general base attacks the hydroxyl side chain of L-serine, which is stabilized by a neighboring aspartate (Asp143; *E. coli* CysE numbering), forming an intermediate, allowing for transfer of the acetyl group from acetyl-CoA to L-serine, releasing products *O*-acetylserine and coenzyme A (Pye et al., 2004) (Figure 2.2). While there is sequence divergence amongst CysE homologues, there is strong conservation of mechanism and active site residues (Pye et al., 2004).

### 2.5.4 Cysteine Inhibition of CysE

Tight control of intracellular cysteine levels is essential for meeting the cysteine requirements of the cell, while preventing unwanted toxic effects of high cysteine concentrations (Park & Imlay, 2003). As mentioned previously, CysE is constitutively expressed (Noji et al., 2001), where the main form of regulation is through formation of the CSC and feedback inhibition by the pathway product L-cysteine (Kredich & Tomkins, 1966). L-cysteine is a potent inhibitor of bacterial CysE enzymes with $IC_{50}$ values of 0.5-10 µM reported

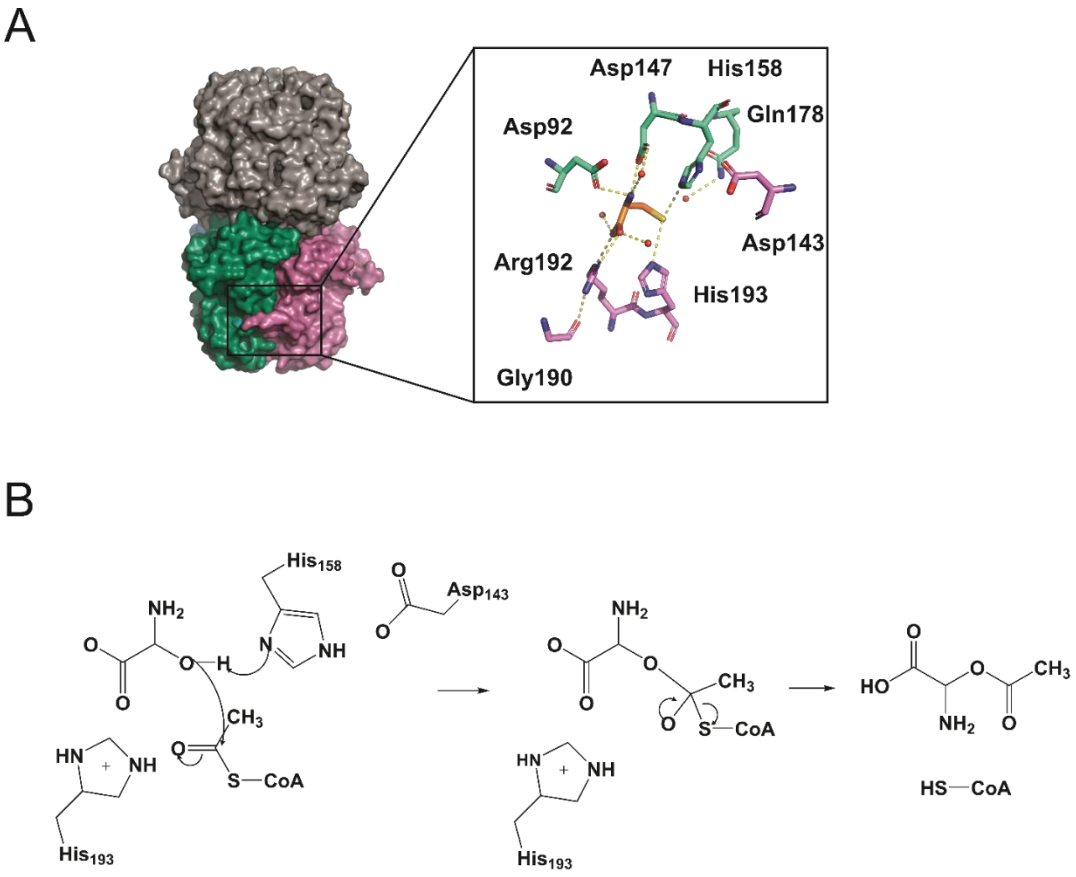


**Figure 2.2:** L-cysteine interactions with L-serine binding pocket in CysE from *E. coli* (1T3D). (A) Active site residues are represented as sticks, colored green (Asp92, Asp147, His158 and Gln178) and pink (Asp143, Gly190, Arg192 and His193), based on chains. Inhibitor L-cysteine is represented as orange sticks. Hydrogen bonds are shown as yellow dashed lines. (B) CysE reaction mechanism for formation of *O*-acetylserine, adapted from (Pye et al., 2004). Figure was produced using PyMOL and ChemDraw Prime (RRID:SCR_016768).

(Benoni et al., 2017; Hindson & Shaw, 2003; Kredich & Tomkins, 1966; Oldham et al., 2022b). Kinetic studies show that cysteine is a competitive inhibitor relative to serine, through binding to the serine binding pocket which has been confirmed through crystallography (Kumar et al., 2014; Olsen et al., 2004; Pye et al., 2004)

(Figure 2.2). Interestingly, cysteine displays competitive inhibition relative to acetyl-CoA even though it binds to the serine binding pocket (Hindson, 2003; Johnson, Huang, Roderick, & Cook, 2004; Oldham et al., 2022b) . This competitive inhibition is explained by observing CysE crystal structures with L-cystein bound. Upon binding of L-cysteine in the serine binding site the C-terminal tail folds up against the CysE monomer, physically blocking the active site and preventing the binding of acetyl-CoA (Olsen et al., 2004). Supporting this, truncation of the last ten C-terminal residues that form the C-terminal tail reduces CysE sensitivity to cysteine inhibition (Koshiki Mino et al., 2000). This is thought to prevent the accidental acetylation of L-cysteine, given its structural similarity to serine. (Koshiki Mino et al., 2000)

### 2.5.5 Development of CysE Inhibitors

CysE enzymes from bacterial pathogens have been extensively characterized, both kinetically and structurally, with numerous high-quality crystal structurers available for inhibitor design. Given the importance of CysE in infection and antibiotic resistance, and its essentiality in some bacterial pathogens, CysE represents an attractive drug target. The inhibition of CysE would deplete the cell of cysteine and *O*-acetylserine, where the latter isomerizes to *N*-acetylserine, the natural inducer of the cysteine biosynthetic operon, leading to metabolic dysregulation. There have been limited studies into inhibitors of CysE enzymes, but promising inhibitors ($IC_{50} \leq 100$ μM) have been identified for a number of bacterial pathogens (Table 2.1) and are discussed below.

#### 2.5.5.1 Natural Compound Inhibitors

Several promising CysE inhibitors have been identified via *in silico* screening of natural compound libraries. Recently, the flavonoid quercetin was found to inhibit CysE from *K. pneumoniae* ($IC_{50}$ = 3.7 μM) (Table 2.1) (Verma et al., 2020). Through docking analysis, quercetin (Figure 2.3) was shown to bind allosterically to the CysE trimer-trimer interface. Although not experimentally investigated by the authors, the binding of quercetin to this interface may inhibit *Kp*CysE through disrupting the trimer-trimer interactions, dissociating the hexamer, which has been shown to reduce CysE activity (Verma et al., 2020). However, quercetin has been shown to inhibit other bacterial enzymes including isocitrate lyase (Shukla et al.,

2015) and glutamate racemase (Pawar, Jha, Chopra, Chaudhry, & Saluja, 2020). This broad inhibition suggests that quercetin inhibition of CysE might be non-specific, which is supported by the targeting of the trimeric interface and not serine or acetyl-CoA binding sites.

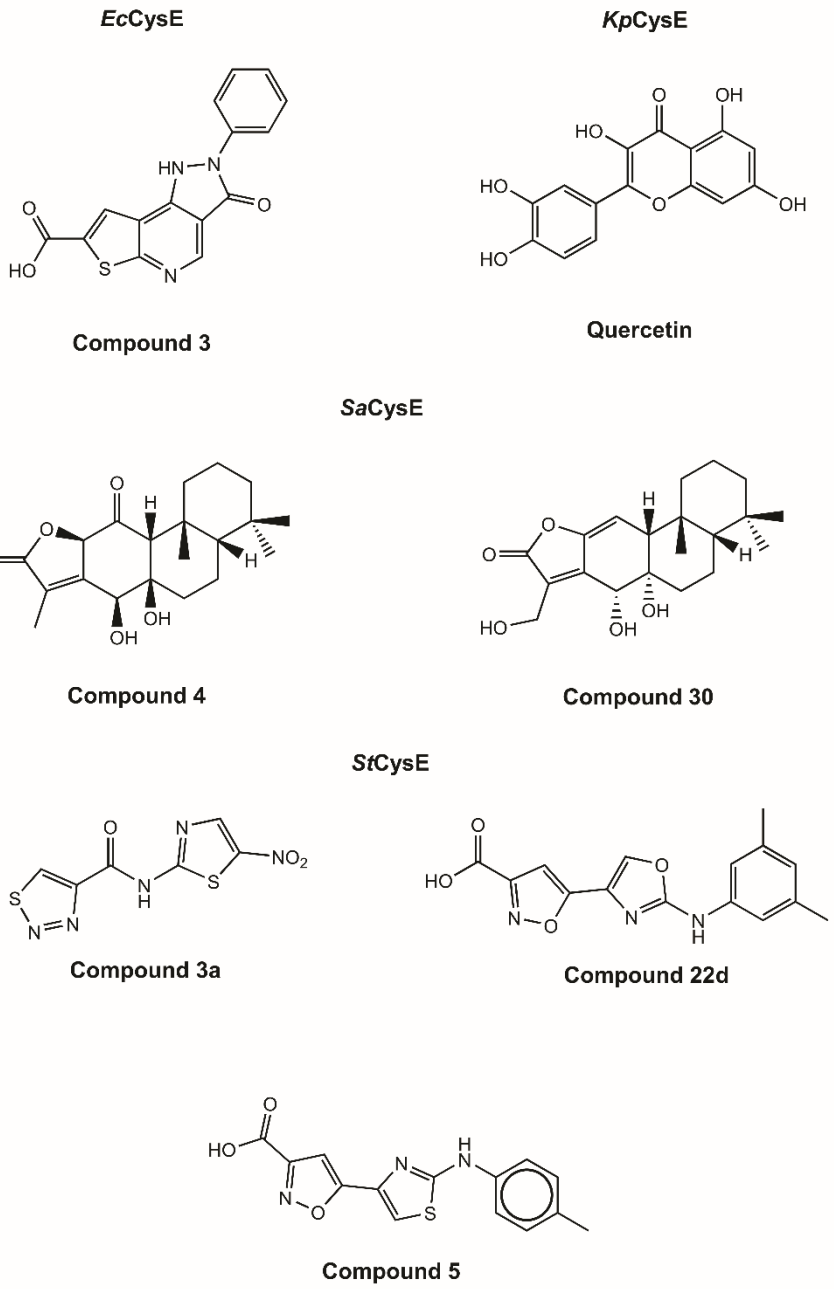


**Figure 2.3:** Chemical structures of CysE inhibitors. Figure produced using ChemDraw Prime (RRID:SCR_016768).

Natural compound inhibitors have also been identified for *Sa*CysE from methicillin-resistant *S. aureus* (MRSA) (Chen et al., 2019). These include two polycyclic diterpenoids; compound 4 (11-oxo-ebracteolatanolide B) and compound 30 ((4R,4aR)-dihydroxy-3-hydroxymethyl-7,7,10a-trimethyl-2,4,4a,5,6,6a,7,8,9,10,10a,l0b-dodecahydrophenanthro[3,2-b]furan-2-one) (Figure 2.3). These compounds share the same chemical scaffold, with substitution of oxygens attached to the phenyl rings. Both compounds inhibited *Sa*CysE (both $IC_{50}$ = 71.84 μM), where compound 4 was shown to display mixed inhibition against serine and competitive inhibition against acetyl-CoA, while the opposite was seen for compound 30. Docking analysis with a structural homology model of *Sa*CysE, shows hydrophilic interactions between compound 4 and key catalytic residue, His95, and the N-terminal domain residues, Ala43 and Gly44. Compound 30 interacts with these identical residues and active site residue Asp94. Given the highly similar chemical structure of these compounds, it is unsurprising that they share CysE residue interactions, however what is interesting is these compounds do not dock in either the acetyl-CoA or serine binding pocket, but instead bind in a pocket between the third α-helix (equivalent to sixth α-helix in *E. coli*; 1T3D) and the serine binding site. This is a unique method of targeting the CysE active site as the inhibitor can interact with the active site residues without occupying the active site, and may explain the mixed and competitive inhibition observed for these compounds.

Both compounds were also able to inhibit MRSA growth with minimum inhibitory concentration (MIC) values of 12.5 and 25 μg/mL for compound 4 and 30, respectively (Chen et al., 2019). Furthermore, both compounds were able to disrupt a mature MRSA-biofilm at one-fold the MIC concentration, and did not display any cytotoxicity to human cells. Both compounds did not inhibit the structurally similar hexapeptide enzyme, GlmU (N-acetylglucosamine-1-phosphate uridyltransferase) demonstrating target specificity. Although the *in vitro* $IC_{50}$ values are relatively high, given that these compounds inhibited growth of the target organism, displayed target specificity and are well tolerated by mammalian cells, these compounds are ideal for further optimization. Natural compounds have become popular for identifying novel antimicrobials, a large number of chemically distinct compounds can be screened and optimized by substituting chemical groups. Promising natural

compound inhibitors discussed here could also be used for targeting other CysE homologs.

#### 2.5.5.2 Chemical Inhibitors

Initial research into the development of CysE inhibitors was by conducted by Agarwal et al. (2008)(Agarwal, Jain, Bhattacharya, & Azam, 2008). The researchers employed virtual screening to identify inhibitors of CysE from *E. coli*. Screening of the crystal structure of *Ec*CysE (1T3D), identified nine compounds with promising docking scores, of which three were characterized *in vitro*. Compound 3, (3-oxo-2-phenyl-3,5-dihydro-2H-pyrazolo(3,4d)thieno(2,3-b)pyridine-7-carboxylic acid) was the only compound identified to inhibit *Ec*CysE (72 μM) and exhibit antimicrobial effects. This compound was tested for growth inhibition of the parasite *E. histolytica* resulting in unexpectedly potent inhibition ($IC_{50}$ = 0.61 μM), suggesting off-target inhibition.

As well as natural products, 2-aminothiazole and 2-aminooxazole compounds have been investigated as inhibitors of CysE enzymes. These compounds mimic binding interactions with key active site residues similar to the natural inhibitor L-cysteine (Figure 2.2). Recent studies have explored 2-aminothiazoles and 2-aminooxazole compounds as inhibitors of CysE from *S. typhimurium* (*St*CysE) (Magalhães et al., 2021; Magalhães et al., 2020). Since the crystal structure for *St*CysE (7E3Y) has been solved only recently (Momitani, Shiba, Sawa, Ono, & Hurukawa, 2022), all virtual screening was carried out against both *Ec*CysE (1T3D) and *H. influenzae* CysE (1SSM) crystal structures, as there is strong conservation of active site residues with *St*CysE. Virtual screening of ~91 000 compounds from three libraries identified six compounds, which *in vitro* had $IC_{50}$ values ranging from 13.6 to 84.1 μM (Magalhães et al., 2020). Further characterization of these compounds, revealed only compound 3a (N-(5-Nitro-1,3-thiazol-2-yl)-1,2,3-thiadiazole-4-carboxamide), a 2-aminothiazole (Figure 2.3), to inhibit *St*CysE with an $IC_{50}$ of 48.6 μM to be bactericidal, with an MIC of 64 μg/mL against *E. coli*. *In silico* docking analysis showed that compound 3a interacts with key active site residues Asp92, Asp157, Arg192, His193 and catalytic His158, mimicking interactions exhibited by the inhibitor L-cysteine (Figure 2.2). Compound 3a was shown to inhibit *E. coli* growth, but only in media low in cysteine. Previous research supports the anti-bacterial

activity of 2-aminothiazoles, with bactericidal activity against *M. tuberculosis* reported (Kesicki et al., 2016; Meissner et al., 2013).

Further research into *St*CysE inhibition was conducted using an in-house library for further virtual screening of *St*CysE (Magalhães et al., 2021; Momitani et al., 2022). Using the same screening method as discussed previously the researchers identified seven compounds that reduced *St*CysE activity, with the most potent being the substituted 2-aminothiazole, compound 5, (5-{2-[(4-Methylphenyl)amino]-1,3-thiazol-4-yl}-1,2-oxazole-3-carboxylic acid) (Figure 2.3), with an $IC_{50}$ of 110 µM, which displayed competitive inhibition relative to acetyl-CoA ($K_i$ = 64 µM). Docking analysis showed compound 5 interacts with the CysE serine active site residues and acetyl-CoA binding pocket, where the carboxylic acid group interacts with the same residues as seen for inhibitor cysteine/substrate serine. The "L-shape" of the inhibitor allows it to mimic acetyl-CoA, explaining the observation of competitive inhibition (Magalhães et al., 2021). Structure-activity relationship analysis was undertaken through *in vitro* screening of compound 5 analogues. Substitution of the 2-aminothiazole ring with a 2-aminooxazole was shown to increase affinity, and the presence of an ester, amide or carboxylic acid group connected to the isoxazole ring was shown to be essential for affinity (Magalhães et al., 2021). Isoxazole-3-ester and isoxazole-3-carboxylic acid derivatives were further optimized through synthesis with different chemical groups connected to the oxazole ring (Magalhães et al., 2021). Affinity was not substantially affected by the side group, but derivatives with electron-withdrawing groups were unstable compared to electron-donating groups. The most potent analogue was compound 22d, (3,5-dimethylphenyl-(2-aminooxazol-4-yl) isoxazole-3- carboxylic Acid) (Figure 2.3), with an $IC_{50}$ of 4.2 µM (Table 2.1). Unfortunately, this compound was unable to inhibit the growth of *E. coli*, requiring further optimization to improve compound permeability.

Overall, CysE inhibitor development is in its early stages, with a number of different strategies employed, with the main challenge in obtaining potent inhibitors that also inhibit bacterial growth. The essentiality of CysE in the notoriously antibiotic-resistant pathogens *S. aureus* and *N. gonorrhoeae*, highlights CysE as an ideal target for antimicrobial development. With more research being undertaken in targeting cysteine biosynthetic enzymes, overcoming the challenge of finding

compounds that are potent and yet specific, while being permeable to target organisms, will lead to the development of promising inihibitors.

**Table 2.1:** List of characterized CysE inhibitors.

| Inhibitor | Enzyme | $IC_{50}$ (µM)* | $K_i$ (µM) AcCoA* | $K_i$ (µM) L-serine | Citation |
|---|---|---|---|---|---|
| Compound 3 | *Ec*CysE | 72[a] | 42[a] | ND | (Agarwal et al., 2008) |
| Compound 4 | *Sa*CysE | 71.84 ± 0.27 | 225.3[a] | 53.9[a] | (Chen et al., 2019) |
| Compound 30 | | 71.84 ± 0.15 | 111.5[a] | 47.66[a] | |
| Quercetin | *Kp*CysE | 3.7[a] | 162 | ND | (Verma et al., 2020) |
| Compound 3a | *St*CysE | 48.6 ± 8.43 | ND | ND | (Magalhães et al., 2020) |
| Compound 5 | | 110 ± 0 | 64 ± 12 | ND | (Magalhães et al., 2021) |
| Compound 22d | | 4.24 ± 0.11 | ND | ND | |

* Error reported as standard error

[a]No error reported

ND- Not determined

## 2.6 *O*-acetylserine sulfhydrylase (CysK/CysM)

*O*-acetylserine sulfhydrylase is a pyridoxal 5'phosphate (PLP) dependent enzyme that catalyzes the second step of the L-cysteine biosynthesis reaction, combining *O*-acetylserine and a sulfur donor into cysteine. OASS is present in bacteria as two isoforms, OASS-A (CysK) that utilizes sulfide for the synthesis of cysteine, and OASS-B (CysM) that utilizes sulfide and thiosulfate. Bacteria with *cysK* or *cysM* deleted from the genome exhibit reduced virulence, compromised fitness and decreased antibiotic resistance. Subsequently, its inactivation is being pursued as a

strategy for the identification of novel antibiotics and/or antibiotic adjuvants that target non-essential proteins.

### 2.6.1 Role and Essentiality of CysK/CysM in Bacterial Pathogens

As the second and final enzyme in the cysteine biosynthetic pathway both OASS isoforms play an important role in bacteria. Transposon mutagenesis screening found that CysK is essential in just two bacterial pathogens, *Campylobacter jejuni* (Mandal, Jiang, & Kwon, 2017), and *Francisella novicida* (Gallagher et al., 2007). Like CysK, CysM is essential in very few bacterial species, including *Burkholderia pseudomallei (Moule et al., 2014),* and two strains of *Burkholderia cenocepacia,* K56-2 (Gislason, Turner, Domaratzki, & Cardona, 2017), and J2315 (Wong et al., 2016). Given that many bacterial species have both OASS isoforms, or even two copies of CysK, it is not surprising CysK and/or CysM are non-essential in many bacterial pathogens. For example, the *M. tuberculosis* genome contains three annotated OASS genes, denoted CysK1, CysK2 and CysM. The nomenclature of these genes is confusing in that OASS-A is denoted as CysK1, OASS-B as CysK2 (not CysM) and the mycobacterial CysM is unique and found only in actinobacteria. *Mtb*CysM uses a small thiocarboxylated protein (CysO) as the sulfur donor and *O*-phosphoserine (not *O*-acetylserine) as the preferred acceptor substrate (Ågren, Schnell, & Schneider, 2009; Burns-Huang & Mundhra, 2019; Burns et al., 2005; Claus, Zocher, Maier, & Schulz, 2005). Disrupting the *de novo* cysteine biosynthesis pathway in *M. tuberculosi*s represents an attractive drug target. Cysteine biosynthesis is consistently upregulated in dormancy models of infection (Schnappinger et al., 2003; Voskuil, Visconti, & Schoolnik, 2004), particularly survival of *M. tuberculosis* in infected macrophages in the granuloma, where it is exposed to an extremely hostile environment. It could be argued that *M. tuberculosis* could obtain cysteine from the host and not be dependent on *de novo* synthesis of cysteine. However, the upregulation of sulfur acquisition and cysteine synthesis genes in persister cells suggests that the host does not provide a sufficient amount of cysteine (Betts, Lukey, Robb, McAdam, & Duncan, 2002; Hampshire et al., 2004; Schnappinger et al., 2003; Voskuil, Bartek, Visconti, & Schoolnik, 2011; Voskuil et al., 2004), and it is likely cysteine is scarce within the granuloma due to host defense strategies such as nutrient depletion. *M. tuberculosis cysO* and *cysM* deletion strains show attenuation in *in vitro* models of dormancy

and also in a mouse model of infection (Sassetti & Rubin, 2003). A target identification pipeline for drug targets in *M. tuberculosis* based on a comprehensive *in silico* analysis using experimental derived phenotype data and proteomics, suggests that both CysE and CysK2 are high confidence drug targets (Raman, Yeturu, & Chandra, 2008).

As discussed earlier, inactivation of the cysteine biosynthetic operon leading to cysteine auxotrophy in *S. typhimurium* led to an increased susceptibility to antibiotics during swarming, which is normally associated with a decreased susceptibility to antibiotics. A *S. typhimurium Δcysk, cysM* double deletion strain was pleiotropic (Turnbull & Surette, 2010), making it difficult to associate a particular phenotype to this strain, presumably due to the accumulation of toxic intermediates, such as 3'phosphoadenoside 5'-phosphosulfate (Neuwald et al., 1992).

Shatalin et al. (2011) linked both the high concentration of $H_2S$, and decreased cysteine concentration to increased resistance to a variety of antibiotics. $H_2S$ is cytoprotective in some bacteria due to its ability to suppress oxidative stress generated by some antibiotics (Shatalin, Shatalina, Mironov, & Nudler, 2011). An *S. typhimurium cysK* deletion strain had decreased cysteine production, resulting in $H_2S$ accumulation causing an eight-fold higher resistance to ofloxacin compared to wild-type (Frávega et al., 2016). This highlights the various roles of CysK in antibiotic susceptibility, enhancing resistance to some and decreasing resistance to others, due to the target of the antibiotic and degree of oxidative stress within the cell.

Metal ions at low concentrations are beneficial to bacteria, however, can become toxic at higher concentrations causing oxidative stress and eventually cell death (Joshi, Gupta, & Gupta, 2019). Studies in *S. typhimurium* LT2 and *E. coli* demonstrated that CysK plays an essential role in mediating resistance to the metal ion, tellurite ($K_2TeO_3$) (Ramírez, Castañeda, Xiqui, Sosa, & Baca, 2006; Vásquez, Saavedra, Loyola, Araya, & Pichuantes, 2001), which exhibits strong oxidizing properties through an unknown mechanism. Deletion of *cysK* from *Azospirllum brasilense* conferred a lower MIC when grown on media with tellurite, whilst

transfer of the *A. brasilense* and *Bacillus stearothermophilus cysK* into *E. coli* and *S. typhimurium* respectively, conferred increased tellurite resistance (Ramírez et al., 2006; Vásquez et al., 2001).

As mentioned previously, disruption of the cysteine biosynthetic pathways can affect biofilm formation. The effect of a number of mutants from the cysteine biosynthetic operon of *Vibrio fischeri,* including Δ*cysH,* Δ*cysJ,* Δ*cysK,* and Δ*cysN* on biofilm formation were tested, with the greatest effect on biofilm formation seen with the Δ*cysK* mutant (Singh, Brooks, Ray, Mandel, & Visick, 2015). Biofilm and pellicle formation are vital to colonization which was observed in early colonization of baby squid where Δ*cysK* resulted in decreased colonization (Singh et al., 2015). Addition of cysteine allowed rescue of the biofilm defect and partial rescue of the pellicle defect, indicating a key role of CysK in initial colonization (Singh et al., 2015).

In a screen for genes important for the switch of *N. meningitidis* from commensal to pathogen, CysK was identified as being important in this switch. Saturated random transposon insertion libraries of *N. meningitidis* were engineered and assessed for fitness during normal growth and colonization of epithelial and endothelial cells, and the CysK mutant was identified as being of particular importance for epithelial cell infection (Capel et al., 2016).

### 2.6.2 Structural Characteristics of CysK and CysM

*O*-acetylserine sulfhydrylase (OASS; EC 2.5.1.47) belongs to the tryptophan synthase β-superfamily, and the β-family of PLP dependent enzymes (Guédon & Martin-Verstraete, 2007; Mino & Ishikawa, 2003; Takumi & Nonaka, 2016). PLP is an essential cofactor, utilized in the active site of OASS enzymes. As briefly discussed above there are two OASS isoforms, which each use an alternate sulfur source; CysK utilizes sulfide, whereas, CysM utilizes both thiosulfate and sulfide, with *O*-acetylserine to form cysteine (Kredich, 2008). Both isoforms are present in most bacteria, enabling the utilization of both thiosulfate and sulfide for cysteine biosynthesis. Expression of these isoforms is influenced by aerobic or anaerobic growth, for example, the genome of the pathogen *S. typhimurium* encodes both OASS isoforms with CysK expressed in excess of CysM under aerobic conditions,

and vice versa under anaerobic conditions (Filutowicz, Wiater, & Hulanicka, 1982). The two isozymes, CysM and CysK, function as homodimers and exhibit 25-45% similarity in their amino acid sequence (Ågren et al., 2009; Schnell, Oehlmann, Singh, & Schneider, 2007; Tai, Nalabolu, Jacobson, Minter, & Cook, 1993; Zhao, Kumada, Imanaka, Imamura, & Nakanishi, 2006). The key difference between these isoenzymes is the ability of CysM to utilize larger sulfur donor substrates including thiosulfate, where CysK is only capable of accepting the small sulfur donor, hydrogen sulfide (Barbara Campanini et al., 2015; Claus et al., 2005; Tai et al., 1993).

CysK and CysM enzymes have been structurally characterized from a range of a bacterial species, enabling comparison of the two isoforms, and providing insight into active site conformation and isoform differences for isoform specific inhibitor design. Within the CysK and CysM homodimer one PLP molecule is bound per subunit in the active site cleft that is formed between the N and C-terminal domains of each monomer. The active site cleft of CysK and CysM are fairly similar and are lined by seven chain segments totaling 16 residues. Six of these chain segments are highly conserved between CysK and CysM isoforms, however, the seventh segment spanning residues 210-216 of CysM (*E. coli* CysM numbering) indicates a key difference between the two enzymes (Chattopadhyay et al., 2007; Claus et al., 2005). CysM contains the three large residues Arg210, Arg211, and Trp212 followed by a three-residue insertion, which bulges towards the surface enlarging the active site. Most of this enlarged active site is occupied by the sidechain tail of Arg210 which most likely binds to thiosulfate or other larger sulfur donor substrates (Claus et al., 2005). Conversely, *St*CysK has three small residues, Gly230, Ala231 and Gly232 (Claus et al., 2005; Rabeh & Cook, 2004). This small change reduces the size of the active site cleft, therefore restricting CysK to using bisulfide as its sulfur donor. Lys41, is highly conserved across both CysK and CysM isozymes as it forms an internal aldimine linkage with PLP in both isoforms (Liang, Han, Tan, Ding, & Li, 2019; Rabeh & Cook, 2004). The enzyme cycles through open and closed conformations during catalysis. Both open (no substrates bound) and closed forms (substrates bound) have been structurally characterized (Burkhard et al., 1998; Burkhard, Tai, Ristroph, Cook, & Jansonius, 1999; Chattopadhyay et al., 2007) with the closed form occurring via binding of the substrate α-carboxylate or acetate

to the substrate binding loop (residues 68-71 in *S. typhimurium*) triggering the active site to close (Burkhard et al., 1999; Chattopadhyay et al., 2007).

The two monomer subunits interact solely at the dimer interface and an allosteric binding site was recently identified in the CysK isoform, that is not present in CysM (Rabeh & Cook, 2004). The structure of CysK with $Cl^-$ bound at the allosteric anion binding site at the subunit interface, shows a closed/inhibited form of the enzyme (Tai et al., 2001). The anion sulfide behaves similarly to chloride and has essentially the same ionic radii and also binds to the anion binding site (Tai et al., 2001), presumably acting as a further regulator of CysK activity and modulating sulfur flux within the cell.

### 2.6.3 CysK/CysM Enzyme Mechanism

As discussed for CysE, a detailed understanding of both structure and enzyme mechanism is important for inhibitor design. OASS catalyzes the replacement of the β-acetoxy group of *O*-acetylserine by either sulfide in the case of CysK or thiosulfate and sulfide in the case of CysM to produce L-cysteine. Both CysM and CysK utilize a bi-bi ping-pong mechanism for cysteine biosynthesis (Tai et al., 1993; Zhao, Kumada, et al., 2006). This involves the release of one of the half reactions products before all substrates have bound to the enzyme, generating an enzyme intermediate in the process (Ulusu, 2015). *O*-acetylserine carries out nucleophilic attack on the C-4' of the internal aldimine (Figure 2.4). As the external aldimine is formed, the active site closes due to interaction of the substrate-carboxylate with an asparagine loop (Figure 2.4). A conserved lysine (Lys41; *E. coli* numbering), initially part of the internal aldimine PLP linkage, serves as a general base to deprotonate Cα in the β-elimination reaction that releases acetate at the conclusion of the first half reaction forming the α-aminoacrylate intermediate (Figure 2.4) (Joshi et al., 2019; Rabeh & Cook, 2004). Acetate diffuses out of the active site as it opens partially to allow entry of bisulfide and product release. Lys41 remains protonated at the beginning of the second half reaction, bisulfide diffuses into the active site attacking the Cβ of the α-aminoacrylate giving the cysteine external Schiff base (Figure 2.4). The cysteine product, *S*-sulfocysteine for CysM, and L-cysteine for CysK, is expelled via transimination (Joshi et al., 2019; Rabeh &

Cook, 2004). *S*-sulfocysteine is reduced to L-cysteine via an unknown mechanism (Kredich, 2008).

### 2.6.4 Cysteine Synthase Complex Formation

The bienzyme cysteine synthase complex (CSC) was first discovered during the purification of *S. typhimurium* CysK and CysE (Kredich, Becker, & Tomkins, 1969; Kredich & Tomkins, 1966). CSC formation has since been confirmed across many other species including *E. coli* (Benoni et al., 2017; Koshiki Mino et al., 2000; K. Mino et al., 2000), *H. influenzae* (Huang, Vetting, & Roderick, 2005; Salsi et al., 2010), and various plant species (Francois, Kumaran, & Jez, 2006; Yi et al., 2013). The formation of the CSC represents a unique avenue for the design of inhibitors.

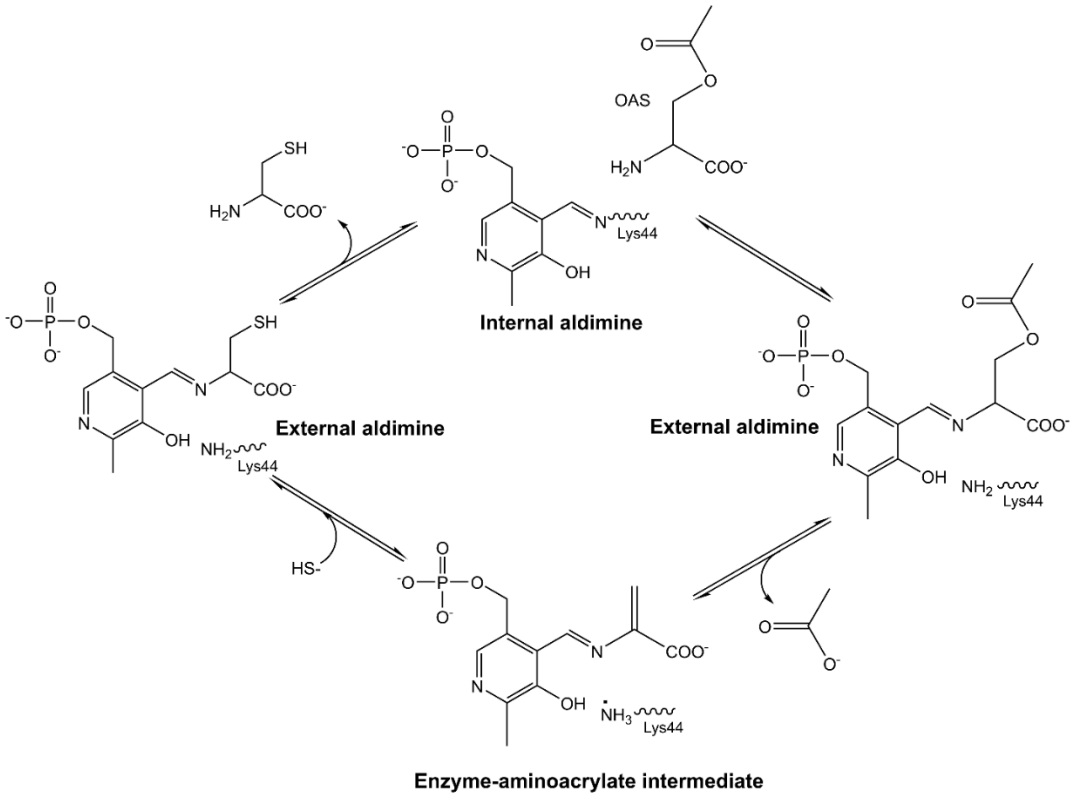


**Figure 2.4:** CysK catalytic mechanism, based on the *M. tuberculosis* CysK enzyme (*Mtb*CysK Lys44 equivalent to Lys41 in text). Figure produced using ChemDraw Prime (RRID:SCR_016768), adapted from (Joshi et al., 2019).

The complex forms via binding of the CysE C-terminal tail into the CysK active site, thus inhibiting CysK activity and therefore cysteine production (Benoni et al., 2017; B. Campanini et al., 2015; Francois et al., 2006; Huang et al., 2005; Koshiki Mino et al., 2000; K. Mino et al., 2000; Salsi et al., 2010). The complex forms in 3:2 CysE:CysK ratio consisting of one CysE hexamer and two CysK dimers (Huang

et al., 2005). Deletion of 20 C-terminal residues from CysE results in an inability to bind to CysK and formation of the CSC does not occur, highlighting the importance of the C-terminal peptide tail of CysE in CSC formation (Koshiki Mino et al., 2000). CSC formation reduces L-cysteine feedback inhibition and L-serine substrate inhibition of CysE activity in *E. coli* (Benoni et al., 2017). Complex formation also reduces CysE cold inactivation at both 0 and 10 °C (K. Mino et al., 2000), presumably due to increased stability caused by structural reorganization at part of the N-terminal domain of CysE, that interacts with CysK leading to allosteric stabilization at the interface between the CysE trimers (Rosa et al., 2021). CysM and CysE have no interactions and do not form a complex, due to differences in the active site structure (Zhao, Kumada, et al., 2006).

Structural studies of CysK in complex with CysE C-terminal peptides have provided insight into the interaction of the C-terminal CysE tail with the active site of CysK as to date there are no atomic structures of the CSC. The PLP cofactor in the OASS active site has fluorescent properties sensitive to its microenvironment and protein conformational changes. These fluorescent properties can be used to monitor formation of the CSC with CysE and with peptides that mimic the C-terminal tail of CysE (Campanini et al., 2005). Fluorescent monitoring of the PLP cofactor binding to the entire CysE protein and a C-terminal decapeptide (mimicking the CysE C-terminal tail), demonstrated that the C-terminal α-carboxylate of the CysE C-terminal decapeptide and the CysE C-terminal tail fit into the same position (Burkhard et al., 1999; Campanini et al., 2005).

At a ratio of 5:1 CysE:CysK (at which full complex formation is assumed to have taken place) the activity of CysK in the *E. coli* CSC is reduced to 10% of free CysK activity (Koshiki Mino et al., 2000; K. Mino et al., 2000; Rosa et al., 2019). Yet the CysE C-terminal decapeptide when bound to CysK reduced activity to 50% at a 500:1 molar ratio of decapeptide to CysK (Koshiki Mino et al., 2000). This can be attributed to full length CysE binding 250-fold tighter to CysK compared to the C-terminal decapeptide (Huang et al., 2005). Dissociation constants ($K_D$) of peptides in complex with CysK compared to full length CysE in complex with CysK further show the stark contrast in binding affinity of peptides compared to the full length CysE in the CSC (Table 2.2). This indicates there may be additional

structural features of CysE that CysK recognizes aside from the C-terminal decapeptide which increase the binding affinity but are not sufficient for directing complex formation without the presence of the C-terminal decapeptide (Huang et al., 2005).

The highly conserved C-terminal isoleucine of the CysE C-terminal peptide is an essential anchor point for correct positioning of the C-terminal tail; in *H. influenzae* accounting for 80% of the total interaction energy (Salsi et al., 2010). This energy contribution is derived from Thr69 and Thr73 hydrogen bonds to the Ile267 α-carboxylate (Figure 2.5) (Salsi et al., 2010). The Ile267 sidechain forms hydrophobic interactions in an apolar pocket formed by the Phe144 and PLP (Figure 2.5) (Salsi et al., 2010). A further 10% of the total interaction energy is split equally between the C-terminal Asn266 and Leu265 (Figure 2.5) (Salsi et al., 2010).

**Table 2.2:** Dissociation constants ($K_D$) of CysE decapeptides and full length CysE in the CSC. H*i*DK = *Hi*CysE C-terminal decapeptide (GIDDGMNLNI) with *Hi*CysK from (Campanini et al., 2005). *Hi*DStK = *Hi*CysE C-terminal decapeptide (GIDDGMNLNI) with *St*CysK from (Campanini et al., 2005). *Ec*CS C1 = full length *Ec*CysE with *Ec*CysK from (Benoni et al., 2017). *Ec*CS C2 = full length *Ec*CysE with *Ec*CysK from (Marchetti et al., 2021). *St*CSC C= full length *St*CysE with *St*CysK from (Marchetti et al., 2021).

| | **CysE Decapeptide** | | **Full length CysE** | | |
|---|---|---|---|---|---|
| | **HiDK** | **HiDStK** | **EcCS C1** | **EcCS C2** | **StCS C** |
| **$K_D$ (nM)** | 515 ± 29* | 972 ± 62* | 4.5/6[a] | 0.63[a] | 0.83[a] |

*Error reported as standard error

[a]No error reported

The dependence of the CSC on sulfur availability indicates regulation of sulfur flux to be the purpose of CSC formation (Benoni et al., 2017; Kredich et al., 1969; Wang & Leyh, 2012; Zhao, Moriga, et al., 2006). The regulation forms a loop beginning with high availability of sulfur to the cell where the CSC is stabilized by bisulfide (Kredich et al., 1969), however, when sulfur availability is low, OAS accumulates via CysE production, thus indicating sulfur starvation and dissociation of the CSC (Benoni et al., 2017; Kredich et al., 1969; Wang & Leyh, 2012; Zhao, Moriga, et al., 2006). Dissociation of the CSC can occur at OAS concentrations upwards of 50

μM (Kredich et al., 1969; Wang & Leyh, 2012), which then non-enzymatically isomerizes to *N*-acetylserine and binds to the transcriptional regulator CysB, thus promoting expression of sulfate acquisition genes (Jovanovic, Lilic, Savic, & Jovanovic, 2003; Kredich et al., 1969; Wang & Leyh, 2012). Expression of sulfate acquisition and reduction genes increases the concentration of sulfur within the cell, completing the loop with high sulfur availability promoting CSC stability and therefore increasing OAS production.

### 2.6.5 Development of Inhibitors for the OASS Isoforms CysK & CysM

#### 2.6.5.1 Peptide Inhibitors

Salsi et al. (2010) and Spyrakis et al. (2013) have paved the way in CysK inhibitor discovery with the identification of multiple potent peptide inhibitors for several key CysK isoforms (Salsi et al., 2010; Francesca Spyrakis et al., 2013). Although more recently, CysK inhibitor studies have focused primarily on chemical inhibitors, these peptide inhibitors stand as key templates for chemical inhibitor designs. The natural inhibition of CysK by CysE has been routinely used for these peptide inhibitor studies as a design platform (B. Campanini et al., 2015; Salsi et al., 2010; F. Spyrakis et al., 2013; Francesca Spyrakis et al., 2013). The three C-terminal residues of CysE contribute the strongest interactions with CysK, and therefore a minimum three-residue peptide is required for CysK inhibition; both Salsi et al. (2010) and Spyrakis et al. (2013) screened pentapeptides – including an additional two residues to better mimic the full length CysE C-terminal peptide (Salsi et al., 2010; F. Spyrakis et al., 2013; Francesca Spyrakis et al., 2013). Salsi et al. (2010) utilized the *Hi*CysK crystal structure (1Y7L) in complex with the *Hi*CysE C-terminal peptide (Huang et al., 2005), replacing this peptide with a panel of 400 pentapeptides into the active site via virtual screening (Salsi et al., 2010). Spyrakis et al. (2013) followed through an analogous computational pipeline, with the inclusion of the *S. typhimurium* apo CysK (*St*CysK) (1OAS) (Burkhard et al., 1998) and *St*CysM (2JC3) (Chattopadhyay et al., 2007) crystal structures.

Peptide inhibitors for both *S. typhimurium* isoforms and *Hi*CysK were identified, which demonstrated improved potencies *in vitro* compared to their respective native CysE C-terminal pentapeptides (Table 2.3). The most potent pentapeptides identified for *Hi*CysK were MNWNI and MNYDI, which both exhibited approximately 1.75 times improved affinity for the enzyme in comparison to the

equivalent native *Hi*CysE pentapeptide (MNLNI). Interestingly, structural analysis (MNWNI, 3IQG; MNYDI, 3IQH) showed the asparagine in MNWNI at position four to

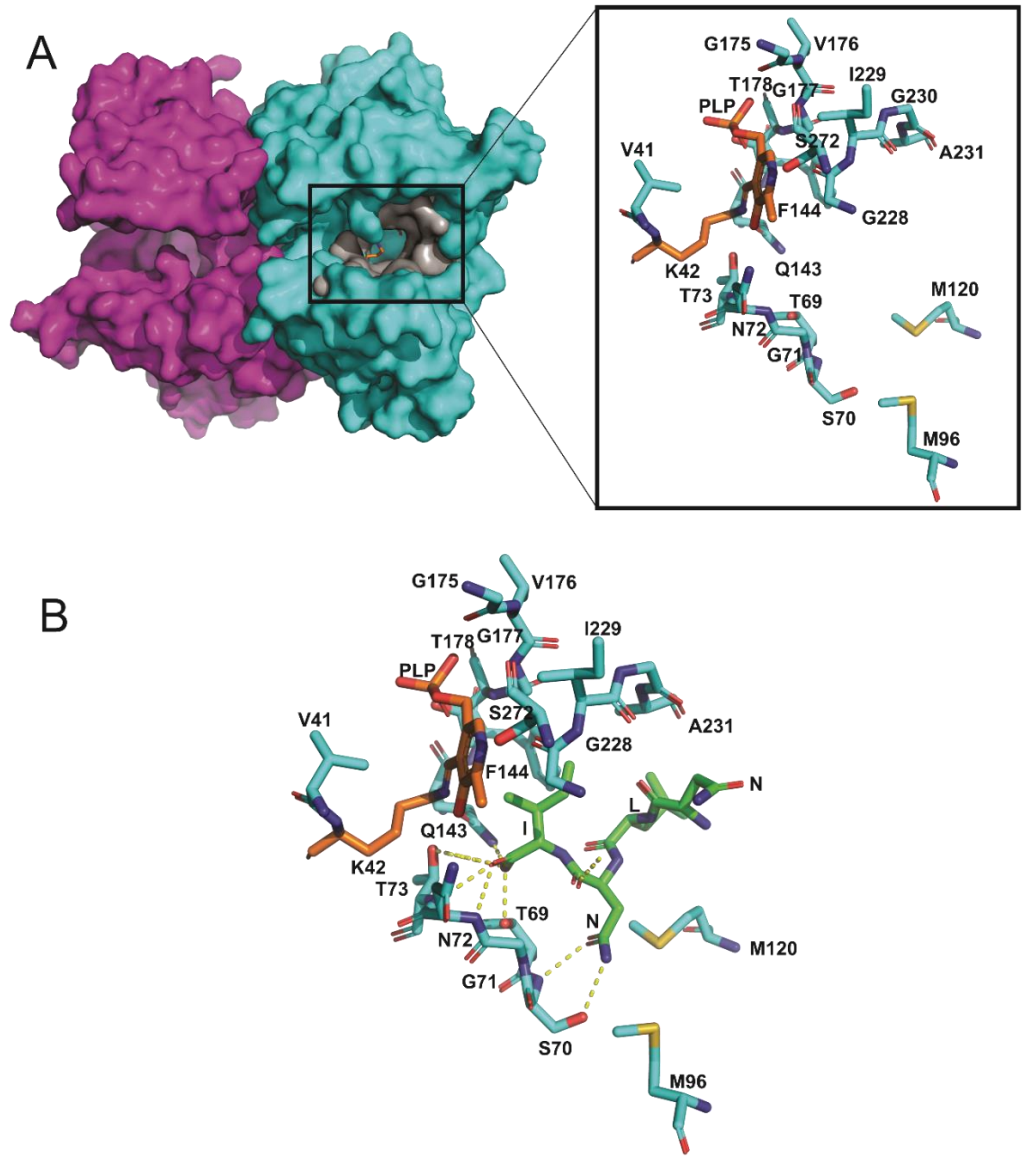


**Figure 2.5:** Overview of *H. influenzae* CysK. (a) *Hi*CysK dimer surface shown with one monomer in magenta and the other in cyan with PLP bound to K42 visible in orange deep in the active site cleft. Zoomed into *H. influenzae* active site residues (V41, K42, 69-TSGNT-73, M96, M120, 143-QF-144, 175-GVGT-178, 228-GIGA-231, and S272) shown in cyan with PLP bound to K42 in orange. Active site is similar to *St*CysK open (0.5 Å, r.m.s.d ) and *St*CysK partially closed anion-inhibited (0.4 Å, r.m.s.d) conformation (Huang et al., 2005) (b) *H. influenzae* active site residues shown in cyan interacting with bound *Hi*CysE C-terminal tetrapeptide shown in green (NLNI). Polar bonds shown with dotted yellow lines. Figure created with 1Y7L from (Huang et al., 2005) using PyMOL.

**Table 2.3:** List of top characterized CysK peptide inhibitors.

| Inhibitor | Enzyme | $K_D$ (μM)* | Citation |
|---|---|---|---|
| MNLNI (*Hi*SAT WT) | *Hi*CysK | 44.0 ± 3.6 | (Salsi et al., 2010) |
| | *St*CysK | 120 ± 12 | (Francesca Spyrakis et al., 2013) |
| | *St*CysM | ~3,000[a] | |
| MNWNI | *Hi*CysK | 24.9 ± 3.6 | (Salsi et al., 2010) |
| | *St*CysK | 10.4 ± 0.9 | (Francesca Spyrakis et al., 2013) |
| MNYDI | *Hi*CysK | 25.8 ± 1.7 | (Salsi et al., 2010) |
| | *St*CysK | 0.22 ± 0.04 | (Francesca Spyrakis et al., 2013) |
| YGDGI (*St*SAT WT) | *St*CysK | 11.8 ± 0.6 | |
| | *St*CysM | 4,922 ± 1,030 | |
| YGYDI | *St*CysK | 0.42 ± 0.02 | |
| MNDGI | *St*CysK | 306 ± 17 | |
| | *St*CysM | 1,100 ± 100 | |

*Error reported as standard error

[a]No error reported

participate in hydrogen-bonding with Ser70; whereas, the aspartate of MNYDI was shown to protrude out towards the protein surface. This protrusion is thought to be a result of the tyrosine at position three participating in an aromatic cluster with Phe144 and Phe233, which allows a sulfate ion to reside within the active site instead, and mimic the interactions of the asparagine in MNWNI (Figure 2.6) (Salsi et al., 2010).

Secondly, and most intriguingly, the top pentapeptide assessed for *St*CysK was MNYDI, which is a pentapeptide based on the *Hi*CysE C-terminus (MNLNI), and not that of the *St*CysE C-terminus (YGDGI) (Salsi et al., 2010). MNYDI showed approximately 60 times improved affinity compared to YGDGI, and around 600 times improved affinity compared to MNLNI. Moreover, the equivalent pentapeptide of MNYDI based on the *St*CysE sequence, YGYDI, still showed reduced potency compared to MNYDI, highlighting that the terminal three residues

of

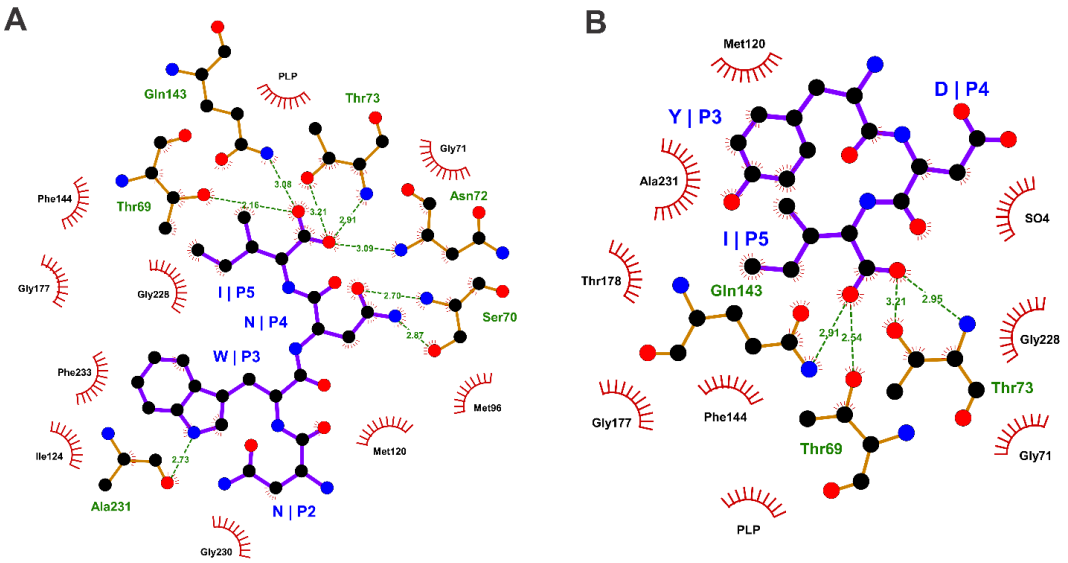


**Figure 2.6:** A: LigPlot showing the interactions between the *Hi*CysK residues and the MNWNI pentapeptide (PDB code 3IQG). B: LigPlot showing the interactions between the *Hi*CysK residues and the MNYDI pentapeptide (PDB code 3IGH).

the pentapeptides are involved in affinity regulation, whereas the preceding two residues are involved in selectivity (Salsi et al., 2010).

Furthermore, the pentapeptide which demonstrated the greatest potency towards *St*CysM was based on *both* the *St* and *Hi*CysE C-terminal sequences – MNDGI. This pentapeptide exhibited approximately 4.5 times greater affinity for the enzyme than YGDGI, and around three times greater affinity than MNLNI (Salsi et al., 2010). This inhibitor is also the most effective against both *S. typhimurium* isoforms, with the difference in $K_D$ values minimized. Correlation analysis of the $K_D$ values of *St* isoform binders, demonstrated an inversely proportional relationship, where a more potent inhibitor of *St*CysK was more likely to possess reduced affinity for *St*CysM.

Reasonable affinity correlation was also noted between binders of CysK *H. influenzae* and *S. typhimurium* homologs. Comparison of the active site architecture of these homologs signified only one minor difference – the orientation of the Gln227 side chain. In *Hi*CysK, the R-group protrudes into the active site; whereas, in *St*CysK this group protrudes towards the enzyme surface. Consequently, it is proposed that this localizes the third and fourth residues of the pentapeptides differentially within the enzyme active sites. Nevertheless, this highlights the

possibility for synthesizing broad-spectrum CysK and CysM compounds (Francesca Spyrakis et al., 2013).

Altogether, these data demonstrate that effective peptide inhibitors of CysK should ideally possess negatively-charged, hydrogen-bond acceptors at position four, and hydrophobic residues at position three. Unfortunately, this trend does not seem to translate to CysM peptide inhibitors, with glycine, a neutral and non-hydrogen bond acceptor at position four, and a negatively-charged, hydrophilic residue at position three.

More recently, Kant et al. (2019) investigated a panel of tetrapeptides for inhibition of the parasite *Leishmania donovani* CysK (*Ld*CysK) (Kant et al., 2019), with the aim to deconvolute the findings of (Raj, Kumar, & Gourinath, 2012), where *Ld*CysK did not demonstrate a preference for tetrapeptides with either long or small residues. Tetrapeptides were designed to contain all possible amino acid combinations for subsequent docking analysis. Docking analysis revealed EWSI and DWSI as the top two binders, respectively, with EWSI observing greater hydrogen-bonding and hence stabilization capabilities (Kant et al., 2019). Therefore, EWSI stands as a starting point for future *Ld*CysK inhibitor designs, alongside the need for *in vitro* characterization. Kant et al. (2019) also followed on to compare the differences between these identified tetrapeptide inhibitors of *Ld*CysK for their affinity for *Mtb*CysK1, given the similarity of these peptides to the native *Mtb*CysE tetrapeptide – DFSI. Interestingly, EWSI demonstrated improved docking into *Mtb*CysK1 compared to both DFSI and EFSI (Kant et al., 2019). This highlights EWSI as a valid starting point for future virtual screening of *Mtb*CysK1 chemical inhibitors.

#### 2.6.5.2 Chemical Inhibitors

Chemical inhibitors stand as superior drug compounds given their improved *in vivo* half-life, bioavailability, and pharmacokinetics compared to peptidic compounds (Amori et al., 2012; Reichelt & Martin, 2006). Since the studies by Salsi (2010) were published, many groups have been working on the design, synthesis, and characterization of chemical inhibitors for both CysK and CysM. The design work

has largely stemmed from structurally mimicking the key chemical

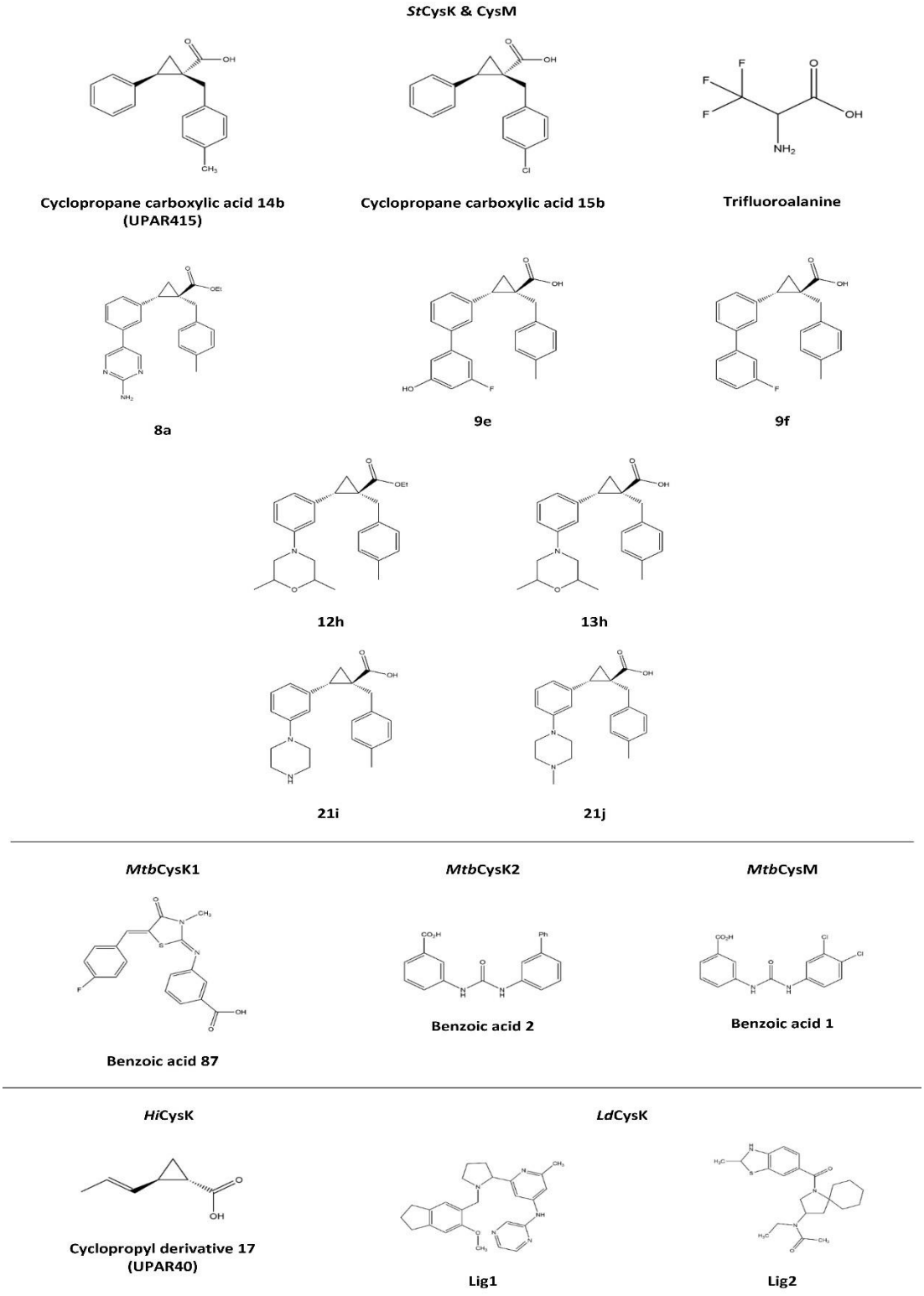


**Figure 2.7:** Chemical structures of top OASS chemical inhibitors. Figure produced using ChemDraw Prime (RRID:SCR_016768).

groups of the peptide inhibitors. Subsequently, many different chemical inhibitors have been identified, including, cyclopropane carboxylic acids (Amori et al., 2012;

Annunziato et al., 2016; Annunziato et al., 2021; Bruno, Amori, & Costantino, 2013; Pieroni et al., 2016), thiazolidinone and pyrimidinone derivatives (Jean Kumar et al., 2013; Kumar et al., 2011; Poyraz et al., 2013), fluoroalanines (Franko et al., 2018), benzoic acids (Brunner et al., 2016), and pyrazinamines and acetamides (Kant et al., 2019). The majority of these compounds were discovered via *in silico* docking experiments using crystal structures of inhibited complexes of the enzymes and subsequent high-throughput virtual screening.

To date, Amori et al. (2012) and Pieroni et al. (2016) have discovered the most potent chemical inhibitors of *Hi*CysK - (±)-trans-2-(ethoxycarbonyl) cyclopropanecarboxylic acid (±)-7 (referred to as UPAR40) (Amori et al., 2012) and trans-2-(prop-1-enyl)-cyclopropanecarboxylic acid (referred to as cyclopropyl derivative 17) (Pieroni et al., 2016), respectively. Both compounds contain a carboxylate and a hydrophobic moiety which reflect the key properties of the CysE C-terminal isoleucine, and are incorporated together between a cyclopropane spacer (Figure 2.7) (cyclopropane spaces are common features in bioactive molecules and also aid in restraining the ligand in its effective conformation for enzymatic interaction) (Amori et al., 2012; B. Campanini et al., 2015). Promisingly, docking and molecular dynamic analyses showed that these inhibitors lock the enzyme in its closed conformation (Amori et al., 2012; Bruno et al., 2013). Despite this success, Pieroni et al. (2016) has noted the impracticality of the chemical properties of these compounds for drug-like synthesis (Pieroni et al., 2016), and given the inactivity against the CysM isoform, efforts should now be directed towards improving the synthetic feasibility of these compounds, and their activity towards *Hi*CysM, alongside *in vivo* and cytotoxicity assays.

The success of the cyclopropane carboxylic acid compounds for *Hi*CysK, has also been shown for both *S. typhimurium* isoforms. Pieroni et al. (2016) identified (1S,2S)-1-(4-Methylbenzyl)-2-phenylcyclopropanecarboxylic acid 14b and (1S,2S)-1-(4-Chlorobenzyl)-2-phenylcyclopropanecarboxylic acid 15b as the most potent inhibitors against *St*CysM to date (Table 2.4) These compounds were adapted from cyclopropyl derivative 17 to contain a phenyl group as opposed to a vinyl group (Figure 2.7), which better embodies the *trans* orientation with the carboxylate displayed by the CysE C-terminal isoleucine, and is more synthetically viable. It was noted that further substitution of cyclopropyl derivative 17 at the α-

carbon position for interaction with both *S. typhimurium* isoforms would better occupy a moderately polar area of the active site, and therefore, benzyl substitution at this site with further para substitution resulted in compounds 14b and 15b (Pieroni et al., 2016). Interestingly, the *para* substitution of compounds 14b (4-$CH_3$) and 15b (4-Cl) represent both electron withdrawing and donating groups, yet reasonably equivalent potencies are observed (Table 2.4) – however, compound 15b shows reduced selectivity towards either isoform. Promisingly, the $IC_{50}$ values of compound 15b for both enzyme isoforms (Table 2.4), in the presence of the natural substrates of the enzyme, corroborate with the dissociation constants reported, indicating competitive inhibition.

Recently, Annunziato et al. (2021) utilized compound 14b, here referred to as UPAR415, as an effective adjuvant for the polymyxin antibiotic, colistin (Annunziato et al., 2021). Interestingly, in the presence of low cysteine levels, administration of UPAR415 alone did not exhibit any bactericidal or bacteriostatic effects on multiple bacterial species (Gram-positive and -negative) (Annunziato et al., 2021). In contrast, when UPAR415 was treated under these same conditions in conjunction with colistin, significant deductions were seen in the MIC of colistin compared to when colistin is dosed on its own. Promisingly, the cytotoxicity of UPAR415 was also shown to be insignificant. The crystal structure of *St*CysK in complex with UPAR415 (6Z4N) was also solved by Annunziato et al. (2021). This demonstrated that UPAR415 is a competitive inhibitor of *St*CysK against its first substrate, *O*-acetylserine, and was found localized in proximity to the PLP cofactor (Figure 2.8). The active site entrance could be seen to be partially blocked by the two aromatic substituents of the cyclopropane-ring, which engaged in hydrophobic interactions with active site residues. The remainder of the UPAR415 molecule was seen to penetrate into the active site. Promisingly, the carboxylate group of UPAR415 was found to localize to the well-studied carboxylic site; engagement with this site has been found to result in a conformational change of the enzyme into its closed active site state through translocation of the substrate-binding loop, which ultimately rotates the N-terminal domain over the active site. Although, UPAR415 positions itself at this carboxylic site, only partial closure of the active site is induced, which can be explained by a steric clash of the substrate-binding loop with the tolyl substituent of UPAR415 (Figure 2.8) (Annunziato et al., 2021).

**Table 2.4:** Top characterized OASS chemical inhibitors.

| Inhibitor | Enzyme | $IC_{50}$ (μM)* | $K_D$ (μM)* | Citation |
|---|---|---|---|---|
| Cyclopropyl derivative 7 (UPAR40) | *Hi*CysK | 700 ± 53 | 1.46 ± 0.25 | (Amori et al., 2012) |
| Cyclopropyl derivative 17 | | ND | 1.45[a] | (Pieroni et al., 2016) |
| Cyclopropane carboxylic acid 14b (UPAR415) | *St*CysK | ND | 0.028 ± 0.005 | |
| | *St*CysM | ND | 0.49 ± 0.05 | |
| Cyclopropane carboxylic acid 15b | *St*CysK | 0.099 ± 0.004 | 0.054 ± 0.008 | |
| | *St*CysM | 0.50 ± 0.03 | 0.42 ± 0.06 | |
| 8a | *St*CysK | ND | - | (Annunziato et al., 2022) |
| | *St*CysM | ND | - | |
| 9e | *St*CysK | ND | 0.035 ± 0.003 | |
| | *St*CysM | ND | 0.61 ± 0.08 | |
| 9f | *St*CysK | ND | 0.051 ± 0.004 | |
| | *St*CysM | ND | 1.45 ± 0.31 | |
| 12h | *St*CysK | ND | - | |
| | *St*CysM | ND | - | |
| 13h | *St*CysK | ND | 0.066 ± 0.005 | |
| | *St*CysM | ND | 3.37 ± 0.72 | |
| 21i | *St*CysK | ND | 0.45 ± 0.09 | |
| | *St*CysM | ND | 83.8 ± 16.1 | |
| 21j | *St*CysK | ND | 0.25 ± 0.06 | |
| | *St*CysM | ND | 23.6 ± 4.5 | |
| Trifluoroalanine | *St*CysK | 130 ± 10 | ND | (Franko et al., 2018) |
| | *St*CysM | 1,290 ± 230 | ND | |
| Benzoic acid 87 | *Mtb*CysK1 | 0.019 ± 0.0011 | ND | (Poyraz et al., 2013) |
| Benzoic acid 1 | *Mtb*CysM | ND | 0.32 ± 0.01 | (Brunner et al., 2016) |
| Benzoic acid 2 | *Mtb*CysK2 | ND | 22.6 ± 2.4 | |

ND = not determined. *Error reported as standard error. [a]No error reported.

A medicinal chemistry campaign to synthesize UPAR415 derivatives and the characterization of ligand-target complexes revealed the presence of an accessory sub-pocket that can be filled by substitutions at the 3' position of UPAR415

(Annunziato et al., 2022). Most compounds synthesized in this study retained good binding *in vitro*. Derivatives with heteroaliphatic or heteroaromatic groups in the 3' position led improved inhibition against both OASS isoforms compared to those previously described (Annunziato et al., 2021). Compounds substituted with a heteroaromatic group at the 3' position for example, trans-2-(3'-fluoro-5'-hydroxy-[1,1'-biphenyl]-3-yl)-1-(4-methylbenzyl)cyclopropane carboxylic acid (compound 9e) and trans-2-(3′-fluoro-[1,1′-biphenyl]-3-yl)-1-(4-methylbenzyl)cyclopropane carboxylic acid (compound 9f), that had a phenyl substituted with a fluorine and hydroxy group, or a fluorine respectively demonstrated potent inhibition (nanomolar range) against CysK (Figure 2.7) (Annunziato et al., 2022). Whereas compounds carrying a 2-aminopyrimidine group at the 3' position showed good inhibition of both isoforms. Compound 13h (trans-2-(3-(2,6-dimethylmorpholino)phenyl)-1-(4-methylbenzyl)cyclopropanecarboxylic acid) had a dimethyl morpholine at the 3' position and had the most potent activity for derivatives substituted with a heteroaliphatic group at position 3' (Figure 2.7). Compounds with a piperazine ring had good activity against CysK but these derivatives were less effective at inhibiting CysM. The majority of all compounds synthesized demonstrated low toxicity in that they were tolerated by mammalian cells. Compound 13h and its corresponding ester derivative 12h showed potent inhibition *in vitro* and good toxicity profiles. These lead compounds were tested as colistin adjuvants, showing effective synergy by reducing the MIC of colistin against *E. coli* and *S. typhimurium* even at low concentrations (Annunziato et al., 2022). Importantly for this study, the most promising derivative 12h (trans-ethyl 2-(3-(2,6-dimethylmorpholino)phenyl)-1-(4-methylbenzyl)cyclopropanecarboxylate) was linked to the chemical inhibition of CysK and CysM *in vivo* using target engagement experiments in *S. typhimurium* in the presence of colistin (the compound on its own does not exert any bactericidal effects) (Annunziato et al., 2022). Compound 12h demonstrated a significant improvement in the active concentration at which it can act as a colistin adjuvant inside cells, thereby paving the way as a prodrug to overcome some of the toxicity issues associated with colistin.

Franko et al. (2018) studied fluoroalanine derivatives *in vitro* against both *S. typhimurium* isoforms as irreversible inhibitors, given the ubiquitous use and

study of these halogens as

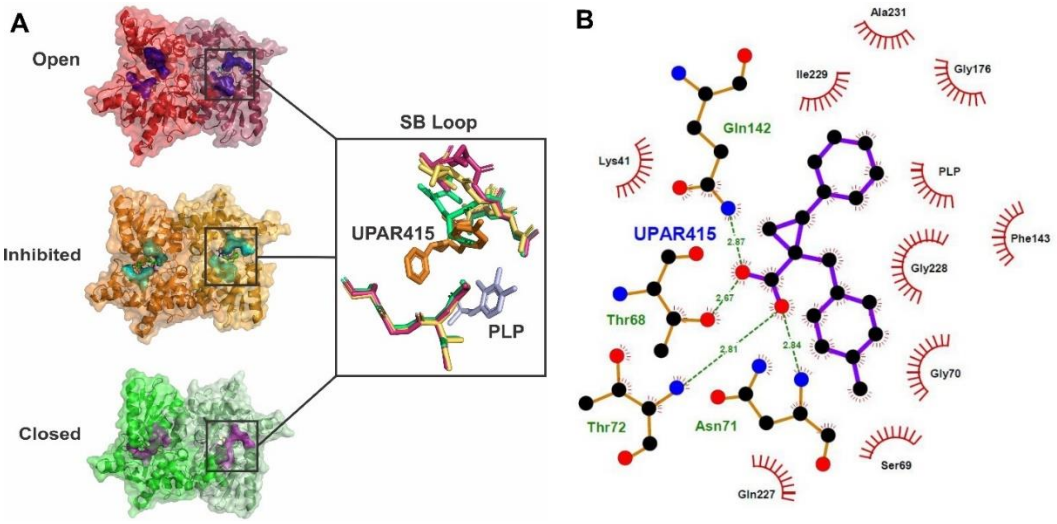


**Figure 2.8:** Inhibition of *St*CysK by UPAR415. A. Structural comparison of the substrate binding loop between the open conformation (1OAS) shown in shades of red, the inhibited conformation (6Z4N) shown in shades of orange, and the closed conformation (1D6S) shown in shades of green. B. LigPlot showing the interactions between the enzyme residues and the UPAR415 molecule. Figure produced using PyMOl and LigPlot.

irreversible inhibitors of PLP-dependent enzymes (Alexeev et al., 2006; Alston, Muramatsu, Ueda, & Bright, 1981; Azam & Jayaram, 2016; John & Tudball, 1972; Passera et al., 2011; Phillips & Dua, 1992; Silverman, 1995; Silverman & Abeles, 1976; Tysoe & Withers, 2014). Halogenated alanine addition to this group of enzymes is known to generate an unsaturated α-aminoacrylate Schiff's base (or α-aminoacrylate-PLP complex) (Alexeev et al., 2006; Poulin, Lu, Ackermann, Bey, & Pegg, 1992) – the subsequent inhibition mechanism is dependent on the specific halogenated alanine and how this reorientates the active site; typically, the catalytic lysine is attacked, and subsequent chemical rearrangement culminates in the disengagement of the halogen ions, allowing for a stable derivative to form, which ultimately inhibits the enzyme (Franko et al., 2018).

*β*,*β*,*β*-trifluoroalanine (triF-Ala), which is a known PLP-dependent enzyme suicide inhibitor (Alexeev et al., 2006; Faraci & Walsh, 1989; Phillips & Dua, 1992; Silverman & Abeles, 1976; Silverman & Abeles, 1977; Tysoe & Withers, 2014; Wang & Walsh, 1981), was the most potent fluoroalanine derivative assessed. This compound had high affinity for the StCysK enzyme active site and slightly lower for that of *St*CysM. The mechanism of inhibition was determined to be irreversible covalent modification of the catalytic amino acids, yet the $IC_{50}$ values of triF-Ala with both enzyme isoforms (Table 2.4) are too high to be an efficient inhibitor.

Poyraz et al. (2013) identified the most potent inhibitor to date for the *M. tuberculosis* enzyme CysK1 (*Mtb*CysK1), a thiazolidinone derivative - 3-((Z)-((Z)-5-(4-fluorobenzylidene)-3-methyl-4-oxothiazolidin-2-ylidene)amino)benzoic acid (Poyraz et al., 2013). E-pharmacophore sites were identified from the *Mtb*CysK1-DFSI crystal structure (2Q3C) (Schnell et al., 2007) – one aromatic ring, two acceptors, and two negative ionizable moieties. The compound benzoic acid 87 was identified from substitution analyses from the initial *in vitro* hit compound - 3-({5-[2-(carboxymethoxy)benzylidene]-3-methyl-4-oxo-1,3-thiazolidin-2-ylidene}amino)benzoic acid 2, where compound 87 represents a C4 fluoro substitution, and showed an approximately five fold greater inhibition effect compared to benzoic acid 2.

The crystal structure of derivative 2 bound to *Mtb*CysK1 (3ZEI) showed the thiazolidinone moiety to not protrude greatly out of the active site as is seen with the native peptide (Poyraz et al., 2013). The thiazolidine core mimics the phenyl group of the DFSI peptide, and contributes to interactions with the enzyme hydrophobic cleft. Although similarly, the carboxylic moiety of the compound benzoic acid 2 (associated with the benzoic acid group) was found docked entirely within the active site with Ser72 interactions and potential for hydrogen-bonding with Thr71 and Gln144, as has previously been shown with the C-terminal isoleucines of peptide inhibitors (Salsi et al., 2010; Francesca Spyrakis et al., 2013). In contrast to previous inhibitor observations, the 2-carboxymethoxy moiety does not participate in any solvent hydrogen-bonding despite protruding out towards the protein surface, which may indicate a key feature in developing future potent inhibitors (B. Campanini et al., 2015; Poyraz et al., 2013) . Nevertheless, this structural analysis revealed an enzyme pocket next to the *para*-position of the benzylidene ring, from which compound 87 verifies (Poyraz et al., 2013).

Brunner et al. (2016) identified the most potent inhibitor to date for *Mtb*CysM - 3-(3-(3,4-dichlorophenyl)ureido) benzoic acid 1, as well as that for *Mtb*CysK2 - 3-(3-([1,1-Biphenyl]-3-yl)ureido)benzoic acid 2 (Brunner et al., 2016). These hit compounds were identified by *in vitro* screening of around 17,000 small molecules, followed by structural analysis. The crystal structure of the compound benzoic acid 1 bound to *Mtb*CysM (5I7A) did not demonstrate large differences compared to the

apo structure – the compound was shown to be bound within the open state of the active site (parallel to PLP pyrimidine ring plane), where stacking interactions were seen between the PLP pyrimidine ring and the urea moiety (Brunner et al., 2016). The meta carboxylate group of the compound was found associated within the active site, similar to the carboxylate moiety of the α-aminoacrylate intermediate of *Mtb*CysK1 (Schnell et al., 2007); whereas the 1,2-dichlorobenzene group interacts within the hydrophobic cleft of the enzyme. The core urea group was found to interact with the Asn221 side chain via its carbonyl moiety, interactions with the carboxyl of Ala323 found within the active site occur through an amide group, with the other amide group forming a hydrogen-bond with a water molecule (Brunner et al., 2016). Promisingly, in a nutrient starvation model (simulating dormancy, when CysM is primarily expressed), compound 1 demonstrated higher potency compared to current clinically-approved first-line tuberculosis antibiotics, with insignificant cytotoxic effects on several mammalian cell lines (Brunner et al., 2016).

Kant et al. (2019) identified two hit molecules for *Ld*CysK - N-(2-{1-[(6-methoxy-2,3-dihydro-1H-inden-5-yl)methyl]pyrrolidin-2-yl}-6-methylpyridin-4-yl)pyrazin-2-amine (Lig1) and N-ethyl-N-{1-[(2-methyl-2,3-dihydro-1,3-benzothiazol-6-yl)carbonyl]-1-azaspiro[4.5]decan-3-yl}acetamide (Lig2) via *in silico* screening of tetrapeptides with shape similarity to EWSI and DWSI (Kant et al., 2019). These ligands were docked into *Ld*CysK and Lig2 demonstrated improved interaction energy and capacity for hydrogen-bonding; this ligand was that which had greater conformational similarity to EWSI compared to DWSI. This potency of Lig2 was reinforced through molecular dynamics and binding energy analysis compared to Lig1 in complex with the enzyme, in terms of stability and compactness. In addition, both docking and molecular dynamic analyses demonstrated hydrogen-bonding interactions between Lig2 and residues, Ser79 and Gln152 (Kant et al., 2019). Characterization of these inhibitors both *in vitro* and *in vivo* remains to be investigated.

It is worth noting that despite the significant advances that have been made in the chemical inhibitor space for CysK and CysM enzymes, the potencies of these inhibitors remain around 100-fold less effective than the complete enzymatic inhibition of CysK by CysE (Table 2.2).

## 2.7 Conclusion

There have been many campaigns aimed at discovering potent and selective inhibitors for the cysteine synthesis enzymes CysE and CysK. Yet despite excellent inhibition of activity seen for certain compounds many failed to inhibit bacterial growth, presumably due to the lack of permeability of the compounds across the bacterial wall. The best inhibitor for CysE that was bactericidal and had an $IC_{50}$ of 48 μM, although this is much greater than the natural inhibitor cysteine, with an $IC_{50}$ between 1-10 μM. Recently inhibitors of CysK were identified that demonstrate potent inhibition (nanomolar binding) and an adjuvant effect when used in combination with the antibiotic colistin. Based on this it is worth testing other promising inhibitors identified with known antibiotics to see if they have an adjuvant effect. Given that cysteine biosynthesis is often dispensable under nutrient rich conditions but becomes more essential during infection and persistence it would also be worth testing if the identified compounds reduces infection and/or enhances clearance by the host immune system. As shown here there is increasing evidence for bacterial *de novo* cysteine biosynthesis as a promising drug target for either new antimicrobials or antibiotic adjuvants. Further validation of this pathway and further exploration of new and existing inhibitor compounds is vital to develop potent and selective inhibitors to overcome antimicrobial resistance in a range of Gram-positive and Gram-negative human pathogens.

## 2.8 References


Abd El-Aleam, R. H., George, R. F., Georgey, H. H., & Abdel-Rahman, H. M. (2021). Bacterial virulence factors: a target for heterocyclic compounds to combat bacterial resistance. *RSC Advances, 11*(58), 36459-36482. 10.1039/d1ra06238g

Agarwal, S. M., Jain, R., Bhattacharya, A., & Azam, A. (2008). Inhibitors of Escherichia coli serine acetyltransferase block proliferation of Entamoeba histolytica trophozoites. *Int J Parasitol, 38*(2), 137-141. 10.1016/j.ijpara.2007.09.009

Ågren, D., Schnell, R., & Schneider, G. (2009). The C-terminal of CysM from Mycobacterium tuberculosis protects the aminoacrylate intermediate and is involved in sulfur donor selectivity. *FEBS Letters, 583*(2), 330-336. 10.1016/j.febslet.2008.12.019

Akerley, B. J., Rubin, E. J., Novick, V. L., Amaya, K., Judson, N., & Mekalanos, J. J. (2002). A genome-scale analysis for identification of genes required for growth or survival of Haemophilus influenzae. *Proc Natl Acad Sci U S A, 99*(2), 966-971. 10.1073/pnas.012602299

Alexeev, D., Baxter, R. L., Campopiano, D. J., Kerbarh, O., Sawyer, L., Tomczyk, N., . . . Webster, S. P. (2006). Suicide inhibition of alpha-oxamine synthases: structures of the covalent adducts of 8-amino-7-oxononanoate synthase with trifluoroalanine. *Org Biomol Chem, 4*(7), 1209-1212. 10.1039/b517922j

Alston, T. A., Muramatsu, H., Ueda, T., & Bright, H. J. (1981). Inactivation of gamma-cystathionase by gamma-fluorinated amino acids. *FEBS Lett, 128*(2), 293-297. 10.1016/0014-5793(81)80102-0

Amori, L., Katkevica, S., Bruno, A., Campanini, B., Felici, P., Mozzarelli, A., & Costantino, G. (2012). Design and synthesis of trans-2-substituted-cyclopropane-1-carboxylic acids as the first non-natural small molecule inhibitors of O-acetylserine sulfhydrylase. *Med. Chem. Comm., 3*(9), 1111-1116. 10.1039/C2MD20100C

Annunziato, G., Pieroni, M., Benoni, R., Campanini, B., Pertinhez, T. A., Pecchini, C., . . . Costantino, G. (2016). Cyclopropane-1,2-dicarboxylic acids as new tools for the biophysical investigation of O-acetylserine sulfhydrylases by fluorimetric methods and saturation transfer difference (STD) NMR. *J Enzyme Inhib Med Chem, 31*(sup4), 78-87. 10.1080/14756366.2016.1218486

Annunziato, G., Spadini, C., Franko, N., Storici, P., Demitri, N., Pieroni, M., . . . Costantino, G. (2021). Investigational Studies on a Hit Compound Cyclopropane–Carboxylic Acid Derivative Targeting O-Acetylserine Sulfhydrylase as a Colistin Adjuvant. *ACS Infectious Diseases, 7*(2), 281-292. 10.1021/acsinfecdis.0c00378

Annunziato, G., Spadini, C., Marchetti, M., Franko, N., Pavone, M., Iannarelli, M., . . . Costantino, G. (2022). Inhibitors of O-Acetylserine Sulfhydrylase with a Cyclopropane-Carboxylic Acid Scaffold Are Effective Colistin Adjuvants in Gram Negative Bacteria. *Pharmaceuticals, 15*(6) 10.3390/ph15060766

Azam, M. A., & Jayaram, U. (2016). Inhibitors of alanine racemase enzyme: a review. *J Enzyme Inhib Med Chem, 31*(4), 517-526. 10.3109/14756366.2015.1050010

Bachman, M. A., Breen, P., Deornellas, V., Mu, Q., Zhao, L., Wu, W., . . . Gilmore, M. S. (2015). Genome-Wide Identification of Klebsiella pneumoniae

Fitness Genes during Lung Infection. *mBio, 6*(3), e00775-00715. doi:10.1128/mBio.00775-15

Becker, D., Selbach, M., Rollenhagen, C., Ballmaier, M., Meyer, T. F., Mann, M., & Bumann, D. (2006). Robust Salmonella metabolism limits possibilities for new antimicrobials. *Nature, 440*(7082), 303-307. 10.1038/nature04616

Becker, M. A., & Tomkins, G. M. (1969). Pleiotropy in a Cysteine-requiring Mutant of *Salmonella typhimurium* Resulting from Altered Protein-Protein Interaction. *J. Biol. Chem., 244*(21), 6023-6030.

Benoni, R., De Bei, O., Paredi, G., Hayes, C. S., Franko, N., Mozzarelli, A., . . . Campanini, B. (2017). Modulation of *Escherichia coli* serine acetyltransferase catalytic activity in the cysteine synthase complex. *FEBS Lett, 591*(9), 1212-1224. 10.1002/1873-3468.12630

Betts, J. C., Lukey, P. T., Robb, L. C., McAdam, R. A., & Duncan, K. (2002). Evaluation of a nutrient starvation model of Mycobacterium tuberculosis persistence by gene and protein expression profiling. *Mol Microbiol, 43*(3), 717-731. 10.1046/j.1365-2958.2002.02779.x

Bhave, D. P., Muse, W. B., 3rd, & Carroll, K. S. (2007). Drug targets in mycobacterial sulfur metabolism. *Infectious disorders drug targets, 7*(2), 140-158. 10.2174/187152607781001772

Brunner, K., Maric, S., Reshma, R. S., Almqvist, H., Seashore-Ludlow, B., Gustavsson, A.-L., . . . Schneider, G. (2016). Inhibitors of the Cysteine Synthase CysM with Antibacterial Potency against Dormant Mycobacterium tuberculosis. *J. Med. Chem, 59*(14), 6848-6859. 10.1021/acs.jmedchem.6b00674

Brunner, K., Steiner, E. M., Reshma, R. S., Sriram, D., Schnell, R., & Schneider, G. (2017). Profiling of in vitro activities of urea-based inhibitors against cysteine synthases from Mycobacterium tuberculosis. *Bioorg Med Chem Lett, 27*(19), 4582-4587. 10.1016/j.bmcl.2017.08.039

Bruno, A., Amori, L., & Costantino, G. (2013). Computational Insights into the Mechanism of Inhibition of OASS-A by a Small Molecule Inhibitor. *Mol Inform, 32*(5-6), 447-457. 10.1002/minf.201200174

Burkhard, P., Rao, G. S., Hohenester, E., Schnackerz, K. D., Cook, P. F., & Jansonius, J. N. (1998). Three-dimensional structure of O-acetylserine sulfhydrylase from *Salmonella typhimurium*. *J Mol Biol, 283*(1), 121-133. 10.1006/jmbi.1998.2037.

Burkhard, P., Tai, C.-H., Ristroph, C. M., Cook, P. F., & Jansonius, J. N. (1999). Ligand binding induces a large conformational change in O-acetylserine sulfhydrylase from Salmonella typhimurium. *Journal of Molecular Biology, 291*(4), 941-953. 10.1006/jmbi.1999.3002

Burns-Huang, K., & Mundhra, S. (2019). Mycobacterium tuberculosis cysteine biosynthesis genes mec+-cysO-cysM confer resistance to clofazimine. *Tuberculosis, 115*, 63-66. https://doi.org/10.1016/j.tube.2019.02.002

Burns, K. E., Baumgart, S., Dorrestein, P. C., Zhai, H., McLafferty, F. W., & Begley, T. P. (2005). Reconstitution of a new cysteine biosynthetic pathway in Mycobacterium tuberculosis. *J Am Chem Soc, 127*(33), 11602-11603. 10.1021/ja053476x

Campanini, B., Benoni, R., Bettati, S., Beck, C. M., Hayes, C. S., & Mozzarelli, A. (2015). Moonlighting O-acetylserine sulfhydrylase: new functions for an old protein *Biochimica et biophysica acta, 1854*(9), 1184-1193. 10.1016/j.bbapap.2015.02.013

Campanini, B., Pieroni, M., Raboni, S., Bettati, S., Benoni, R., Pecchini, C., . . . Mozzarelli, A. (2015). Inhibitors of the sulfur assimilation pathway in bacterial pathogens as enhancers of antibiotic therapy. *Curr Med Chem, 22*(2), 187-213. 10.2174/0929867321666141112122553

Campanini, B., Speroni, F., Salsi, E., Cook, P. F., Roderick, S. L., Huang, B., . . . Mozzarelli, A. (2005). Interaction of serine acetyltransferase with O-acetylserine sulfhydrylase active site: evidence from fluorescence spectroscopy. *Protein science : a publication of the Protein Society, 14*(8), 2115-2124. 10.1110/ps.051492805

Capel, E., Zomer, A. L., Nussbaumer, T., Bole, C., Izac, B., Frapy, E., . . . Coureuil, M. (2016). Comprehensive Identification of Meningococcal Genes and Small Noncoding RNAs Required for Host Cell Colonization. *mBio, 7*(4) 10.1128/mBio.01173-16

Chattopadhyay, A., Meier, M., Ivaninskii, S., Burkhard, P., Speroni, F., Campanini, B., . . . Cook, P. F. (2007). Structure, mechanism, and conformational dynamics of O-acetylserine sulfhydrylase from *Salmonella typhimurium*: comparison of A and B isozymes. *Biochemistry, 46*(28), 8315-8330. 10.1021/bi602603c

Chaudhuri, R. R., Allen, A. G., Owen, P. J., Shalom, G., Stone, K., Harrison, M., . . . Charles, I. G. (2009). Comprehensive identification of essential Staphylococcus aureus genes using Transposon-Mediated Differential Hybridisation (TMDH). *BMC genomics, 10*, 291-291. 10.1186/1471-2164-10-291

Chen, C., Yan, Q., Tao, M., Shi, H., Han, X., Jia, L., . . . Ma, Y. (2019). Characterization of serine acetyltransferase (CysE) from methicillin-resistant Staphylococcus aureus and inhibitory effect of two natural products on CysE. *Microbial Pathogenesis, 131*, 218-226. 10.1016/j.micpath.2019.04.002

Claus, M. T., Zocher, G. E., Maier, T. H. P., & Schulz, G. E. (2005). Structure of the O-Acetylserine Sulfhydrylase Isoenzyme CysM from Escherichia coli. *Biochemistry, 44*(24), 8620-8626. 10.1021/bi050485+

Colyer, T. E., & Kredich, N. M. (1996). In vitro characterization of constitutive CysB proteins from Salmonella typhimurium. *Mol Microbiol, 21*(2), 247-256. 10.1046/j.1365-2958.1996.6301347.x

Faraci, W. S., & Walsh, C. T. (1989). Mechanism of inactivation of alanine racemase by beta, beta, beta-trifluoroalanine. *Biochemistry, 28*(2), 431-437. 10.1021/bi00428a004

Fasnacht, M., & Polacek, N. (2021). Oxidative Stress in Bacteria and the Central Dogma of Molecular Biology. *Front. Mol. Biosci, 8*, 671037-671037. 10.3389/fmolb.2021.671037

Filutowicz, M., Wiater, A., & Hulanicka, D. (1982). Delayed inducibility of sulphite reductase in cysM mutants of Salmonella typhimurium under anaerobic conditions. *J Gen Microbiol, 128*(8), 1791-1794. 10.1099/00221287-128-8-1791

Francois, J. A., Kumaran, S., & Jez, J. M. (2006). Structural basis for interaction of O-acetylserine sulfhydrylase and serine acetyltransferase in the Arabidopsis cysteine synthase complex. *The Plant cell, 18*(12), 3647-3655. 10.1105/tpc.106.047316

Franko, N., Grammatoglou, K., Campanini, B., Costantino, G., Jirgensons, A., & Mozzarelli, A. (2018). Inhibition of O-acetylserine sulfhydrylase by

fluoroalanine derivatives. *Journal of Enzyme Inhibition and Medicinal Chemistry, 33*(1), 1343-1351. 10.1080/14756366.2018.1504040

Frávega, J., Álvarez, R., Díaz, F., Inostroza, O., Tejías, C., Rodas, P. I., . . . Gil, F. (2016). Salmonella Typhimurium exhibits fluoroquinolone resistance mediated by the accumulation of the antioxidant molecule H2S in a CysK-dependent manner. *Journal of Antimicrobial Chemotherapy, 71*(12), 3409-3415. 10.1093/jac/dkw311

Gallagher, L. A., Ramage, E., Jacobs, M. A., Kaul, R., Brittnacher, M., & Manoil, C. (2007). A comprehensive transposon mutant library of Francisella novicida, a bioweapon surrogate. *Proc Natl Acad Sci U S A, 104*(3), 1009-1014. 10.1073/pnas.0606713104

Gislason, A. S., Turner, K., Domaratzki, M., & Cardona, S. T. (2017). Comparative analysis of the Burkholderia cenocepacia K56-2 essential genome reveals cell envelope functions that are uniquely required for survival in species of the genus Burkholderia. *Microb Genom, 3*(11) 10.1099/mgen.0.000140

Gorman, J., & Shapiro, L. (2004). Structure of serine acetyltransferase from *Haemophilus influenzae Rd*. *Acta Crystallogr D Biol Crystallogr, 60*(Pt 9), 1600-1605. 10.1107/s0907444904015240

Guédon, E., & Martin-Verstraete, I. (2007). Cysteine Metabolism and Its Regulation in Bacteria. In V. F. Wendisch (Ed.), *Amino Acid Biosynthesis ~ Pathways, Regulation and Metabolic Engineering* (pp. 195-218). Berlin, Heidelberg: Springer Berlin Heidelberg.

Hampshire, T., Soneji, S., Bacon, J., James, B. W., Hinds, J., Laing, K., . . . Butcher, P. D. (2004). Stationary phase gene expression of Mycobacterium tuberculosis following a progressive nutrient depletion: a model for persistent organisms? *Tuberculosis (Edinb), 84*(3-4), 228-238. 10.1016/j.tube.2003.12.010

Hicks, J. L., & Mullholland, C. V. (2018). Cysteine biosynthesis in Neisseria species. *Microbiology, 164(12)*, 1471-1480. doi:10.1099/mic.0.000728

Hindson, V. J. (2003). Serine acetyltransferase of Escherichia coli: substrate specificity and feedback control by cysteine. *The Biochemical journal, 375*(Pt 3), 745-752. 10.1042/BJ20030429

Hindson, V. J., & Shaw, W. V. (2003). Random-Order Ternary Complex Reaction Mechanism of Serine Acetyltransferase from Escherichia coli. *Biochemistry, 42*(10), 3113-3119. 10.1021/bi0267893

Hryniewicz, M. M., & Kredich, N. M. (1994). Stoichiometry of binding of CysB to the cysJIH, cysK, and cysP promoter regions of *Salmonella typhimurium*. *Journal of Bacteriology, 176*(12), 3673-3682. 10.1128/jb.176.12.3673-3682.1994.

Huang, B., Vetting, M. W., & Roderick, S. L. (2005). The active site of O-acetylserine sulfhydrylase is the anchor point for bienzyme complex formation with serine acetyltransferase. *J Bacteriol, 187*(9), 3201-3205. 10.1128/jb.187.9.3201-3205.2005

Jean Kumar, V. U., Poyraz, O., Saxena, S., Schnell, R., Yogeeswari, P., Schneider, G., & Sriram, D. (2013). Discovery of novel inhibitors targeting the *Mycobacterium tuberculosis* O-acetylserine sulfhydrylase (CysK1) using virtual high-throughput screening. *Bioorg Med Chem Lett, 23*(5), 1182-1186. 10.1016/j.bmcl.2013.01.031

John, R. A., & Tudball, N. (1972). Evidence for induced fit of a pseudo-substrate of aspartate aminotransferase. *Eur J Biochem, 31*(1), 135-138. 10.1111/j.1432-1033.1972.tb02510.x

Johnson, C. M., Huang, B., Roderick, S. L., & Cook, P. F. (2004). Kinetic mechanism of the serine acetyltransferase from Haemophilus influenzae. *Archives of Biochemistry and Biophysics, 429*(2), 115-122. 10.1016/j.abb.2004.06.006

Joshi, P., Gupta, A., & Gupta, V. (2019). Insights into multifaceted activities of CysK for therapeutic interventions. *3 Biotech, 9*(2) 10.1007/s13205-019-1572-4

Jovanovic, M., Lilic, M., Savic, D. J., & Jovanovic, G. (2003). The LysR-type transcriptional regulator CysB controls the repression of hslJ transcription in Escherichia coli. *Microbiology (Reading), 149*(Pt 12), 3449-3459. 10.1099/mic.0.26609-0

Kant, V., Vijayakumar, S., Sahoo, G. C., Ali, V., Singh, K., Chaudhery, S. S., & Das, P. (2019). In-silico screening and validation of high-affinity tetra-peptide inhibitor of Leishmania donovani O-acetyl serine sulfhydrylase (OASS). *J Biomol Struct Dyn, 37*(2), 481-492. 10.1080/07391102.2018.1429315

Kesicki, E. A., Bailey, M. A., Ovechkina, Y., Early, J. V., Alling, T., Bowman, J., . . . Parish, T. (2016). Synthesis and Evaluation of the 2-Aminothiazoles as Anti-Tubercular Agents. *PLOS ONE, 11*(5), e0155209. 10.1371/journal.pone.0155209

Kim, Y., Zhou, M., Peterson, S., Anderson, W. F., & Joachimiak, A. (2009). Crystal Structure of Serine Acetyltransferase CysE from Yersinia pestis. 10.2210/pdb3GVD/pdb

Kredich, N. M. (1992). The molecular basis for positive regulation of cys promoters in Salmonella typhimurium and Escherichia coli. *Molecular Microbiology, 6*(19), 2747-2753. 10.1111/j.1365-2958.1992.tb01453.x

Kredich, N. M. (2008). Biosynthesis of Cysteine. *EcoSal Plus, 3*(1) 10.1128/ecosalplus.3.6.1.11

Kredich, N. M., Becker, M. A., & Tomkins, G. M. (1969). Purification and Characterization of Cysteine Synthetase, a Bifunctional Protein Complex, from Salmonella typhimurium. *Journal of Biological Chemistry, 244*(9), 2428-2439. 10.1016/s0021-9258(19)78241-6

Kredich, N. M., & Tomkins, G. M. (1966). The Enzymic Synthesis of L-Cysteine in Escherichia coli and Salmonella typhimurium. *Journal of Biological Chemistry, 241*(21), 4955-4965. 10.1016/s0021-9258(18)99657-2

Kumar, S., Kumar, N., Alam, N., & Gourinath, S. (2014). Crystal structure of serine acetyl transferase from Brucella abortus and its complex with coenzyme A. *Biochim Biophys Acta, 1844*(10), 1741-1748. 10.1016/j.bbapap.2014.07.009

Kumar, S., Raj, I., Nagpal, I., Subbarao, N., & Gourinath, S. (2011). Structural and Biochemical Studies of Serine Acetyltransferase Reveal Why the Parasite Entamoeba histolytica Cannot Form a Cysteine Synthase Complex. *Journal of Biological Chemistry, 286*(14), 12533-12541. 10.1074/jbc.m110.197376

Le Faou, A. (1984). Sulphur nutrition and metabolism in various species of Neisseria. *Annales de l'Institut Pasteur / Microbiologie, 135B*, 3-11. 10.1016/S0769-2609(84)80037-X

Liang, J., Han, Q., Tan, Y., Ding, H., & Li, J. (2019). Current Advances on Structure-Function Relationships of Pyridoxal 5′-Phosphate-Dependent Enzymes. *Frontiers in Molecular Biosciences, 6* 10.3389/fmolb.2019.00004

Lithgow, J. K., Hayhurst, E. J., Cohen, G., Aharonowitz, Y., & Foster, S. J. (2004). Role of a cysteine synthase in Staphylococcus aureus. *J Bacteriol, 186*(6), 1579-1590. 10.1128/jb.186.6.1579-1590.2004

Lochowska, A., Iwanicka-Nowicka, R., Plochocka, D., & Hryniewicz, M. M. (2001). Functional dissection of the LysR-type CysB transcriptional regulator. Regions important for DNA binding, inducer response, oligomerization, and positive control. *J Biol Chem, 276*(3), 2098-2107. 10.1074/jbc.M007192200

Magalhães, J., Franko, N., Raboni, S., Annunziato, G., Tammela, P., Bruno, A., . . . Costantino, G. (2021). Discovery of Substituted (2-Aminooxazol-4-yl)Isoxazole-3-carboxylic Acids as Inhibitors of Bacterial Serine Acetyltransferase in the Quest for Novel Potential Antibacterial Adjuvants. *Pharmaceuticals (Basel, Switzerland), 14*(2), 174. 10.3390/ph14020174

Magalhães, J., Franko, N., Raboni, S., Annunziato, G., Tammela, P., Bruno, A., . . . Costantino, G. (2020). Inhibition of Nonessential Bacterial Targets: Discovery of a Novel Serine O-Acetyltransferase Inhibitor. *ACS Med. Chem. Lett, 11*(5), 790-797. 10.1021/acsmedchemlett.9b00627

Mandal, R. K., Jiang, T., & Kwon, Y. M. (2017). Essential genome of Campylobacter jejuni. *BMC Genomics, 18*(1), 616. 10.1186/s12864-017-4032-8

Marchetti, M., De Angelis, F. S., Annunziato, G., Costantino, G., Pieroni, M., Ronda, L., . . . Bettati, S. (2021). A Competitive O-Acetylserine Sulfhydrylase Inhibitor Modulates the Formation of Cysteine Synthase Complex. *Catalysts, 11*(6), 700. 10.3390/catal11060700

Meissner, A., Boshoff, H. I., Vasan, M., Duckworth, B. P., Barry, C. E., 3rd, & Aldrich, C. C. (2013). Structure-activity relationships of 2-aminothiazoles effective against Mycobacterium tuberculosis. *Bioorg Med Chem, 21*(21), 6385-6397. 10.1016/j.bmc.2013.08.048

Mino, K., Hiraoka, K., Imamura, K., Sakiyama, T., Eisaki, N., Matsuyama, A., & Nakanishi, K. (2000). Characteristics of Serine Acetyltransferase fromEscherichia coliDeleting Different Lengths of Amino Acid Residues from the C-Terminus. *Bioscience, Biotechnology, and Biochemistry, 64*(9), 1874-1880. 10.1271/bbb.64.1874

Mino, K., & Ishikawa, K. (2003). A novelO-phospho-L-serine sulfhydrylation reaction catalyzed byO-acetylserine sulfhydrylase fromAeropyrum pernixK1. *FEBS Letters, 551*(1-3), 133-138. 10.1016/s0014-5793(03)00913-x

Mino, K., Yamanoue, T., Sakiyama, T., Eisaki, N., Matsuyama, A., & Nakanishi, K. (2000). Effects of bienzyme complex formation of cysteine synthetase from *Escherichia coli* on some properties and kinetics. *Biosci Biotechnol Biochem, 64*(8), 1628-1640. 10.1271/bbb.64.1628

Momitani, K., Shiba, T., Sawa, T., Ono, K., & Hurukawa, S. (2022). Crystal structure of serine acetyltransferase from Salmonella typhimurium. 10.2210/pdb7E3Y/pdb

Moule, M. G., Hemsley, C. M., Seet, Q., Guerra-Assunção, J. A., Lim, J., Sarkar-Tyson, M., . . . Wren, B. W. (2014). Genome-wide saturation mutagenesis of Burkholderia pseudomallei K96243 predicts essential genes and novel targets for antimicrobial development. *mBio, 5*(1), e00926-00913. 10.1128/mBio.00926-13

Muir, A., Gurung, I., Cehovin, A., Bazin, A., Vallenet, D., & Pelicic, V. (2020). Construction of a complete set of Neisseria meningitidis mutants and its use

for the phenotypic profiling of this human pathogen. *Nature Communications, 11*(1), 5541. 10.1038/s41467-020-19347-y

Neuwald, A. F., Krishnan, B. R., Brikun, I., Kulakauskas, S., Suziedelis, K., Tomcsanyi, T., . . . Berg, D. E. (1992). cysQ, a gene needed for cysteine synthesis in Escherichia coli K-12 only during aerobic growth. *Journal of Bacteriology, 174*(2), 415-425. doi:10.1128/jb.174.2.415-425.1992

Noji, M., Takagi, Y., Kimura, N., Inoue, K., Saito, M., Horikoshi, M., . . . Saito, K. (2001). Serine Acetyltransferase Involved in Cysteine Biosynthesis from Spinach: Molecular Cloning, Characterization and Expression Analysis of cDNA Encoding a Plastidic Isoform. *Plant and Cell Physiology, 42*(6), 627-634. 10.1093/pcp/pce078

Oldham, K. E. A., Prentice, E. J., Summers, E. L., & Hicks, J. L. (2022a). Serine acetyltransferase from Neisseria gonorrhoeae; structural and biochemical basis of inhibition. *Biochemical Journal, 479*(1), 57-74. 10.1042/BCJ20210564

Oldham, K. E. A., Prentice, E. J., Summers, E. L., & Hicks, J. L. (2022b). Serine acetyltransferase from Neisseria gonorrhoeae; structural and biochemical basis of inhibition. *Biochem. J., 479*(1), 57-74. 10.1042/bcj20210564

Olsen, L. R., Huang, B., Vetting, M. W., & Roderick, S. L. (2004). Structure of serine acetyltransferase in complexes with CoA and its cysteine feedback inhibitor. *Biochemistry, 43*(20), 6013-6019. 10.1021/bi0358521

Oppezzo, O. J., & Antón, D. N. (1995). Involvement of cysB and cysE genes in the sensitivity of Salmonella typhimurium to mecillinam. *J Bacteriol, 177*(15), 4524-4527. 10.1128/jb.177.15.4524-4527.1995

Park, S., & Imlay, J. A. (2003). High levels of intracellular cysteine promote oxidative DNA damage by driving the fenton reaction. *Journal of bacteriology, 185*(6), 1942-1950. 10.1128/JB.185.6.1942-1950.2003

Passera, E., Campanini, B., Rossi, F., Casazza, V., Rizzi, M., Pellicciari, R., & Mozzarelli, A. (2011). Human kynurenine aminotransferase II – reactivity with substrates and inhibitors. *The FEBS Journal, 278*(11), 1882-1900. 10.1111/j.1742-4658.2011.08106.x

Pawar, A., Jha, P., Chopra, M., Chaudhry, U., & Saluja, D. (2020). Screening of natural compounds that targets glutamate racemase of Mycobacterium tuberculosis reveals the anti-tubercular potential of flavonoids. *Scientific Reports, 10*(1), 949. 10.1038/s41598-020-57658-8

Phillips, R. S., & Dua, R. K. (1992). Indole protects tryptophan indole-lyase, but not tryptophan synthase, from inactivation by trifluoroalanine. *Arch Biochem Biophys, 296*(2), 489-496. 10.1016/0003-9861(92)90602-s

Pieroni, M., Annunziato, G., Beato, C., Wouters, R., Benoni, R., Campanini, B., . . . Costantino, G. (2016). Rational Design, Synthesis, and Preliminary Structure-Activity Relationships of α-Substituted-2-Phenylcyclopropane Carboxylic Acids as Inhibitors of Salmonella typhimurium O-Acetylserine Sulfhydrylase. *J Med Chem, 59*(6), 2567-2578. 10.1021/acs.jmedchem.5b01775

Poulin, R., Lu, L., Ackermann, B., Bey, P., & Pegg, A. E. (1992). Mechanism of the irreversible inactivation of mouse ornithine decarboxylase by alpha-difluoromethylornithine. Characterization of sequences at the inhibitor and coenzyme binding sites. *J Biol Chem, 267*(1), 150-158. 10.1016/S0021-9258(18)48472-4

Poyraz, O., Jeankumar, V. U., Saxena, S., Schnell, R., Haraldsson, M., Yogeeswari, P., . . . Schneider, G. (2013). Structure-guided design of novel thiazolidine

inhibitors of O-acetyl serine sulfhydrylase from *Mycobacterium tuberculosis*. *J Med Chem, 56*(16), 6457-6466. 10.1021/jm400710k

Pye, V. E., Tingey, A. P., Robson, R. L., & Moody, P. C. E. (2004). The Structure and Mechanism of Serine Acetyltransferase from Escherichia coli. *Journal of Biological Chemistry, 279*(39), 40729-40736. 10.1074/jbc.m403751200

Rabeh, W. M., & Cook, P. F. (2004). Structure and Mechanism of O-Acetylserine Sulfhydrylase. *Journal of Biological Chemistry, 279*(26), 26803-26806. 10.1074/jbc.R400001200

Raetz, C. R., & Roderick, S. L. (1995). A left-handed parallel beta helix in the structure of UDP-N-acetylglucosamine acyltransferase. *Science, 270*(5238), 997-1000. 10.1126/science.270.5238.997

Raj, I., Kumar, S., & Gourinath, S. (2012). The narrow active-site cleft of O-acetylserine sulfhydrylase from Leishmania donovani allows complex formation with serine acetyltransferases with a range of C-terminal sequences. *Acta Crystallogr D Biol Crystallogr, 68*(Pt 8), 909-919. 10.1107/s0907444912016459

Rakonjac, J., Milic, M., & Savic, D. J. (1991). cysB and cysE mutants of Escherichia coli K12 show increased resistance to novobiocin. *Mol Gen Genet, 228*(1-2), 307-311. 10.1007/bf00282481

Raman, K., Yeturu, K., & Chandra, N. (2008). targetTB: a target identification pipeline for Mycobacterium tuberculosis through an interactome, reactome and genome-scale structural analysis. *BMC Syst Biol, 2*, 109. 10.1186/1752-0509-2-109

Ramírez, A., Castañeda, M., Xiqui, M. L., Sosa, A., & Baca, B. E. (2006). Identification, cloning and characterization of cysK, the gene encoding O-acetylserine (thiol)-lyase from Azospirillum brasilense, which is involved in tellurite resistance. *FEMS Microbiology Letters, 261*(2), 272-279. 10.1111/j.1574-6968.2006.00369.x

Reichelt, A., & Martin, S. F. (2006). Synthesis and Properties of Cyclopropane-Derived Peptidomimetics. *Accounts of Chemical Research, 39*(7), 433-442. 10.1021/ar030255s

Remmele, C. W., Xian, Y., Albrecht, M., Faulstich, M., Fraunholz, M., Heinrichs, E., . . . Rudel, T. (2014). Transcriptional landscape and essential genes of *Neisseria gonorrhoeae*. *Nucleic Acids Res., 42*(16), 10579-10595. 10.1093/nar/gku762

Rengarajan, J., Bloom, B. R., & Rubin, E. J. (2005). Genome-wide requirements for *Mycobacterium tuberculosis* adaptation and survival in macrophages. *Proceedings of the National Academy of Sciences, 102*(23), 8327-8332. doi:10.1073/pnas.0503272102

Roop, R. M., Gaines, J. M., Anderson, E. S., Caswell, C. C., & Martin, D. W. (2009). Survival of the fittest: how Brucella strains adapt to their intracellular niche in the host. *Medical Microbiology and Immunology, 198*(4), 221-238. 10.1007/s00430-009-0123-8

Rosa, B., Dickinson, E. R., Marchetti, M., Campanini, B., Pioselli, B., Bettati, S., & Rand, K. D. (2021). Revealing the Dynamic Allosteric Changes Required for Formation of the Cysteine Synthase Complex by Hydrogen-Deuterium Exchange MS. *Molecular & Cellular Proteomics, 20*, 100098. 10.1016/j.mcpro.2021.100098

Rosa, B., Marchetti, M., Paredi, G., Amenitsch, H., Franko, N., Benoni, R., . . . Bettati, S. (2019). Combination of SAXS and Protein Painting Discloses the Three-Dimensional Organization of the Bacterial Cysteine Synthase

Complex, a Potential Target for Enhancers of Antibiotic Action. *International Journal of Molecular Sciences, 20*(20), 5219. 10.3390/ijms20205219

Salsi, E., Bayden, A. S., Spyrakis, F., Amadasi, A., Campanini, B., Bettati, S., . . . Mozzarelli, A. (2010). Design of O-Acetylserine Sulfhydrylase Inhibitors by Mimicking Nature. *Journal of Medicinal Chemistry, 53*(1), 345-356. 10.1021/jm901325e

Sassetti, C. M., & Rubin, E. J. (2003). Genetic requirements for mycobacterial survival during infection. *Proc Natl Acad Sci U S A, 100*(22), 12989-12994. 10.1073/pnas.2134250100

Schnappinger , D., Ehrt , S., Voskuil , M. I., Liu , Y., Mangan , J. A., Monahan , I. M., . . . Schoolnik , G. K. (2003). Transcriptional Adaptation of Mycobacterium tuberculosis within Macrophages : Insights into the Phagosomal Environment. *Journal of Experimental Medicine, 198*(5), 693-704. 10.1084/jem.20030846

Schnell, R., Oehlmann, W., Singh, M., & Schneider, G. (2007). Structural insights into catalysis and inhibition of O-acetylserine sulfhydrylase from *Mycobacterium tuberculosis*. Crystal structures of the enzyme alpha-aminoacrylate intermediate and an enzyme-inhibitor complex. *J Biol Chem, 282*(32), 23473-23481. 10.1074/jbc.M703518200

Shatalin, K., Shatalina, E., Mironov, A., & Nudler, E. (2011). $H_2S$: A Universal Defense Against Antibiotics in Bacteria. *Science, 334*(6058), 986-990. doi:10.1126/science.1209855

Shukla, H., Kumar, V., Singh, A. K., Rastogi, S., Khan, S. R., Siddiqi, M. I., . . . Akhtar, M. S. (2015). Isocitrate lyase of Mycobacterium tuberculosis is inhibited by quercetin through binding at N-terminus. *Int J Biol Macromol, 78*, 137-141. 10.1016/j.ijbiomac.2015.04.005

Silverman, R. B. (1995). Mechanism-based enzyme inactivators *Methods in Enzymology* (Vol. 249, pp. 240-283): Academic Press.

Silverman, R. B., & Abeles, R. H. (1976). Inactivation of pyridoxal phosphate dependent enzymes by mono- and polyhaloalanines. *Biochemistry, 15*(21), 4718-4723. 10.1021/bi00666a028

Silverman, R. B., & Abeles, R. H. (1977). Mechanism of inactivation of gamma-cystathionase by beta,beta,beta-trifluoroalanine. *Biochemistry, 16*(25), 5515-5520. 10.1021/bi00644a019

Singh, P., Brooks, J. F., Ray, V. A., Mandel, M. J., & Visick, K. L. (2015). CysK Plays a Role in Biofilm Formation and Colonization by Vibrio fischeri. *Appl. Environ. Microbiol., 81*(15), 5223-5234. 10.1128/aem.00157-15

Spyrakis, F., Felici, P., Bayden, A. S., Salsi, E., Miggiano, R., Kellogg, G. E., . . . Campanini, B. (2013). Fine tuning of the active site modulates specificity in the interaction of O-acetylserine sulfhydrylase isozymes with serine acetyltransferase. *Biochim Biophys Acta, 1834*(1), 169-181. 10.1016/j.bbapap.2012.09.009

Spyrakis, F., Singh, R., Cozzini, P., Campanini, B., Salsi, E., Felici, P., . . . Mozzarelli, A. (2013). Isozyme-Specific Ligands for O-acetylserine sulfhydrylase, a Novel Antibiotic Target. *PLOS ONE, 8*(10), e77558. 10.1371/journal.pone.0077558

Stipanuk, M. H., Dominy, J. E., Lee, J.-I., & Coloso, R. M. (2006). Mammalian Cysteine Metabolism: New Insights into Regulation of Cysteine Metabolism. *The Journal of Nutrition, 136*(6), 1652S-1659S. 10.1093/jn/136.6.1652s

Sturgill, G., Toutain, C. M., Komperda, J., O'Toole, G. A., & Rather, P. N. (2004). Role of CysE in production of an extracellular signaling molecule in Providencia stuartii and Escherichia coli: loss of CysE enhances biofilm formation in Escherichia coli. *Journal of bacteriology, 186*(22), 7610-7617. 10.1128/JB.186.22.7610-7617.2004

Tai, C. H., Burkhard, P., Gani, D., Jenn, T., Johnson, C., & Cook, P. F. (2001). Characterization of the allosteric anion-binding site of O-acetylserine sulfhydrylase. *Biochemistry, 40*(25), 7446-7452. 10.1021/bi015511s

Tai, C. H., Nalabolu, S. R., Jacobson, T. M., Minter, D. E., & Cook, P. F. (1993). Kinetic mechanisms of the A and B isozymes of O-acetylserine sulfhydrylase from *Salmonella typhimurium* LT-2 using the natural and alternative reactants. *Biochemistry, 32*(25), 6433-6442. 10.1021/bi00076a017.

Takumi, K., & Nonaka, G. (2016). Bacterial Cysteine-Inducible Cysteine Resistance Systems. *Journal of Bacteriology, 198*(9), 1384-1392. 10.1128/jb.01039-15

Turnbull, A. L., & Surette, M. G. (2008). L-Cysteine is required for induced antibiotic resistance in actively swarming *Salmonella enterica* serovar Typhimurium. *Microbiology, 154*(Pt 11), 3410-3419. 10.1099/mic.0.2008/020347-0

Turnbull, A. L., & Surette, M. G. (2010). Cysteine biosynthesis, oxidative stress and antibiotic resistance in *Salmonella typhimurium*. *Res Microbiol, 161*(8), 643-650. 10.1016/j.resmic.2010.06.004

Tysoe, C., & Withers, G. S. (2014). Fluorinated Mechanism-Based Inhibitors: Common Themes and Recent Developments. *Current Topics in Medicinal Chemistry, 14*(7), 865-874. 10.2174/1568026614666140202204602

Ulusu, N. N. (2015). Evolution of Enzyme Kinetic Mechanisms. *Journal of Molecular Evolution, 80*(5-6), 251-257. 10.1007/s00239-015-9681-0

Varesio, L. M., Fiebig, A., & Crosson, S. (2021). Brucella ovis Cysteine Biosynthesis Contributes to Peroxide Stress Survival and Fitness in the Intracellular Niche. *Infect Immun, 89*(6) 10.1128/iai.00808-20

Vásquez, C. C., Saavedra, C. P., Loyola, C. A., Araya, M. A., & Pichuantes, S. (2001). The product of the cysK gene of Bacillus stearothermophilus V mediates potassium tellurite resistance in Escherichia coli. *Curr Microbiol, 43*(6), 418-423. 10.1007/s002840010331

Verma, D., Gupta, S., Saxena, R., Kaur, P., R, R., Srivastava, S., & Gupta, V. (2020). Allosteric inhibition and kinetic characterization of Klebsiella pneumoniae CysE: An emerging drug target. *Int J Biol Macromol, 151*, 1240-1249. 10.1016/j.ijbiomac.2019.10.170

Voskuil, M. I., Bartek, I. L., Visconti, K., & Schoolnik, G. K. (2011). The response of mycobacterium tuberculosis to reactive oxygen and nitrogen species. *Front Microbiol, 2*, 105. 10.3389/fmicb.2011.00105

Voskuil, M. I., Visconti, K. C., & Schoolnik, G. K. (2004). Mycobacterium tuberculosis gene expression during adaptation to stationary phase and low-oxygen dormancy. *Tuberculosis (Edinb), 84*(3-4), 218-227. 10.1016/j.tube.2004.02.003

Wang, E. A., & Walsh, C. (1981). Characteristics of beta, beta-difluoroalanine and beta, beta, beta -trifluoroalanine as suicide substrates for Escherichia coli B alanine racemase. *Biochemistry, 20*(26), 7539-7546. 10.1021/bi00529a032

Wang, T., & Leyh, T. S. (2012). Three-stage Assembly of the Cysteine Synthase Complex from Escherichia coli. *Journal of Biological Chemistry, 287*(6), 4360-4367. 10.1074/jbc.m111.288423

Warr, A. R., Hubbard, T. P., Munera, D., Blondel, C. J., Abel zur Wiesch, P., Abel, S., . . . Waldor, M. K. (2019). Transposon-insertion sequencing screens unveil requirements for EHEC growth and intestinal colonization. *PLOS Pathogens, 15*(8), e1007652. 10.1371/journal.ppat.1007652

Wong, Y. C., Abd El Ghany, M., Naeem, R., Lee, K. W., Tan, Y. C., Pain, A., & Nathan, S. (2016). Candidate Essential Genes in Burkholderia cenocepacia J2315 Identified by Genome-Wide TraDIS. *Front Microbiol, 7*, 1288. 10.3389/fmicb.2016.01288

Yi, H., Dey, S., Kumaran, S., Lee, S. G., Krishnan, H. B., & Jez, J. M. (2013). Structure of Soybean Serine Acetyltransferase and Formation of the Cysteine Regulatory Complex as a Molecular Chaperone. *Journal of Biological Chemistry, 288*(51), 36463-36472. 10.1074/jbc.m113.527143

Zhao, C., Kumada, Y., Imanaka, H., Imamura, K., & Nakanishi, K. (2006). Cloning, overexpression, purification, and characterization of O-acetylserine sulfhydrylase-B from Escherichia coli. *Protein Expression and Purification, 47*(2), 607-613. https://doi.org/10.1016/j.pep.2006.01.002

Zhao, C., Moriga, Y., Feng, B., Kumada, Y., Imanaka, H., Imamura, K., & Nakanishi, K. (2006). On the interaction site of serine acetyltransferase in the cysteine synthase complex from Escherichia coli. *Biochemical and Biophysical Research Communications, 341*(4), 911-916. https://doi.org/10.1016/j.bbrc.2006.01.054

# Chapter Three: Identification of inhibitors of *O*-acetylserine sulfhydrylase A from *Neisseria gonorrhoeae*

## 3.1 Preface

Antimicrobial resistance (AMR) poses a significant and growing threat to public health, necessitating novel approaches to antibiotic development. *Neisseria gonorrhoeae* is one such pathogen, now classified as a high priority pathogen due to its increasing resistance to all current front-line antibiotics (WHO, 2024). Targeting the central pathway to bacterial sulfur metabolism, *de novo* L-cysteine biosynthesis is a promising new avenue of research. Given the essential role of L-cysteine in oxidative stress mitigation and bacterial survival, inhibiting key enzymes in this pathway, such as the final step of the pathway *O*-acetylserine sulfhydrylase A (CysK), presents a viable strategy for developing new antimicrobial agents and adjuvants. This chapter builds upon the previous review chapter on strategies for targeting L-cysteine biosynthesis for combatting antimicrobial resistance by investigating one such strategy. In this chapter we have conducted structural analysis of the NgCysK crystal structure (using X-ray crystallography), developed a computational NgCysK homology model with PLP bound, performed structure-based virtual inhibitor screening of commercial libraries, ordered and evaluated hit compounds identified *in silico*, and have evaluated these compounds in NgCysK via *in vitro* analysis, with the most potent compound being promising for downstream optimisation.

The work presented in this chapter is shown in a publication format as a manuscript prepared for submission to the journal; Computational and Structural Biotechnology Journal. Included in this chapter is a Future Directions section (3.8), which is not part of the manuscript, but has been included to discuss the future work directly related to this project; these results will be included in future publications.

Supplementary information is available in Appendix A. Citation for this work is as follows:

**McGarvie, J.**, Warrender, A. K., Oldham, K. E. A., Jiao, W., & Hicks, J. L. (2025). Identification of inhibitors of *O*-acetylserine sulfhydrylase A from *Neisseria gonorrhoeae.*

## 3.2 Author contributions

I led the experimental work for this research, as first author, which involved enzyme purification, robot screen crystallisation, X-ray crystallography structural analysis, optimisation of inhibitor screening assays, inhibitor compound *in vitro* screening, analysis of compound 5 interactions with NgCysK. Additionally, I prepared all figures as well as drafting and editing this manuscript. Wanting Jiao generated a homology model of NgCysK with PLP bound, conducted virtual inhibitor screening, including preparation and screening of the ligand libraries against the NgCysK homology model, and manuscript drafting. Annmaree Warrender laid the fine screen for the NgCysK crystal. Keely Oldham collected and integrated the crystal structure files. Joanna Hicks conceptualised the research, provided funding for the project, and was involved in manuscript drafting and editing. The authorship contribution form can be found in Appendix C.

## 3.3 Abstract

Antimicrobial resistance (AMR) is an escalating global health crisis and is considered one of the top 10 global public health threats. *Neisseria gonorrhoeae*, the causative agent of gonorrhoea is classified as a high-priority pathogen due to its extensive drug resistance. Given its essential role in mitigating oxidative stress and its absence in humans, targeting *de novo* biosynthesis of L-cysteine is a promising avenue for design of novel antimicrobial and adjuvants. This study investigates the inhibition of the cysteine biosynthesis enzyme, O-acetylserine sulfhydrylase (CysK), from *N. gonorrhoeae* (NgCysK) using a structure-based virtual screening approach to identify potential inhibitors.

The crystal structure of NgCysK was solved to a 2.49 Å resolution, revealing conserved active site features and indicating alternate conformations for each monomer, indicative of positive cooperativity. A homology model incorporating pyridoxal 5'-phosphate (PLP) was generated to facilitate in silico screening. A library of ~10.5 million drug-like compounds from the ZINC15 database was computationally screened, leading to the selection of 42 candidate inhibitors. Among the experimentally tested compounds, one inhibitor (compound 5) demonstrated a dose-dependent inhibition of NgCysK with an $IC_{50}$ of 253.5 ± 56.25 μM. Docking and molecular dynamics simulations revealed that compound 5 forms hydrogen bonds with key active site residues, supporting its potential as an antimicrobial adjuvant.

This study highlights the efficacy of virtual screening in identifying inhibitors targeting NgCysK, reinforcing the viability of cysteine biosynthesis as an antimicrobial target. Given the critical role of L-cysteine in bacterial pathogenesis and oxidative stress management, further optimization of compound 5 may yield more potent inhibitors with clinical applicability against drug-resistant *N. gonorrhoeae* and related pathogens.

## 3.4 Introduction

Antimicrobial resistance also called the silent pandemic is a growing health crisis and is considered one of the top 10 global public health threats. Antibiotic resistant bacteria cause a range of infections that threaten people's health and wellbeing, including sexually transmitted infections. For example, the extensively drug-resistant bacterium *Neisseria gonorrhoeae* (gonococcus) is classified as a high priority pathogen by the World Health Organisation (WHO, 2024) for the research and development of public health initiatives, vaccines and new antimicrobial therapies. Annually there are approximately 87 million gonorrhoea infections globally (Unemo et al., 2019), incidence is rising, and extensive drug resistance further complicates treatment.

To combat rising antimicrobial resistance new antibiotics are needed, alongside alternative strategies such as targeting non-essential targets that enhance susceptibility to existing antibiotics and/or immune clearance. Targeting metabolic pathways is emerging as a promising avenue for the development of new antibiotics and/or antibiotic enhancers (Carfrae & Brown, 2023; Murima, John, & Pethe, 2014). Targeting the synthesis of the key amino acid L-cysteine is one of these avenues (Campanini et al., 2015; Hicks, Oldham, McGarvie, & Walker, 2022). Many pathogens spend at least part of their lifecycle in the challenging host environment, where survival relies on molecules with detoxifying capabilities and reducing power such as thiamine, Fe-S clusters, thioredoxin, glutathione and biotin. These sulfur containing molecules rely on cysteine for their synthesis. Accordingly inhibition of cysteine synthesis disrupts the pathogens ability to establish long term infection and overcome oxidative stress from the host (Abd El-Aleam, George, Georgey, & Abdel-Rahman, 2021; Brunner et al., 2016; Brunner et al., 2017; Campanini et al., 2015). Cysteine metabolism is a promising drug target in bacterial pathogens including *Salmonella enterica* serovar Typhimurium (Becker & Tomkins, 1969; Turnbull & Surette, 2008; Turnbull & Surette, 2010) and *Mycobacterium tuberculosis* (Brunner et al., 2016; Brunner et al., 2017; Burns-Huang & Mundhra, 2019). Inhibition of cysteine biosynthesis has also been associated with a dysregulated oxidative stress response, enhancing the antimicrobial activity of existing antibiotics (Campanini et al., 2015; Turnbull & Surette, 2008; Turnbull & Surette, 2010).

Cysteine is synthesised via a two-step pathway consisting of two enzymes; serine acetyltransferase (SAT/CysE EC 2.3.1.30) and O-acetylserine sulfhydrylase (OASS-A/OASS-B; CysK/CysM EC 4.2.99.8). CysE catalyses the acetylation of L-serine using acetyl coenzyme A (acetyl-CoA) to produce O-acetylserine which is subsequently condensed with sulfide by CysK or thiosulfate in the case of CysM to form L-cysteine. The synthesis of L-cysteine is regulated by feedback inhibition of CysE by L-cysteine, transcriptional regulation by the transcription factor CysB and formation of the cysteine synthase complex. The reversible cysteine synthase complex is formed by the association of two CysK dimers with one CysE hexamer, where the C-terminal tail of CysE inserts into the active site of CysK to drastically reduce its activity, while activity of CysE is enhanced (Abd El-Aleam et al., 2021; Benoni et al., 2017; Kumaran, Yi, Krishnan, & Jez, 2009; Rosa et al., 2019; Wang & Leyh, 2012). The complex acts to regulate sulfur flux within the bacterium and is dissociated by high concentrations of the pathway intermediate O-acetylserine.

Given the absence of the biosynthetic machinery for the *de novo* synthesis of cysteine in mammals we propose that targeting the cysteine synthesis enzymes CysE and CysK within the gonococcus is a good strategy for the development of new antimicrobials and antibiotic enhancers respectively. CysE is an essential gene in the gonococcus (Remmele et al., 2014), even in the presence of cysteine, whereas CysK is not essential but its deletion in the closely related *Neisseria meningitidis* has a severe effect on bacterial fitness (Capel et al., 2016; Turnbull & Surette, 2010). We have demonstrated that despite the absence of sulfate reduction pathway in the gonococcus (that provides sulfide for the synthesis of cysteine) (Hicks & Mullholland, 2018) CysK from *N. gonorrhoeae* (NgCysK) is a functional enzyme with kinetic parameters similar to those of CysK homologues from other bacteria (McGarvie, Oldham, Warrender, Prentice, & Hicks, 2025). Additionally, we have shown that CysK from *N. gonorrhoeae* does not form the cysteine synthase complex (McGarvie et al., 2025) which will likely alter sulfur flux within the bacterium. A common strategy in developing inhibitors to CysK enzymes is designing peptide inhibitors that mimic the C-terminal tail of CysE to inhibit the enzyme (Bruno, Amori, & Costantino, 2013; Kant et al., 2019; E. Salsi et al., 2010). However, given that the CysE and CysK enzymes from *N. gonorrhoeae* do not form the cysteine synthase complex we employed a structure based virtual screening

approach. Here we present the structure of NgCysK and the computational screening of compound libraries to identify potential CysK inhibitors whose scaffold can be used for the development of more potent inhibitors.

## 3.5 Materials and methods

### 3.5.1 Cloning of Neisseria gonorrhoeae *cysK* for expression in Escherichia coli

The *Neisseria gonorrhoeae cysK* gene, NGO_0340, was cloned as in (McGarvie et al., 2025). Briefly a synthetic *E. coli* codon optimised *cysK* gene was cloned into expression vector pET28b-PstI for expression with a C-terminal hexahistidine-tag, between PstI and XhoI restriction sites. The *cysK* pET28b plasmid was then transformed into *E. coli* BL21 (DE3) for protein expression.

### 3.5.2 NgCysK expression, purification and crystallisation

*Ng*CysK was expressed and purified as in (McGarvie et al., 2025) for inhibitor screening assays. *Ng*CysK protein for crystallisation was expressed and purified as per (McGarvie et al., 2025) with minor modifications. PLP was not added to the enzyme at any stage during this purification for crystallisation. CysK pellets were resuspended in lysis buffer (50 mM Tris pH 8.0, 200 mM NaCl, 20 mM imidazole). The pre-equilibrated HisTrap™ column (GE Healthcare) was washed with 20 ml lysis buffer before the elution of CysK using a 50% gradient over 25 ml (50 mM Tris pH 8.0, 200 mM NaCl, 1 M imidazole). IMAC-purified CysK was concentrated at 15 °C using an Amicon® Ultra-15 Centrifugal Filter Units (10 kDa molecular weight cutoff) to a final volume of 5 ml.

Initial crystals were grown by vapor diffusion using CrystalHT™-HR2-130 crystallisation screen (Hampton Research), dispensed into a low profile 96-2 well Intelli Plate (Hampton Research) using a Mosquito crystallisation robot (TTP LabTech Ltd). Sitting drops were comprised of a 1:1 ratio (100 nl:100 nl) of reservoir solution and concentrated protein (40 $mg.ml^{-1}$ of purified NgCysK) with 100 µl in the reservoir well. Crystals for diffraction were grown by hanging drop vapor diffusion at 18°C in 0.1 M HEPES sodium, pH 7.5, 2% polyethylene glycol 400 (v/v), 2.0 M Ammonium sulphate 28% (v/v). Drop composition consisted of a 1 : 1 mix (1 µl:1 µl) of reservoir and protein with 500 µl in the reservoir well. For

data collection, all crystals were transferred to a cryo-protectant solution, consisting of crystallisation solution with 15% (v/v) glycerol, prior to snap-freezing in liquid nitrogen.

### 3.5.3 Data collection, indexing, integrating and scaling

X-ray diffraction data was collected at the Australian Synchrotron (Melbourne, Victoria) on the MX2 beamline (McPhillips et al., 2002), equipped with an EIGER x 16M detector (Dectris, Switzerland). The NgCysK diffraction images were indexed, integrated and scaled, using XDS (Kabsch, 2010). Datasets were scaled together using XDS (Kabsch, 2010) and reflections merged using AIMLESS (Evans & Murshudov, 2013) from the CCP4 suite (Winn et al., 2011). Data quality was assessed through AIMLESS (Evans & Murshudov, 2013) and visual inspection of diffraction images using ALBULA (Dectris). FreeR flag dataset (5% of dataset reflections not to be used in refinement and used to compute $R_{free}$) was generated in AIMLESS (Evans & Murshudov, 2013).

#### 3.5.3.1 Indexing, integration and scaling

Datasets 0016 and 0017 were the best of three datasets obtained from the crystal diffraction. Unit cell dimensions of 0017 were changed to match 0016 and the space group changed from sg 19 ($P2_12_12_1$) to sg 4 ($P2_1$) via rerun of XDS (Kabsch, 2010). The original space group was found to be incorrect as the resulting model had unexpectedly high $R_{work}$ and $R_{free}$ values. Datasets 0016 and 0017 were scaled together using XDS (Kabsch, 2010) and reflections merged using AIMLESS (Evans & Murshudov, 2013) from the CCP4 suite (Winn et al., 2011). Data quality was assessed through AIMLESS (Evans & Murshudov, 2013). The total number of monomers present in the asymmetric unit was determined by calculating the solvent content using the Matthew's coefficient programme (Matthews, 1968), as a part of the CCP4 program suite (Winn et al., 2011). The R free flag dataset was generated in AIMLESS (Evans & Murshudov, 2013). Data was analysed for evidence of twinning and translational non-crystallographic symmetry (tNCS) in AIMLESS from the CCP4 suite (Evans & Murshudov, 2013; Winn et al., 2011) and *phenix.xtriage* from the PHENIX suite (Adams et al., 2010).

#### 3.5.3.2 Structure building and refinement

The NgCysK structure was solved using molecular replacement, with the CysK structure from *Mycobacterium tuberculosis* (3ZEI) retrieved from the protein data bank (PDB). A single monomer was extracted from this file in PyMOL (The PyMOL Molecular Graphics System, Version 2.3.2 Schrödinger, LLC) and water and ligands were removed. This *M. tuberculosis* monomer was used as the search model in molecular replacement carried out using *phenix.phaser* (McCoy et al., 2007) from the PHENIX suite (Adams et al., 2010). The model was initially built and refined using the programme *phenix.autobuild* (Terwilliger et al., 2008) from the PHENIX suite (Adams et al., 2010). The resulting structure was further built and refined manually using COOT (Emsley & Cowtan, 2004). For manual building, the 2Fo-Fc and Fo-Fc electron density maps, were set to 1σ and 3σ, respectively. Mobile sidechains lacking supported density were removed from models. Translation-liberation-screw (TLS) was carried out in the late stages of model refinement using TLS groups determined by *phenix.refine* (Terwilliger et al., 2008). After each round of structure manipulation, *phenix.refine* and *phenix.autobuild* were used to run rounds of real-space refinement (Terwilliger et al., 2008).

#### 3.5.3.3 Ligand fitting and refinement

The structures were prepared for ligand fitting through building and refinement of the protein structure, and addition of waters using *phenix.refine* (Terwilliger et al., 2008). CheckMyBlob was used to search for potential ligands in unmodelled density (Kowiel et al., 2019). Visual inspection and manual real-space refinement was carried out in COOT (Emsley & Cowtan, 2004).

#### 3.5.3.4 Structural analysis

Final structure statistics were generated using *phenix.table_one,* from the PHENIX suite (Adams et al., 2010). Structure images were produced using PyMOL (Schrödinger, LLC). The final co-ordinate and structure amplitude files for NgCysK were deposited to the PDB, under the accession code 9NLD.

### 3.5.4 Computational inhibitor screening

The crystal structure of NgCysK was missing key active site and pyridoxal 5'-phosphate (PLP) interacting residues, and for the purposes of virtual screening inhibitor compounds, these sections needed to be modelled.

#### 3.5.4.1 Generation of PLP-bound NgCysK structural model

A homology model of PLP-bound NgCysK was generated using the PLP and inhibitor bound crystal structure of MtCysK (PDB 3ZEI) as the template. The homology model was built using multiple sequence viewer/editor tool in Schrödinger Suite 2021-1. The NgCysK model was generated using energy-based calculation and the inhibitor bound in the template MtCysK was maintained in the homology model. The PLP cofactor from 3ZEI was manually merged into the homology model as it was not recognized as a ligand by the homology modelling tool. The Schiff base linkage between Lys-44 and PLP was manually created in Maestro, and the model was prepared using the Protein Preparation Wizard by assigning bond orders, adding hydrogen atoms, generating protonation states at pH $7 \pm 2$ using Epik, and optimizing hydrogen geometries. PROPKA was used to refine protonation states at pH 7, followed by restrained minimization of heavy atoms to an RMSD of 0.3 Å.

Two loop regions (residues 136-139 and 301-310) were built without a template due to missing regions in the template structure. These loops were refined using the Prime Refine Loops tool with a serial loop sampling method. A dimeric structure was generated based on the refined loop model using crystallographic symmetry mates and further optimized to remove steric clashes using the Protein Preparation Wizard with restrained minimization, converging heavy atoms to an RMSD of 0.3 Å.

#### 3.5.4.2 Virtual screening against PLP-bound NgCysK

The active site in Chain A of the homology model was used as the receptor. The grid file was generated with the centre defined as the centroid of residues 44, 70-76, 98, 102, 120-123, 126, 145, 146, 179, 180, 216, 219, 222-228, 307, 308, and the PLP cofactor. The size of the grid was set to allow docking of ligands with a length $\leqslant$ 20 Å. Rotatable groups for Thr71, Ser72, Thr75, Thr180, Thr231, and PLP1301 were allowed.

A drug-like compound library with neutral charge was obtained from the ZINC15 database (accessed on 2019-08-28, with the following criteria: Rep: 3D, React: Anodyne, Purch: In-stock, pH: Ref Mid, Charge: 0, Drug-Like). This library

contains approximately seven million compounds. The library was filtered using PAINS filters and prepared for modelling with LigPrep using the OPLS3 force field. Possible ligand states at pH 6-8 were generation using Epik. Tautomers were generated. Chiral centers were retained if they were specified in the structural file, otherwise the chiral centers were varied to obtain combinations of different stereocentres. A maximum of two stereoisomers was generated per ligand. This resulted in a prepared library of 10,479,301 compounds.

The compound library was screened against the receptor prepared above using the virtual screening workflow in Schrödinger Suite 2021-1. Prior to any docking, the ligands were first filtered by Lipinski's Rule. Screening was conducted in three stages with increasing precision, HTVS (high-throughput VS), SP (standard precision), and XP (extra precision). Top 10 % ranked compounds from the HTVS stage were subject to SP docking, and the best 10 % compounds from the SP stage were then subject to the final XP docking state. One pose was written out for each ligand, and the top ranked 1000 compounds were written out for evaluation.

#### 3.5.4.3 Virtual screening results evaluation and MD validation

The top 1000 poses showed docking scores ranging from -13 to -10 kcal/mol and were analysed further using Pose Explorer. To ensure diversity in selected hits, the compounds were clustered into 5x5 maps based on SIFT (interaction fingerprints) and 2D fingerprints (Figure 3.1). For each clustering method, the highest-scoring compound per cluster was selected, yielding 42 unique compounds for further evaluation using MM-GBSA calculations. These calculations were performed using the VSGB solvation model with the OPLS4 force field, allowing protein flexibility for residues within 5 Å of the docked ligand.

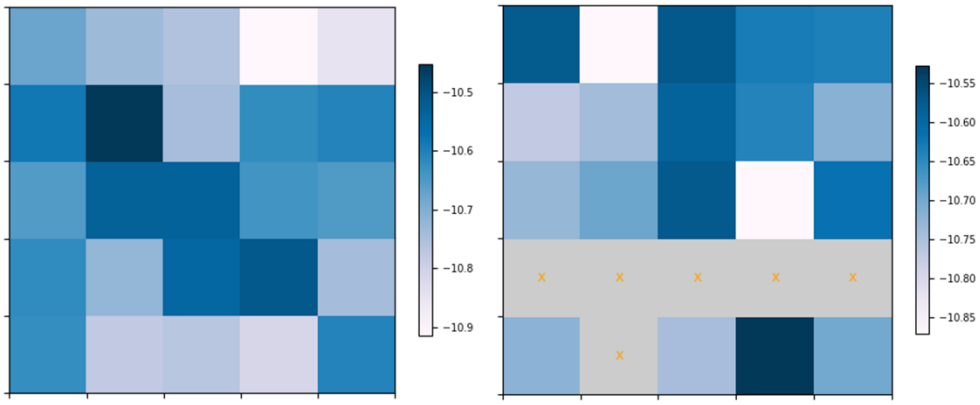


**Figure 3.1:** Docking score Mean on clustered 1000 compounds based on SIFT (Interaction Fingerprints, left) and 2D Fingerprints (right).

The 42 selected compounds had predicted binding energies ranging from -48 to -83 kcal/mol. A total of 27 compounds with predicted binding energies below -60 kcal/mol were selected for molecular dynamics (MD) simulations. The MD system was prepared using OPLS4 force field. The protein-ligand complexes were solvated in SPC explicit water within an orthorhombic box, with a 10 Å buffer in each dimension. The box volume was minimized by rotating the complex, the system charge was neutralized by adding $Na^+$ or $Cl^-$ ions, followed by addition of 0.15 M NaCl. MD simulations were performed using Desmond for NPT ensembles at 310 K and 1.01325 bar. The system was relaxed before the production run using a Langevin thermostat/barostat, and MD simulations were conducted for 2 ns. Compounds that stayed close to the docked position and retained most of the predicted interactions during the MD simulations were recommended for testing.

### 3.5.5 NgCysK Inhibition assays

CysK for inhibition assays was purified immediately prior to assays. Enzyme was stored at 4 °C for the duration of the assay, as a rapid decrease in activity was observed when stored at room temperature. Assays were conducted within 14 h post-purification as CysK activity slowly decreased over time. CysK activity was measured by adapting a method from (Gaitonde, 1967). CysK activity was monitored via absorbance measurements of L-cysteine at 560 nm ($A_{560}$) using a SpectraMax ® M Series Multi-Mode Microplate Reader (Molecular devices**).**

Assays were carried out in 96-well PCR microplates (Axygen), with a reaction volume of 75 µL, containing variable volumes of 100 mM MOPs, 2 mM of OAS, 0.7 mM of sodium sulfide ($Na_2S$), and variable concentrations of the inhibitor compounds (0.01-1 mM). Both substrates, OAS and $Na_2S$, were slightly below their $K_M$ to allow for the most sensitive detection of any mechanisms of inhibition (Attaallah & Amine, 2021; Garcia-Molina et al., 2022). Only the 5 hydrophilic compounds were tested, referred to as compounds 1-5. The reaction was performed at 37 °C after the addition and subsequent spin down (30 seconds at 2500 ***g***) of 0.4 µg of purified CysK. Reactions were stopped with addition of TCA (15 µl of 25% w/v). After addition of acid ninhydrin (100 µl) and glacial acetic acid (100 µl), reaction mixtures were incubated at 95 °C (5 min) and subsequently incubated on ice (5 min). Ice cold ethanol (100%) was added to 100 µl of each reaction mixture and absorbance (560nm) measured. Enzyme concentration and measurement time in inhibition assays was optimised by testing two concentrations (0.2 ug and 0.4 ug) and a variety of time points (from 1-40 mins) to determine the linear region of rates. All substrate stocks were prepared in MQ $H_2O$. Inhibitor compounds were prepared in MQ $H_2O$ and DMSO (Dimethylsulfoxide) (maximum concentration of 10%). Enzyme working stocks of 0.05 $mg.ml^{-1}$ (1.48 µM NgCysK monomer, 33.791 kDa) were stored at 4 °C for the duration of assays. The initial velocity of the reaction was derived from linear-regression analysis of the first 2 minutes of the reaction using a cysteine standard curve (Equation 3.1; Figure A.1Figure A.1). All concentrations of inhibitor compounds were collected in triplicate. Cysteine produced was calculated using a cysteine standard curve equation **(**Equation 3.1). The $IC_{50}$ values were determined by fitting Equation 3.2 using GraphPad Prism (GraphPad Software Version 10.2.3) (Gesztelyi et al., 2012; Weiss, 1997).

**Equation 3.1.** L-cysteine standard curve for determining cysteine produced$x = \frac{y-0.0164}{1.8856}$

$$x = \frac{y - 0.0164}{1.8856}$$

**Equation 3.2:** Log (inhibitor) versus normalized response—variable slope equation

$$Rate = \frac{100}{(1 + 10^{((LogIC_{50} - X)HillSlope)})}$$

## 3.6 Results and discussion

### 3.6.1 Purification and stoichiometry of NgCysK

NgCysK was purified by IMAC followed by a final SEC purification. NgCysK eluted as a single peak from a size exclusion column with an elution volume of 14.2 ml corresponding to an approximate molecular weight of 52.862 kDa (Figure A.2). The predicted molecular mass of an NgSCysK monomer is 33.791 kDa, confirming a dimer of NgCysK monomers (2 x 33.791 kDa = 67.582 kDa). SDS-PAGE analysis of NgCysK shows >95% purity (Figure A.2Figure A.2).

### 3.6.2 Analysis of the NgCysK crystal structure for virtual inhibitor screening

The NgCysK structure was solved by X-ray crystallography for computational inhibitor screening of the enzyme. The NgCysK crystal structure was solved by molecular replacement to 2.49 Å. The final model was refined to an R and free R of 0.198 and 0.255, respectively (Table 3.1). The asymmetric unit contained four monomers arranged as one complete homodimer (Monomer A and D) and one monomer either side of the homodimer (Monomers B and C). All four subunits were between 87-88% complete with 278/279 residues out of the 318-residue polypeptide built (Table A.1). Electron density corresponding to the uncleaved 8-residue C-terminal his-tag was not present in any subunit. All subunits had poor electron density for the C-terminal tail, missing 18 residues in subunit A and B from Tyr300 onwards, and 22 residues in subunits C and D from Tyr296 onwards. This is consistent across CysK homologue structures (Poyraz et al., 2013; Enea Salsi et al., 2010), and is most likely a result of the flexibility of the C-terminal tail. Electron density for the NgCysK co-factor PLP is not apparent in any of the subunits. Further analysis was completed for the functional homodimer only (Monomers A and D). The NgCysK monomer consists of two distinct domains, an N- terminal domain (residues Val43-Gln145), and a C-terminal domain (residues Ile11-Ser42,

**Table 3.1:** Data collection and refinement statistics

| ***Data collection***[a] | **NgCysK** |
|---|---|
| Wavelength (Å) | 0.9537 |
| Resolution range (Å) | 47.53-2.49 (2.58-2.49) |
| Space group | P1 $2_1$ 1 |
| Unit cell parameters a, b, c (Å) | 102.74/62.18/105.67 |
| α, β, γ (º) | 90/90.082/90 |
| No. of molecules in asymmetric unit | 4 |
| Total reflections | 330233 (32079) |
| Unique reflections | 47132 (4605) |
| Multiplicity | 7.0 (7.0) |
| Completeness (%) | 100.0 (99.9) |
| Mean $I/\sigma(I)$ | 19.2 (2.6) |
| $R_{merge}$[b] | 0.056 (0.654) |
| ***Refinement*** | |
| Reflections used in refinement | 46502 (4593) |
| Reflections used for $R_{free}$ | 4749 (424) |
| $R_{work}$ | 0.198 (0.2328) |
| $R_{free}$ | 0.255 (0.3039) |
| No. protein atoms | 7895 |
| No. solvent atoms | 90 |
| No. ligand atoms | |
| $SO_4$ | 21 |
| PEG | 8 |
| Glycerol | 1 |
| Protein residues | 1115 |
| r.m.s.d bonds (Å) | 0.003 |
| r.m.s.d angles (º) | 0.56 |
| Ramachandran favoured (%) | 95.16 |
| Ramachandran allowed (%) | 4.11 |
| Ramachandran outliers (%) | 0.73 |
| Average B ($Å^2$) | 64.39 |
| Macromolecules | 63.85 |
| Ligands | 92.93 |
| Solvent | 59.32 |

| | |
|---|---|
| Clashscore | 13 |
| No. of TLS groups | 1 |
| PDB entry | 9NLD |

[a]Statistics for the highest resolution shell are shown in parentheses

[b]$R_{merge} = \sum_{j=1} \left| I_{hkl\ j} - \langle I_{hkl} \rangle \right| / \sum_{hkl} \sum_{j} I_{hkl}$

and Asn151-Tyr300). Each domain has an α/β-fold, typical of the fold type II, PLP dependant enzymes (Grishin, Phillips, & Goldsmith, 1995; Schneider, Käck, & Lindqvist, 2000). The N-terminal domain consists of a central three-stranded *β*-sheet, flanked by three α-helices on one side and a single α-helix on the other side (Figure 3.2B, Figure 3.2C and Figure 3.4). The formation of the functional homodimer occurs through hydrogen bonding and hydrophobic interactions between each monomer, with the active site pocket consisting of residues all from a single subunit, characteristic of the fold type II family (Liang, Han, Tan, Ding, & Li, 2019). The dimeric state, overall fold, and secondary structures of the NgCysK monomer are similar to many bacterial and plant homologues, with strict residue conservation of active site and PLP-interacting residues (Figure 3.3 and Figure 3.4). A small portion (5993.6 $Å^2$, 26.7% of the dimers surface area (22452.0 $Å^2$) is buried at the monomer-monomer interface.

NgCysK is part of the tryptophan synthase β-superfamily (fold type II) and PLP dependant β-family of enzymes (Guédon & Martin-Verstraete, 2007; Mino & Ishikawa, 2003; Takumi & Nonaka, 2016). Alignment of the NgCysK protein sequence with homologues, shows moderate sequence similarities (average of 57.35% sequence similarity), but strong conservation of the active site residues 71-TSGNTG-76 (Joshi, Gupta, & Gupta, 2019) (except the moderately conserved Ser72) and 223-GIGA-226 (Joshi et al., 2019), and PLP interacting residues Lys-44, Val-40, Ser-266, the asparagine loop at Asn-74, the substrate carboxylate binding Gln-145 and the PLP interacting 179-GTGGT-183 motif (Figure 3.3 and Figure 3.4). The closest structural relatives to the NgCysK enzyme are from *M. tuberculosis* (Poyraz et al., 2013) and *H. influenzae* (Huang, Vetting, & Roderick, 2005) with root mean square deviation values after structural

superposition of 1.13 Å (237 equivalent C-atoms) and 1.24 Å (223 equivalent C-atoms), respectively.

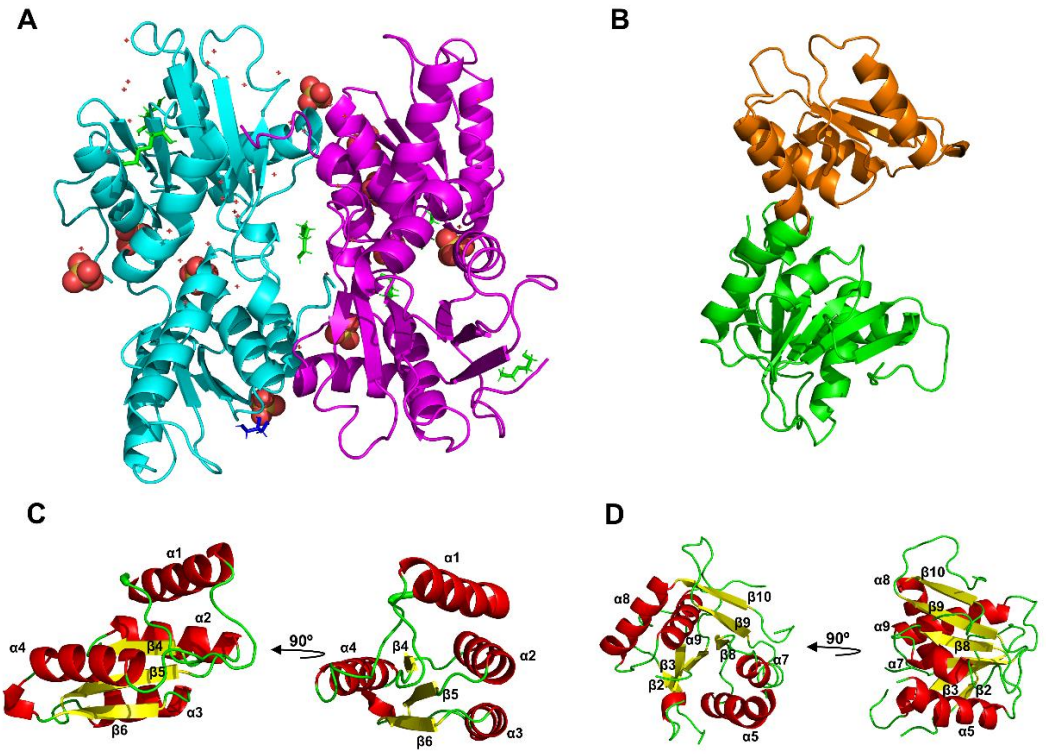


**Figure 3.2:** Structure of apo-NgCysK. (**A**) Functional NgCysK homodimer consisting of monomer A (shown in cyan) and monomer D (shown in magenta). PEG shown in green, glycerol shown in blue, sulfate shown as yellow spheres with four red spheres attached, and waters shown as small red crosses. (**B**) Structure of the NgCysK monomer. N-terminal domain shown in orange. C-terminal domain shown in green. (**C**) Structure of the NgCysK N-terminal domain. (**D**) Structure of the NgCysK C-terminal domain. In (**C**) and (**D**), helices are coloured red and labelled with an α, β-sheets are coloured yellow and labelled with a β. Loops and turns are coloured green. Figure generated in PyMOL

Due to the absence of PLP in our purification and therefore our crystal structure, to determine NgCysK PLP interacting and active site residues, we overlaid the NgCysK with the closest structural relative, MtCysK (PDB ID: 3ZEI) (Figure 3.5). This alignment indicates each NgCysK monomer has an alternate conformation in its homodimer arrangement. The NgCysK monomer D active site cleft residues are arranged in the same conformation as MtCysK, allowing them to form an almost identical active site cleft (Figure 3.5A and Figure 3.5B). Due to resolution constraints and the flexibility of the active site loop, the 223-GIGA-226 active site

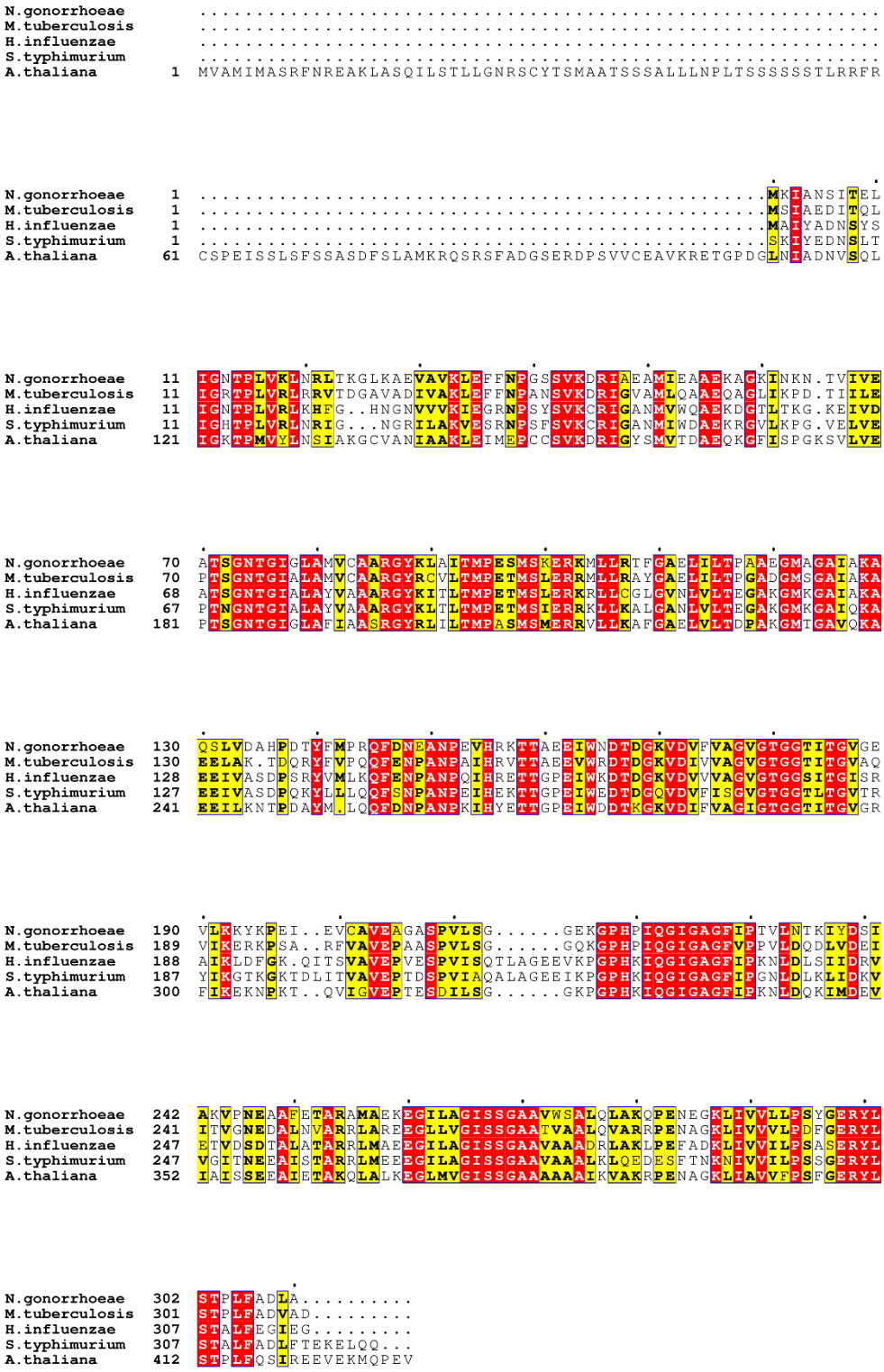


**Figure 3.3:** CysK sequence alignment. The *N. gonorrhoeae* FA1090 CysK structure (9NLD) was aligned to the following CysK homologues; *M. tuberculosis* (3ZEI_A: 65.70% sequence similarity); *H. influenzae* (1Y7L_A: 55.37% sequence similarity); *S. typhimurium* (1FCJ_A: 54.72% sequence similarity); and *A. thaliana* (4AEC_A: 55.99% sequence similarity). Highly conserved residues are highlighted in red, whilst less conserved residues are shown in yellow.

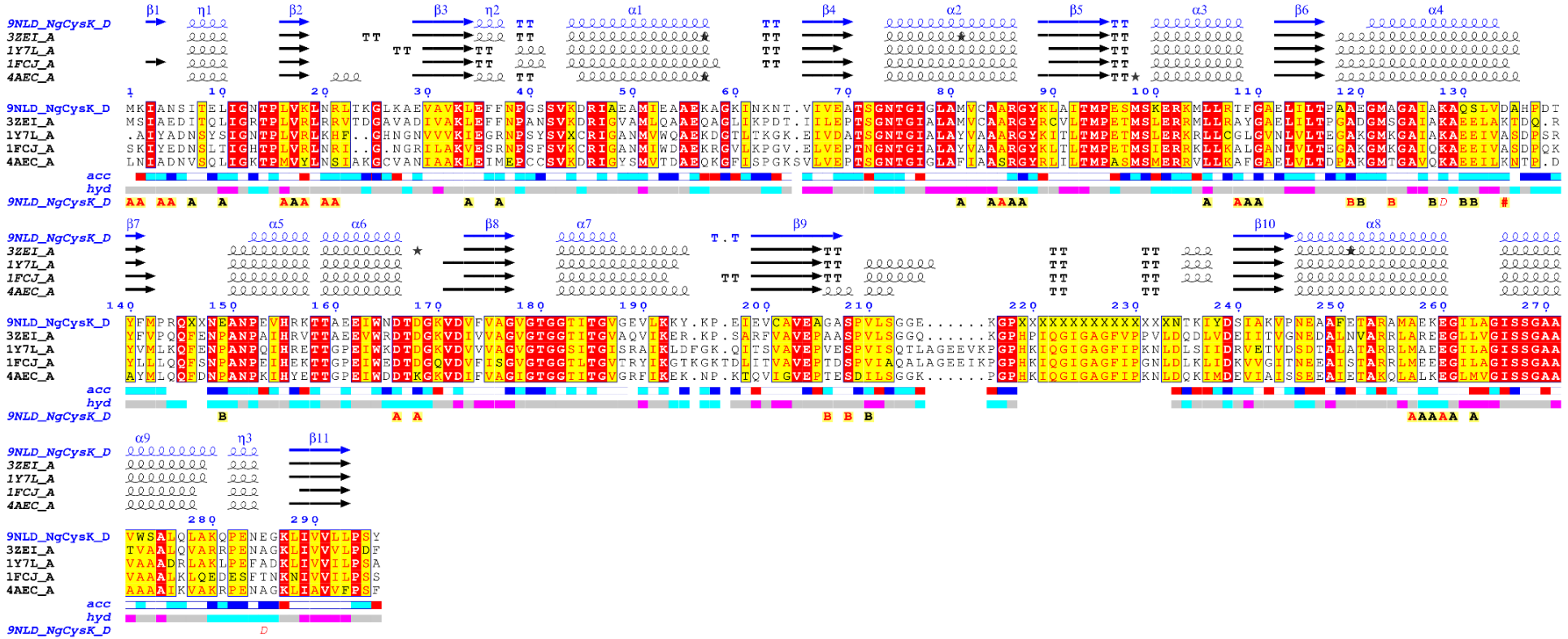


**Figure 3.4:** CysK protein structure alignment and ENDscript secondary structure analysis. The *N. gonorrhoeae* FA1090 CysK structure (9NLD) was aligned to the following CysK homologues; *M. tuberculosis* (3ZEI_A: 65.48% sequence similarity); *H. influenzae* (1Y7L_A: 55.19% sequence similarity); *S. typhimurium* (1FCJ_A: 53.82% sequence similarity); and *A. thaliana* (4AEC_A: 54.89% sequence similarity). Highly conserved residues are highlighted in red, whilst les conserved residues are shown in yellow. Solvent Chain D was used for secondary structure analysis. for chain labelling a nd statistics of the NgCysK monomers in the ASU.

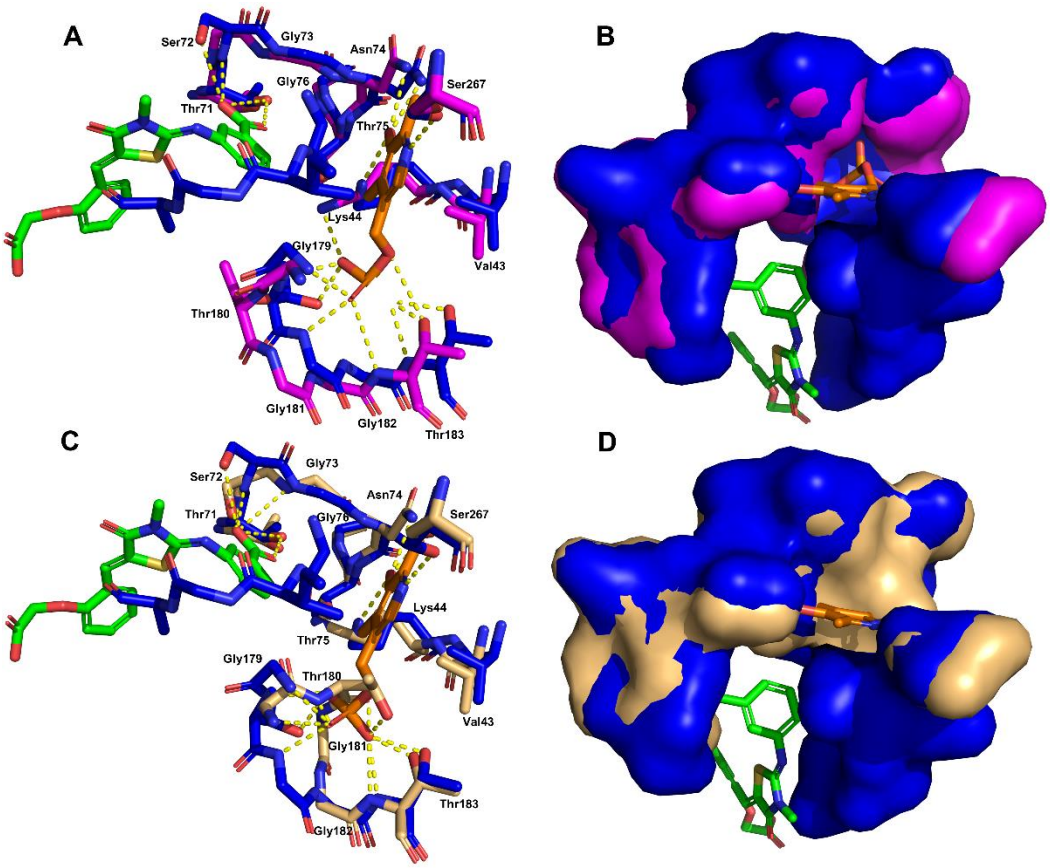


**Figure 3.5:** Alignment of NgCysK and MtCysK active site cleft residues. (**A**) Alignment of NgCysK monomer D active site cleft in licorice stick format. NgCysK active site residues 71-TSGNTG-76 and PLP interacting residues; Val-43, Lys-44, Asn loop at Asn-74, Ser-267 and 179-GTGGT-183 motif are labelled. MtCysK active site residues 223-GIGA-226 are not labelled. NgCysK residues shown in magenta. MtCysK residues shown in blue. PLP shown in orange. Alignment of NgCysK monomer A active site cleft in licorice stick format. NgCysK active site residues 71-TSGNTG-76 and PLP interacting residues; Val-43, Lys-44, Asn loop at Asn-74, Ser-267 and 179-GTGGT-183 motif are labelled. MtCysK active site residues 223-GIGA-226 are not labelled. NgCysK residues shown in light orange/gold. MtCysK residues shown in blue. PLP shown in orange.

motif is missing from the NgCysK structure. Visual inspection of (Figure 3.5B) shows this motif from MtCysK forming the right-hand side of the active site pocket for the AWH (an OAS mimicking substrate) substrate to bind into. Given the similar conformation of all other residues of the active site cleft between NgCysK and MtCysK it can be assumed that NgCysK forms the active site pocket in the same manner. Polar contacts of PLP indicate Schiff base formation between the PLP aldehyde and the NgCysK Lys44 residue, whilst the Val43 is providing hydrophobic stabilisation via van der Waals forces (Figure 3.5A). The side chain of Asn74 forms a hydrogen bond with the 3'-hydroxyl group of PLP assisting with stabilisation of the cofactor while the NgCysK Ser267 hydroxyl group hydrogen bonds to N1 nitrogen atom of the pyridine ring (Figure 3.5A). The glycine rich 179-

GTGGT-183 region loops around the PLP phosphate group forming hydrogen bonds with the phosphate oxygen atoms (Figure 3.5A). The formation of these bonds indicate PLP can successfully bind into the NgCysK monomer D, indicating an active conformation in this monomer. Alternatively, the NgCysK monomer A active site cleft residues are arranged in a different conformation to MtCysK, with the 179-GTGGT-183 motif blocking the binding of the PLP co-factor (Figure 3.5C and Figure 3.5D). Given CysK is a PLP dependant enzyme (Guédon & Martin-Verstraete, 2007; Mino & Ishikawa, 2003; Takumi & Nonaka, 2016), this inability to bind PLP indicates monomer A must be inactive. We hypothesise that the binding of a substrate to monomer D will cause a conformation change in monomer A, allowing PLP to bind and making monomer A now active. This suggests positive cooperativity between the monomers of the dimer which is supported by the kinetic data of NgCysK (McGarvie et al., 2025).

### 3.6.3 CysK is highly conserved across *Neisseria gonorrhoeae* strains

To ensure broad spectrum activity against different *N. gonorrhoeae* strains, high conservation of active site residues is vital. We determined the presence and conservation of CysK (*cysK*) amongst *N. gonorrhoeae* strains using *N. gonorrhoeae* FA1090 CysK as a query against all available *N. gonorrhoeae* genomes in the NCBI database. *cysK* was highly conserved in *N. gonorrhoeae* (97.74-100% sequence identity) over the length of the sequence (933 nucleotides, 310 residues). Although there were only two strains with an identical isoform (2/739) to FA1090, there are only 11 variations to the CysK enzyme across 739 genomes (Figure A.3). All active site residues and PLP interacting residues are conserved across all 739 *N. gonorrhoeae* CysK reference sequences (Figure A.3). Overall, CysK is highly conserved across *N. gonorrhoeae* reference strains, thus making it a suitable target for antimicrobial adjuvant applications.

### 3.6.4 Computational inhibitor screening and characterisation

Although *cysK* is not essential in *N. gonorrhoeae* (Remmele et al., 2014), it is vital for colonisation of epithelial cells in the closely related pathogen *N. meningitidis,* and deletion of *cysK* confers both decreased fitness and an increased antibiotic susceptibility (Capel et al., 2016; Turnbull & Surette, 2010). A commonly used strategy for inhibiting the CysK enzyme is the design of peptide inhibitors that mimic the CysE C-terminal tail (Bruno et al., 2013; Kant et al., 2019; Enea Salsi et

al., 2010). Due to the inability of NgCysK and NgCysE to form the cysteine synthase complex (McGarvie et al., 2025), we used virtual screening to identify potential NgCysK inhibitors that can be used downstream for more potent inhibitor development. Due to the missing PLP co-factor from the NgCysK structure, a homology model was generated using the MtCysK (PDB ID: 3ZEI) with PLP and an inhibitor bound in the active site. This homology model of PLP-bound NgCysK was used as the receptor for virtual screening. The ZINC15 database was used to obtain compounds with neutral charge and drug-like properties (Sterling & Irwin, 2015) which, once prepared, contained 10,479,301 compounds. After the MM-GBSA evaluation and molecular dynamics (MD) simulations, the 12 compounds that remained close to the docked position and retained most of the predicted MD simulated interactions were recommended for testing. Of these 12 compounds, only 10 were available for purchase at the time of the study. Only 5 of these compounds were tested due to the insolubility of the other 5 compounds.

### 3.6.5 *In vitro* NgCysK inhibitor screening

Preliminary testing of compounds 1-5 indicated inhibition of the NgCysK reaction (Figure 3.6) and were therefore subjected to $IC_{50}$ screening. Upon further testing over the 10-1000 μM concentration range, compounds 2-4 indicated no distinct inhibition, whilst compound 1 displayed concentration independent inhibition of NgCysK (Figure A.5), and were therefore classified as false positives. Compound 5 demonstrated clear inhibition and collection of a dose response curve produced and $IC_{50}$ of 253.5 ± 56.25 μM ($R^2$ = 0.7801) (Figure 3.7).

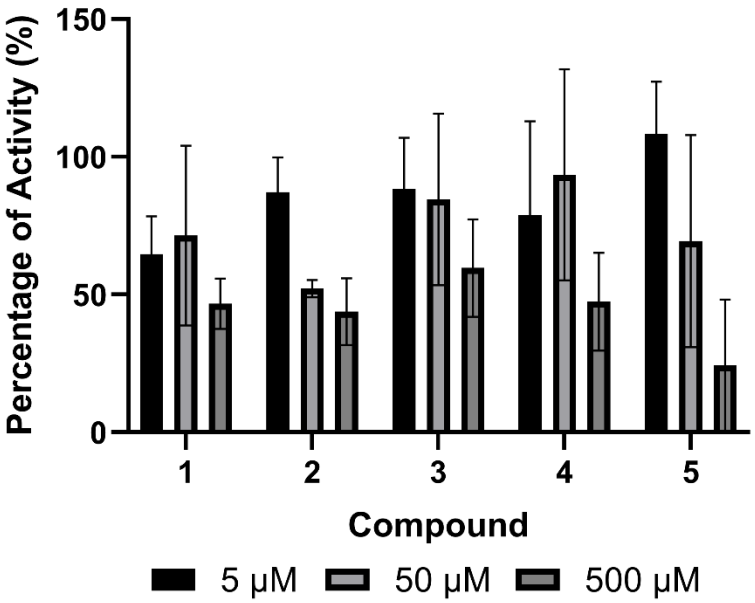


**Figure 3.6:** Preliminary testing of NgCysK inhibitor compounds 1-5. Compounds are numbered. 5 µM concentrations are labelled black. 50 µM concentrations are labelled light grey. 500 µM concentrations are labelled dark grey.

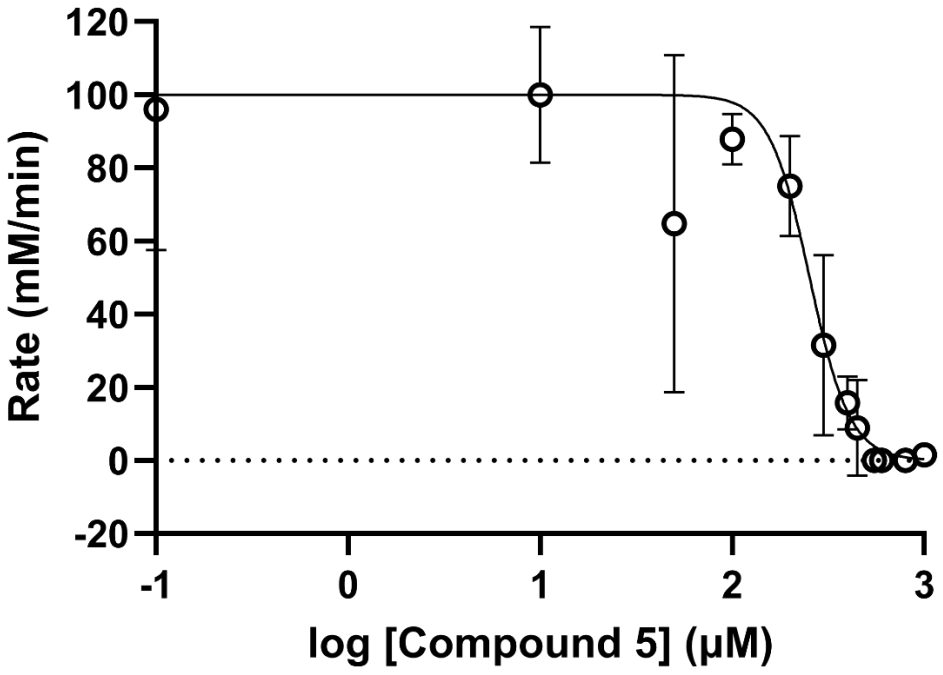


**Figure 3.7:** $IC_{50}$ dose response curve for Compound 5. NgCysK activity measured in the presence of 2 mM OAS and 0.7 mM $Na_2S$. Plotted data points represent mean alongside SEM of three replicates.

### 3.6.6 Docking interactions of Compound 5

Compound 5 (2-[[ethyl-[2-hydroxy-3-(4-methylphenoxy)propyl]amino]methyl]-3H-quinazolin-4-one), consists of; a quinazolinone core connected to a tertiary amine, which is connected to an ether linked to the para-methoxyphenol group, with a central chiral carbon linked hydroxyl group (Figure 3.8). This compound has drug-like compound consistent qualities (Table 3.2) and does not violate any Lipinski's rules (Lipinski, 2000) making it a promising antimicrobial adjuvant for *in vitro* testing.

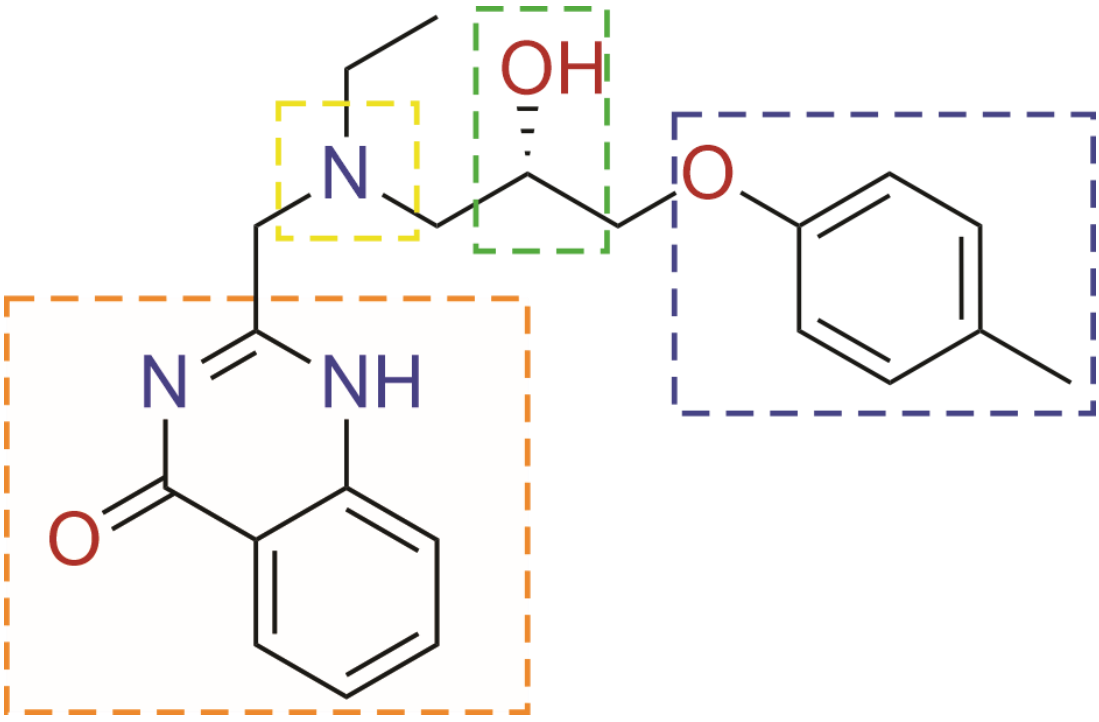


**Figure 3.8:** Structure of Compound 5 ((2-[[ethyl-[2-hydroxy-3-(4-methylphenoxy)propyl]amino]methyl]-3H-quinazolin-4-one). Functional groups quinazolinone and para-methoxyphenol are highlighted in orange and blue, respectively. Tertiary amine (highlighted yellow) and central chiral carbon linked hydroxyl group (highlighted green) are shown. Figure created using ChemDraw Prime.

**Table 3.2:** Compound 5 chemical properties. tPSA refers to the polar surface area (Å$^2$). logP refers to the partition coefficient.

| Chemical formula | Net charge | H-bond donors | H-bond acceptors | Molecular weight (g/mol) | logP | tPSA | Rotatable bonds | Apolar desolvation | Polar desolvation |
|---|---|---|---|---|---|---|---|---|---|
| $C_{21}H_{25}N_3O_3$ | 0 | 2 | 5 | 367.449 | 2.493 | 78 | 8 | 5.65 | -13.95 |

Examination of the NgCysK homology model with PLP bound with compound 5 docked shows notable active site interactions with the O-acetylserine binding site.

There are multiple H-bond interactions between compound 5 and the NgCysK homology models active site residues, mainly involving the asparagine loop residues with one H-bond to Thr71, two H-bonds to Ser72, one hydrogen bond to Gly73, and a hydrogen bond to Ala226. These are complimented by a number of hydrophobic interactions, including the active site pocket residues Gly223 and Ile224 with the central chiral carbon linked hydroxyl group, and the Schiff base forming Lys44 and Glycine rich loop residues Gly179 and Thr180 with the quinazolinone group (Figure 3.9). The residues involved in the active site pocket formation and those directly interacting with compound 5 are strictly conserved not only in *Neisseria* species, but also other Proteobacterial species (Figure 3.10), indicating the downstream product of our compound to have potential as an antimicrobial adjuvant against other pathogens as well as *N. gonorrhoeae*.

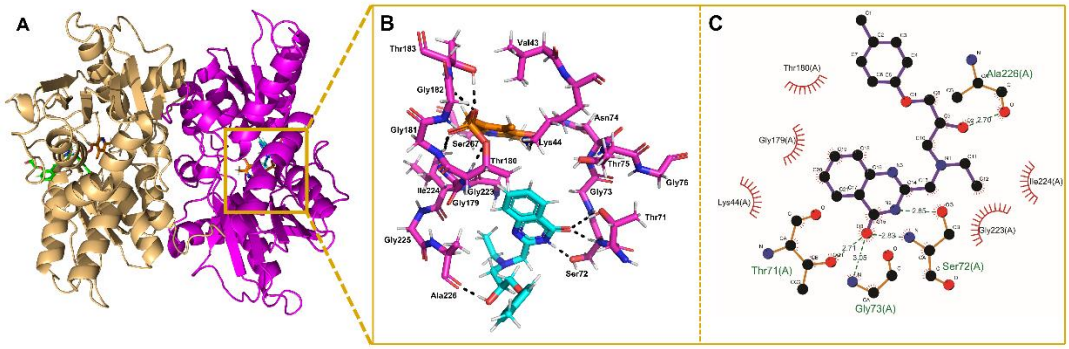


**Figure 3.9:** Docked interactions of Compound 5 binding to homology model of NgCysK with PLP bound. (**A**) NgCysK homology model with compound 5 bound into monomer A (shown in magenta) and AWH from MtCysK (PDB ID: 3ZEI) bound into monomer B (shown in light orange). Compound 5 shown in cyan. AWH shown in green. PLP shown in orange. (**B**) Hydrogen bond interactions (black) between compound 5 (cyan sticks) and NgCysK residues (magenta sticks). (**C**) Two-dimensional LigPlot schematic of H-bonds and hydrophobic interactions between compound 5 and the active site and PLP-interacting residues from the NgCysK homology model (bond lengths not to scale). H-bonds are shown as dark grey dashes and hydrophobic interactions are represented as red radiating lines. All bond lengths are reported in Angstroms (Å). Figures created using PyMOL and LigPlot$^{+}$ (Laskowski & Swindells, 2011).

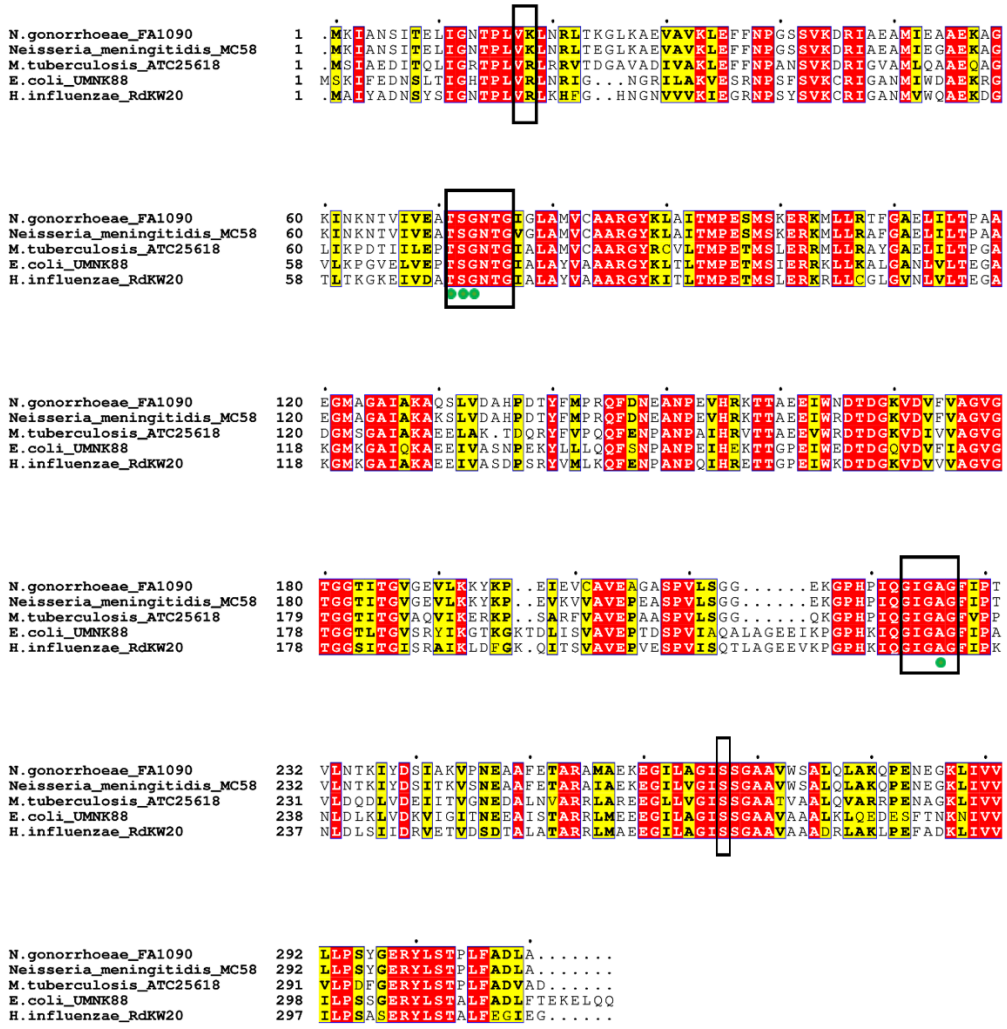


**Figure 3.10:** Multiple sequence alignment of bacterial CysK isoforms. Highly conserved residues are highlighted in red, whilst les conserved residues are shown in yellow. Active site and PLP-interacting residues are highlighted by a black box. Residues forming hydrogen bonds with compound 5 are annotated with green dots. Sequences: *N. gonorrhoeae*_FA1090; *N. meningitidis*_MC58; *M. tuberculosis*_ATC254618 (PDB ID: 3ZEI); *E. coli*_UMNK88; *H. influenzae*_RdKW20 (PDB ID: 4HO1).

## 3.7 Conclusions

Antimicrobial resistance is an ever-increasing issue and is considered one of the top 10 global public health threats. The extensively drug-resistant bacterium *N. gonorrhoeae* is one such issue and has become a global burden on human health. In the absence of an effective vaccine, the front-line combatant for managing the gonococcal disease remains in the hands of antimicrobials. The *de novo* L-cysteine biosynthesis pathway has been identified as a promising avenue for development of new antimicrobial and adjuvant compounds due to the vital role of L-cysteine derived compounds in the mitigation of oxidative stress and the absence of this pathway in humans. We have demonstrated the success of structure-based virtual inhibitor screening as a strategy for identifying inhibitors and report the first inhibitor of NgCysK. After computationally screening a library of ~10.5 million compounds from the ZINC15 database, 42 compounds were identified that met in silico criteria, and of the 5 compounds tested experimentally, compound 5 was the best inhibitor of NgCysK activity *in vitro*. Docking analysis revealed notable H-bond interactions between compound 5 and the active site and PLP-interacting residues of our NgCysK homology model, alongside complimenting hydrophobic interactions. Dose-response analysis of compound 5 showed it to be a promising inhibitor of NgCysK for downstream optimisation with an $IC_{50}$ of 253.5 μM.

The combination of virtual and experimental testing is required for rapid identification of novel inhibitors and has been a proven strategy for identifying bacterial NgCysK inhibitors. The inhibition observed for compound 5 is in the mid-range of previously identified chemical inhibitors reported to date (Hicks et al., 2022). Micro-molar inhibitors have been reported, although ensuring the compound is membrane permeable remains an issue particularly in gram-negative bacteria such as *N. gonorrhoeae* (Maher & Hassan, 2023). Therefore, determining the MIC of the compound 5 downstream optimised molecule is vital to determine the compounds bioactivity and assess its viability as an antimicrobial adjuvant.

Validation of CysK inhibitors to date has mostly been conducted *in vitro* with a particular focus on compounds that inhibit both the CysK and CysM isoforms, however, little to no *in vivo* testing to determine cytotoxicity or MIC of compounds has been included (Hicks et al., 2022). Annunziato and colleagues showed a

complete lack of antibacterial activity when using their compound in isolation, however, they managed to utilise the inhibitor as an effective adjuvant alongside colistin (Annunziato et al., 2021). This work highlights the effective nature of CysK inhibitors for use alongside current antibiotics to increase their efficacy and reduce resistance.

Targeting *de novo* L-cysteine biosynthesis for antimicrobial and adjuvant design has one apparent obstacle in the possibility of developing resistance via upregulation of alternative sulfur acquisition and assimilation pathways to obtain L-cysteine (Toyomoto et al., 2023). However, sulfur acquisition in *N. gonorrhoeae* is unique as it has ABC transporters for sulfate/thiosulfate (Hicks & Mullholland, 2018), transporters for thiol containing amino acids methionine (Semchenko, Day, & Seib, 2017), cysteine, and cystine (Bulut et al., 2012; Semchenko et al., 2017), but lacks taurine and glutathione thiol compound transporters (Seib et al., 2006). Given the lack of both, glutathione importers and the glutathione recycler γ-glutamyl transpeptidase (Seib et al., 2006; Takahashi & Watanabe, 2005), it is interesting to note the maintenance of high intracellular glutathione levels in *N. gonorrhoeae* (15 mM vs 5mM in *E. coli* (Archibald & Duong, 1986)), indicating a reliance on *de novo* glutathione production which in turn relies on L-cysteine biosynthesis to maintain these high intracellular glutathione concentrations. *N. gonorrhoeae* is also lacking the sulfate reduction pathway (Hicks & Mullholland, 2018), further limiting its ability to utilise sulfur and metabolise sulfur containing compounds. Given the distinct lack of alternative sulfur acquisition pathways and the high demand for resisting oxidative stress during infection, *N. gonorrhoeae* is unlikely to develop resistance to a CysK inhibitor making it an ideal target for inhibition of *de novo* L-cysteine biosynthesis.

Looking at the only other pathogenic *Neisseria* species, CysK is of particular importance in *N. meningitidis* for colonisation of epithelial cells (Capel et al., 2016), and upon exposure to epithelial cells, the sulfate reduction pathway involved in *de novo* L-cysteine biosynthesis is differentially expressed (Grifantini et al., 2002; Joseph et al., 2010). CysK when knocked out of *S. typhimurium*, also causes an increased susceptibility to antibiotics alongside decreased fitness (Turnbull & Surette, 2010). Annunziato and colleagues demonstrated cross-species inhibition of

CysK enzymes (Annunziato et al., 2021), and given the high degree of sequence conservation between NgCysK and NmCysK homologues (95.16% sequence identity, Figure 3.10), the hit compounds tested here could be screened against NmCysK.

We have demonstrated the success of structure-based virtual inhibitor screening for identifying NgCysK inhibitors and report compound 5 to inhibit NgCysK at a mid-range µM range placing it in the middle of CysK inhbitors to date. Therefore, compound 5 is a promising candidate for downstream optimisation as an antimicrobial adjuvant against this pathogen.

## 3.8 Future directions

This work demonstrates important progress into the development of novel inhibitors for NgCysK. Although the identified inhibitor, compound 5, inhibits in the mid-range of already existing inhibitors, it is a promising compound for downstream optimisation. Identification of compound 5 demonstrated the suitability of structure-based virtual screening for identification of NgCysK inhibitors. This work lays the foundation for future work into characterising the nature of compound 5 to improve the potency of this promising inhibitor.

In this work, we identified compound 5 to exhibit inhibition at mid-range micromolar concentrations, which is too high for ideal antimicrobial adjuvants. Inhibition in the nanomolar range is ideal, indicating the necessity for further optimisation of the compound. To improve this compounds efficacy, we will conduct medicinal chemistry screening of compound 5 with collaborators, Dr. Farah Lamiable-Oulaidi and Dr. Wanting Jiao, from the Ferrier Research Institute at Victoria, the University of Wellington. This would allow for structure-activity relationship studies of compound 5, to determine which functional groups and residue interactions are vital for potent inhibition.

Alongside the structure-activity studies, we will further characterise the compound 5 inhibiton, by determining the mode of inhibition and the binding kinetics through further kinetic analysis. To improve the quality of the medicinal chemistry we will co-crystallise the compound with NgCysK to experimentally validate the

compound—NgCysK interactions. Alongside this, we will co-crystallise the active site binding substrate OAS to attain a crystal structure with the active site residues present, removing the need for the generated NgCysK homology model with PLP bound. Binding of the OAS substrate should hold the NgCysK in a more rigid structure allowing effective crystallisation of the active site residues and the PLP co-factor. Obtaining the OAS bound NgCysK and compound 5 bound NgCysK crystal structures will allow for more accurate screening and improvements in the medicinal chemistry investigation.

### 3.8.1 Characterising the *Neisseria gonorrhoeae cysK* knockout strain

Characterising an antimicrobial adjuvant target *in vivo* is essential for drug target validation and success. CysK is encoded by the *cysK* gene in *N. gonorrhoeae* and the development of a *cysK* deletion and corresponding complement strains has already begun. We designed a *cysK* deletion construct where a kanamycin resistance gene was flanked on the 5' and 3' ends with 150 base pairs (bp) of homologous sequence to the regions flanking *cysK* in the *N. gonorrhoeae* FA19 genome. The construct was ordered as a synthetic DNA gene block from Twist Bioscience. Given the natural competency of *N. gonorrhoeae,* piliated *N. gonorrhoeae* was streaked through 10ng of the DNA construct, spotted on gonococcal broth (GCB) agar supplemented with Isovitalex (1% final volume, contains L-cysteine and L-cystine) and kanamycin (50 $\mu g.ml^{-1}$) following an adapted spot transformation protocol (Dillard, 2011). Successful transformants were confirmed by colony PCR and DNA sequencing. However, the corresponding complement strain has not yet been generated, due to problems cloning cysK into the complementation plasmid for subsequent genome integration. Future research will generate the complement strain, after which phenotypic characterisation will be conducted via growth curves of the three strains (WT, Δ*cysK*, and the *cysK* complement). Host association assays using human endocervical cells will also be conducted to determine the effect of the *cysK* deletion on gonococcal infection and adhesion, alongside peroxide assays to determine the effect on resisting oxidative stress and antibiotic susceptibility testing. These assays are vital for validation of CysK as a target for antimicrobial adjuvant development and will also give further insight into the function of CysK in

*N. gonorrhoeae*, which is especially important considering the missing sulfate reduction pathway (Hicks & Mullholland, 2018) and inability to use thiosulfate as a sulfur donor for L-cysteine biosynthesis (McGarvie et al., 2025). This is an excellent starting point for *in vivo* characterisation and a *cysK* deletion strain will be crucial for understanding the role of *cysK* in *N. gonorrhoeae*.

## 3.9 References


Abd El-Aleam, R. H., George, R. F., Georgey, H. H., & Abdel-Rahman, H. M. (2021). Bacterial virulence factors: a target for heterocyclic compounds to combat bacterial resistance. *RSC Advances, 11*(58), 36459-36482. 10.1039/d1ra06238g

Adams, P. D., Afonine, P. V., Bunkóczi, G., Chen, V. B., Davis, I. W., Echols, N., . . . Zwart, P. H. (2010). PHENIX: a comprehensive Python-based system for macromolecular structure solution. *Acta Crystallographica Section D Biological Crystallography, 66*(2), 213-221. 10.1107/s0907444909052925

Annunziato, G., Spadini, C., Franko, N., Storici, P., Demitri, N., Pieroni, M., . . . Costantino, G. (2021). Investigational Studies on a Hit Compound Cyclopropane–Carboxylic Acid Derivative Targeting O-Acetylserine Sulfhydrylase as a Colistin Adjuvant. *ACS Infectious Diseases, 7*(2), 281-292. 10.1021/acsinfecdis.0c00378

Archibald, F. S., & Duong, M. N. (1986). Superoxide dismutase and oxygen toxicity defenses in the genus Neisseria. *Infect Immun, 51*(2), 631-641. 10.1128/iai.51.2.631-641.1986

Attaallah, R., & Amine, A. (2021). The Kinetic and Analytical Aspects of Enzyme Competitive Inhibition: Sensing of Tyrosinase Inhibitors. *Biosensors, 11*(9), 322. 10.3390/bios11090322

Becker, M. A., & Tomkins, G. M. (1969). Pleiotrophy in a cysteine-requiring mutant of Samonella typhimurium resulting from altered protein-protein interaction. *J Biol Chem, 244*(21), 6023-6030.

Benoni, R., De Bei, O., Paredi, G., Hayes, C. S., Franko, N., Mozzarelli, A., . . . Campanini, B. (2017). Modulation of Escherichia coli serine acetyltransferase catalytic activity in the cysteine synthase complex. *FEBS Letters, 591*(9), 1212-1224. 10.1002/1873-3468.12630

Brunner, K., Maric, S., Reshma, R. S., Almqvist, H., Seashore-Ludlow, B., Gustavsson, A.-L., . . . Schneider, G. (2016). Inhibitors of the Cysteine Synthase CysM with Antibacterial Potency against Dormant Mycobacterium tuberculosis. *Journal of Medicinal Chemistry, 59*(14), 6848-6859. 10.1021/acs.jmedchem.6b00674

Brunner, K., Steiner, E. M., Reshma, R. S., Sriram, D., Schnell, R., & Schneider, G. (2017). Profiling of in vitro activities of urea-based inhibitors against cysteine synthases from Mycobacterium tuberculosis. *Bioorg Med Chem Lett, 27*(19), 4582-4587. 10.1016/j.bmcl.2017.08.039

Bruno, A., Amori, L., & Costantino, G. (2013). Computational Insights into the Mechanism of Inhibition of OASS-A by a Small Molecule Inhibitor. *Mol Inform, 32*(5-6), 447-457. 10.1002/minf.201200174

Bulut, H., Moniot, S., Licht, A., Scheffel, F., Gathmann, S., Saenger, W., & Schneider, E. (2012). Crystal structures of two solute receptors for L-cystine and L-cysteine, respectively, of the human pathogen Neisseria gonorrhoeae. *J Mol Biol, 415*(3), 560-572. 10.1016/j.jmb.2011.11.030

Burns-Huang, K., & Mundhra, S. (2019). Mycobacterium tuberculosis cysteine biosynthesis genes mec+-cysO-cysM confer resistance to clofazimine. *Tuberculosis, 115*, 63-66. https://doi.org/10.1016/j.tube.2019.02.002

Campanini, B., Pieroni, M., Raboni, S., Bettati, S., Benoni, R., Pecchini, C., . . . Mozzarelli, A. (2015). Inhibitors of the sulfur assimilation pathway in

bacterial pathogens as enhancers of antibiotic therapy. *Curr Med Chem, 22*(2), 187-213. 10.2174/0929867321666141112122553

Capel, E., Zomer, A. L., Nussbaumer, T., Bole, C., Izac, B., Frapy, E., . . . Coureuil, M. (2016). Comprehensive Identification of Meningococcal Genes and Small Noncoding RNAs Required for Host Cell Colonization. *mBio, 7*(4) 10.1128/mBio.01173-16

Carfrae, L. A., & Brown, E. D. (2023). Nutrient stress is a target for new antibiotics. *Trends Microbiol, 31*(6), 571-585. 10.1016/j.tim.2023.01.002

Dillard, J. P. (2011). Genetic Manipulation of *Neisseria gonorrhoeae*. *Current protocols in microbiology, 0 4*, Unit4A.2-Unit4A.2. 10.1002/9780471729259.mc04a02s23

Emsley, P., & Cowtan, K. (2004). Coot: model-building tools for molecular graphics. *Acta Crystallographica Section D Biological Crystallography, 60*(12), 2126-2132. 10.1107/s0907444904019158

Evans, P. R., & Murshudov, G. N. (2013). How good are my data and what is the resolution? *Acta Crystallographica Section D Biological Crystallography, 69*(7), 1204-1214. 10.1107/s0907444913000061

Gaitonde, M. (1967). A spectrophotometric method for the direct determination of cysteine in the presence of other naturally occurring amino acids. *Biochemical Journal, 104*(2), 627-633. 10.1042/bj1040627

Garcia-Molina, P., Garcia-Molina, F., Teruel-Puche, J. A., Rodriguez-Lopez, J. N., Garcia-Canovas, F., & Muñoz-Muñoz, J. L. (2022). The Relationship between the IC50 Values and the Apparent Inhibition Constant in the Study of Inhibitors of Tyrosinase Diphenolase Activity Helps Confirm the Mechanism of Inhibition. *Molecules, 27*(10), 3141. 10.3390/molecules27103141

Gesztelyi, R., Zsuga, J., Kemeny-Beke, A., Varga, B., Juhasz, B., & Tosaki, A. (2012). The Hill equation and the origin of quantitative pharmacology. *Archive for History of Exact Sciences, 66*(4), 427-438. 10.1007/s00407-012-0098-5

Grifantini, R., Bartolini, E., Muzzi, A., Draghi, M., Frigimelica, E., Berger, J., . . . Grandi, G. (2002). Gene expression profile in Neisseria meningitidis and Neisseria lactamica upon host-cell contact: from basic research to vaccine development. *Ann N Y Acad Sci, 975*, 202-216. 10.1111/j.1749-6632.2002.tb05953.x

Grishin, N. V., Phillips, M. A., & Goldsmith, E. J. (1995). Modeling of the spatial structure of eukaryotic ornithine decarboxylases. *Protein Science, 4*(7), 1291-1304. 10.1002/pro.5560040705

Guédon, E., & Martin-Verstraete, I. (2007). Cysteine Metabolism and Its Regulation in Bacteria. In V. F. Wendisch (Ed.), *Amino Acid Biosynthesis ~ Pathways, Regulation and Metabolic Engineering* (pp. 195-218). Berlin, Heidelberg: Springer Berlin Heidelberg.

Hicks, J. L., & Mullholland, C. V. (2018). Cysteine biosynthesis in Neisseria species. *Microbiology, 164*(12), 1471-1480. 10.1099/mic.0.000728

Hicks, J. L., Oldham, K. E. A., McGarvie, J., & Walker, E. J. (2022). Combatting antimicrobial resistance via the cysteine biosynthesis pathway in bacterial pathogens. *Biosci Rep, 42*(10) 10.1042/bsr20220368

Huang, B., Vetting, M. W., & Roderick, S. L. (2005). The Active Site of O-Acetylserine Sulfhydrylase Is the Anchor Point for Bienzyme Complex Formation with Serine Acetyltransferase. *Journal of Bacteriology, 187*(9), 3201-3205. 10.1128/jb.187.9.3201-3205.2005

Joseph, B., Schneiker-Bekel, S., Schramm-Glück, A., Blom, J., Claus, H., Linke, B., . . . Schoen, C. (2010). Comparative genome biology of a serogroup B carriage and disease strain supports a polygenic nature of meningococcal virulence. *J Bacteriol, 192*(20), 5363-5377. 10.1128/jb.00883-10

Joshi, P., Gupta, A., & Gupta, V. (2019). Insights into multifaceted activities of CysK for therapeutic interventions. *3 Biotech, 9*(2) 10.1007/s13205-019-1572-4

Kabsch, W. (2010). XDS. *Acta Crystallographica Section D Biological Crystallography, 66*(2), 125-132. 10.1107/s0907444909047337

Kant, V., Vijayakumar, S., Sahoo, G. C., Ali, V., Singh, K., Chaudhery, S. S., & Das, P. (2019). In-silico screening and validation of high-affinity tetra-peptide inhibitor of Leishmania donovani O-acetyl serine sulfhydrylase (OASS). *J Biomol Struct Dyn, 37*(2), 481-492. 10.1080/07391102.2018.1429315

Kowiel, M., Brzezinski, D., Porebski, P. J., Shabalin, I. G., Jaskolski, M., & Minor, W. (2019). Automatic recognition of ligands in electron density by machine learning. *Bioinformatics, 35*(3), 452-461. 10.1093/bioinformatics/bty626

Kumaran, S., Yi, H., Krishnan, H. B., & Jez, J. M. (2009). Assembly of the Cysteine Synthase Complex and the Regulatory Role of Protein-Protein Interactions. *Journal of Biological Chemistry, 284*(15), 10268-10275. 10.1074/jbc.m900154200

Laskowski, R. A., & Swindells, M. B. (2011). LigPlot+: multiple ligand-protein interaction diagrams for drug discovery. *J Chem Inf Model, 51*(10), 2778-2786. 10.1021/ci200227u

Liang, J., Han, Q., Tan, Y., Ding, H., & Li, J. (2019). Current Advances on Structure-Function Relationships of Pyridoxal 5′ -Phosphate-Dependent Enzymes. *Frontiers in Molecular Biosciences, 6* 10.3389/fmolb.2019.00004

Lipinski, C. A. (2000). Drug-like properties and the causes of poor solubility and poor permeability. *J Pharmacol Toxicol Methods, 44*(1), 235-249. 10.1016/s1056-8719(00)00107-6

Maher, C., & Hassan, K. A. (2023). The Gram-negative permeability barrier: tipping the balance of the in and the out. *mBio, 14*(6) 10.1128/mbio.01205-23

Matthews, B. W. (1968). Solvent content of protein crystals. *Journal of Molecular Biology, 33*(2), 491-497. https://doi.org/10.1016/0022-2836(68)90205-2

McCoy, A. J., Grosse-Kunstleve, R. W., Adams, P. D., Winn, M. D., Storoni, L. C., & Read, R. J. (2007). Phasercrystallographic software. *Journal of Applied Crystallography, 40*(4), 658-674. 10.1107/s0021889807021206

McGarvie, J., Oldham, K., Warrender, A., Prentice, E., & Hicks, J. (2025). Characterisation of O-acetylserine sulfhyrdrylase (CysK) enzymes from bacteria lacking a sulfate reduction pathway. *bioRxiv*, 2025.2003.2026.645513. 10.1101/2025.03.26.645513

McPhillips, T. M., McPhillips, S. E., Chiu, H. J., Cohen, A. E., Deacon, A. M., Ellis, P. J., . . . Kuhn, P. (2002). Blu-Ice and the Distributed Control System: software for data acquisition and instrument control at macromolecular crystallography beamlines. *J Synchrotron Radiat, 9*(Pt 6), 401-406. 10.1107/s0909049502015170

Mino, K., & Ishikawa, K. (2003). A novel O-phospho-L-serine sulfhydrylation reaction catalyzed by O-acetylserine sulfhydrylase from Aeropyrum pernix K1. *FEBS Letters, 551*(1-3), 133-138. 10.1016/s0014-5793(03)00913-x

Murima, P., John, & Pethe, K. (2014). Targeting Bacterial Central Metabolism for Drug Development. *Chemistry & Biology, 21*(11), 1423-1432. 10.1016/j.chembiol.2014.08.020

Poyraz, Ö., Jeankumar, V. U., Saxena, S., Schnell, R., Haraldsson, M., Yogeeswari, P., . . . Schneider, G. (2013). Structure-Guided Design of Novel Thiazolidine Inhibitors of O-Acetyl Serine Sulfhydrylase from Mycobacterium tuberculosis. *Journal of Medicinal Chemistry, 56*(16), 6457-6466. 10.1021/jm400710k

Remmele, C. W., Xian, Y., Albrecht, M., Faulstich, M., Fraunholz, M., Heinrichs, E., . . . Rudel, T. (2014). Transcriptional landscape and essential genes of Neisseria gonorrhoeae. *Nucleic Acids Research, 42*(16), 10579-10595. 10.1093/nar/gku762

Robert, X., & Gouet, P. (2014). Deciphering key features in protein structures with the new ENDscript server. *Nucleic Acids Research, 42*(W1), W320-W324. 10.1093/nar/gku316

Rosa, B., Marchetti, M., Paredi, G., Amenitsch, H., Franko, N., Benoni, R., . . . Bettati, S. (2019). Combination of SAXS and Protein Painting Discloses the Three-Dimensional Organization of the Bacterial Cysteine Synthase Complex, a Potential Target for Enhancers of Antibiotic Action. *International Journal of Molecular Sciences, 20*(20), 5219. 10.3390/ijms20205219

Salsi, E., Bayden, A. S., Spyrakis, F., Amadasi, A., Campanini, B., Bettati, S., . . . Mozzarelli, A. (2010). Design of O-Acetylserine Sulfhydrylase Inhibitors by Mimicking Nature. *Journal of Medicinal Chemistry, 53*(1), 345-356. 10.1021/jm901325e

Salsi, E., Campanini, B., Bettati, S., Raboni, S., Roderick, S. L., Cook, P. F., & Mozzarelli, A. (2010). A two-step process controls the formation of the bienzyme cysteine synthase complex. *J Biol Chem, 285*(17), 12813-12822. 10.1074/jbc.M109.075762

Schneider, G., Käck, H., & Lindqvist, Y. (2000). The manifold of vitamin B6 dependent enzymes. *Structure, 8*(1), R1-R6. 10.1016/s0969-2126(00)00085-x

Seib, K. L., Wu, H.-J., Kidd, S. P., Apicella, M. A., Jennings, M. P., & McEwan, A. G. (2006). Defenses against Oxidative Stress in*Neisseria gonorrhoeae* a System Tailored for a Challenging Environment. *Microbiology and Molecular Biology Reviews, 70*(2), 344-361. 10.1128/mmbr.00044-05

Semchenko, E. A., Day, C. J., & Seib, K. L. (2017). MetQ of Neisseria gonorrhoeae Is a Surface-Expressed Antigen That Elicits Bactericidal and Functional Blocking Antibodies. *Infect Immun, 85*(2) 10.1128/iai.00898-16

Sterling, T., & Irwin, J. J. (2015). ZINC 15 – Ligand Discovery for Everyone. *Journal of Chemical Information and Modeling, 55*(11), 2324-2337. 10.1021/acs.jcim.5b00559

Takahashi, H., & Watanabe, H. (2005). A gonococcal homologue of meningococcal γ-glutamyl transpeptidase gene is a new type of bacterial pseudogene that is transcriptionally active but phenotypically silent. *BMC Microbiology, 5*(1), 56. 10.1186/1471-2180-5-56

Takumi, K., & Nonaka, G. (2016). Bacterial Cysteine-Inducible Cysteine Resistance Systems. *Journal of Bacteriology, 198*(9), 1384-1392. 10.1128/jb.01039-15

Terwilliger, T. C., Grosse-Kunstleve, R. W., Afonine, P. V., Moriarty, N. W., Zwart, P. H., Hung, L.-W., . . . Adams, P. D. (2008). Iterative model building,

structure refinement and density modification with thePHENIX AutoBuildwizard. *Acta Crystallographica Section D Biological Crystallography, 64*(1), 61-69. 10.1107/s090744490705024x

Toyomoto, T., Ono, K., Shiba, T., Momitani, K., Zhang, T., Tsutsuki, H., . . . Sawa, T. (2023). Alkyl gallates inhibit serine O-acetyltransferase in bacteria and enhance susceptibility of drug-resistant Gram-negative bacteria to antibiotics. *Front Microbiol, 14*, 1276447. 10.3389/fmicb.2023.1276447

Turnbull, A. L., & Surette, M. G. (2008). L-Cysteine is required for induced antibiotic resistance in actively swarming *Salmonella enterica* serovar Typhimurium. *Microbiology, 154*(Pt 11), 3410-3419. 10.1099/mic.0.2008/020347-0

Turnbull, A. L., & Surette, M. G. (2010). Cysteine biosynthesis, oxidative stress and antibiotic resistance in Salmonella typhimurium. *Research in Microbiology, 161*(8), 643-650. https://doi.org/10.1016/j.resmic.2010.06.004

Unemo, M., Seifert, H. S., Hook, E. W., Hawkes, S., Ndowa, F., & Dillon, J.-A. R. (2019). Gonorrhoea. *Nature Reviews Disease Primers, 5*(1), 79. 10.1038/s41572-019-0128-6

Wang, T., & Leyh, T. S. (2012). Three-stage Assembly of the Cysteine Synthase Complex from Escherichia coli. *Journal of Biological Chemistry, 287*(6), 4360-4367. 10.1074/jbc.m111.288423

Weiss, J. N. (1997). The Hill equation revisited: uses and misuses. *The FASEB Journal, 11*(11), 835-841. https://doi.org/10.1096/fasebj.11.11.9285481

WHO. (2024). *WHO Bacterial Priority Pathogens List, 2024.* Retrieved from https://iris.who.int/bitstream/handle/10665/376776/9789240093461-eng.pdf?sequence=1

Winn, M. D., Ballard, C. C., Cowtan, K. D., Dodson, E. J., Emsley, P., Evans, P. R., . . . Wilson, K. S. (2011). Overview of theCCP4 suite and current developments. *Acta Crystallographica Section D Biological Crystallography, 67*(4), 235-242. 10.1107/s0907444910045749

# Chapter Four: Characterisation of O-acetylserine sulfhydrylase (CysK) from

# bacteria lacking a sulfate reduction pathway

## 4.1 Preface

Investigating alternative sulfur metabolic pathways is a promising avenue for understanding the deeper mechanisms of our planet and of evolution. There are a vast array of sulfur acquisition, assimilation and metabolic pathways yet to be characterised. Scavenging of nutrients such as sulfur, is well-established to play a key role in the success of a pathogen to adapt to the host environment. All bacterial sulfur metabolism converged on *de novo* L-cysteine biosynthesis which is highly conserved across bacteria, protists, and plant species. Previous research has discovered a genomic disruption in the sulfate reduction arm of L-cysteine biosynthesis in both *Staphylococcus aureus* and *Neisseria gonorrhoeae* (Hicks & Mullholland, 2018; Lithgow, Hayhurst, Cohen, Aharonowitz, & Foster, 2004; Soutourina et al., 2009), however the key biosynthetic enzymes Serine *O*-acetyltransferase (SAT/CysE) and *O*-acetylserine sulfhydrylase (OASS-A/CysK) remained intact. *N. gonorrhoeae* and *S. aureus* have been reported to grow using thiosulfate as a sole sulfur source (Le Faou, 1984; Lithgow et al., 2004). However, *S. aureus* is unable to import thiosulfate (Lithgow et al., 2004; Soutourina et al., 2009), and the *N. gonorrhoeae* OASS isoform sequence matches more closely to a CysK isoform (which is unable to use thiosulfate) (Hicks & Mullholland, 2018) raising intriguing questions as to how sulfate metabolism functions in these two pathogens. This chapter builds upon the previous work in Chapter Three where we presented analysis of the NgCysK crystal structure and the promising hit, compound 5 we will use for downstream optimisation to inhibit NgCysK as an antimicrobial adjuvant. In this chapter, we have analysed the substrate specificity of CysK from *Staphylococcus aureus* and *Neisseria* gonorrhoeae, evaluated the structural changes induced by substrate binding, as well as determining the ability of *N. gonorrhoeae* to form the cysteine synthase complex using small angle X-ray scattering (SAXS) and kinetic assay analysis.

The work presented in this chapter is shown in a publication format as a manuscript submitted for publication to the journal; *Biochemcial Journal*. Included in this

chapter is a Future directions section (4.8), which itself is not part of the manuscript, but has been included to discuss ongoing future work directly related to the project; these results will be included in future publications. Supplementary information available in Appendix B.

The citation for this publication is as follows:

**McGarvie, J.**, Oldham, K., Warrender, A., Prentice, E., & Hicks, J. (2025). Characterisation of O-acetylserine sulfhyrdrylase (CysK) enzymes from bacteria lacking a sulfate reduction pathway. *bioRxiv*, 2025.2003.2026.645513. 10.1101/2025.03.26.645513

## 4.2 Author contributions

I led the experimental work for this research, as first author, which involved enzyme purification, method optimisation, collection and analysis of kinetic assay data; sample preparation, running and analysis of SAXS data; as well as figure preparation, writing and editing of the manuscript. Erica Prentice contributed to the interpretation and analysis of kinetic data. Jessica Usu was responsible for collection of some of the SAXS data. Joanna Hicks conceptualised the research, provided funding for the project, cloned NgCysK, collected some of the SAXS data, contributed to manuscript writing and editing, and prepared the manuscript for submission. The authorship contribution form can be found in Appendix C.

# Characterisation of O-acetylserine sulfhyrdrylase (CysK) enzymes from bacteria lacking a sulfate reduction pathway.

**Jack McGarvie[1,2]**, Keely E.A. Oldham[2], Annmaree Warrender[2], Erica Prentice[2], & Joanna L. Hicks[1]

Joanna L. Hicks[1], Keely E.A. Oldham[1,2], **Jack McGarvie[1]** and Emma J. Walker[1]

[1] *Te Huataki Waiora, School of Health, University of Waikato, Hamilton, New Zealand*

[2] *Te Aka Matuatua, School of Science, University of Waikato, Hamilton, New Zealand*

## 4.3 Abstract

Sulfur metabolism plays an important role in bacterial pathogenesis. Elucidation of differences in sulfur metabolism across bacterial pathogens furthers our understanding of host survival and offers opportunities to disrupt these pathways for new therapies. Within bacteria sulfur metabolism converges at the synthesis of L-cysteine. One of the key mechanisms of obtaining sulfur for the synthesis of L-cysteine is the successive reduction of sulfate to sulfide via the sulfate reduction pathway. Accordingly, L-cysteine biosynthesis is a critical metabolic pathway for bacterial survival, particularly in pathogenic species such as *Neisseria gonorrhoeae* and *Staphylococcus aureus*, which lack the sulfate reduction pathway. O-acetylserine sulfhydrylase catalyses the second step of the two-step synthesis reaction, condensing sulfide or thiosulfate (in the case of OASS-A/CysK or OASS-B/CysM respectively) with O-acetylserine to synthesize cysteine. Here we investigate the enzymatic properties and functional characterization of O-acetylserine sulfhydrylase, from *N. gonorrhoeae* and *S. aureus*, with a focus on substrate specificity, kinetic parameters, and cysteine synthase complex (CSC) formation. Using small angle X-ray scattering and kinetic assays we demonstrate that both *N. gonorrhoeae* and *S. aureus* CysK enzymes utilise only sodium sulfide for the synthesis of cysteine, despite the lack of a sulfate reduction pathway (to

generate sulfide) in these organisms. Both enzymes demonstrate a higher affinity for *O*-acetylserine (OAS) compared to sodium sulfide ($Na_2S$). We also show that the two cysteine synthesis enzymes, CysE and CysK that traditionally form the cysteine synthase complex do not form a complex in *N. gonorrhoeae*. These findings highlight the functional divergence in sulfur metabolism strategies among bacteria lacking sulfate reduction and provide deeper insights into the adaptive mechanisms of *N. gonorrhoeae* and *S. aureus* in sulfur flux.

## 4.4 Introduction

Sulfur, biblically referred to as brimstone, is the fifth most common element found on earth (Sosa Torres, Rito Morales, Solano Peralta, & Kroneck, 2020). Sulfur is readily available in many different forms, including the inorganic compounds elemental sulfur ($S_8$), sulfate ($SO_4^{2-}$), sulfide ($S^{2-}$), sulfite ($SO_3^{2-}$), thiosulfate ($S_2O_3^{2-}$), and the polythionates ($S_3O_6^{2-}$; $S_4O_6^{2-}$) (Sosa Torres et al., 2020). Sulfur also plays a vital role within central biochemistry as a redox active and structural element, due to its wide array of stable oxidation states (Kertesz, 2000; Sosa Torres et al., 2020). The survival of bacteria is dependent on sulfur metabolism with sulfur comprising 0.5-1% of microbial cells dry weight, found in amino acids (e.g. methionine and cysteine), enzyme co-factors (e.g. coenzyme A/M, lipoic acid, biotin, and thiamine), and the foundations of redox reactions (e.g. iron-sulfur complexes, and the redox-active components of disulfide bonds) (Kertesz, 2000; Wu et al., 2021).

Bacterial sulfur metabolism is crucial for bacterial survival. Import of sulfur containing metabolites for biosynthetic processes is derived from assimilation of inorganic sulfate by plants and bacteria (Kertesz, 2000). *De novo* biosynthesis of L-cysteine is the main pathway for bacteria to acquire environmental inorganic sulfur. Within most bacteria, cysteine biosynthesis begins with the import of sulfate into the cell where it is subsequently reduced via the reductive sulfate assimilation pathway (RSAP) (Campanini et al., 2015). The major facilitator superfamily (MFS) and the ATP-binding cassette (ABC) superfamily are the two main families of sulfate transporter proteins responsible for the uptake of inorganic sulfate into microbial cells, via active import (Guédon & Martin-Verstraete, 2007; Kertesz, 2001). Once inside the cell, successive reduction of sulfate prepares the sulfide for

incorporation into L-cysteine (Figure 4.1). *Escherichia coli* first reduces sulfate to adenosine 5'-phosphosulfate (APS) using the multi-enzyme complex ATP sulfyhdrylase (CysDN) (Sekowska, Kung, & Danchin, 2000). In most bacteria, APS is reduced to phosphoadenosylphosphosulfate (PAPS) by ATP-kinase (CysC), and PAPS reductase (CysH) subsequently reduces PAPS to sulfite and phosphoadenosylphosphate (PAP) (Kredich, 2008; Sekowska et al., 2000). In *Neisseria* species, the reduction of APS to PAPS, and subsequent reduction to sulfite and PAP, is completed in a single step reaction by APS reductase (Rusniok et al., 2009). Finally, sulfite reductase (CysIJ) reduces sulfite to sulfide (Kredich, 2008) which is subsequently combined with *O*-acetylserine, forming L-cysteine (Figure 4.1).

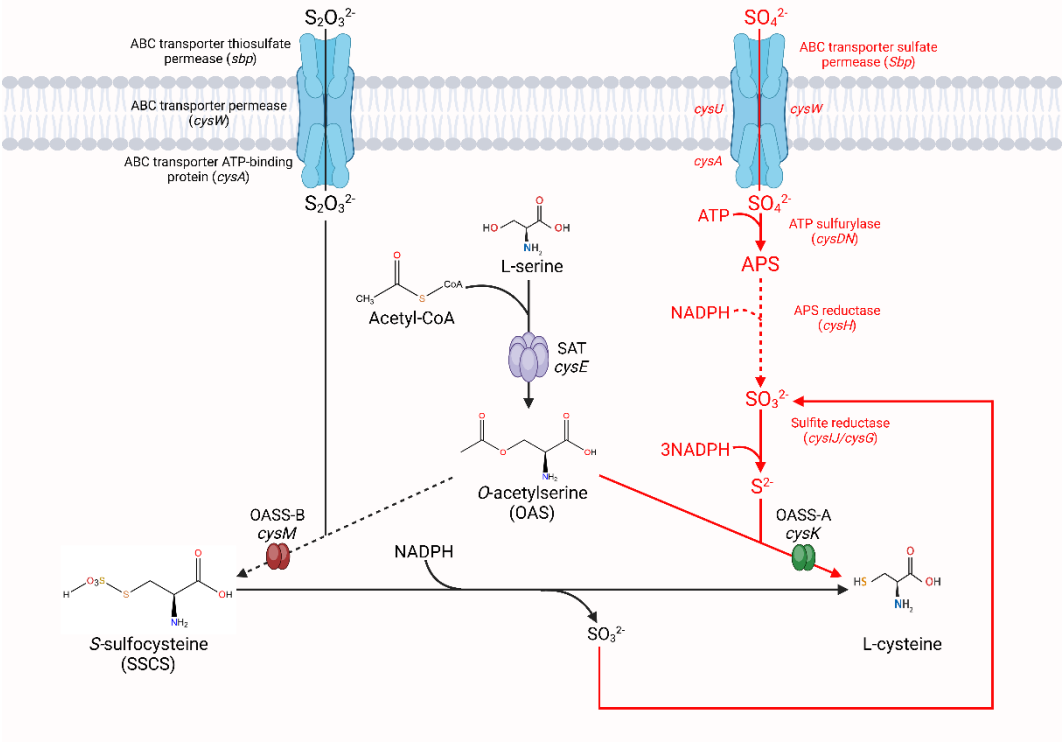


**Figure 4.1:** Sulfate acquisition and cysteine biosynthetic pathways in *Neisseria* species

Interestingly, some bacterial pathogens are missing sections of the sulfate reduction pathway, including the notable pathogens *Neisseria gonorrhoeae* and *Staphylococcus aureus*. *N. gonorrhoeae* has only a single sulfate uptake system from the ABC transporter superfamily in its genome (Hicks & Mullholland, 2018) composed of a transporter permease (*cysW*), an ATP-binding protein (*cysA*), a periplasmic sulfate-binding protein (*sbp*), and a sulfate permease (*cysU*) which is present in all *N. gonorrhoeae* strains except for FA1090 (Hicks & Mullholland,

2018; Kertesz, 2001). However, there is a 3.5 kb deletion between the *cysG* and *cysN* genes in all *N. gonorrhoeae* strains, resulting in the removal of *cysH* and *cysD* from this operon (Hicks & Mullholland, 2018). These genes are not present anywhere else in the *N. gonorrhoeae* genome. An in-frame stop codon present in each coding sequence of the sulfite reductase encoding genes, *cysIJ*, within the *N. gonorrhoeae* genome, renders these proteins non-functional (Hicks & Mullholland, 2018). The combination of these deletions and stop codons culminate in a non-functional sulfate reduction pathway in *N. gonorrhoeae.* Unlike *N. gonorrhoeae, S. aureus* is completely lacking any sulfate, thiosulfate or R-sulfonate importers (Lithgow et al., 2004; Soutourina et al., 2009). Not only does it lack the ability to import these important sulfur sources, but similar to *N. gonorrhoeae, S. aureus* lacks the sulfate reductase gene *cysI*, preventing it from reducing sulfate to sulfite (Lithgow et al., 2004; Soutourina et al., 2009). Accordingly, *N. gonorrhoeae* and *S. aureus* share an inability to grow on sulfate as a sole sulfur source, consistent with a non-functional sulfate reduction pathway as described. They are, however, able to use thiosulfate as a sole sulfur source (Le Faou, 1984; Soutourina et al., 2009), with the L-cysteine requirement of both bacteria being met by thiosulfate, suggesting the ABC transporter complex in *N. gonorrhoeae* is able to import thiosulfate (Hicks & Mullholland, 2018), and the presence of a yet unknown thiosulfate uptake system in *S. aureus* (Lithgow et al., 2004).

The final step of the pathway is the biosynthesis of L-cysteine. Cysteine is a key amino acid in proteins, and other biomolecules such as coenzyme A and is required for the synthesis of reducing agents such as thioredoxin and glutathione, which are essential for mitigating intracellular oxidants and resisting host immune responses (Carmel-Harel & Storz, 2000; Hicks & Mullholland, 2018; Kredich, 2008). One of the primary challenges for bacteria, in particular pathogenic bacteria, is surviving the hostile host environment and evading the host immune system, both of which *N. gonorrhoeae* and *S. aureus* are proficient in (de Jong Nienke, van Kessel Kok, & van Strijp Jos, 2019; Quillin & Seifert, 2018). Both pathogens are constantly under pressure of oxidative killing from the host (de Jong Nienke et al., 2019; Gaupp, Ledala, & Somerville, 2012; Seib et al., 2006), making mechanisms to mitigate this oxidative stress extremely important. The immune system exerts this

oxidative killing mechanism primarily through polymorphonuclear neutrophils (PMNs) (de Jong Nienke et al., 2019; Gaupp et al., 2012; Quillin & Seifert, 2018; Seib et al., 2006). To mitigate this oxidative stress, an effective intracellular reducing system is required, and most compounds within this system are derived from L-cysteine. Glutathione, synthesised by glutathione reductase, prevents unwanted oxidation of cellular compounds, and regulates the redox balance when encountering free radicals released by the host cell (Meister & Anderson, 1983; Pinto et al., 2013). Thus, intracellular glutathione levels are one of the main oxidative stress mitigating mechanisms deployed during infection. Here is where distinct differences between *N. gonorrhoeae* and *S. aureus* sulfur metabolism can be seen. *N. gonorrhoeae* lacks the ability to recycle glutathione (Seib et al., 2006) and lacks glutathione import machinery (Hicks & Mullholland, 2018), whereas, *S. aureus* only lacks the ability to synthesise glutathione, therefore relying on its import (Lensmire et al., 2023).

Bacteria also retain the ability to obtain L-cysteine from the environment. The ability to import L-cysteine and L-cystine is well conserved across many bacterial species, particularly in pathogens, giving a distinct advantage over the energetically expensive *de novo* biosynthesis of L-cysteine (Takahashi, Watanabe, Kim, Yokoyama, & Yanagisawa, 2018). In an oxidative environment such as those of *N. gonorrhoeae* and *S. aureus* infection sites (Edwards & Butler, 2011; Gaupp et al., 2012), L-cysteine is commonly found in its oxidised form, L-cystine (Korshunov, Imlay, & Imlay, 2020). *N. gonorrhoeae* has ABC transporters for both L-cysteine (*ngo2011-2014*), and L-cystine (*ngo0372-0374*) (Figure 4.1) (Bulut et al., 2012; Hicks & Mullholland, 2018). *S. aureus* is also capable of importing L-cysteine and L-cystine using its symporter tcyP (*SA0368*) and ABC transporter tycABC (*SA2202-SA2200*) (Soutourina et al., 2009). However, in the cysteine/cystine deplete or oxidative environment of *N. gonorrhoeae* and *S. aureus* infection, transportation alone would not fulfil L-cysteine requirements, therefore justifying the need for *de novo* biosynthesis of L-cysteine.

L-cysteine biosynthesis occurs in a two-step reaction, catalysed by two enzymes, serine acetyltransferase (SAT) and *O*-acetylserine sulfydrylase (OASS), denoted as CysE and CysK/CysM (OASS isoforms), respectively. Initially CysE, acetylates L-

serine, forming *O*-acetylserine and CoA (Figure 4.2). In the final step, CysK catalyses a condensation reaction of *O*-acetylserine with sulfide, producing L-cysteine (Figure 4.2).

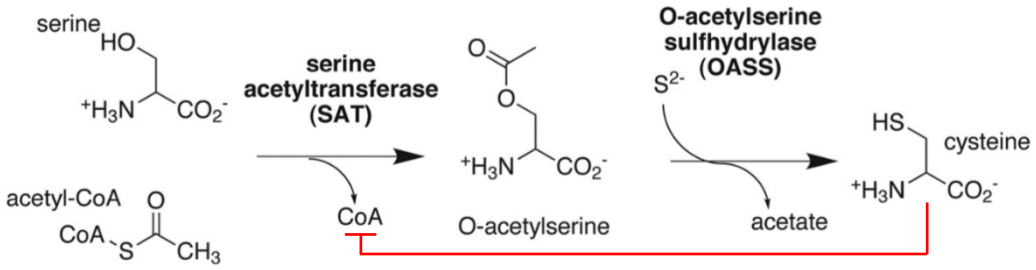


**Figure 4.2:** Cysteine biosynthesis pathway. CysE denoted as SAT and CysK denoted as OASS

CysE belongs to the left-handed parallel β-helix family and catalyses the first step of this reaction in both bacteria and plants (Johnson, Roderick, & Cook, 2005). In both *S. aureus* and *N. gonorrhoeae,* CysE has been identified as an essential gene (Chaudhuri et al., 2009; Remmele et al., 2014), and whilst non-essential in *N. meningitidis,* the *cysE* deletion strain confers impaired growth in media (Capel et al., 2016). L-cysteine feedback inhibition of CysE is well conserved across bacteria, regulates the first step of the two-step biosynthesis pathway (Figure 4.2), and acts as the primary method of prevention for high concentrations of intracellular L-cysteine, which are toxic to bacteria (Benoni, De Bei, et al., 2017a; Takumi & Nonaka, 2016).

OASS is a PLP dependent enzyme belonging to both the tryptophan synthase β superfamily, and the β-family of pyridoxal 5'-phopshate (PLP) dependent enzymes (Guédon & Martin-Verstraete, 2007; Mino & Ishikawa, 2003; Takumi & Nonaka, 2016). There are two commonly found isoforms of OASS, OASS-A (CysK) and OASS-B (CysM) (Kredich, 2008). Most bacteria have both isoforms, using CysK (OASS-A) and CysM (OASS-B) for cysteine biosynthesis using sulfide or thiosulfate respectively. *Salmonella enterica* Servovar typhimurium is one such example, however, expression was found to be environmentally dependent, where CysK (OASS-A) was expressed in excess of CysM (OASS-B) under aerobic conditions, and vice versa under anaerobic conditions (Tai, Nalabolu, Jacobson, Minter, & Cook, 1993). CysM, unlike CysK, can directly use thiosulfate to produce S-sulfocysteine, which is subsequently reduced to L-cysteine (Tai et al., 1993). Interestingly, *N. gonorrhoeae* and *S. aureus* have only one OASS isoform, which has higher homology to CysK (OASS-A) and is hypothesised to use sulfide for

L-cysteine biosynthesis (Hicks & Mullholland, 2018; Pederick et al., 2024). With *N. gonorrhoeae* and *S. aureus* lacking the ability to reduce sulfate to sulfide, and relying on thiosulfate for cysteine biosynthesis, a substrate which only the CysM isoform utilises, intriguing questions regarding the role of OASS within these pathogenic bacteria arise, especially considering the annotation of the OASS from *S. aureus* as the CysM isoform (Lithgow et al., 2004).

Due to the cytotoxic nature of high L-cysteine concentrations, L-cysteine biosynthesis is well regulated in bacteria. The L-cysteine regulon is controlled at the transcriptional level by CysB, a homotetramer, and a member of the LysR family of transcription factors (Hicks & Mullholland, 2018; Jovanovic, Lilic, Savic, & Jovanovic, 2003). CysB can bind to DNA due to the helix-turn-helix motif within the N-terminal domain (Lochowska et al., 2004). The CysE product OAS is unstable and rapidly isomerises to *N*-acetylserine (NAS) (Kredich, 1992; Wirtz & Hell, 2006), both of which bind to CysB, causing positive regulation of L-cysteine biosynthesis and sulfate acquisition genes, however, NAS produces an estimated 15-fold higher response (Hryniewicz & Kredich, 1991; Kredich, 1992; Ostrowski & Kredich, 1989). CysB upregulates the sulfate acquisition genes *cysJIH, cysK,* and *csyP,* whilst negatively autoregulating its own transcription via upstream binding of its own promoter (Lochowska et al., 2004; Ostrowski & Kredich, 1989, 1991). Pathogenic bacteria depend on their ability to adapt and overcome host defences rapidly, making transcriptional regulation of both the L-cysteine regulon and the sulfate acquisition pathway vital. Interestingly, *cysB* has been identified as an essential gene in *N. gonorrhoeae* (Remmele et al., 2014), but not in *S. aureus* (Chaudhuri et al., 2009).

Feedback inhibition of CysE, and transcriptional regulation are not the only methods of regulating sulfur metabolism and flux. Another mechanism within this pathway lies with the formation of the cysteine synthase complex (CSC). The complex combines the two enzymes that catalyse L-cysteine biosynthesis, CysE and CysK, proven by gel chromatography and fluorescence to consist of one CysE hexamer and two CysK dimers giving a 3:2 protomer ratio (Benoni, De Bei, et al., 2017a; Hicks & Mullholland, 2018; Johnson et al., 2005; Kredich, Becker, & Tomkins, 1969). The CSC was first characterised from *S. typhimurium* (Kredich et

al., 1969; Kredich & Tomkins, 1966) and there is further evidence of CSC formation in other bacterial species, including *E. coli* (Benoni, De Bei, et al., 2017a, 2017b; Mino, Yamanoue, et al., 2000a, 2000b), *Haemophilus influenzae* (Huang, Vetting, & Roderick, 2005), and *Mycobacterium tuberculosis* (Schnell, Oehlmann, Singh, & Schneider, 2007). CSC formation is controlled by the availability of sulfur and involves the C-terminal tail of CysE inserting into the active site of CysK, almost completely inhibiting its activity (Saito, Yokoyama, Noji, & Murakoshi, 1995). When in the complex, CysE loses sensitivity to feedback inhibition by L-cysteine, has reduced substrate inhibition from L-serine and therefore increased catalytic activity (Benoni, De Bei, et al., 2017a).

When sulfur is readily available to the cell, the CSC is stabilised by bisulfide, however, with low sulfur availability, OAS accumulates, dissociating the complex and signalling sulfur starvation (Benoni, De Bei, et al., 2017a; Zhao et al., 2006). This dissociation can occur at μM OAS concentrations (upwards of 50μM OAS) (Kredich et al., 1969; Wang & Leyh, 2012), OAS then chemically isomerises to NAS, which binds to transcriptional regulator CysB, promoting expression of sulfate acquisition genes (Jovanovic et al., 2003; Kredich, 2008; Wang & Leyh, 2012). Fluorescent spectroscopy confirmed binding of the CysE C-terminal peptide binding in the CysK active site, where binding affinity was monitored by CysK activity and PLP fluorescence (Campanini et al., 2015). The CSC structure has yet to be elucidated, however, there is a crystal structure of CysK from *H. influenzae,* with a CysE 10 residue C-terminal peptide bound in the active site (Huang et al., 2005). The key residues for binding were determined via tetrapeptide library screening, indicating a C-terminal isoleucine (Ile) is essential for binding and inhibition of CysK, which remains well conserved across CSC forming bacteria, including *S. typhimurium, H. influenzae* and *E. coli* (Benoni, De Bei, et al., 2017a; Huang et al., 2005; Salsi et al., 2010).

## 4.5 Materials and methods

### 4.5.1 Cloning of Neisseria gonorrhoeae, Staphylococcus aureus, and Escherichia coli cysK for expression in Escherichia coli

The *cysK* genes NGO_0340 (*N. gonorrhoeae*), SAA6008_00518 (*S. aureus*), and NP_416909.1 (*E. coli*) were codon optimised for *E. coli* and ordered from Geneart

(ThermoFisher) and Twist Bioscience. The synthetic *cysK* constructs were cloned into expression vector pET28b-PstI with a C-terminal hexahistidine-tag, between PstI and XhoI restriction sites. The plasmids for each *cysK* pET28b plasmid were confirmed by DNA sequencing before transformation into *E. coli* BL21 (DE3) for protein expression. Positive transformants were selected for by growing overnight at 37°C, in Luria-Bertani (LB) agar supplemented with 50 $\mu g.ml^{-1}$ kanamycin.

### 4.5.2 CysK expression and purification

The same method was used for all CysK variants. *E. coli* BL21 (DE3) containing the NGO_0340_pET28b, SAA6008_00518_pET28b, and NP_416909.1_pET28b plasmid were cultured in 1 L LB broth, supplemented with 50 $\mu g.ml^{-1}$ kanamycin. Cultures were incubated at 37 °C (200 rpm) until an $OD_{600}$ of 0.5-0.7. Protein expression was induced by the addition of 0.75 mM IPTG and cultures were incubated at 22 °C (200 rpm) overnight. Cultures were centrifuged at 4,600 ***g*** for 20 min at 4 °C and the resulting cell pellet was resuspended in lysis buffer (50 mM potassium phosphate pH 7.0, 200 mM NaCl, 20 mM imidazole). One Complete Mini, EDTA-free protease inhibitor tablet (Roche), and 0.1 mM PLP were added prior to cell lysis by sonication. Lysate was centrifuged at 29,097 ***g*** for 25 min at 4 °C and 0.2 µm filtered supernatant was loaded onto a pre-equilibrated HisTrap™ column (GE Healthcare). The column was washed with 20 ml lysis buffer before the elution of CysK using a 50% gradient over 25 ml (50 mM potassium phosphate pH 7.0, 200 mM NaCl, 1 M imidazole).

Immobilised-metal ion affinity chromatography-purified (IMAC-purified) CysK was concentrated at 4 °C using an Amicon® Ultra-15 Centrifugal Filter Units (10 kDa molecular weight cutoff) to a final volume of 5 ml. Concentrated CysK was loaded and run through a HiLoad™ 16/60 Superdex™ 75 column (GE Healthcare), preequilibrated in 50 mM Potassium phosphate pH 7.0, 100 mM NaCl and eluted CysK was collected and stored at 4 °C. Protein concentration was measured by absorbance at 280 nm by Nanodrop™. All CysK enzymes showed strong yellow colour post-purification, and fluorescent emission spectra at ~500 nm when excited at 400 nm was seen in NgCysK, indicating the presence of the internal PLP, as a ketoenamine tautomer (Figure B.1).

### 4.5.3 CysK Kinetic assays

CysK for kinetic characterisation was purified immediately prior to assays. Enzyme was stored at 4 °C for the duration of the assay, as a rapid decrease in activity was observed when stored at room temperature. Assays were conducted within 14 h post-purification as CysK activity slowly decreased over time. CysK activity was measured by adapting a method from (Gaitonde, 1967). CysK activity was monitored via absorbance measurements of L-cysteine at 560 nm ($A_{560}$) using a SpectraMax ® M Series Multi-Mode Microplate Reader (Molecular devices**).**

To measure the $K_M$ and $V_{max}$ for the substrate *O*-acetylserine (OAS), assays were carried out in 96-well PCR microplates, with a reaction volume of 75 µL, containing variable volumes of 100 mM MOPs (pH 7.0), sodium sulfide ($Na_2S$) (30 mM for NgCysK without glycerol, 7 mM for NgCysK with glycerol, and 15 mM for SaCysK with and without glycerol), and variable amounts of OAS. The reaction was performed at 37 °C after the addition and subsequent spin down (30 seconds at 2500 ***g***) of 0.2 µg of purified CysK. After addition of acid ninhydrin (100 µl) and glacial acetic acid (100 µl), reaction mixtures were incubated at 95 °C (5 min) forming a pink chromophore (an L-cysteine + ninhydrin derivative), and subsequently incubated on ice (5 min). Ice cold ethanol (100%) was added to 100 µl of each reaction mixture and absorbance of the pink chromophore (560 nm) measured. Enzyme concentration in activity assays was optimised for SaCysK (as SaCysK had noticeably higher reaction rates than NgCysK) by testing various amounts of SaCysK (0.0058, 0.058, 0.2, 0.4, 0.58, 0.75, 1, 2.5, 3.5, 5.8, and 58 ug; Figure B.2) and matched by NgCysK. All substrate stocks were prepared in MQ $H_2O$. Other components of the reactions and measurement step reagents can be found in the supplementary information. Enzyme working stocks of 0.05 $mg.ml^{-1}$ (1.47 µM SaCysK monomer, 34.011 kDa; 1.47 µM SaCysK monomer, 34.011 kDa, 25% glycerol v/v; 1.48 µM NgCysK monomer, 33.791 kDa; 1.48 µM NgCysK monomer, 33.791 kDa, 25% glycerol v/v) were stored at 4 °C for the duration of assays. The $K_M$ and $V_{max}$ were calculated for $Na_2S$, by varying the amount of $Na_2S$ and keeping the concentration of OAS constant at 10 mM across all enzymes. $K_M$ and $V_{max}$ values were determined by non-linear regression fit of the Michaelis Menten (Equation 4.1), allosteric sigmoidal (Equation 4.2), substrate inhibition **(**Equation 4.3), or the allosteric sigmoidal with substrate inhibition equation **(**Equation 4.4) using GraphPad Prism (GraphPad Software Version 10.2.3). The

initial velocity of the reaction was derived from linear-regression analysis of the first 5 minutes of the reaction using a cysteine standard curve (Equation 3.1; Figure B.2). All concentrations were collected in triplicate. Cysteine produced was calculated using a cysteine standard curve equation **(**Equation 3.1), and $k_{cat}$ was calculated by dividing the $V_{max}$ rate ($M.s^{-1}$) by the molar concentration of dimeric enzyme. The catalytic efficiency $k_{cat}/K_M$ ($M^{-1}s^{-1}$) was calculated by dividing the $k_{cat}$ ($s^{-1}$) by the $K_M$ (M). Catalytic efficiency values were calculated for each substrate.

**Equation 4.1.** The Michaelis Menten equation $Rate = \frac{V_{max}[S]}{K_M+[S]}$

$$Rate = \frac{V_{max}[S]}{K_M + [S]}$$

**Equation 4.2.** The allosteric sigmoidal equation $Rate = \frac{V_{max}[S^h]}{K_{half}+[S^h]}$

$$Rate = \frac{V_{max}[S^h]}{K_{half} + [S^h]}$$

**Equation 4.3.** The substrate inhibition equation $Rate = \frac{V_{max}[S]}{(K_m+S(\frac{1+S}{K_i}))}$

$$Rate = \frac{V_{max}[S]}{(K_m + S(\frac{1+S}{K_i}))}$$

**Equation 4.4.** The allosteric sigmoidal with substrate inhibition equation $Rate = \frac{v_{max}[S^h]}{(K_m^h+\left(S\left(1+\frac{S}{K_i}\right)\right)^h)}$

$$Rate = \frac{v_{max}[S^h]}{(K_m^h + \left(S\left(1 + \frac{S}{K_i}\right)\right)^h)}$$

**Equation 4.5.** L-cysteine standard curve for determining cysteine produced $x = \frac{y-0.0164}{1.8856}$

$$x = \frac{y - 0.0164}{1.8856}$$

### 4.5.4 Thiosulfate substrate assays

Thiosulfate substrate assays were conducted using a modified method from above. The key modification was substitution of thiosulfate for sodium sulfide in the reaction. Thiosulfate was added at low to high varied concentrations (final reaction concentration, 1-50 mM).

### 4.5.5 Small angle X-ray scattering (SAXS)

#### 4.5.5.1 Purification of CysE

NgCysE and EcCysE were purified using IMAC and gel filtration chromatography with minor modifications. CysE pellets were resuspended in lysis buffer (50 mM Tris pH 8.0, 200 mM NaCl, 20 mM imidazole). No PLP was added prior to sonication. Lysate was centrifuged at 20000 ***g*** for 20 min at room temperature. The pre-equilibrated HisTrap™ column (GE Healthcare) was washed with 20 ml lysis buffer before the elution of CysE using a 50% gradient over 25 ml (50 mM Tris pH 8.0, 200 mM NaCl, 1 M imidazole) (Oldham, Prentice, Summers, & Hicks, 2022). IMAC-purified CysE was concentrated at 15 °C using an Amicon® Ultra-15 Centrifugal Filter Units (10 kDa molecular weight cutoff) to a final volume of 0.75 ml (Oldham et al., 2022). Concentrated CysE was run through an Enrich 650 analytical gel filtration column (BioRad), pre-equilibrated in 50 mM Tris pH 8.0, 100 mM NaCl and stored at room temperature.

#### 4.5.5.2 Preparation of samples

NgCysK, EcCysK, SaCysK, NgCysE, and EcCysE were expressed and purified as mentioned above. SaCysE was unable to be purified as it remained insoluble. All CysK samples were concentrated using Amicon® Ultra-15 Centrifugal Filter Units (10 kDa molecular weight cutoff, centrifuged at 4 ºC and 3000 ***g***) and made up with glycerol (25% v/v final) and transported on ice. All CysE samples were prepared as close to the time of departure as possible (one or two days beforehand) and transported at room temperature to avoid cold inactivation (Mino, Yamanoue, et al., 2000a) or aggregation due to overconcentration. CysE samples were concentrated on site at the Australian Synchrotron using Amicon® Ultra-0.5 Centrifugal Filter Units (10 kDa molecular weight cutoff, centrifuged at 4 ºC and 13,000 ***g***).

#### 4.5.5.3 Data Collection

Experiments were conducted using the Australian Synchrotron SAXS/WAXS beamline equipped with a Dectris PILATUS 1M/200k detector coupled to a size exclusion chromatography (SEC) with a sheath flow cell (Kirby et al., 2016). Protein samples not analysed for CSC formation (non-CSC formation) were prepared in Potassium phosphate buffer (50 mM Potassium phosphate pH 7.0, 100 mM NaCl), and protein samples for potential CSC formation analysis were prepared in TRIS buffer (50 mM Tris pH 8.0, 100 mM NaCl)**.** Non-CSC formation samples were prepared to final concentrations of 4, 6 and 8 mg/ml in a 96-well plate (45 µl total volume). This allowed for correction of concentration dependent behaviours and the mitigation of potential sample aggregation. Potential CSC forming samples were prepared to a 3:2 CysE:CysK monomeric ratio with a 6 mg/ml final concentration in a 96-well plate (60 µl total volume). SEC was conducted using either a 3.2 mL Superdex S200 5/150 (Cytiva) for individual CysK non-CSC formation samples, or a 24 mL Superdex S200 5/150 (Cytiva) for CysK and CysE samples analysed for CSC formation, respectively. Each column was equilibrated with the appropriate buffer prior to sample loading; Potassium phosphate for the 3.2 mL Superdex S200 5/150 (Cytiva) column (for non-CSC samples); and TRIS (pH 8.0) for the 24 mL Superdex S200 5/150 (Cytiva) column (for potential CSC forming samples).

Scattering images were collected using instrument parameters as seen in Table 4.1 (Kirby et al., 2013). Scattering intensity was measured as a function of momentum transfer ($q$), where $q = 4\pi\sin(\theta)/\lambda$ and $2\theta$ is the scattering angle in Å (Kikhney & Svergun, 2015). Samples (45 or 60 µl injection volume) were run through the size exclusion columns at a flow rate of 0.4 ml/min (Table 4.2) and into a 1.5 mm thin-walled glass capillary where they were exposed to continuous one second x-ray bursts over an ~10 (3.2 ml column) or ~60 (24 ml column) minute elution period.

**Table 4.1.** SEC-SAXS Data Collection Parameters

| | |
|---|---|
| **Instrument** | Australian Synchotron SAXS/WAXS beamline with Dectris PILATUS 1M/200k detector (Kirby et al., 2013) |
| **Wavelength (Å)** | 1.033 |

| | |
|---|---|
| **Beam size (µm)** | 250 x 450 |
| **Camera length (m)** | 2.683 |
| ***q* measurement range (Å$^{-1}$)** | 0.0015-3.0 |
| **Absolute scaling method** | Comparison with scattering from 1 mm pure $H_2O$ |
| **Normalisation** | To transmitted intensity by beam-stop counter |
| **Monitoring for radiation damage** | X-ray dose maintained below 210 Gy, data frame-by-frame comparison |
| **Exposure time** | Continuous 1s data-frame measurements of SEC elution |
| **Sample configuration** | SEC-SAXS with sheath-flow cell (Kirby et al., 2016), effective sample path length 0.49 mm |
| **Sample temperature (ºC)** | 8 |

**Table 4.2.** SAXS sample details

| | NgCysK | EcCysK | SaCysK | NgCysE | EcCysE | NgCSC | EcCSC |
|---|---|---|---|---|---|---|---|
| **Organism** | *Neisseria gonorrhoeae* | *Escherichia coli* | *Staphylococcus aureus* | *Neisseria gonorrhoeae* | *Escherichia coli* | *Neisseria gonorrhoeae* | *Escherichia coli* |
| **Source** | *E. coli* expressed | *E. coli* expressed | *E. coli* expressed | *E. coli* expressed | *E. coli* expressed | *E. coli* expressed | *E. coli* expressed |
| **UniProt sequence ID (residues in construct)** | Q5F9Q2 (1-310) + C-terminal Hexa His-tag | P0ABK5 (1-323) + C-terminal Hexa His-tag | A0A0U1ME23 (1-301) + C-terminal Hexa His-tag | A0A1D3FX11 (1-272) + N-terminal Hexa His-tag | P0A9D4 (1-273) + N-terminal Hexa His-tag | Q5F9Q2 (1-310) C-terminal Hexa His-tag + A0A1D3F (1-272) N-terminal Hexa His-tag | P0ABK5 (1-323) C-terminal Hexa His-tag + P0A9D4 (1-273) N-terminal Hexa His-tag |
| **Extinction coefficient [$A_{280}$, 0.1% (*w/v*)]** | 0.594 | 0.535 | 1.112 | 0.598 | 0.855 | - | - |
| **$\bar{\upsilon}$ from chemical composition ($cm^3\ g^{-1}$)** | 0.743 | 0.743 | 0.733 | 0.740 | 0.739 | - | 0.741 |
| **Particle contrast from sequence and solvent constituent, $\Delta p$ ($p_{protein} - p_{solvent}$; $10^{10}\ cm^{-2}$)** | 2.775 | 2.780 | 2.895 | 2.799 | 2.811 | - | 2.798 |
| ***M* from chemical composition (Da)** | 32726 | 36780 | 32946 | 31600 | 31600 | 320504 | 336720 |
| **SEC-SAXS column (3.2 mL Superdex S200 5/150 (Cytiva))** | | | | | | | |
| **Loading concentration ($mg.ml^{-1}$)** | 6 | 6 | 6 | 6 | - | - | - |
| **Injection volume (ul)** | 45 | 45 | 45 | 45 | - | - | - |
| **Flow rate ($ml.min^{-1}$)** | 0.4 | 0.4 | 0.4 | 0.4 | - | - | - |
| **SEC-SAXS column (24 mL Superdex S200 5/150 (Cytiva))** | | | | | | | |
| **Loading concentration ($mg.ml^{-1}$)** | - | 6 | - | - | 6 | 6 | 6 |
| **Injection volume (ul)** | - | 45 | - | - | 45 | 60 | 60 |
| **Flow rate ($ml.min^{-1}$)** | - | 0.4 | - | - | 0.4 | 0.4 | 0.4 |
| **Solvent** | 50 mM TRIS, 100 mM NaCl, 0.1% Azide, pH 8.0 | | | | | | |

#### 4.5.5.4 Data Processing

The beamline intensity normalisation and subsequent data reduction was performed using the Australian Synchrotron developed software scatterBrain (version 2.71) (Table 4.3). Scattering files produced were aligned with the inline SEC profile using CHROMIXS (Panjkovich & Svergun, 2018). The sample-scattering frames were selected from the largest peak, corresponding with the dimeric or hexameric protein for all CysK and CysE enzymes respectively. In CSC samples, sample-scattering frames were selected from the initial peak corresponding to the decameric complex. In all cases, the buffer-scattering region was selected from upstream of the first protein elution peak. The buffer-scattering was subtracted from the selected sample-scattering and the processed scattering profiles were exported as *.dat files which are readable by the ATSAS package programmes. Unless stated otherwise, all downstream data processing was performed using the ATSAS program suite (version 3.1.0) (Manalastas-Cantos et al., 2021).

**Table 4.3.** Reduction and analysis software

| | |
|---|---|
| **SAXS data reduction** | *I(q) versus q* using s*catterBrain* 2.71 (http://www.synchotron.org.au/aussyncbeamlines/saxswaxs/software-saxswaxs), solvent subtraction using CHROMIXS (Panjkovich & Svergun, 2018) |
| **Extinction coefficient estimate** | *ProtParam (Gasteiger et al., 2005)* |
| **Calculation of Δ*p* and ῡ values** | *MULCh* 1.1 (Whitten, Cai, & Trewhella, 2008) |
| **Basic analyses: Guinier, *P*(*r*), $V_P$** | *PRIMUSqt* from *ATSAS 3.1.0 (Petoukhov et al., 2012)* |
| **Atomic structure modelling** | *CRYSOL* from *PRIMUSqt* in *ATSAS 3.1.0 (Svergun, Barberato, & Koch, 1995)* |

Subtracted scattering data was analysed using the PRIMUSqt software (Manalastas-Cantos et al., 2021; Petoukhov et al., 2012). Within PRIMUSqt, the "Radius of Gyration" and the "Distance Distribution" analysis functions were both used to determine the radius of gyration ($R_g$) and the relative intensity (forward scattering intensity, I(0)) for each sample. The "Radius of Gyration" function uses the Guinier Approximation of low-resolution scattering data (the low-*q* region) to calculate reciprocal space values. Keeping in line with the standard criteria for globular

proteins, the plotted range of Guinier plots was kept below $qR_g = 1.3$ (Kikhney & Svergun, 2015; Putnam, 2016; Skou, Gillilan, & Ando, 2014; Trewhella et al., 2017). These plots were assessed for quality of fit using the fidelity of the model (ranging from 0.0 being the lowest in quality, to 1.0 being the highest quality) alongside the random distribution of residuals averaging around zero. Aggregation of the protein samples was evaluated based on the linearity of the Guinier plots (non-linear regions indicate aggregation). The "Distance Distribution" uses the pair distance distribution function (P(r)) to calculate the maximum particle dimensions ($D_{max}$), the real-space $R_g$, and I(0). Interatomic distance distributions (r) are calculated using GNOM (Svergun, 1992) from the "Distance Distribution" function. $D_{max}$ was defined by the value of r where the P(r) curve reaches zero. This distance distribution data was fit to an approximate maximum $q$ of 0.3 $Å^{-1}$ (Table 4.1, Table 4.2, Table 4.3, and Figure B.4). $D_{max}$ was manually adjusted to the lowest possible value whilst still producing a smooth curve, with P(r)>0 and a random distribution of residuals around zero. The P(r) curves were normalised by dividing by I(0) (from the "Guinier analysis") to remove any confounding effects of concentration.

The "Porod Volume" function in PRIMUSqt was used to calculate the Porod Volume ($V_P$), using a $q$-range limited to the Porod-Debye region and reciprocal space values determined by the "Radius of Gyration" function. The Porod-Debye region plotted was defined by the scattering data that reached and maintained a plateau within the Porod plot (Figure B.4) (Rambo & Tainer, 2011). This subset of data was used to determine the $V_p$ which in turn was used together with calculated molecular weights (MW) to determine the particle densities ($d_{particle}$) for each CysK variant in each condition tested. The MW was determined using the protein sequence analysis programme ProtParam (Gasteiger et al., 2005). The $d_{particle}$ was calculated using Equation 4.6, where MW is the molecular weight of the protein and $V_p$ is the calculated porod volume (Rambo & Tainer, 2011).

**Equation 4.6.** Formula for calculating particle density

$$d_{particle} = (MW/V_p)$$

Dimensionless Kratky plots were created by multiplying $q$ by the $R_g$ (from the "Guinier analysis") to remove effects of protein size and molecular weight. The

intensity was normalised by dividing by I(0) (from the "Guinier analysis") to remove any confounding effects of concentration.

Theoretical scattering of known enzyme structures overlayed onto experimental scattering data plots were created using "CRYSOL online" from ATSAS online 3.2.1 web services tool. All CysK enzymes experimental scattering data were overlaid with the theoretical scattering of our *N. gonorrhoeae* CysK crystal structure (NgCysK, 9NLD) from the PDB. All CysE enzymes experimental scattering data were overlaid with the theoretical data of their corresponding organisms' crystal structure from the PDB (NgCysE with 6WYE, and EcCysE with 1T3D). Crysol was used to determine any similarities or differences between enzymes in solution (SAXS) and rigid models (X-ray crystallography).

### 4.5.6 Cysteine synthase complex formation

The protocol for forming the cysteine synthase complex (CSC) was based on a method by (Benoni, De Bei, et al., 2017a).

#### 4.5.6.1 Monitoring cysteine synthase complex formation by gel filtration chromatography

A 1 ml solution of NgCysE 6 μM: NgCysK 4 μM (monomer ratios) was manually injected into the injection loop of the FPLC for injection into the Enrich 650 analytical gel filtration column (Bio-Rad Laboratories, USA), preequilibrated in gel filtration buffer (50 mM Potassium phopshate pH 7.0, 100 mM NaCl). After sample injection, the column was washed with 28 ml of gel filtration buffer (50 mM Potassium phosphate pH 7.0, 100 mM NaCl). Fractions were collected and run on a 12% SDS PAGE gel. This was repeated with a NgCysE 4 μM: NgCysK 0.05 μM 1 ml solution, without fractions being run on a 12% SDS PAGE gel. The same method was repeated using a EcCysE 6 μM: EcCysK 4 μM monomeric ratio.

#### 4.5.6.2 Monitoring cysteine synthase complex formation by small angle X-ray scattering

NgCysK, EcCysK, NgCysE, and EcCysE were expressed and purified and prepared as mentioned above. Data was processed in the same manner as discussed above with particular emphasis on the scattering plots, which display the key differences between CysK, CysE and CSC scattering.

## 4.6 Results and discussion

### 4.6.1 Substrate specificity of CysK from two bacteria lacking the sulfate reduction pathway

Given the importance of sulfur metabolism, and its central role in L-cysteine biosynthesis in bacteria, investigating the kinetic function of the final step of L-cysteine biosynthesis in these two pathogenic bacteria lacking the sulfate reduction pathway is vital. Kinetic analyses of CysK from *N. gonorrhoae* and *S. aureus* were conducted as we endeavour to elucidate the differences in substrate utilisation and in turn sulfur metabolism (Figure 4.1). The production of L-cysteine by CysK was determined by measuring the absorbance of a pink chromophore that forms when ninhydrin interacts with L-cysteine (Friedman, 2004). It is well documented that addition of 25% (v/v) glycerol (final concentration) significantly improves stability of the enzyme, mitigating decreases in activity caused by freeze/thawing (Vagenende, Yap, & Trout, 2009). Glycerol has been used on many occasions for CysK stabilisation during storage (Bertagnolli & Wedding, 1977; Kuske et al., 1994), resuspension of pellets and samples (Ramirez, Castneda, Xiqui, Sosa, & Baca, 2006; Singh, Brooks, Ray, Mandel, & Visick, 2015), elution, and dialysis (Benoni, De Bei, et al., 2017a; Ramirez et al., 2006). However, we discovered the presence of glycerol had a significant effect on the kinetics of NgCysK and SaCysK (Figure B.4, Figure B.5, Table B.1, and Table B.2). Therefore, kinetic analyses presented here were completed in the absence of glycerol, using freshly purified enzyme.

The kinetic parameters of NgCysK for substrate OAS (Table 4.4) were calculated from fitting an Allosteric sigmoidal model ($R^2 = 0.9702$) of rate versus OAS (Figure 4.3A). The overall fit for the Allosteric sigmoidal equation is good, giving a $K_{half\ (OAS)}$ of 1.541 mM, a $k_{cat\ (OAS)}$ of 87.5 $s^{-1}$, and a $k_{cat}/K_{M\ (OAS)}$ of 5.67 x $10^4$ $M.s^{-1}$ for the dimer (Table 4.4). A saturating concentration of 30 mM $Na_2S$ was used for the collection of the Allosteric sigmoidal plot. The kinetic parameters of NgCysK for substrate $Na_2S$ were calculated from fitting an Allosteric sigmoidal model ($R^2 = 0.9088$) of rate versus $Na_2S$ (Figure 4.3B). The overall fit for the Allosteric

sigmoidal equation is good, giving a $K_{half\ (Na2S)}$ of 23.620 mM, a $k_{cat\ (Na2S)}$ of 100.94 $s^{-1}$, and a $k_{cat}/K_{M\ (Na2S)}$ of 4.27 x $10^3$ $M.s^{-1}$ for the dimer (Table 4.4).

**Table 4.4:** Kinetic parameters of NgCysK in the absence of glycerol

| Parameter | *O*-acetylserine (OAS)[a] | Sodium sulfide ($Na_2S$)[a] |
|---|---|---|
| $v_{max}$ ($mM.min^{-1}$) | 0.207 ± 0.016 | 0.239 ± 0.111 |
| $K_{half}$ (mM) | 1.541 ± 0.306 | 23.620 ± 10.780 |
| $k_{cat}$ ($s^{-1}$) [b] | 87.47 ± 7.12 | 100.94 ± 46.92 |
| $k_{cat}/K_M$ ($M.s^{-1}$) | (5.67 ± 1.22) x $10^4$ | (4.27 ± 2.78) x$10^3$ |
| h | 1.725 ± 0.513 | 2.669 ± 1.086 |
| $R^2$ | 0.9702 | 0.9088 |

[a] Error is SEM of three replicates
[b] $k_{cat}$ calculated by dividing the rate ($M.s^{-1}$) by enzyme concentration using the concentration of the NgCysK dimer (67.582 kDa)

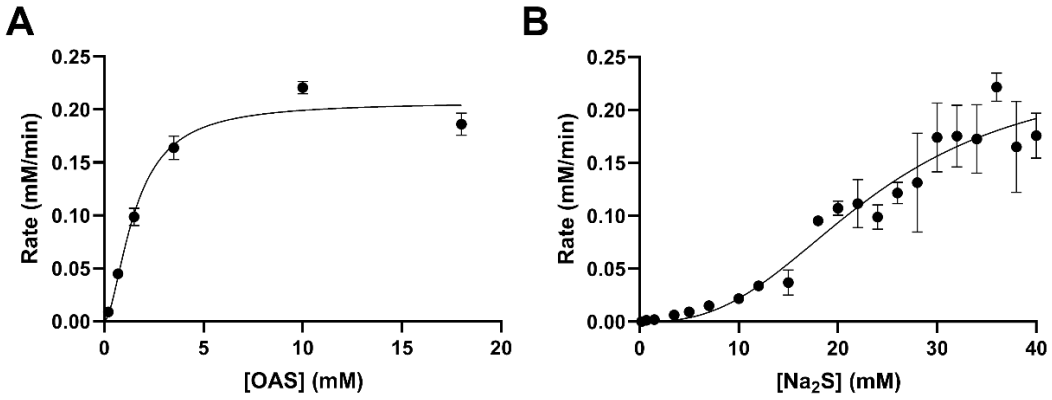


**Figure 4.3:** Kinetic analysis of NgCysK substrates OAS and $Na_2S$ in the absence of glycerol. (**A**) Allosteric sigmoidal fit (occuring when the enzyme has cooperative subunits) for OAS. (**B**) Allosteric sigmoidal fit for $Na_2S$. OAS and $Na_2S$ assays were collected at saturating concentrations of 10 mM OAS and 30 mM $Na_2S$, respectively. Plotted data points represent mean alongside SEM of three replicates.

The kinetic parameters of SaCysK for substrate OAS (Table 4.5) were calculated from fitting a Substrate inhibition model ($R^2 = 0.9301$) of rate versus OAS (Figure 4.4A). The overall fit for the Substrate inhibition equation is good, giving a $K_{M\ (OAS)}$ of 1.378 mM, a $k_{cat\ (OAS)}$ of 53.57 $s^{-1}$, and a $k_{cat}/K_{M\ (OAS)}$ of 3.89 x $10^4$ $M.s^{-1}$ for the dimer (Table 4.5). A saturating concentration of 15 mM $Na_2S$ was used for the collection of the Substrate inhibition plot. The kinetic parameters of SaCysK for substrate $Na_2S$ were also calculated from fitting a Substrate inhibition model ($R^2 = 0.6206$) of rate versus $Na_2S$ (Figure 4.4B). The overall fit for the Substrate inhibition equation is poorer than that of OAS due to the error at 12 and 15 mM $Na_2S$ concentrations, alongside the low rate at 8 mM $Na_2S$. However, kinetic

parameters were obtained from the data, giving a $K_{M\ (Na2S)}$ of 2.306 mM, a $k_{cat\ (Na2S)}$ of 22.96$s^{-1}$, and a $k_{cat}/K_{M\ (Na2S)}$ of 9.96 x $10^3$ $M.s^{-1}$ for the dimer (Table 4.5).

**Table 4.5:** Kinetic parameters of SaCysK in the absence of glycerol

| Parameter | *O*-acetylserine (OAS)[a] | Sodium sulfide ($Na_2S$)[a] |
|---|---|---|
| $v_{max}$ ($mM.min^{-1}$) | 0.126 ± 0.032 | 0.054 ± 0.034 |
| $K_M$ (mM) | 1.378 ± 0.592 | 2.306 ± 3.573 |
| $k_{cat}$ ($s^{-1}$) [b] | 53.57 ± 13.6 | 22.96 ± 14.5 |
| $k_{cat}/K_M$ ($M.s^{-1}$) | (3.89 ± 1.94) x $10^4$ | (9.96 ± 1.66) x $10^3$ |
| $K_i$ (mM) | 6.265 ± 2.489 | 15.970 ± 12.793 |
| $R^2$ | 0.9301 | 0.6206 |

[a] Error is SEM of three replicates
[b] $k_{cat}$ calculated by dividing the rate ($M.s^{-1}$) by enzyme concentration using the concentration of the SaCysK dimer (68.022 kDa)

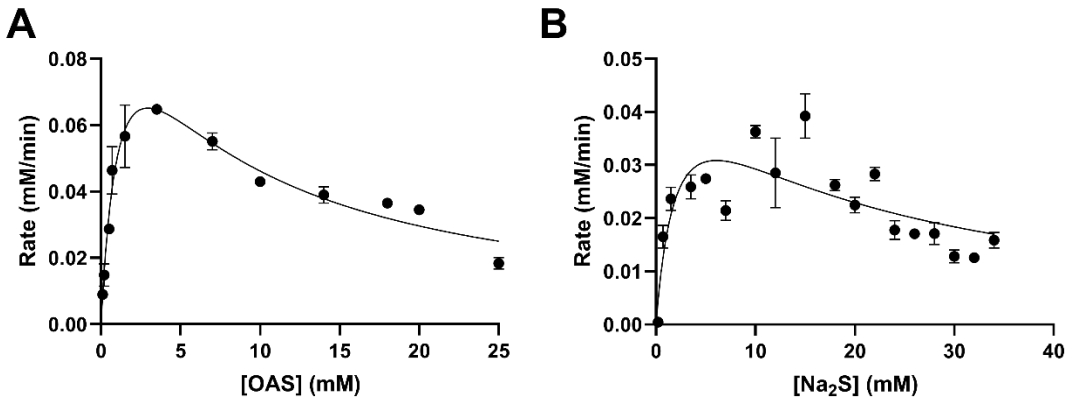


**Figure 4.4:** Kinetic analysis of SaCysK substrates OAS and $Na_2S$ in the absence of glycerol. (**A**) Substrate inhibition fit (occurs when the enzyme exhibits inhibition at high substrate concentrations) for OAS. (**B**) Substrate inhibition fit for $Na_2S$. OAS and $Na_2S$ assays were collected at saturating concentrations of 10 mM OAS and 15 mM $Na_2S$, respectively. Plotted data points represent mean alongside SEM of three replicates.

The difference in $K_{half}$ and $K_M$ values for each substrate in NgCysK (1.541 mM OAS versus 23.620 mM $Na_2S$) and SaCysK (1.378 mM OAS versus 2.306 mM $Na_2S$), respectively, indicates a greater affinity for OAS compared with $Na_2S$ in both enzymes. Interestingly, this substrate affinity is similar to the plant *O*-acetylserine sulfhydrylase isozyme A and C from *Datura innoxia* (Kuske et al., 1994), but not to other bacterial homologues (Bertagnolli & Wedding, 1977; Cook & Wedding, 1976; Tai et al., 1993). However, the earlier studies were conducted in the presence of glycerol, which we have determined to largely affect the kinetics of each substrate. The specificity constants, $k_{cat}/K_M$, are 5.67 x $10^4$ $M.s^{-1}$ (OAS) and 4.27 x $10^3$ $M.s^{-1}$ ($Na_2S$) for NgCysK, and 3.89 x $10^4$ $M.s^{-1}$ (OAS) and 9.96 x $10^3$ $M.s^{-1}$

($Na_2S$) for SaCysK. Catalytic efficiency ($k_{cat}/K_M$) values of $\geq 10^8$ $M.s^{-1}$ indicate the enzyme's reaction rate is diffusion limited (Roskoski, 2007), and in the case of NgCysK the reaction rate is not limited by diffusion of OAS ($k_{cat}/K_{M:}$ 5.67 x $10^4$ $M.s^{-1}$), or $Na_2S$ ($k_{cat}/K_{M:}$ 4.27 x $10^3$ $M.s^{-1}$). For SaCysK the reaction rate is also not limited by diffusion of either substrate, OAS ($k_{cat}/K_{M:}$ 3.89 x $10^4$ $M.s^{-1}$), and $Na_2S$ ($k_{cat}/K_{M:}$ 9.96 x $10^3$ $M.s^{-1}$).

There is a ~13.3-fold increase in $k_{cat}/K_M$ for OAS compared to $Na_2S$ attributable to NgCysK having a ~15.33-fold increased affinity for OAS ($K_{half}$: 1.541 mM) compared to $Na_2S$ ($K_{half}$: 23.620 mM). In SaCysK, there is a ~3.89-fold increase in $k_{cat}/K_M$ for OAS compared to $Na_2S$ attributable to SaCysK having a ~1.67-fold increased affinity for OAS ($K_M$: 1.378 mM) compared to $Na_2S$ ($K_M$: 2.306 mM). Intriguingly, the kinetics parameters for substrates OAS and $Na_2S$ vary extensively across CysK homologues. For OAS, positive cooperativity is seen at low concentrations with substrate inhibition above 25 mM in the plant species *D. innoxia* (Kuske et al., 1994). Plant species *Phaseolus vulgaris* and *Phaseolus polyanthus* exhibit Michaelis-Menten kinetics (Bertagnolli & Wedding, 1977), and *S. typhimurium* exhibits substrate inhibition above 7.5 mM (Cook & Wedding, 1976; Tai et al., 1993). For NgCysK there is an allosteric sigmoidal relationship to OAS with positive cooperativity at low concentrations and an eventual plateau beginning at ~5 mM. In comparison SaCysK displays a strictly substrate inhibition relationship, beginning to drop after ~5 mM OAS. For $Na_2S$, substrate inhibition in *P. vulgaris* is observed after reaching a maximal rate at ~1.5 mM $S^{2-}$ with positive cooperativity (an allosteric sigmoidal model) observed at concentrations below 0.3 mM (Bertagnolli & Wedding, 1977). Similarly, *D. innoxia* OASS (isozyme C) exhibits positive cooperativity below ~0.18 mM $S^{2-}$ with substantial substrate inhibition after 0.2 mM (Kuske et al., 1994). *P. polyanthus* CysK shows no allosteric sigmoidal (positive cooperativity) response to $S^{2-}$, however, fits a substrate inhibition model (Bertagnolli & Wedding, 1977), which is also found in *S. typhimurium* after 0.25 mM $S^{2-}$ (Cook & Wedding, 1976), similar to the response seen in SaCysK after ~8 mM $Na_2S$. For NgCysK, only an allosteric sigmoidal response is seen with positive cooperativity at low concentrations and a slight plateau beginning at ~30 mM. It is intriguing to see such variable relationships of the CysK enzyme with its substrates, and of particular interest is the stark difference

we see between SaCysK and NgCysK, two enzymes from organisms lacking the same sulfate reduction pathway (Figure 4.1). Based on the reaction mechanism of CysK homologues (Joshi, Gupta, & Gupta, 2019; Rabeh & Cook, 2004), and their shared substrates, we predict that both NgCysK and SaCysK function through a bi-bi ping-pong mechanism, in keeping with the proposed alternating cycle of binding and releasing each substrate, being unable to have both substrates bound at the same time.

Both *S. aureus* and *N. gonorrhoeae* lack the sulfate reduction pathway. However, with their ability to grow on media with thiosulfate as the only sulfur source, this raised questions regarding the functionality and characterisation of the CysK enzyme in both *S. aureus* and *N. gonorrhoeae*. The CysM isoform can use both sulfide and thiosulfate as sulfur donors during L-cysteine biosynthesis, therefore, although the kinetic parameters fit with other CysK enzymes, we checked for dual substrate usage, especially due to the previous annotation of the OASS from *S. aureus* as the CysM isoform (Lithgow et al., 2004). To establish both enzymes as a CysK isoform of OASS, we conducted the same kinetic assays as above, replacing $Na_2S$ with thiosulfate ($S_2O_3^{2-}$) (Table 4.6, Figure 4.5). Non-linear regression fit of a Michaelis-Menten model gave a very poor fit to the data ($R^2$ = 0.2058 (NgCysK) and 0.1426 (SaCysK)) (Table 4.6) resulting in a $V_{max}$ and $K_M$ of 0.002 ± 0.003 $mM.min^{-1}$ and 5.780 ± 11.476 mM, respectively, for NgCysK (Table 4.6), and 0.000 ± 373,758.5 $mM.min^{-1}$ and 7.727 ± ∞ mM, respectively, for SaCysK (Table 4.6). The error present in the $K_M$ of both enzymes is greater than the $K_M$, taking the $K_M$ below 0 mM (Table 4.6). This, alongside the exceptionally low $V_{max}$ (Table 4.6), which lays outside the values measured, indicates there is no enzyme activity detected for any thiosulfate concentration, therefore, establishing these enzymes from both *S. aureus* and *N. gonorrhoeae* are in fact CysK isoforms, incapable of utilising thiosulfate as a sulfur donor for the synthesis of cysteine.

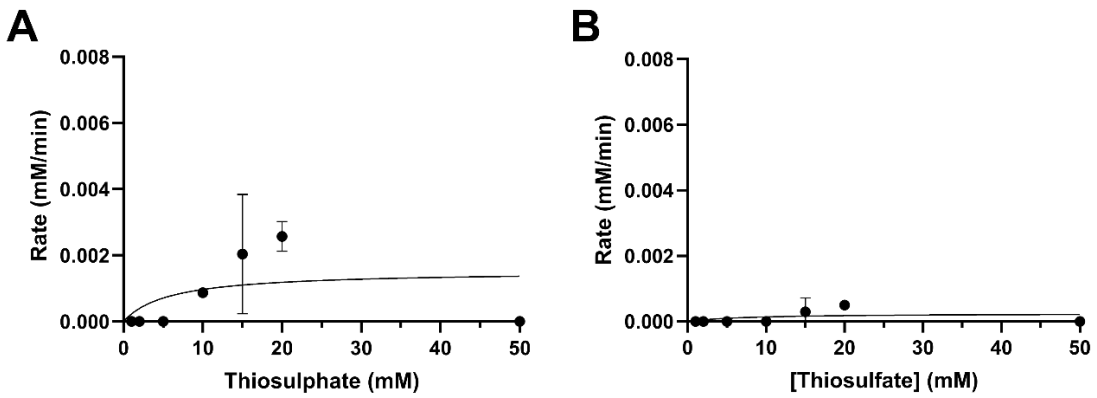


**Figure 4.5:** Thiosulfate activity assays for NgCysK and SaCysK. Michaelis-Menten model is fit to both data sets. (**A**) NgCysK thiosulfate activity. (**B**) SaCysK thiosulfate activity. Both assays were conducted at saturating concentrations of OAS (10 mM).

**Table 4.6:** Kinetic parameters of thiosulfate in NgCysK and SaCysK

| Parameter | NgCysK[a] | SaCysK[a] |
|---|---|---|
| $v_{max}$ ($mM.min^{-1}$) | 0.002 ± 0.003 | 0.000 ± 373,758.5 |
| $K_M$ (mM) | 5.780 ± 11.476 | 7.727 ± ∞ |
| $k_{cat}$ ($s^{-1}$) [b] | (8.589 ± 16.300) x $10^3$ | (1.417 ± 2.117 x$10^{12}$) x$10^3$ |
| $k_{cat}/K_M$ ($M^{-1}.s^{-1}$) | (1.486 ± 4.080) x $10^6$ | (1.834 ± ∞) x $10^5$ |
| $R^2$ | 0.2058 | 0.1426 |

[a] Error is SEM of two replicates
[b] $k_{cat}$ calculated by dividing the rate ($M.s^{-1}$) by enzyme concentration using the concentration of the CysK dimer (NgCysK: 33.791 kDa; SaCysK: 34.011 kDa)
[∞] Infinity symbol indicates error was so high it could not be calculated and is therefore infinity

### 4.6.2 Small angle X-ray scattering shows no conformational change in the presence of OAS

Size exclusion chromatography (SEC) combined with small angle X-ray scattering (SEC-SAXS) analysis (Kirby et al., 2016) was performed on CysK enzymes from both, *N. gonorrhooeae* and *S. aureus,* two organisms lacking the sulfate reduction pathway, to determine the effect of OAS binding to both NgCysK and SaCysK in solution. Throughout our analysis, we used the well-characterised CysK enzyme from *E. coli* as a comparison to a "true" CysK (Benoni, Beck, et al., 2017; Kredich & Tomkins, 1966; Mino, Yamanoue, et al., 2000a; Owais & Gharaibeh, 1990; Sekowska et al., 2000; Yamamoto, Oshima, Nonaka, Ito, & Ishihama, 2011). The scattering data of NgCysK and SaCysK with and without OAS, and the EcCysK, indicated a folded globular protein (Figure 4.6A, C and E), and the calculated

molecular mass (Qp, MoW Fischer method, Vc), combined with the pair wise distribution (P(r)) analysis (Figure 4.6G) support a dimer of CysK monomers for all organisms. However, when comparing MW calculations of all four methods, we see the Porod volume MW calculation consistently gives a 1.39-1.66-fold higher molecular weight estimation for all CysK enzymes, including both NgCysK and SaCysK, in the presence of OAS (Table 4.7 and Table 4.8). This overestimation can occur due to two limitations of this particular method, a large hydration shell as a result of proteins surface residues interacting with water molecules in solution, and high flexibility of particular regions (Hopkins, Gillilan, & Skou, 2017; Rambo & Tainer, 2011). The C-terminal region of the CysK enzymes alongside their active site regions, are particularly flexible, combined with the hydration shell of the enzymes in solution may have led to the overestimation of the molecular weight.

**Table 4.7:** Structural parameters of Guinier fits, P(r) functions, MW estimates for *Ng*CysK, *Ng*CysE, *Ec*CysK, *Ec*CysE, and *Sa*CysK ran individually. 3.2 and 24 refer to the column volume used during SEX-SAXS run.

| | ***Ng*CysK (3.2)** | ***Ec*CysK (24)** | ***Sa*CysK (3.2)** | ***Ec*CysE (24)** | ***Ng*CysE (3.2)** |
|---|---|---|---|---|---|
| **Qp MW (Da) (ratio to predicted value)** | 63626 (0.94) | 47609 (0.73) | 62861 (0.95) | 168062 (0.89) | 206817 (1.09) |
| **MoW MW (Da) using the Fischer method (ratio to predicted value)** | 67924 (1.01) | 53332 (0.81) | 67828 (1.03) | 177320 (0.94) | 204792 (1.08) |
| **Vc MW (Da) (ratio to predicted value)** | 58815 (0.87) | 48791 (0.75) | 59571 (0.90) | 167351 (0.88) | - |
| **Radius of gyration analysis** | | | | | |
| ***I*(0) ($cm^{-1}$) [from Guinier]** | 0.043 ± 0.000037 | 0.01048 ± 0.000021 | 0.049 ± 0.00004 | 0.038 ± 0.000047 | 0.05343 ± 0.00013 |
| **$R_g$ (Å) [from Guinier]** | 26.30 ± 0.04 | 26.45 ± 0.09 | 26.08 ± 0.04 | 38.80 ± 0.07 | 39.42 ± 0.16 |
| ***q*$R_g$ limits** | 0.22-1.29 | 0.29-1.28 | 0.35-1.30 | 0.48-1.30 | 0.26-1.29 |
| **Fidelity** | 1.00 | 1.00 | 1.00 | 1.00 | 1.00 |
| **Distance distribution analysis** | | | | | |
| ***I*(0) ($cm^{-1}$) [from Guinier]** | 0.043 | 0.010 | 0.049 | 0.038 | 0.053 |
| **$R_g$ (Å) [from Guinier]** | 26.14 | 26.45 | 26.08 | 39.18 | 39.42 |
| ***I*(0) ($cm^{-1}$) [from P(r)]** | 0.043 ± 0.00006941 | 0.01048 ± 0.00003455 | 0.04878 ± 0.00007179 | 0.03796 ± 0.00007145 | 0.05410 ± 0.0002185 |
| **$R_g$ (Å) [from P(r)]** | 26.13 ± 0.05968 | 26.44 ± 0.1183 | 26.07 ± 0.05021 | 39.20 ± 0.1095 | 40.53 ± 0.1761 |
| **$d_{max}$ (Å)** | 83.60 | 83.16 | 81.98 | 131.87 | 130.38 |
| **Points** | 208 | 208 | 208 | 169 | 202 |
| **Alpha** | 19.18 | 8.44 | 13.98 | 8.77 | 9.41 |
| ***q* range ($Å^{-1}$)** | 0.0084-0.3039 | 0.0110-0.3026 | 0.0123-0.3047 | 0.0123-0.2059 | 0.0064-0.1973 |
| ***P*(r) total quality estimate from GNOM** | 0.9005 | 0.8837 | 0.9030 | 0.8663 | 0.8308 |
| **Porod volume analysis** | | | | | |
| **MW (kDa)** | 67.6 | 73.6 | 68.0 | 189.6 | 189.7 |
| **Porod volume ($Å^{-3}$) (ratio: $V_P$/calculated $M_W$)** | 97410.90 (1.44) | 108823 (1.66) | 96731.10 (1.47) | 307037.00 (1.62) | 294247.00 (1.55) |
| **$d_{particle}$ (g $cm^{-3}$)** | 1.15 | 1.12 | 1.17 | 1.03 | 1.07 |

**Table 4.8.** Structural parameters of Guinier fits, P(r) functions, MW estimates for *Ng*CysK and *Sa*CysK ran with OAS

| | ***Ng*CysK + OAS** | ***Sa*CysK + OAS** |
|---|---|---|
| **Qp MW (Da) (ratio to predicted value)** | 63093 (0.93) | 62861 (0.92) |
| **MoW MW (Da) using the Fischer method (ratio to predicted value)** | 60876 (0.90) | 67828 (0.99) |
| **Vc MW (Da) (ratio to predicted value)** | 61531 (0.91) | 59571 (0.88) |
| **Radius of gyration analysis** | | |
| ***I*(0) ($cm^{-1}$)** | 0.025 ± 0.0001 | 0.031 ± 0.0001 |
| ***R*g (Å)** | 26.11 ± 0.18 | 25.96 ± 0.16 |
| ***q*Rg limits ($Å^{-1}$)** | 0.22-1.29 | 0.28-1.25 |
| **Fidelity** | 0.80 | 0.82 |
| **Distance distribution analysis** | | |
| ***I*(0) ($cm^{-1}$) [from Guinier]** | 0.025 | 0.031 |
| ***R*g (Å) [from Guinier]** | 25.90 | 26.11 |
| ***I*(0) ($cm^{-1}$) [from P(r)]** | 0.02520 ± 0.0001026 | 0.03098 ± 0.00008989 |
| ***R*g (Å) [from P(r)]** | 25.89 ± 0.1487 | 26.11 ± 0.07990 |
| $d_{max}$ (Å) | 77.69 | 81.98 |
| **Points** | 170 | 169 |
| **Alpha** | 0.1294 | 12.12 |
| ***q* range ($Å^{-1}$)** | 0.0083-0.3064 | 0.0083-0.3084 |
| ***P*(r) total quality estimate from GNOM** | 0.98 | 0.98 |
| **Porod volume analysis** | | |
| **MW (kDa)** | 67.58 | 68.02 |
| **Porod volume ($Å^{-3}$) (ratio: $V_P$/calculated $M_W$)** | 95074.90 (1.41) | 94602.70 (1.39) |
| $d_{particle}$ (g $cm^{-3}$) | 1.18 | 1.19 |

However, if we look at the MW calculations given by the Volume of correlation ($V_c$), Fischer estimation (MoW), and the Porod invariant or dimensionless Kratky plot ($Q_P$) methods, we see more accurate values. The MW calculations for all three CysK enzymes give a ratio to the ProtParam calculated MW, consistent with that of a functional homodimer (EcCysK: 0.73-0.81 (Table 4.7); NgCsyK with and without OAS: 0.87-1.01 (Table 4.7 and Table 4.8); SaCysK with and without OAS: ranging from 0.88-1.03 (Table 4.7 and Table 4.8)). The Guinier and P(r) calculated $R_g$ values for all three enzymes are very similar, all ranging from 26.07-26.45 Å (Table 4.7), indicating the SaCysK and NgCysK behave in a similar manner to EcCysK, our "true" CysK, positive control. The *Ec*CysK, *Ng*CysK, and *Sa*CysK SAXS profiles were fit with the theoretical calculated scattering from the *Ng*CysK crystal structure (PDB ID: 9NLD). Visual inspection indicates a good fit for all data,

holo enzymes and the *Sa*CysK and *Ng*CysK with OAS. The chi-square values of fit indicate a worse fit for the holo enzymes compared to the OAS crysol (Supplementary Table 4). This is due to the increased noise in the OAS data which the model misconstrues as a better fit.

Comparison of the NgCysK and SaCysK SAXS profiles in the presence and absence of OAS show negligible differences (Figure 4.6), indicating no major change in conformation or flexibility of the enzyme (Rambo & Tainer, 2011). This indicates there is no change in the compactness of the enzymes when OAS is bound, compared to when it is not as shown by the $R_g$ values derived from Guinier analysis. Values from the Guinier analysis tool (radius of gyration analysis) are used as this assumes a globular shape (Eryilmaz et al., 2013) of which NgCysK and SaCysK are. There is no change in $R_g$, from holo NgCysK to NgCysK with OAS bound (26.30 ± 0.04 - 26.11 ± 0.18) (Table 4.7 and Table 4.8), or from holo SaCysK to SaCysK with OAS bound (26.08 ± 0.04 - 25.96 ± 0.16) (Table 4.7 and Table 4.8).

The Kratky plots for both NgCysK and SaCysK with and without OAS, alongside EcCysK indicate a bell-shaped curve, consistent with the expected shape exhibited by a typical folded protein (Figure 4.6). This confirms that NgCysK and SaCysK enzymes remain folded in the presence of OAS.

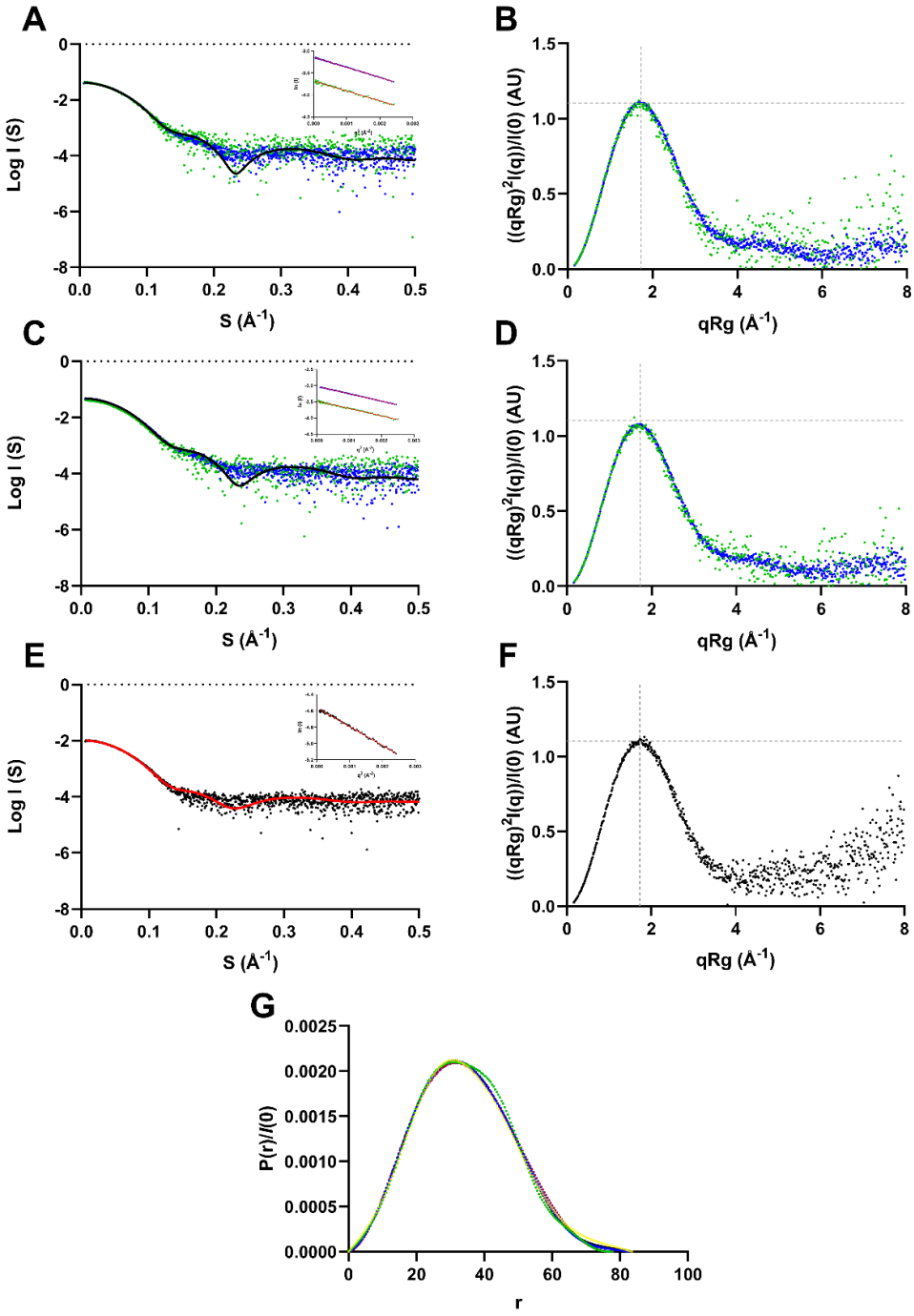


**Figure 4.6:** SAXS profiles of NgCysK and SaCysK in the presence and absence of OAS, and EcCysK. (**A**) Scattering profiles of NgCysK in the absence (blue circles) and presence (green circles) of 10 mM OAS. (**B**) Kratky plot of NgCysK in the absence (blue circles) and presence (green circles) of 10 mM OAS. (**C**) Scattering profiles of SaCysK in the absence (blue circles) and presence (green circles) of 10 mM OAS. (**D**) Kratky plot of SaCysK in the absence (blue circles) and presence (green circles) of 10 mM OAS. (**E**) Scattering profile of EcCysK. Experimental EcCysK scattering shown in black. Theoretical scattering (red line) calculated from NgCysK crystal structure (9NLD). (**F**) Kratky plot of EcCysK. (**G**) Pair distance distribution function (P(r)) analysis of NgCysK and SaCysk in the absence and presence of OAS, and EcCysK. NgCysK shown in black; NgCysK + OAS shown in green; SaCysK shown in blue; SaCysK + OAS shown in burgundy; EcCysK shown in yellow. The P(r) values are normalised by relative intensity for comparison of all enzymes on the same scale. Theoretical scattering shown in black in (**A**) and (**C**) and red in (**E**), calculated from OAS-free NgCysK crystal structure (9NLD). Guinier plots for all enzymes are inlaid in the scattering plots, enzymes without OAS are shown in blue, enzymes with OAS are shown in green and EcCysK is shown in black. A red trend line is present in all Guinier plots. The grey dashed lines in the Kratky plots represent the expected peak maxima for folded, globular proteins, where $(qRg)^2I(q)/I(0) = 1.104$ in a q range of 0.05 – 0.1 $Å^{-1}$ (Makowski et al., 2020; Receveur-Brechot & Durand, 2012).

### 4.6.3 Formation of the Cysteine Synthase Complex (CSC)

There are three main mechanisms for regulating L-cysteine metabolism and therefore sulfur flux. The first is transcriptional regulation by CysB, and the second is feedback inhibition of CysE by L-cysteine which is seen in other CysE homologues (Kumar, Raj, Nagpal, Subbarao, & Gourinath, 2011; Pye, Tingey, Robson, & Moody, 2004), including *N. gonorrhoeae* (Oldham et al., 2022). The final, which we will investigate here, is formation of the CSC which occurs within many bacterial and plant species (Benoni, De Bei, et al., 2017a; Kredich et al., 1969; Kredich & Tomkins, 1966; Mino, Yamanoue, et al., 2000a; Salsi et al., 2010; Yi et al., 2013) and is hypothesised to modulate sulfur flux (Hell & Wirtz, 2002; Wirtz et al., 2012; Wirtz & Hell, 2006). Due to the use of the CSC in modulating sulfur flux, combined with both, L-cysteine mediated CysE inhibition and a lack of the sulfate reduction pathway, it is of particular interest whether *N. gonorrhoeae* and *S. aureus* can form the CSC. Using Clustal Omega (Madeira et al., 2019), a sequence alignment of CysE bacterial homologues was generated and analysed using ESPript 3.0 (Figure 4.7) (Robert & Gouet, 2014). This analysis showed the CysE from *N. gonorrhoeae* (*Ng*CysE) and *S. aureus* (*Sa*CysE), had moderate (49.51%) and low to moderate (38.69%) sequence similarities to other CysE homologues, respectively (Figure 4.7). The C-terminus four peptide fragment, GDGI was well conserved across three species with DFMI and DYII being the C-terminal tetrapeptide sequence in NgCysE and *Sa*CysE, respectively. The conservation of the C-terminal isoleucine in both species indicates their potential for CSC formation. The CysK active site has also been confirmed as the anchor for CSC formation (Campanini et al., 2015). The CSC is an important regulator of the cysteine biosynthesis pathway and has yet to be characterised in *N. gonorrhoeae* or *S. aureus*.

Characterising the CSC would provide further insight into elucidating the sulfur assimilation and synthesis of L-cysteine in *N. gonorrhoeae* and *S. aureus*. However, we were unable to purify the SaCysE enzyme, therefore, only the NgCSC formation was tested using *E. coli* as a positive control as it is known to form the CSC (Benoni, De Bei, et al., 2017a; Mino, Hiraoka, et al., 2000).

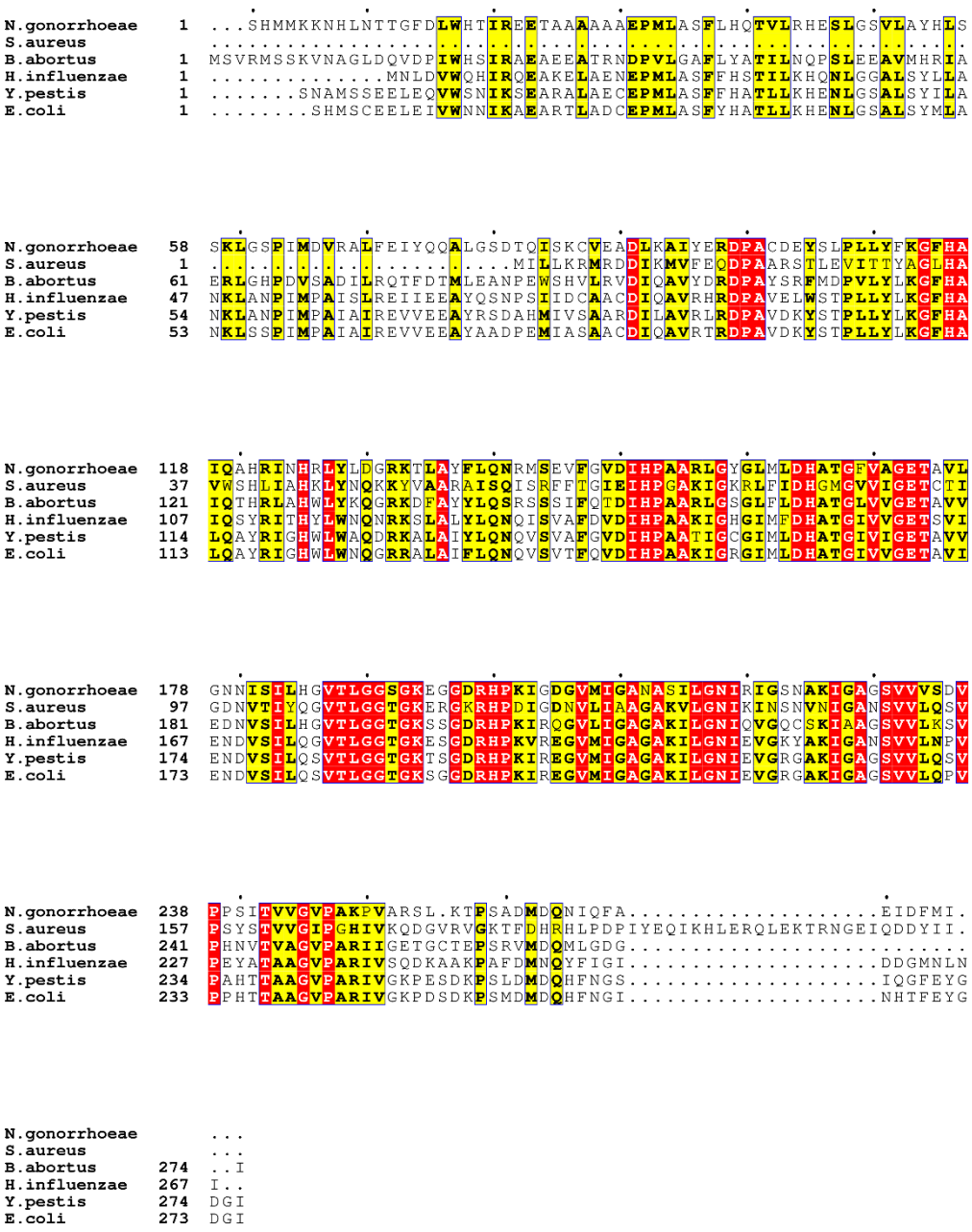


**Figure 4.7:** CysE protein sequence alignment. The *N. gonorrhoeae* and *S. aureus* CysE amino acid sequences were aligned to the following CysE homologues; *Brucella abortus* (*Ng*CysE 47.96% and *Sa*CysE 41.27% sequence similarity); *Haemophilus influenzae* (*Ng*CysE 51.89% and *Sa*CysE 39.49% sequence similarity); *Yersinia pestis* (*Ng*CysE 53.14% and *Sa*CysE 36.92% sequence similarity); *Escherichia coli* (*Ng*CysE 53.70% and *Sa*CysE 36.92% sequence similarity); and *Ng*CysE and *Sa*CysE have 39.18% sequence similarity to each other. Highly conserved residues are highlighted red, whilst less conserved residues are highlighted yellow. Sequence alignment created using Clustal Omega (Madeira et al., 2019). Figure created using ESPript 3.0 (Robert & Gouet, 2014).

.

#### 4.6.3.1 Investigation of CSC formation by gel filtration chromatography

Formation of the CSC was investigated by gel filtration chromatography using freshly purified CysK and CysE. Both proteins were purified individually, and analysed using a calibrated gel filtration column. NgCysE elutes from an Enrich 650 analytical gel filtration column (BioRad) at 12.28 ml, corresponding to a molecular weight of 193.8 kDa, consistent with an NgCysE hexamer (Figure 4.8A). NgCysK elutes at 14.6 ml, corresponding to a molecular weight of 52.862 kDa, consistent with a dimer (Figure 4.8C). EcCysE elutes from an Enrich 650 analytical gel filtration column (BioRad) at 13.4 ml, corresponding to a molecular weight of 198.5 kDa, consistent with an EcCysE hexamer (Figure 4.8B). EcCysK elutes at 15 ml, corresponding to a molecular weight of 80.1 kDa, consistent with a dimer (Figure 4.8D).

NgCysE and NgCsyK were mixed and analysed by gel filtration chromatography at 3:2 and 1:1 monomeric molar ratios. The homologous CSC from *E. coli* indicates the composition to be one CysE hexamer and two CysK dimers (3:2 monomeric molar ratio) (Benoni, De Bei, et al., 2017a). Given this conformation, the NgCSC formation would give an elution peak of ~332 kDa corresponding to an elution volume of 11.9 ml, prior to the NgCysE and NgCysK elution peaks seen, however, we observe no such peak indicating no CSC formation (Figure 4.8).

In comparison, given the established 3:2 ratio of CysE to CysK in *E. coli* (Benoni, De Bei, et al., 2017a), the EcCSC formation would give an elution peak of ~337 kDa corresponding to an elution volume of 11.8 ml, prior to the EcCysE and EcCysK elution peaks seen. Given the presence of this peak in the elution profile (Figure 4.8F), this indicates successful formation of the EcCSC.

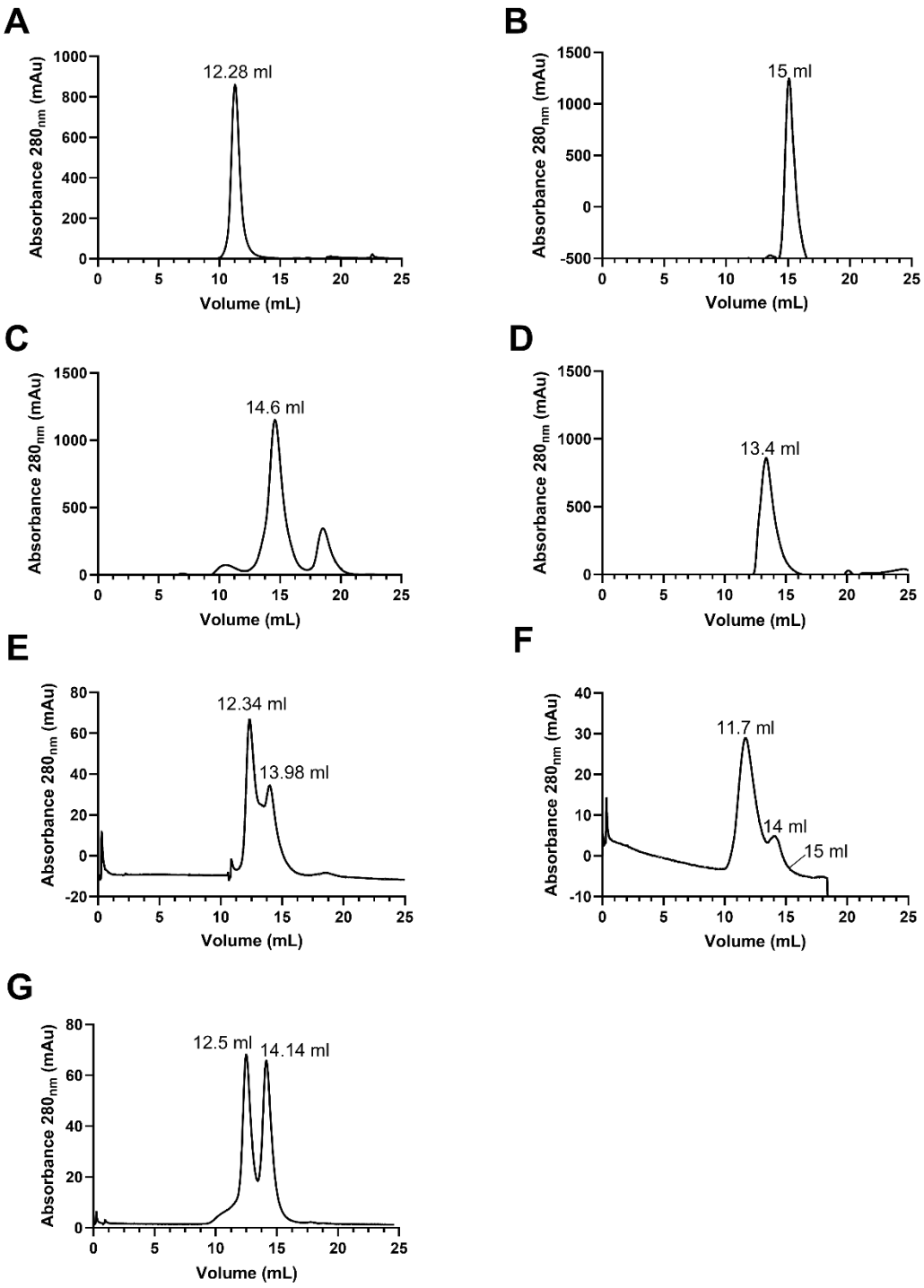


**Figure 4.8:** Monitoring formation of the CSC in *N. gonorrhoeae* and *E. coli* by gel filtration chromatography

### 4.6.3.2 Investigation of CSC formation by SAXS

Following our gel filtration chromatography experiments, we looked at the potential CSC formation in *N. gonorrhoeae* in comparison to our *E. coli* positive control using SEC-SAXS. Both the EcCSC and NgCSC forming enzymes were run as per Table 4.2**.** Visual inspection of the UV trace of the SEC run prior to beam exposure and the CHROMIXS scattering profile, shows the presence of three distinct peaks

in the EcCSC run compared to the presence of only two distinct peaks in the NgCSC run (Figure 4.9). The first peak seen in the EcCSC profiles indicates the expected larger CSC followed by the elution of the excess (hasn't formed the CSC) EcCysE, and the third and final peak being the excess EcCysK (Figure 4.9B). This was expected as the CSC formation functions in an equilibrium (Kumaran, Yi, Krishnan, & Jez, 2009; Wang & Leyh, 2012), unless driven by other factors such as the presence of OAS, which can dissociate the complex at concentrations upwards of 50 µM (Benoni, Beck, et al., 2017; Kredich et al., 1969; Wang & Leyh, 2012) or the presence of sulfide, which promotes complex formation (Wirtz & Hell, 2006). In comparison, visual inspection of the UV trace and CHROMIXS scattering for the NgCSC run, shows only the elution peaks for NgCysE and NgCysK (Figure 4.9A).

Analysis of the scattering data from these runs also shows a distinct difference between the EcCSC and NgCSC runs. The scattering points from each of the peaks were isolated and analysed separately, and once extrapolated, showed a distinctly different scattering pattern for the EcCSC in comparison to the individual enzymes (EcCysE and EcCysK) scattering patterns (Figure 4.8A). The scattering of the individual enzymes is typical of a folded globular protein, further consolidated by the bell shape curve of their Kratky plots (Figure 4.8B), and the P(r) distribution analysis (Figure 4.8C). However, the EcCSC peak has a distinct scattering pattern indicating the presence of a large molecule with multiple species (i.e. EcCysE and EcCysK) together in a complex (Figure 4.8A). This is also evident in the EcCSC Kratky plot (Figure 4.8B) and P(r) distribution analysis (Figure 4.8C).

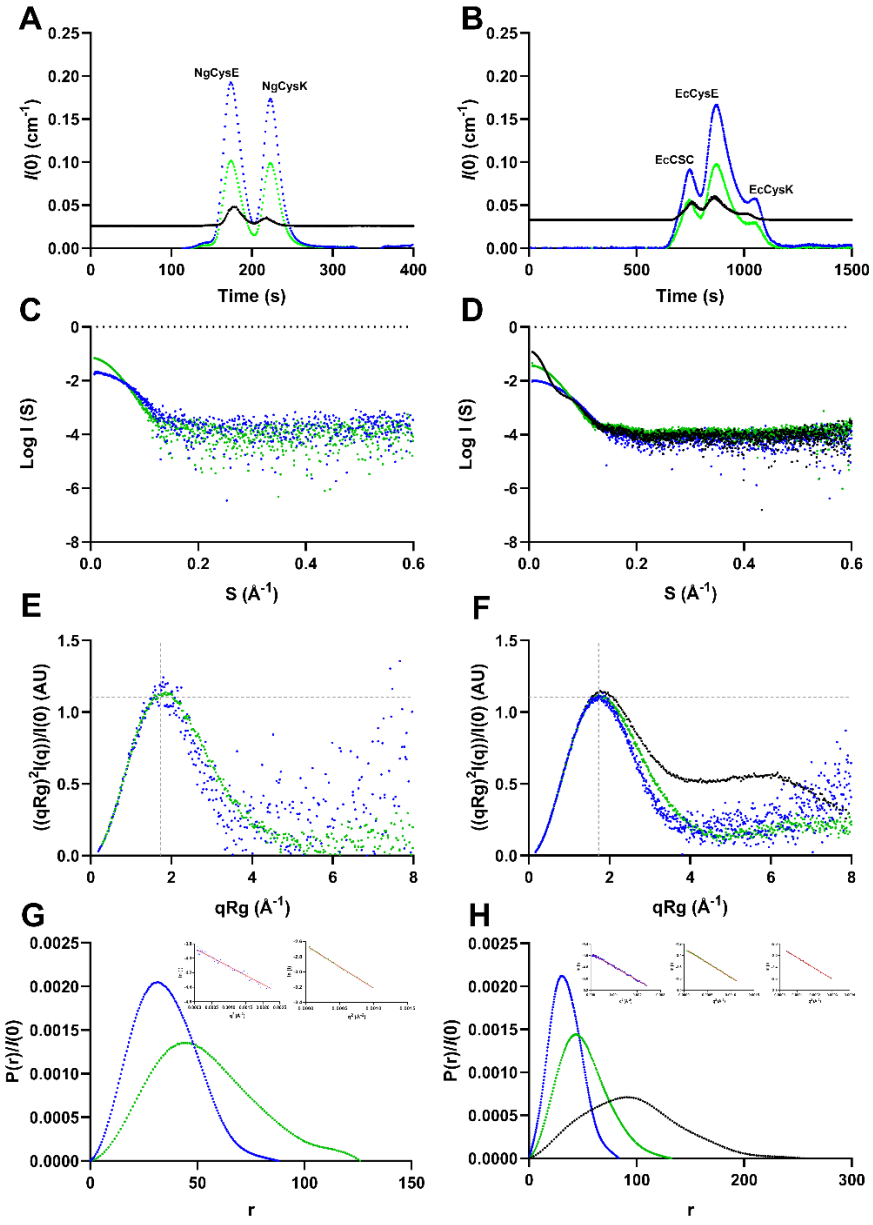


**Figure 4.9:** SAXS profiles of attempted CSC formation in *N. gonorrhoeae* and *E .coli.* (**A**) UV trace and CHROMIXS scattering of attempted NgCSC formation. (**B**) UV trace and CHROMIXS scattering of EcCSC formation. (**C**) Scattering profiles of NgCysK (blue circles) and NgCysE (green circles) from attempted NgCSC formation. (**D**) Scattering profiles of of EcCysK (blue circles), EcCysE (green circles), and EcCSC (black circles) from EcCSC formation. (**E**) Kratky plot of NgCysK (blue circles) and NgCysE (green circles) from attempted NgCSC formation. (**F**) Kratky plot of EcCysK (blue circles), EcCysE (green circles), and EcCSC (black circles) from EcCSC formation. (**G**) Pair distance distribution function (P(r)) analysis of NgCysK (blue circles) and NgCysE (green circles) from attempted NgCSC formation. (**H**) Pair distance distribution function (P(r)) analysis of EcCysK (blue circles), EcCysE (green circles), and EcCSC (black circles) from EcCSC formation. Individual enzymes present in the UV trace and CHROMIXS scattering are labelled in black. UV $A_{280}$ trace is shown in blue. UV $A_{260}$ trace is shown in green. CHROMIXS scattering is shown in black. The grey dashed lines in the Kratky plots represent the expected peak maxima for folded, globular proteins, where $(qRg)^2I(q)/I(0) = 1.104$ in a q range of 0.05 – 0.1 Å$^{-1}$ (Makowski et al., 2020; Receveur-Brechot & Durand, 2012). Guinier plots for all enzymes are inlaid on the P(r) distributions. A red trend line is present in all Guinier plots.

Given the conservation of the C-terminal isoleucine in *N. gonorrhoeae* and the confirmation of their successful folding into functional globular proteins, the

potential for CSC formation is there. However, through both gel filtration chromatography and SAXS analysis, we have confirmed the inability of *N. gonorrhoeae* to form the CSC *in vitro*. It is therefore possible that the CSC is completely unable to form in *N. gonorrhoeae*. This would result in a CysK enzyme that is not inhibited by CSC formation, allowing an increase in L-cysteine production. Additionally, due to the unregulated OAS consumption by CysK, sulfate acquisition genes would be downregulated. Given the necessity of reducing compounds such as glutathione (Seib et al., 2006), therefore creating high demand for L-cysteine, it may be advantageous for *N. gonorrhoeae* to be incapable of CSC formation. This lack of CSC formation may in fact be linked to the inability of *N. gonorrhoeae* to reduce sulfate to sulfide, and that the transcriptional regulator CysB controls two of the deleted genes from this pathway via operon control.

**Table 4.9:** Structural parameters of Guinier fits, P(r) functions, MW estimates for CSC formation

| | *Ng*CysE (3.2 ml column) | *Ng*CysK (3.2 ml column) | *Ec*CSC (24 ml column) |
|---|---|---|---|
| **Qp MW (Da) (ratio to predicted value)** | 216494 (1.14) | 64574 (0.96) | 742926 (2.21) |
| **MoW MW (Da) using the Fischer method (ratio to predicted value)** | 190215 (1.00) | 66520 (0.98) | - |
| **Vc MW (Da) (ratio to predicted value)** | 208954 (1.10) | 60934 (0.90) | - |
| **Radius of gyration analysis** | | | |
| ***I*(0) ($cm^{-1}$)** | 0.07 ± 0.0002 | 0.021 ± 0.00018 | 0.1284 ± 0.00017 |
| **$R_g$ (Å)** | 40.94 ± 0.19 | 27.09 ± 0.39 | 74.85 ± 0.14 |
| **$qR_g$ limits ($Å^{-1}$)** | 0.34-1.26 | 0.21-1.30 | 0.53-1.30 |
| **Fidelity** | 0.75 | 0.72 | 0.99 |
| **Distance distribution analysis** | | | |
| ***I*(0) ($cm^{-1}$) [from Guinier]** | 0.070 | 0.021 | 0.128 |
| **$R_g$ (Å) [from Guinier]** | 41.15 | 26.87 | 74.85 |
| ***I*(0) ($cm^{-1}$) [from P(r)]** | 0.07022 ± 0.0001692 | 0.02085 ± 0.0001642 | 0.1284 ± 0.0002387 |
| **$R_g$ (Å) [from P(r)]** | 41.16 ± 0.1118 | 26.87 ± 0.2545 | 74.91 ± 0.1793 |
| **$d_{max}$ (Å)** | 144.74 | 81.91 | 255.85 |
| **Points** | 134 | 167 | 122 |
| **Alpha** | 14.60 | 3.31 | 18.69 |
| ***q* range ($Å^{-1}$)** | 0.0083-0.1947 | 0.0077-0.2952 | 0.0071-0.1074 |
| ***P*(r) total quality estimate from GNOM** | 0.8094 | 0.9257 | 0.9009 |
| **Porod volume analysis** | | | |
| **MW (kDa)** | 189.7 | 67.6 | 336.72 |
| **Porod volume ($Å^{-3}$) (ratio: $V_P$/calculated $M_W$)** | 313606.00 (1.65) | 99147.40 (1.47) | 1465780.00 (4.35) |
| **$d_{particle}$ (g $cm^{-3}$)** | 1.00 | 1.13 | 0.38 |

## 4.7 Conclusions

Sulfur metabolism across plant and bacterial species is vital to many life cycles within our planetary ecosystem. Investigating the various avenues of sulfur metabolism will not only garner a profoundly deeper understanding of the planet we live on, but offer the capability to develop new medicines, new environmentally friendly production methods, new engineering processes, or even ways to break down and remediate already existing environmental damage. Given that L-cysteine biosynthesis is at the center of sulfur metabolism, particularly in bacterial organisms, investigating bacterial sulfur metabolism, particularly of two pathogens with the same non-functional sulfur reduction pathway such as *N. gonorrhoeae* and *S. aureus* is of vital importance.

Here we have presented the kinetic and SEC-SAXS analysis of CysK from both *N. gonorrhoeae* and *S. aureus*. Small angle X-ray scattering analysis confirms that both enzymes function as dimers in solution with no other oligomeric states detected. We have characterised the kinetics of both enzymes, and hypothesise a bi-bi ping-pong mechanism, with *O*-acetylserine being first to bind, and once the acetyl group is released, sulfide enters the active site replacing the acetyl group with a thiol group, to form L-cysteine. We suggest positive cooperativity at low concentrations of OAS with a plateau beginning at concentrations ≥5 mM, and positive cooperativity at $Na_2S$ concentrations of ≤15 mM for NgCysK. We suggest substrate inhibition at OAS concentrations ≥5 mM and $Na_2S$ concentrations ≥12 mM for SaCysK. Both enzymes have a higher affinity for OAS (NgCysK: 1.541 mM, SaCysK: 1.378mM) compared to $Na_2S$ (NgCysK: 23.620 mM, SaCysK: 2.306 mM), which is intriguingly similar to the plant *O*-acetylserine sulfhydrylase isozyme A and C from *D. innoxia* (Kuske et al., 1994), but not to other bacterial homologues (Bertagnolli & Wedding, 1977; Cook & Wedding, 1976; Tai et al., 1993). The kinetic relationship to both substrates is substantially varied across CysK homologues, however, some similarities do exist. NgCysK exhibits positive cooperativity for both OAS (also seen in *D. innoxia* (Kuske et al., 1994), and $Na_2S$ (also seen in *P. vulgaris* and *D. innoxia* (Bertagnolli & Wedding, 1977; Kuske et al., 1994)). Conversely, SaCysK exhibits substrate inhibition for both OAS (also

seen in *D. innoxia* and *S.* typhimurium (Cook & Wedding, 1976; Kuske et al., 1994; Tai et al., 1993)) and $Na_2S$ (also seen in *P. vulgaris, D. innoxia* OASS (isozyme C), *P. polyanthus,* and *S. typhimurium* (Bertagnolli & Wedding, 1977; Cook & Wedding, 1976; Kuske et al., 1994)). The cooperativity seen in NgCysK indicates an interconnectedness between active sites of the NgCysK dimer. This is not observed in the SaCysK. SaCysK and NgCysK are both incapable of utilising thiosulfate as a sulfur donor in L-cysteine biosynthesis, confirming their characterisation as CysK enzymes.

Binding of OAS into the active sites of both enzymes causes some manner of conformational shift or rigidity as indicated by the improved chi-square value of both NgCysK and SaCysK in the presence of 10 mM OAS, compared to without OAS. However, this substrate binding does not cause a change in the overall flexibility or density of the enzymes, indicating a small internal conformation change.

Further elucidation of the mechanisms of sulfur metabolism also led us to the investigation of CSC formation. Using both, gel chromatography and SAXS analysis, we have shown that *N. gonorrhoeae* is incapable of CSC formation *in vitro.* This raises further questions as to the regulation of sulfur metabolism in this organism. The lack of CSC formation would mean a lack of NgCysK inhibition which may be an evolutionary advantage for *N. gonorrhoeae,* due to the high demand for L-cysteine production to produce vital reducing compounds such as glutathione. Combined with the L-cysteine feedback inhibition of NgCysE (Oldham et al., 2022), this may indicate an alternate mechanism of sulfur flux regulation in *N. gonorrhoeae.*

In bacteria, all primary pathways for inorganic sulfur assimilation converge on L-cysteine biosynthesis. Our two organisms, *S. aureus* and *N. gonorrhoeae,* both lack the ability to use inorganic sulfate as a sulfur source, but can fulfil their requirement for sulfur with thiosulfate (Le Faou, 1984; Soutourina et al., 2009). Both CysK enzymes from these pathogenic bacteria are unable to use thiosulfate for L-cysteine production, indicating the presence of an alternate sulfur acquisition pathway in both *S. aureus* and *N. gonorrhoeae.* Given the inability of *N.*

*gonorrhoeae* to form the CSC, combined with an inability to reduce sulfate or use thiosulfate for L-cysteine production, there are many more questions as to the mechanisms of sulfur regulation, acquisition and metabolism in *N. gonorrhoeae.*

Our NgCysK and SaCysK kinetics, alongside the SAXS analysis of both enzymes gives unique insight into the function of two bacteria lacking the same sulfate reduction pathway. This, combined with the inability of *N. gonorrhoeae* to form the CSC, indicates another yet undetermined sulfur metabolising pathway that will lead to a deeper understanding of our ecosystem, and may lead to advances in medicinal, climate change, and biotechnological research.

## 4.8 Supplementary information

Supplementary information associated with this chapter can be found in Appendix B: Supplementary material for Chapter Four

## 4.9 Future directions

This work demonstrates important progress into the elucidation of sulfur metabolism in bacteria. Characterising the vast array of different sulfur metabolic pathways among bacteria will give us invaluable insights, allowing further development and manipulation of natural mechanisms and pathways for engineering, environmental or medicinal research. Here we have characterised the biochemistry of the final enzyme in the two step L-cysteine biosynthetic pathway for two human pathogens, *N. gonorrhoeae* and *S. aureus* with the same sulfur reduction pathway absence (Hicks & Mullholland, 2018; Lithgow et al., 2004; Soutourina et al., 2009). This work lays the foundation for further exploration of the final enzymes function in sulfur metabolism in these two pathogens.

In this work, we characterised the kinetic relationship NgCysK and SaCysK have with their two substrates, OAS and $Na_2S$. However, Tai and colleagues have shown the presence of anions, in particular $Cl^-$, in a non-specific anion binding site in CysK from *S. typhimurium* (Tai et al., 2001). Therefore, using the established reaction we will collect kinetic data with increasing $Cl^-$ concentrations to further elucidate the mechanism of NgCysK catalysis. Given that high intracellular levels of L-cysteine are cytotoxic to bacteria, and the catalytic activity of CysK enzymes is a reversible reaction, investigating the kinetic relationship of NgCysK and SaCysK to

L-cysteine may be invaluable. This may provide insight into why the CSC does not form in *N. gonorrhoeae. N. gonorrhoeae* may not require regulation of sulfur flux in the same manner as other bacterial and plant species. Given the inability to form the CSC, this indicates there is no requirement by *N. gonorrhoeae* to limit the activity of NgCysK.

In this research, we have shown the inability of *N. gonorrhoeae* to form the CSC at µM concentrations, significantly higher concentrations than those used to form the CSC in *E. coli* (Benoni, De Bei, et al., 2017a). However, further experimentation will completely rule out the CSC formation. We will attempt co-expression of the NgCysE and NgCysK enzyme with an N-terminal his-tag on the NgCysE enzyme. This should determine whether the lack of complex formation is simply due to the *in vitro* environment we have thus far attempted to form the CSC, or if given a cytoplasmic environment within a bacterial cell, the two enzymes will successfully form a complex. If the complex is successfully formed, it should elute successfully from a Nickel IMAC purification and give a peak at ~11.9 ml from an analytical SEC. Alternatively, *Brucella abortus* was unable to form the CSC, despite the required residues being present in the CysE C-terminal tetrapeptide (Dharavath, Raj, & Gourinath, 2017). This was a result of two CysK active site residues occupying the active site and preventing the C-terminal tetrapeptide of CysE from binding (Dharavath et al., 2017). We will create two, point mutation NgCysK enzymes, E96A and E96Q. If the E96A NgCysK forms the CSC, this will indicate the formation was prevented due to the size of the residue in the active site pocket, however if the E96Q NgCysK forms the complex, this will indicate the negative charge of the Glu96 residue may have repelled the negatively charged Asp from the C-terminal tetrapeptide of NgcysE (DFMI). Overall, this is an excellent starting point for characterisation of this alternate sulfur metabolic pathway observed in both *N. gonorrhoeae* and *S. aureus.*

## 4.10 References


Benoni, R., Beck, C. M., Garza-Sánchez, F., Bettati, S., Mozzarelli, A., Hayes, C. S., & Campanini, B. (2017). Activation of an anti-bacterial toxin by the biosynthetic enzyme CysK: mechanism of binding, interaction specificity and competition with cysteine synthase. *Scientific Reports, 7*(1) 10.1038/s41598-017-09022-6

Benoni, R., De Bei, O., Paredi, G., Hayes, C. S., Franko, N., Mozzarelli, A., . . . Campanini, B. (2017a). Modulation of Escherichia coli serine acetyltransferase catalytic activity in the cysteine synthase complex. *FEBS Letters, 591*(9), 1212-1224. 10.1002/1873-3468.12630

Benoni, R., De Bei, O., Paredi, G., Hayes, C. S., Franko, N., Mozzarelli, A., . . . Campanini, B. (2017b). Modulation ofEscherichia coliserine acetyltransferase catalytic activity in the cysteine synthase complex. *FEBS Letters, 591*(9), 1212-1224. 10.1002/1873-3468.12630

Bertagnolli, B. L., & Wedding, R. T. (1977). Purification and initial kinetic characterization of different forms of o-acetylserine sulfhydrylase from seedlings of two species of phaseolus. *Plant Physiol, 60*(1), 115-121. 10.1104/pp.60.1.115

Bulut, H., Moniot, S., Licht, A., Scheffel, F., Gathmann, S., Saenger, W., & Schneider, E. (2012). Crystal Structures of Two Solute Receptors for l-Cystine and l-Cysteine, Respectively, of the Human Pathogen Neisseria gonorrhoeae. *Journal of Molecular Biology, 415*(3), 560-572. 10.1016/j.jmb.2011.11.030

Campanini, B., Pieroni, M., Raboni, S., Bettati, S., Benoni, R., Pecchini, C., . . . Mozzarelli, A. (2015). Inhibitors of the sulfur assimilation pathway in bacterial pathogens as enhancers of antibiotic therapy. *Curr Med Chem, 22*(2), 187-213. 10.2174/0929867321666141112122553

Capel, E., Zomer, A. L., Nussbaumer, T., Bole, C., Izac, B., Frapy, E., . . . Coureuil, M. (2016). Comprehensive Identification of Meningococcal Genes and Small Noncoding RNAs Required for Host Cell Colonization. *mBio, 7*(4) 10.1128/mBio.01173-16

Carmel-Harel, O., & Storz, G. (2000). Roles of the Glutathione- and Thioredoxin-Dependent Reduction Systems in theEscherichia ColiandSaccharomyces CerevisiaeResponses to Oxidative Stress. *Annual Review of Microbiology, 54*(1), 439-461. 10.1146/annurev.micro.54.1.439

Chaudhuri, R. R., Allen, A. G., Owen, P. J., Shalom, G., Stone, K., Harrison, M., . . . Charles, I. G. (2009). Comprehensive identification of essential Staphylococcus aureus genes using Transposon-Mediated Differential Hybridisation (TMDH). *BMC Genomics, 10*(1), 291. 10.1186/1471-2164-10-291

Cook, P. F., & Wedding, R. T. (1976). A reaction mechanism from steady state kinetic studies for O-acetylserine sulfhydrylase from Salmonella typhimurium LT-2. *Journal of Biological Chemistry, 251*(7), 2023-2029. 10.1016/s0021-9258(17)33649-9

de Jong Nienke, W. M., van Kessel Kok, P. M., & van Strijp Jos, A. G. (2019). Immune Evasion by Staphylococcus aureus. *Microbiology Spectrum, 7*(2), 10.1128/microbiolspec.gpp1123-0061-2019. 10.1128/microbiolspec.gpp3-0061-2019

Dharavath, S., Raj, I., & Gourinath, S. (2017). Structure-based mutational studies of O-acetylserine sulfhydrylase reveal the reason for the loss of cysteine

synthase complex formation in Brucella abortus. *Biochemical Journal, 474*(7), 1221-1239. 10.1042/bcj20161062

Edwards, J. L., & Butler, E. K. (2011). The Pathobiology of Neisseria gonorrhoeae Lower Female Genital Tract Infection. *Frontiers in Microbiology, 2* 10.3389/fmicb.2011.00102

Eryilmaz, E., Janda, A., Kim, J., Cordero, R. J. B., Cowburn, D., & Casadevall, A. (2013). Global structures of IgG isotypes expressing identical variable regions. *Molecular Immunology, 56*(4), 588-598. 10.1016/j.molimm.2013.06.006

Friedman, M. (2004). Applications of the Ninhydrin Reaction for Analysis of Amino Acids, Peptides, and Proteins to Agricultural and Biomedical Sciences. *Journal of Agricultural and Food Chemistry, 52*(3), 385-406. 10.1021/jf030490p

Gaitonde, M. (1967). A spectrophotometric method for the direct determination of cysteine in the presence of other naturally occurring amino acids. *Biochemical Journal, 104*(2), 627-633. 10.1042/bj1040627

Gasteiger, E., Hoogland, C., Gattiker, A., Duvaud, S. e., Wilkins, M. R., Appel, R. D., & Bairoch, A. (2005). Protein Identification and Analysis Tools on the ExPASy Server. In J. M. Walker (Ed.), *The Proteomics Protocols Handbook* (pp. 571-607). Totowa, NJ: Humana Press.

Gaupp, R., Ledala, N., & Somerville, G. A. (2012). Staphylococcal response to oxidative stress. *Frontiers in Cellular and Infection Microbiology, 2* 10.3389/fcimb.2012.00033

Guédon, E., & Martin-Verstraete, I. (2007). Cysteine Metabolism and Its Regulation in Bacteria. In V. F. Wendisch (Ed.), *Amino Acid Biosynthesis ~ Pathways, Regulation and Metabolic Engineering* (pp. 195-218). Berlin, Heidelberg: Springer Berlin Heidelberg.

Hell, R., & Wirtz, M. (2002). Molecular Biology, Biochemistry and Cellular Physiology of Cysteine Metabolism in *Arabidopsis thaliana*. *The Arabadopsis Book*, 1-19. 10.1199/tab.0154.full

Hicks, J. L., & Mullholland, C. V. (2018). Cysteine biosynthesis in Neisseria species. *Microbiology, 164*(12), 1471-1480. 10.1099/mic.0.000728

Hopkins, J. B., Gillilan, R. E., & Skou, S. (2017). *BioXTAS RAW*: improvements to a free open-source program for small-angle X-ray scattering data reduction and analysis. *Journal of Applied Crystallography, 50*(5), 1545-1553. 10.1107/s1600576717011438

Hryniewicz, M. M., & Kredich, N. M. (1991). The cysP promoter of Salmonella typhimurium: characterization of two binding sites for CysB protein, studies of in vivo transcription initiation, and demonstration of the anti-inducer effects of thiosulfate. *Journal of Bacteriology, 173*(18), 5876-5886. 10.1128/jb.173.18.5876-5886.1991

Huang, B., Vetting, M. W., & Roderick, S. L. (2005). The Active Site of O-Acetylserine Sulfhydrylase Is the Anchor Point for Bienzyme Complex Formation with Serine Acetyltransferase. *Journal of Bacteriology, 187*(9), 3201-3205. 10.1128/jb.187.9.3201-3205.2005

Johnson, C. M., Roderick, S. L., & Cook, P. F. (2005). The serine acetyltransferase reaction: acetyl transfer from an acylpantothenyl donor to an alcohol. *Archives of Biochemistry and Biophysics, 433*(1), 85-95. 10.1016/j.abb.2004.08.014

Joshi, P., Gupta, A., & Gupta, V. (2019). Insights into multifaceted activities of CysK for therapeutic interventions. *3 Biotech, 9*(2) 10.1007/s13205-019-1572-4

Jovanovic, M., Lilic, M., Savic, D. J., & Jovanovic, G. (2003). The LysR-type transcriptional regulator CysB controls the repression of hslJ transcription in Escherichia coli. *Microbiology, 149*(12), 3449-3459. 10.1099/mic.0.26609-0

Kertesz, M. A. (2000). Riding the sulfur cycle – metabolism of sulfonates and sulfate esters in Gram-negative bacteria. *FEMS Microbiology Reviews, 24*(2), 135-175. 10.1016/s0168-6445(99)00033-9

Kertesz, M. A. (2001). Bacterial transporters for sulfate and organosulfur compounds. *Research in Microbiology, 152*(3-4), 279-290. 10.1016/s0923-2508(01)01199-8

Kikhney, A. G., & Svergun, D. I. (2015). A practical guide to small angle X-ray scattering (SAXS) of flexible and intrinsically disordered proteins. *FEBS Letters, 589*(19PartA), 2570-2577. 10.1016/j.febslet.2015.08.027

Kirby, N., Cowieson, N., Hawley, A. M., Mudie, S. T., McGillivray, D. J., Kusel, M., . . . Ryan, T. M. (2016). Improved radiation dose efficiency in solution SAXS using a sheath flow sample environment. *Acta Crystallogr D Struct Biol, 72*(Pt 12), 1254-1266. 10.1107/s2059798316017174

Kirby, N. M., Mudie, S. T., Hawley, A. M., Cookson, D. J., Mertens, H. D. T., Cowieson, N., & Samardzic-Boban, V. (2013). A low-background-intensity focusing small-angle X-ray scattering undulator beamline. *Journal of Applied Crystallography, 46*(6), 1670-1680. https://doi.org/10.1107/S002188981302774X

Korshunov, S., Imlay, K. R. C., & Imlay, J. A. (2020). Cystine import is a valuable but risky process whose hazardsEscherichia coliminimizes by inducing a cysteine exporter. *Molecular Microbiology, 113*(1), 22-39. 10.1111/mmi.14403

Kredich, N. M. (1992). The molecular basis for positive regulation of *cys* promoters in *Salmonella typhimurium* and *Escherichia coli Molecular Microbiology, 6*(19), 2747-2753. 10.1111/j.1365-2958.1992.tb01453.x

Kredich, N. M. (2008). Biosynthesis of Cysteine. *EcoSal Plus, 3*(1) 10.1128/ecosalplus.3.6.1.11

Kredich, N. M., Becker, M. A., & Tomkins, G. M. (1969). Purification and Characterization of Cysteine Synthetase, a Bifunctional Protein Complex, from Salmonella typhimurium. *Journal of Biological Chemistry, 244*(9), 2428-2439. 10.1016/s0021-9258(19)78241-6

Kredich, N. M., & Tomkins, G. M. (1966). The Enzymic Synthesis of L-Cysteine in Escherichia coli and Salmonella typhimurium. *Journal of Biological Chemistry, 241*(21), 4955-4965. 10.1016/s0021-9258(18)99657-2

Kumar, S., Raj, I., Nagpal, I., Subbarao, N., & Gourinath, S. (2011). Structural and Biochemical Studies of Serine Acetyltransferase Reveal Why the Parasite Entamoeba histolytica Cannot Form a Cysteine Synthase Complex. *Journal of Biological Chemistry, 286*(14), 12533-12541. 10.1074/jbc.m110.197376

Kumaran, S., Yi, H., Krishnan, H. B., & Jez, J. M. (2009). Assembly of the Cysteine Synthase Complex and the Regulatory Role of Protein-Protein Interactions. *Journal of Biological Chemistry, 284*(15), 10268-10275. 10.1074/jbc.m900154200

Kuske, C. R., Ticknor, L. O., Guzmán, E., Gurley, L. R., Valdez, J. G., Thompson, M. E., & Jackson, P. J. (1994). Purification and characterization of O-

acetylserine sulfhydrylase isoenzymes from Datura innoxia. *Journal of Biological Chemistry, 269*(8), 6223-6232. 10.1016/s0021-9258(17)37591-9

Le Faou, A. (1984). Sulphur nutrition and metabolism in various species of Neisseria. *Annales de l'Institut Pasteur / Microbiologie, 135*(1, Supplement B), 3-11. https://doi.org/10.1016/S0769-2609(84)80037-X

Lensmire, J. M., Wischer, M. R., Kraemer-Zimpel, C., Kies, P. J., Sosinski, L., Ensink, E., . . . Hammer, N. D. (2023). The glutathione import system satisfies the Staphylococcus aureus nutrient sulfur requirement and promotes interspecies competition. *PLOS Genetics, 19*(7), e1010834. 10.1371/journal.pgen.1010834

Lithgow, J. K., Hayhurst, E. J., Cohen, G., Aharonowitz, Y., & Foster, S. J. (2004). Role of a Cysteine Synthase in Staphylococcus aureus. *Journal of Bacteriology, 186*(6), 1579-1590. 10.1128/jb.186.6.1579-1590.2004

Lochowska, A., Iwanicka-Nowicka, R., Zaim, J., Witkowska-Zimny, M., Bolewska, K., & Hryniewicz, M. M. (2004). Identification of activating region (AR) of Escherichia coli LysR-type transcription factor CysB and CysB contact site on RNA polymerase alpha subunit at the cysP promoter. *Molecular Microbiology, 53*(3), 791-806. 10.1111/j.1365-2958.2004.04161.x

Madeira, F., Park, Y. M., Lee, J., Buso, N., Gur, T., Madhusoodanan, N., . . . Lopez, R. (2019). The EMBL-EBI search and sequence analysis tools APIs in 2019. *Nucleic Acids Research, 47*(W1), W636-W641. 10.1093/nar/gkz268

Makowski, L., Berkowitz, S., & Houde, D. (2020). Scattering techniques for the characterization of biopharmaceuticals (pp. 185-223).

Manalastas-Cantos, K., Konarev, P. V., Hajizadeh, N. R., Kikhney, A. G., Petoukhov, M. V., Molodenskiy, D. S., . . . Franke, D. (2021). *ATSAS 3.0*: expanded functionality and new tools for small-angle scattering data analysis. *Journal of Applied Crystallography, 54*(1), 343-355. 10.1107/s1600576720013412

Meister, A., & Anderson, M. E. (1983). GLUTATHIONE. *Annual Review of Biochemistry, 52*(1), 711-760. 10.1146/annurev.bi.52.070183.003431

Mino, K., Hiraoka, K., Imamura, K., Sakiyama, T., Eisaki, N., Matsuyama, A., & Nakanishi, K. (2000). Characteristics of Serine Acetyltransferase from Escherichia coli Deleting Different Lengths of Amino Acid Residues from the C-Terminus. *Bioscience, Biotechnology, and Biochemistry, 64*(9), 1874-1880. 10.1271/bbb.64.1874

Mino, K., & Ishikawa, K. (2003). A novel O-phospho-L-serine sulfhydrylation reaction catalyzed by O-acetylserine sulfhydrylase from Aeropyrum pernix K1. *FEBS Letters, 551*(1-3), 133-138. 10.1016/s0014-5793(03)00913-x

Mino, K., Yamanoue, T., Sakiyama, T., Eisaki, N., Matsuyama, A., & Nakanishi, K. (2000a). Effects of Bienzyme Complex Formation of Cysteine Synthetase from Escherichia coli on Some Properties and Kinetics. *Bioscience, Biotechnology, and Biochemistry, 64*(8), 1628-1640. 10.1271/bbb.64.1628

Mino, K., Yamanoue, T., Sakiyama, T., Eisaki, N., Matsuyama, A., & Nakanishi, K. (2000b). Effects of Bienzyme Complex Formation of Cysteine Synthetase fromEscherichia colion Some Properties and Kinetics. *Bioscience, Biotechnology, and Biochemistry, 64*(8), 1628-1640. 10.1271/bbb.64.1628

Oldham, K. E. A., Prentice, E. J., Summers, E. L., & Hicks, J. L. (2022). Serine acetyltransferase from Neisseria gonorrhoeae; structural and biochemical

basis of inhibition. *Biochemical Journal, 479*(1), 57-74. 10.1042/BCJ20210564

Ostrowski, J., & Kredich, N. M. (1989). Molecular characterization of the cysJIH promoters of Salmonella typhimurium and Escherichia coli: regulation by cysB protein and N-acetyl-L-serine. *Journal of Bacteriology, 171*(1), 130-140. 10.1128/jb.171.1.130-140.1989

Ostrowski, J., & Kredich, N. M. (1991). Negative autoregulation of cysB in Salmonella typhimurium: in vitro interactions of CysB protein with the cysB promoter. *Journal of Bacteriology, 173*(7), 2212-2218. 10.1128/jb.173.7.2212-2218.1991

Owais, W. M., & Gharaibeh, R. (1990). Cloning of the E. coli O-acetylserine sulfhydrylase gene: ability of the clone to produce a mutagenic product from azide and O-acetylserine. *Mutat Res, 245*(3), 151-155. 10.1016/0165-7992(90)90043-j

Panjkovich, A., & Svergun, D. I. (2018). CHROMIXS: automatic and interactive analysis of chromatography-coupled small-angle X-ray scattering data. *Bioinformatics, 34*(11), 1944-1946. 10.1093/bioinformatics/btx846

Pederick, J. L., Vandborg, B. C., George, A., Bovermann, H., Boyd, J. M., Freundlich, J. S., & Bruning, J. B. (2024). Identification of cysteine metabolism regulator (CymR)-derived pentapeptides as nanomolar inhibitors of*Staphylococcus aureus*O-acetyl-L-serine sulfhydrylase (CysK). Cold Spring Harbor Laboratory. Retrieved from https://dx.doi.org/10.1101/2024.09.19.614015

Petoukhov, M. V., Franke, D., Shkumatov, A. V., Tria, G., Kikhney, A. G., Gajda, M., . . . Svergun, D. I. (2012). New developments in the ATSAS program package for small-angle scattering data analysis. *J Appl Crystallogr, 45*(Pt 2), 342-350. 10.1107/s0021889812007662

Pinto, R., Leotta, L., Shanahan, E. R., West, N. P., Leyh, T. S., Britton, W., & Triccas, J. A. (2013). Host Cell–Induced Components of the Sulfate Assimilation Pathway Are Major Protective Antigens of Mycobacterium tuberculosis. *The Journal of Infectious Diseases, 207*(5), 778-785. 10.1093/infdis/jis751

Putnam, C. D. (2016). Guinier peak analysis for visual and automated inspection of small-angle X-ray scattering data. *Journal of Applied Crystallography, 49*(5), 1412-1419. 10.1107/s1600576716010906

Pye, V. E., Tingey, A. P., Robson, R. L., & Moody, P. C. E. (2004). The Structure and Mechanism of Serine Acetyltransferase from Escherichia coli. *Journal of Biological Chemistry, 279*(39), 40729-40736. 10.1074/jbc.m403751200

Quillin, S. J., & Seifert, H. S. (2018). Neisseria gonorrhoeae host adaptation and pathogenesis. *Nature Reviews Microbiology, 16*(4), 226-240. 10.1038/nrmicro.2017.169

Rabeh, W. M., & Cook, P. F. (2004). Structure and Mechanism of O-Acetylserine Sulfhydrylase. *Journal of Biological Chemistry, 279*(26), 26803-26806. 10.1074/jbc.R400001200

Rambo, R. P., & Tainer, J. A. (2011). Characterizing flexible and intrinsically unstructured biological macromolecules by SAS using the Porod-Debye law. *Biopolymers, 95*(8), 559-571. 10.1002/bip.21638

Ramirez, A., Castneda, M., Xiqui, M. L., Sosa, A., & Baca, B. E. (2006). Identification, cloning and characterization of*cysK* the gene encoding*O*acetylserine (thiol)-lyase from*Azospirillum brasilense* which is

involved in tellurite resistance. *FEMS Microbiology Letters, 261*(2), 272-279. 10.1111/j.1574-6968.2006.00369.x

Receveur-Brechot, V., & Durand, D. (2012). How random are intrinsically disordered proteins? A small angle scattering perspective. *Curr Protein Pept Sci, 13*(1), 55-75. 10.2174/138920312799277901

Remmele, C. W., Xian, Y., Albrecht, M., Faulstich, M., Fraunholz, M., Heinrichs, E., . . . Rudel, T. (2014). Transcriptional landscape and essential genes of Neisseria gonorrhoeae. *Nucleic Acids Research, 42*(16), 10579-10595. 10.1093/nar/gku762

Robert, X., & Gouet, P. (2014). Deciphering key features in protein structures with the new ENDscript server. *Nucleic Acids Research, 42*(W1), W320-W324. 10.1093/nar/gku316

Rosa, B., Marchetti, M., Paredi, G., Amenitsch, H., Franko, N., Benoni, R., . . . Bettati, S. (2019). Combination of SAXS and Protein Painting Discloses the Three-Dimensional Organization of the Bacterial Cysteine Synthase Complex, a Potential Target for Enhancers of Antibiotic Action. *International Journal of Molecular Sciences, 20*(20), 5219. 10.3390/ijms20205219

Roskoski, R. (2007). Michaelis-Menten Kinetics. In S. J. Enna & D. B. Bylund (Eds.), *xPharm: The Comprehensive Pharmacology Reference* (pp. 1-10). New York: Elsevier.

Rusniok, C., Vallenet, D., Floquet, S., Ewles, H., Mouzé-Soulama, C., Brown, D., . . . Pelicic, V. (2009). NeMeSys: a biological resource for narrowing the gap between sequence and function in the human pathogen Neisseria meningitidis. *Genome Biology, 10*(10), R110. 10.1186/gb-2009-10-10-r110

Saito, K., Yokoyama, H., Noji, M., & Murakoshi, I. (1995). Molecular Cloning and Characterization of a Plant Serine Acetyltransferase Playing a Regulatory Role in Cysteine Biosynthesis from Watermelon. *Journal of Biological Chemistry, 270*(27), 16321-16326. 10.1074/jbc.270.27.16321

Salsi, E., Bayden, A. S., Spyrakis, F., Amadasi, A., Campanini, B., Bettati, S., . . . Mozzarelli, A. (2010). Design of O-Acetylserine Sulfhydrylase Inhibitors by Mimicking Nature. *Journal of Medicinal Chemistry, 53*(1), 345-356. 10.1021/jm901325e

Schnell, R., Oehlmann, W., Singh, M., & Schneider, G. (2007). Structural Insights into Catalysis and Inhibition of O-Acetylserine Sulfhydrylase from Mycobacterium tuberculosis. *Journal of Biological Chemistry, 282*(32), 23473-23481. 10.1074/jbc.m703518200

Seib, K. L., Wu, H.-J., Kidd, S. P., Apicella, M. A., Jennings, M. P., & McEwan, A. G. (2006). Defenses against Oxidative Stress in*Neisseria gonorrhoeae* a System Tailored for a Challenging Environment. *Microbiology and Molecular Biology Reviews, 70*(2), 344-361. 10.1128/mmbr.00044-05

Sekowska, A., Kung, H. F., & Danchin, A. (2000). Sulfur metabolism in Escherichia coli and related bacteria: facts and fiction. *J Mol Microbiol Biotechnol, 2*(2), 145-177.

Singh, P., Brooks, J. F., Ray, V. A., Mandel, M. J., & Visick, K. L. (2015). CysK Plays a Role in Biofilm Formation and Colonization by Vibrio fischeri. *Applied and Environmental Microbiology, 81*(15), 5223-5234. 10.1128/aem.00157-15

Skou, S., Gillilan, R. E., & Ando, N. (2014). Synchrotron-based small-angle X-ray scattering of proteins in solution. *Nature Protocols, 9*(7), 1727-1739. 10.1038/nprot.2014.116

Sosa Torres, M. E., Rito Morales, A., Solano Peralta, A., & Kroneck, P. M. H. (2020). Sulfur, the Versatile Non-metal. *Met Ions Life Sci, 20* 10.1515/9783110589757-008

Soutourina, O., Poupel, O., Coppée, J. Y., Danchin, A., Msadek, T., & Martin-Verstraete, I. (2009). CymR, the master regulator of cysteine metabolism in *Staphylococcus aureus* controls host sulphur source utilization and plays a role in biofilm formation. *Molecular Microbiology, 73*(2), 194-211. 10.1111/j.1365-2958.2009.06760.x

Svergun, D., Barberato, C., & Koch, M. H. J. (1995). CRYSOL– a Program to Evaluate X-ray Solution Scattering of Biological Macromolecules from Atomic Coordinates. *Journal of Applied Crystallography, 28*(6), 768-773. https://doi.org/10.1107/S0021889895007047

Svergun, D. I. (1992). Determination of the regularization parameter in indirect-transform methods using perceptual criteria. *Journal of Applied Crystallography, 25*(4), 495-503. https://doi.org/10.1107/S0021889892001663

Tai, C.-H., Burkhard, P., Gani, D., Jenn, T., Johnson, C., & Cook, P. F. (2001). Characterization of the Allosteric Anion-Binding Site ofO-Acetylserine Sulfhydrylase†. *Biochemistry, 40*(25), 7446-7452. 10.1021/bi015511s

Tai, C. H., Nalabolu, S. R., Jacobson, T. M., Minter, D. E., & Cook, P. F. (1993). Kinetic mechanisms of the A and B isozymes of O-acetylserine sulfhydrylase from Salmonella typhimurium LT-2 using the natural and alternate reactants. *Biochemistry, 32*(25), 6433-6442. 10.1021/bi00076a017

Takahashi, H., Watanabe, H., Kim, K. S., Yokoyama, S., & Yanagisawa, T. (2018). The Meningococcal Cysteine Transport System Plays a Crucial Role in *Neisseria meningitidis* Survival in Human Brain Microvascular Endothelial Cells. *mBio, 9*(6) 10.1128/mbio.02332-18

Takumi, K., & Nonaka, G. (2016). Bacterial Cysteine-Inducible Cysteine Resistance Systems. *Journal of Bacteriology, 198*(9), 1384-1392. 10.1128/jb.01039-15

Trewhella, J., Duff, A. P., Durand, D., Gabel, F., Guss, J. M., Hendrickson, W. A., . . . Whitten, A. E. (2017). 2017 publication guidelines for structural modelling of small-angle scattering data from biomolecules in solution: an update. *Acta Crystallographica Section D Structural Biology, 73*(9), 710-728. 10.1107/s2059798317011597

Vagenende, V., Yap, M. G. S., & Trout, B. L. (2009). Mechanisms of Protein Stabilization and Prevention of Protein Aggregation by Glycerol. *Biochemistry, 48*(46), 11084-11096. 10.1021/bi900649t

Wang, T., & Leyh, T. S. (2012). Three-stage Assembly of the Cysteine Synthase Complex from Escherichia coli. *Journal of Biological Chemistry, 287*(6), 4360-4367. 10.1074/jbc.m111.288423

Whitten, A. E., Cai, S., & Trewhella, J. (2008). *MULCh*: modules for the analysis of small-angle neutron contrast variation data from biomolecular assemblies. *Journal of Applied Crystallography*(41), 222-226. 10.1107/S0021889807055136

Wirtz, M., Beard, K. F. M., Lee, C. P., Boltz, A., Schwarzländer, M., Fuchs, C., . . . Hell, R. (2012). Mitochondrial Cysteine Synthase Complex Regulates O-Acetylserine Biosynthesis in Plants. *Journal of Biological Chemistry, 287*(33), 27941-27947. 10.1074/jbc.m112.372656

Wirtz, M., & Hell, R. (2006). Functional analysis of the cysteine synthase protein complex from plants: Structural, biochemical and regulatory properties. *Journal of Plant Physiology, 163*(3), 273-286. 10.1016/j.jplph.2005.11.013

Wu, B., Liu, F., Fang, W., Yang, T., Chen, G.-H., He, Z., & Wang, S. (2021). Microbial sulfur metabolism and environmental implications. *Science of The Total Environment, 778*, 146085. https://doi.org/10.1016/j.scitotenv.2021.146085

Yamamoto, K., Oshima, T., Nonaka, G., Ito, H., & Ishihama, A. (2011). Induction of the Escherichia colicysK gene by genetic and environmental factors. *FEMS Microbiology Letters, 323*(1), 88-95. 10.1111/j.1574-6968.2011.02364.x

Yi, H., Dey, S., Kumaran, S., Lee, S. G., Krishnan, H. B., & Jez, J. M. (2013). Structure of Soybean Serine Acetyltransferase and Formation of the Cysteine Regulatory Complex as a Molecular Chaperone. *Journal of Biological Chemistry, 288*(51), 36463-36472. 10.1074/jbc.m113.527143

Zhao, C., Moriga, Y., Feng, B., Kumada, Y., Imanaka, H., Imamura, K., & Nakanishi, K. (2006). On the interaction site of serine acetyltransferase in the cysteine synthase complex from Escherichia coli. *Biochemical and Biophysical Research Communications, 341*(4), 911-916. https://doi.org/10.1016/j.bbrc.2006.01.054

# Chapter Five: Conclusions and Future Perspectives

## 5.1 Thesis summary

*Neisseria gonorrhoeae* is the causative agent of the sexually transmitted infection (STI), gonorrhoea. Rapid emergence of antimicrobial-resistant strains has given rise to resistance to every class of frontline antibiotic used for treatment (Unemo et al., 2019). The appearance of ceftriaxone-resistant strains led to the World Health Organisation categorising *N. gonorrhoeae* as a high priority pathogen, emphasising the urgent need for new antimicrobials (WHO, 2024). Absence of the *de novo* L-cysteine biosynthesis pathway in humans makes this pathway an excellent target for the development of new antimicrobials (Campanini et al., 2015). Interestingly, another high priority pathogen, *Staphylococcus aureus,* is missing the same sulfate reduction pathway as *N. gonorrhoeae.* Characterising the sulfur acquisition strategies of bacteria provides important insights into our ecosystems and provides new strategies for developing medicines and biotechnologies. Identifying inhibitors for CysK and CysE enzymes in both Gram-negative and Gram-positive bacterial pathogens has progressed well. This thesis demonstrates my work to characterise kinetics and structural changes in the *N. gonorrhoeae* and *S. aureus* CysK enzymes, and to characterise the structure and use structure-based virtual inhibitor screening for the *N. gonorrhoeae* CysK (NgCysK).

We hypothesised that NgCysK was a promising target for antimicrobial adjuvant development, given the stress encountered in the host environment (Seib et al., 2006), and despite its non-essentiality in *N. gonorrhoeae* (Remmele et al., 2014), it's importance for epithelial cell colonisation in the closely related *N. meningitidis* (Capel et al., 2016), and decreased fitness and increased antibiotic susceptibility in *S. typhimurium* (Capel et al., 2016; Turnbull & Surette, 2010). As NgCysK was uncharacterised, the collection and analysis of structural data was vital for structure-based virtual inhibitor screening for NgCysK inhibitors. For NgCysK characterisation, methods for expression and purification were optimised. Using our purification methods, we were able to produce NgCysK of sufficient purity and yield for downstream analysis.

Using size exclusion chromatography (SEC), we show that NgCysK elutes as a dimer. These findings are supported by our SEC-small angle X-ray scattering (SAXS) data where only the NgCysK species was observed with no other oligomeric states present, therefore showing that, overall, NgCysK exists solely as a dimer in solution which is consistent with characterised CysK homologues.

To identify NgCysK inhibitors, we used a structure-based virtual inhibitor screening strategy, which required a high quality NgCysK model. This was generated using the 2.49 Å NgCysK crystal structure, combined with the highest sequence similarity CysK enzyme, MtCysK (PDB ID: 3ZEI). An NgCysK homology model with PLP bound was generated due to some missing active site residues and the lack of electron density for the co-factor PLP. Using recombinant NgCysK an optimal crystallisation condition was identified resulting in collection of a 2.49 Å dataset. Model refinement revealed NgCysK had crystallised as a homodimer. Each dimer was formed through the hydrogen bonds and hydrophobic interactions between each monomer. NgCysK active sites are comprised of residues all within each subunit of the dimer resulting in two active sites per dimer. Intriguingly, when overlaid with MtCysK, we see each monomer of the NgCysK dimer is in a different conformation indicating positive cooperativity. One monomer is inactive due to its conformation not allowing PLP binding into the active site, and one is in an active conformation allowing PLP binding. This positive cooperativity is also supported by the allosteric relationship NgCysK seen in our kinetic analysis of both substrates, OAS and $Na_2S$. Overall, we have shown that NgCsyK has a dimeric oligomeric structure consistent with CysK homologues.

To conduct structure-based virtual inhibitor screening the NgCysK structure had to be prepared for library screening. The NgCysK missing active site residues and the missing PLP co-factor were modelled, creating a homology model with MtCysK as the schematic for missing sections. The screening of a commercially available drug-like library was conducted, producing a total of 42 hit compounds, of which 10 were ordered, and 5 were tested downstream. To test for inhibitory activity *in vitro,* a colourimetric stopped assay was adapted for high throughput screening of inhibitors against NgCysK. This screening demonstrated the best inhibitor was compound 5,

producing an $IC_{50}$ of 253.5 μM, placing it in the mid-range of CysK inhibitors to date. Analysis of docking interactions between compound 5 and NgCysK shows key hydrogen bonds between active site residues in the binding pocket supported by hydrophobic interactions from active site cleft residues. Overall, this research presents the first characterisation and inhibitor for NgCysK, and is the second published attempt to target a sulfur metabolism pathway in *Neisseria* species. This thesis demonstrates the targeting of *de novo* L-cysteine biosynthesis to be a promising source of new antimicrobial adjuvant targets for *N. gonorrhoeae*.

In addition, given the absence of the sulfate reduction pathway in *N. gonorrhoeae* and *S. aureus,* investigation of this alternate sulfur metabolism was necessary. Both human pathogens share the same sulfate reduction pathway and yet are reliant upon sulfur containing compound such as thiols for resisting the oxidatively stressed environments they colonise. L-cysteine biosynthesis is where all bacterial sulfur metabolism converges, making investigation of the final enzyme in the L-cysteine biosynthesis pathway vital. Using an adapted colourimetric stopped assay, the kinetics of both NgCsyK and SaCysK were determined showing an allosteric sigmoidal relationship of NgCysK with both substrates, and a substrate inhibition relationship of SaCysK with both substrates. Structural changes caused by OAS substrate binding were also explored indicating no large-scale change in the overall size of the enzymes when bound. The formation of the cysteine synthase complex has been identified to regulate sulfur flux. Therefore, given the missing sulfate reduction pathway, the formation of this complex was also investigated. *N. gonorrhoeae* is unable to form the cysteine synthase complex *in vitro* which raises further questions as to the role of CysK in *N. gonorrhoeae* sulfur metabolism and how *N. gonorrhoeae* regulates said sulfur metabolism. Overall, we have demonstrated the inability of *N. gonorrhoeae* to form the CSC and the kinetic relationship of NgCysK and SaCysK to their substrates, OAS and $Na_2S$.

## 5.2 Future perspectives

Future perspective sections are available at the end of each chapter under the heading “Future directions”.

## 5.3 Concluding statement

The results presented in this thesis have enhanced our understanding of CysK enzymes and their role in *de novo* L-cysteine biosynthesis in *N. gonorrhoeae* and *S. aureus*. The biochemical characterisation of NgCysK was fundamental, not only for understanding its role in L-cysteine biosynthesis but was also essential to our discovery of the first NgCysK inhibitors. The kinetic and SAXS structural characterisation of NgCysK and SaCysK is a vital stepping stone to understanding the sulfur utilisation strategy of two high priority pathogens. Elucidation of the CSC in *N. gonorrhoeae* deepens our understanding of sulfur metabolism. This thesis is a testament to the antimicrobial adjuvant potential of CysK inhibition and lays a foundation for targeting CysK in other bacterial pathogens.

# Appendix A: Supplementary information for Chapter Three

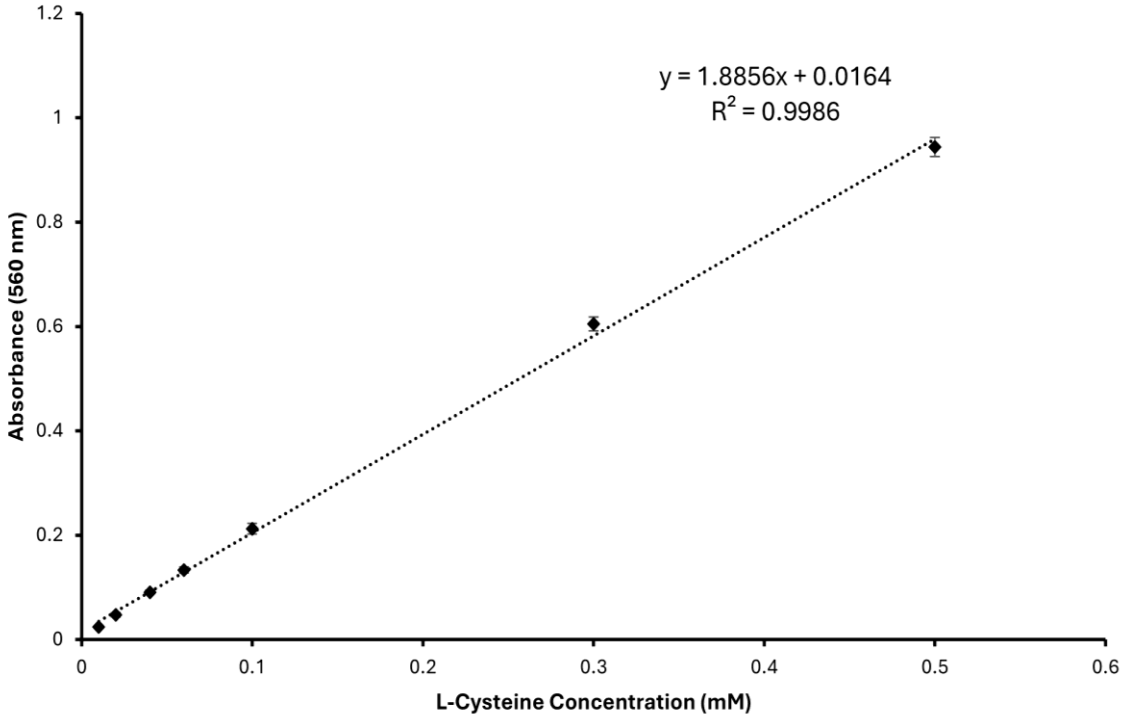


**Figure A.1:** Standard curve of L-cysteine. Concentration (mM) of L-cysteine plotted on the x-axis. Absorbance ($A_{560}$) of L-cysteine plotted on the y-axis. Cysteine produced in kinetic assays was calculated from absorbance readings ($A_{560}$) using the equation from the line of best fit.

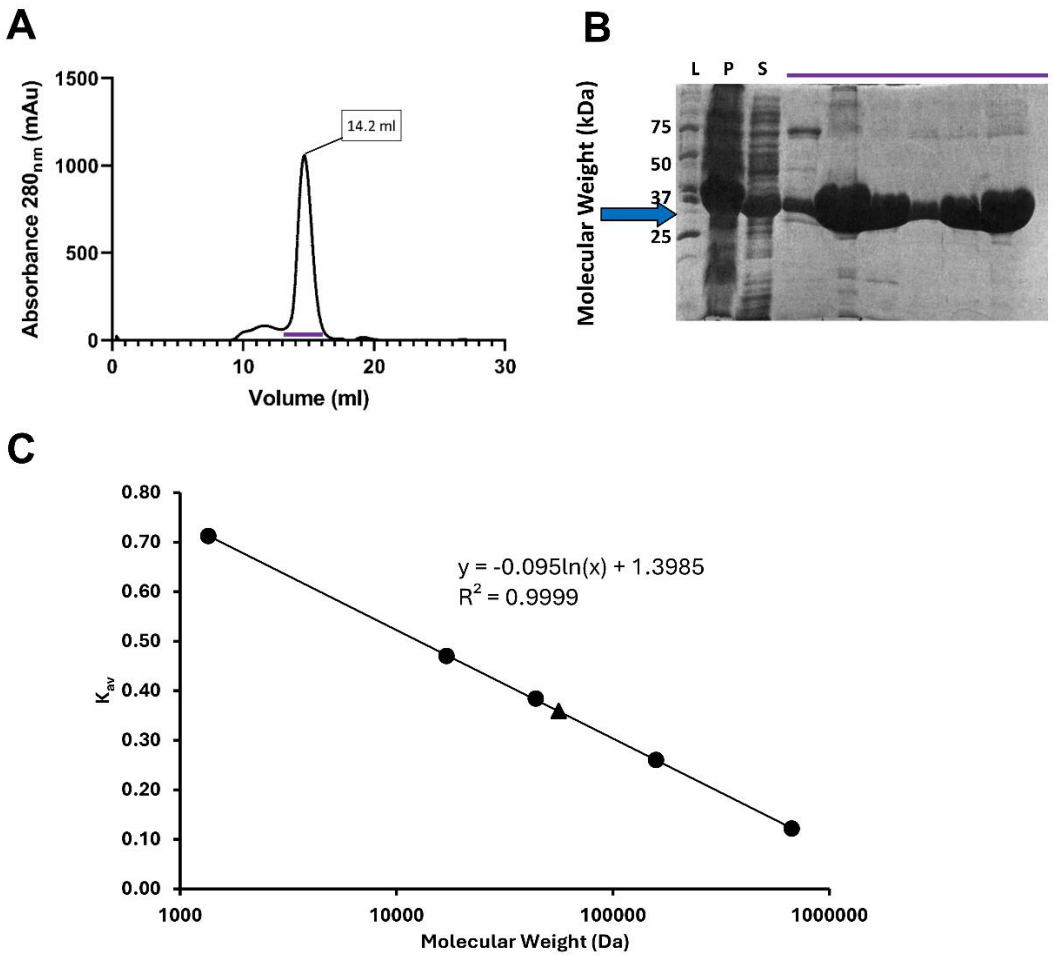


**Figure A.2:** Gel filtration purification of NgCysK. (A) Gel filtration chromatogram purified NgCysK using an Enrich 650 Gel filtration Column (Bio-Rad) with a single elution peak at 14.2 ml. (B) Corresponding 12% SDS-PAGE gel of column fractions (indicated by the purple line in the chromatogram and above the gel) showing a high yield and purity of NgCysK. Molecular weights of the Precision Plus Protein Standards (Bio-Rad) in kDa are labelled. (C) calibration of the Enrich 650 Gel Filtration Column. Molecular weights of gel filtration calibration standards (Bio-Rad) plotted on the x-axis. $K_{av}$ plotted on the y-axis. $K_{av}$ of NgCysK (0.36) indicated by a triangle $K_{av}$ calculated by subtracting column void volume from the protein elution volume and dividing by the total column volume. Equation from line of best fit used for determining molecular weight of unknown proteins.

**Table A.1:** NgCysK structure statistics for each monomer in the ASU.

| Chain | Residue chain built | Residues missing | Total built |
|---|---|---|---|
| **A** | Met1-Ala-207 | 39 | 279/318 |
| | Ile229-Tyr300 | | |
| **B** | Met1-Ala207 | 39 | 279/318 |
| | Ile229-Tyr300 | | |
| **C** | Met1-Gln145 | 40 | 278/318 |
| | Asn148-Pro218 | | |
| | Tyr235-Tyr296 | | |
| **D** | Met1-Gln145 | 39 | 279/318 |
| | Asn148-Pro218 | | |
| | Asn234-Tyr296 | | |

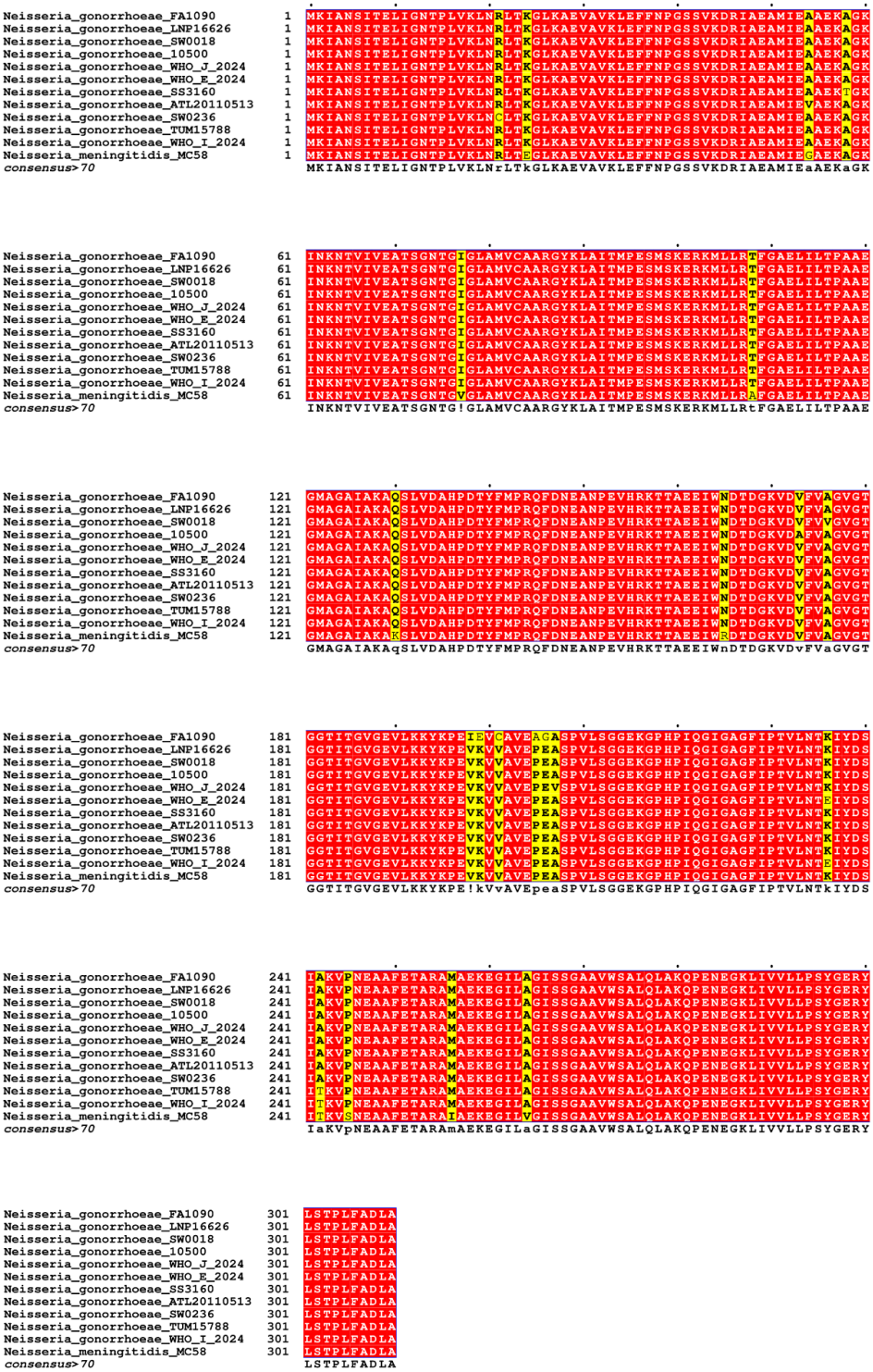


**Figure A.3:** Multiple sequence alignment of the CysK sequences from pathogenic *Neisseria*. Each *N. gonorrhoeae* strain is representative of a portion of the *N. gonorrhoeae* CysK sequences in NCBI; FA1090 = 2/732, LNP16626 = 387/732, SW0018 = 1/732, 10500 = 3/732, WHO_J_2024 = 2/732, WHO_E_2024 = 18/732, SS3160 = 2/732, ATL20110513 = 2/732, SW0236 = 1/732, TUM15788 = 15/732, and WHO_I_2024 = 299/732. *N. meningitidis* MC58 has been included for comparison. Highly conserved residues are highlighted red. Moderately conserved residues are highlighted in yellow.

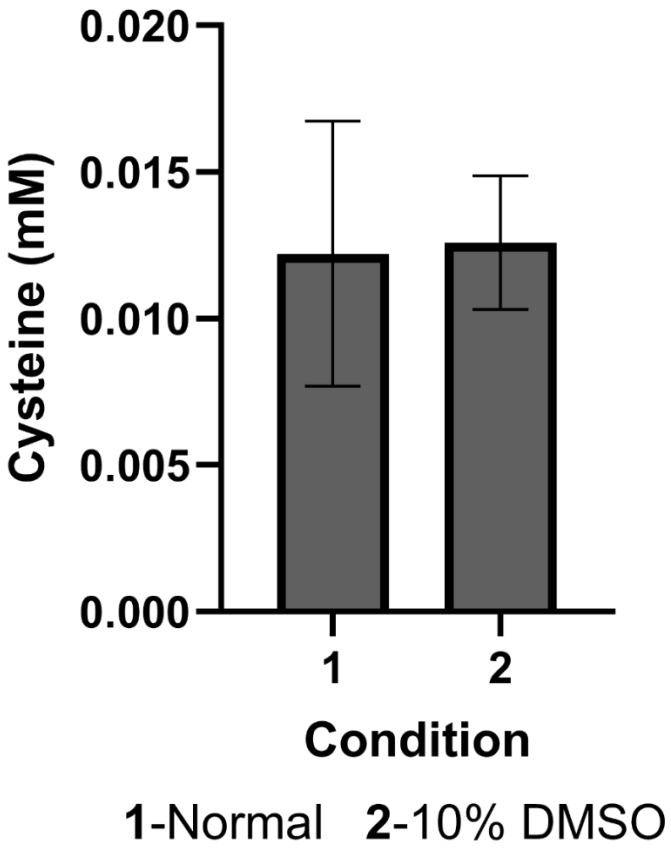


**Figure A.4:** Column graph showing there is no effect of 10% DMSO (this is the highest concentration of DMSO present in the inhibitor compounds tested) on the activity of NgCysK.

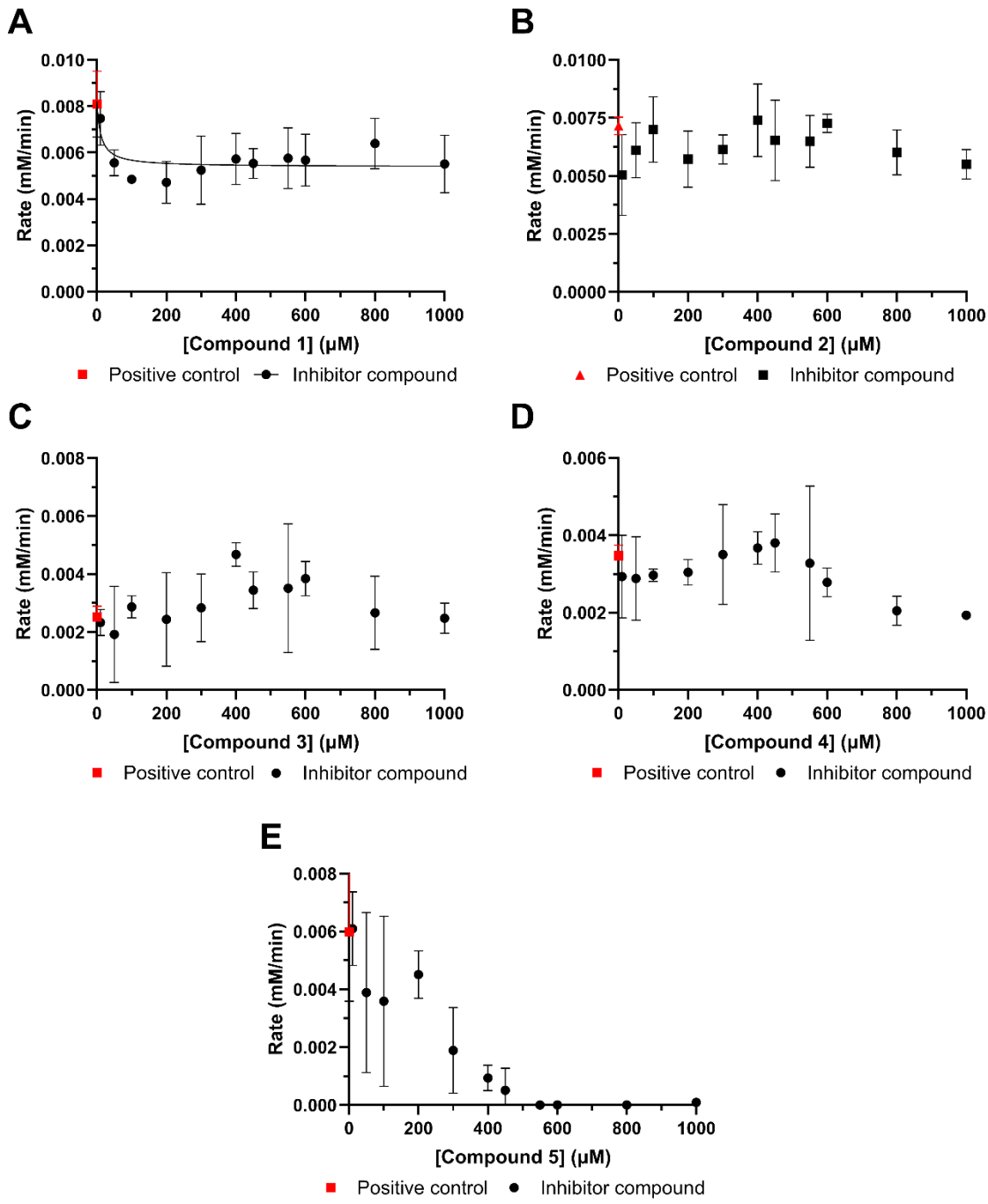


**Figure A.5:** Kinetic analysis of all 5 potential NgCysK inhibitor compounds tested. Compounds tested across a concentration range of 10-1000 μM. data was collected at 2 mM OAS and 0.7 mM $Na_2S$. Plotted data points represent mean alongside SEM of three replicates. (**A**) Compound 1. (**B**) Compound 2. (**C**) Compound 3. (**D**) Compound 4. (**E**) Compound 5.

**Required reagents and kinetic assay reagent compositions:**

**PLP (Pyridoxal 5'-phopshate, 2mM)**

4.94 mg PLP

10 ml $MQH_2O$

***O*-acetylserine (50 mM)**

45.9 mg *O*-acetyl-L-serine hydrochloride

5 ml $MQH_2O$

***O*-acetylserine (5 mM)**

1 ml *O*-acetylserine (50 mM)

9 ml $MQH_2O$

**Sodium sulfide (50 mM)**

19.51 mg Sodium sulphide

5 ml $MQH_2O$

**Sodium sulfide (5.25 mM)**

1.050 ml Sodium sulfide (50 mM)

8.950 ml $MQH_2O$

**Acid Ninhydrin Reagent**

250 mg Ninhydrin

6 ml Glacial acetic acid

4 ml Concentrated hydrochloric acid (10 M)

**Trichloroacetic acid (25% v/v)**

1.25 g Trichloroacetic acid

5 ml $MQH_2O$

**MOPs buffer (100mM, pH 7)**

2.093 g MOPs

Make up to 10 ml $MQH_2O$

**DTT (Dithiothreitol, 481.5mM)**

371.379 mg DTT

Make up to 5 ml with MOPs buffer

pH to 7 with NaOH

**L-cysteine (50mM)**

60.58 mg L-cysteine

10 ml MQ $H_2O$

pH to 2.0

**L-cysteine (5 mM)**

1 ml of 50mM L-cysteine

9 ml MQ $H_2O$

**Compound 1 (100 mM)**

5 mg of Compound 1

128.71 µl MQ $H_2O$

**Compound 1 (50 mM)**

64.36 µl of 100 mM Compound 1

64.36 µl MQ $H_2O$

**Compound 1 (10 mM)**

20 µl of 50 mM Compound 1

80 µl MQ $H_2O$

**Compound 1 (5 mM)**

200 µl of 10 mM Compound 1

200 µl MQ $H_2O$

**Compound 1 (1 mM)**

120 µl of 5 mM Compound 1

480 µl MQ $H_2O$

**Compound 1 (500 µM)**

175 µl of 1 mM Compound 1

175 µl MQ $H_2O$

**Compound 1 (250 µM)**

150 µl of 500 µM Compound 1

150 µl MQ $H_2O$

**Compound 1 (50 µM)**

40 µl of 250 µM Compound 1

60 µl MQ $H_2O$

**Compound 2 (100 mM)**

5 mg of Compound 2

142.3 µl MQ $H_2O$

**Compound 2 (50 mM)**

71.15 µl of 100 mM Compound 2

71.15 µl MQ $H_2O$

**Compound 2 (10 mM)**

20 µl of 50 mM Compound 2

80 µl MQ $H_2O$

**Compound 2 (5 mM)**

200 µl of 10 mM Compound 2

200 µl MQ $H_2O$

**Compound 2 (1 mM)**

120 µl of 5 mM Compound 2

480 µl MQ $H_2O$

**Compound 2 (500 µM)**

175 µl of 1 mM Compound 2

175 µl MQ $H_2O$

**Compound 2 (250 µM)**

150 µl of 500 µM Compound 2

150 µl MQ $H_2O$

**Compound 2 (50 µM)**

40 µl of 250 µM Compound 2

60 µl MQ $H_2O$

**Compound 3 (100 mM)**

5 mg of Compound 3

114.82 µl MQ $H_2O$

**Compound 3 (50 mM)**

57.41 µl of 100 mM Compound 3

57.41 µl MQ $H_2O$

**Compound 3 (10 mM)**

20 µl of 50 mM Compound 3

80 µl MQ $H_2O$

**Compound 3 (5 mM)**

200 µl of 10 mM Compound 3

200 µl MQ $H_2O$

**Compound 3 (1 mM)**

120 µl of 5 mM Compound 3

480 µl MQ $H_2O$

**Compound 3 (500 µM)**

175 µl of 1 mM Compound 3

175 µl MQ $H_2O$

**Compound 3 (250 µM)**

150 µl of 500 µM Compound 3

150 µl MQ $H_2O$

**Compound 3 (50 µM)**

40 µl of 250 µM Compound 3

60 µl MQ $H_2O$

**Compound 4 (100 mM)**

5 mg of Compound 4

132.5 µl MQ $H_2O$

**Compound 4 (50 mM)**

66.24 µl of 100 mM Compound 4

66.24 µl MQ $H_2O$

**Compound 4 (10 mM)**

20 µl of 50 mM Compound 4

80 µl MQ $H_2O$

**Compound 4 (5 mM)**

200 µl of 10 mM Compound 4

200 µl MQ $H_2O$

**Compound 4 (1 mM)**

120 µl of 5 mM Compound 4

480 µl MQ $H_2O$

**Compound 4 (500 µM)**

175 µl of 1 mM Compound 4

175 µl MQ $H_2O$

**Compound 4 (250 µM)**

150 µl of 500 µM Compound 4

150 µl MQ $H_2O$

**Compound 4 (50 µM)**

40 µl of 250 µM Compound 4

60 µl MQ $H_2O$

**Compound 5 (100 mM)**

5 mg of Compound 5

136.07 µl MQ $H_2O$

**Compound 5 (50 mM)**

68.04 µl of 100 mM Compound 5

68.04 µl MQ $H_2O$

**Compound 5 (10 mM)**

20 µl of 50 mM Compound 5

80 µl MQ $H_2O$

**Compound 5 (5 mM)**

200 µl of 10 mM Compound 5

200 µl MQ $H_2O$

**Compound 5 (1 mM)**

120 µl of 5 mM Compound 5

480 µl MQ $H_2O$

**Compound 5 (500 µM)**

175 µl of 1 mM Compound 5

175 µl MQ $H_2O$

**Compound 5 (250 µM)**

150 µl of 500 µM Compound 5

150 µl MQ $H_2O$

**Compound 5 (50 µM)**

40 µl of 250 µM Compound 5

60 µl MQ $H_2O$

# Appendix B: Supplementary information for Chapter Four

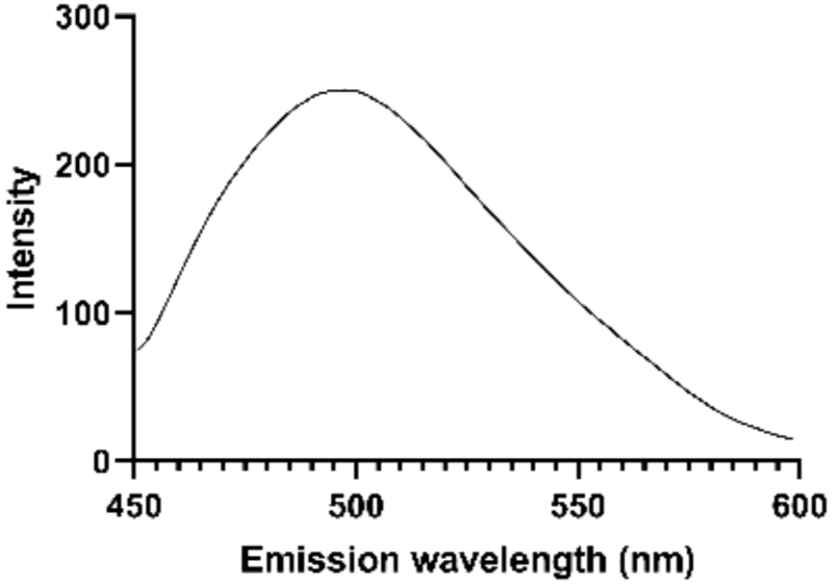


**Figure B.1:** Fluorescent spectroscopy emission wavelength scan of NgCysK. Measured at room temperature 22 ºC. Excitation wavelength 400nm. Emission wavelength measured between 450-600nm.

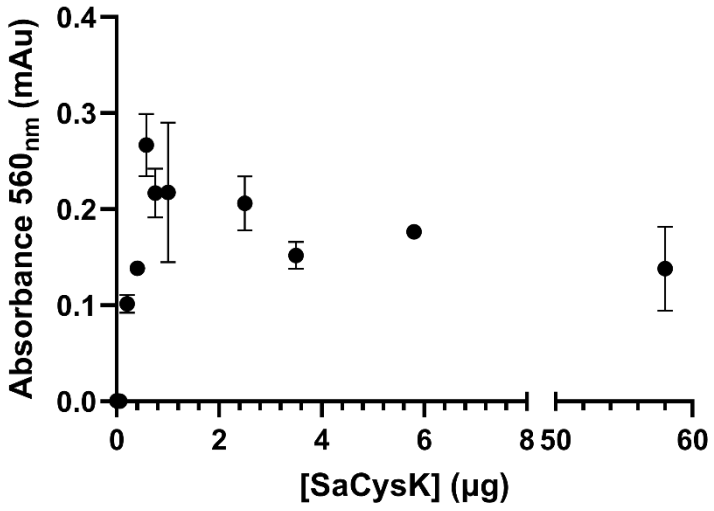


**Figure B.2:** Absorbance readings of Cysteine produced from various SaCysK concentrations. Given the error in the points above 0.2 µg, and the plateau at ~0.15 mAu, 0.2 µg was selected as the appropriate concentration for further testing.

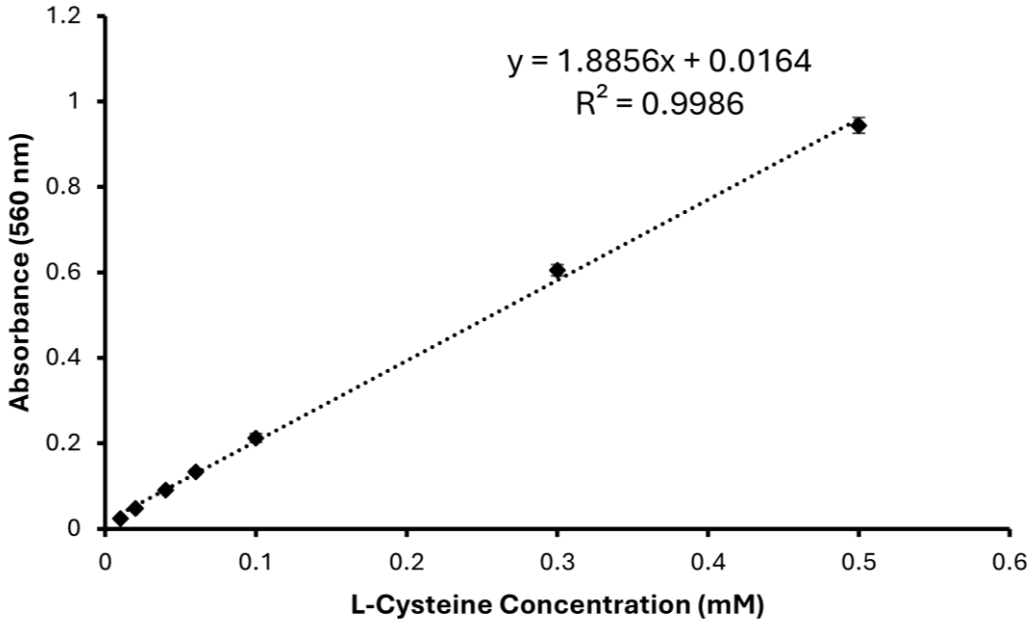


**Figure B.3:** Standard curve of L-cysteine. Concentration (mM) of L-cysteine plotted on the x-axis. Absorbance ($A_{560}$) of L-cysteine plotted on the y-axis. Cysteine produced in kinetic assays was calculated from absorbance readings ($A_{560}$) using the equation from the line of best fit.

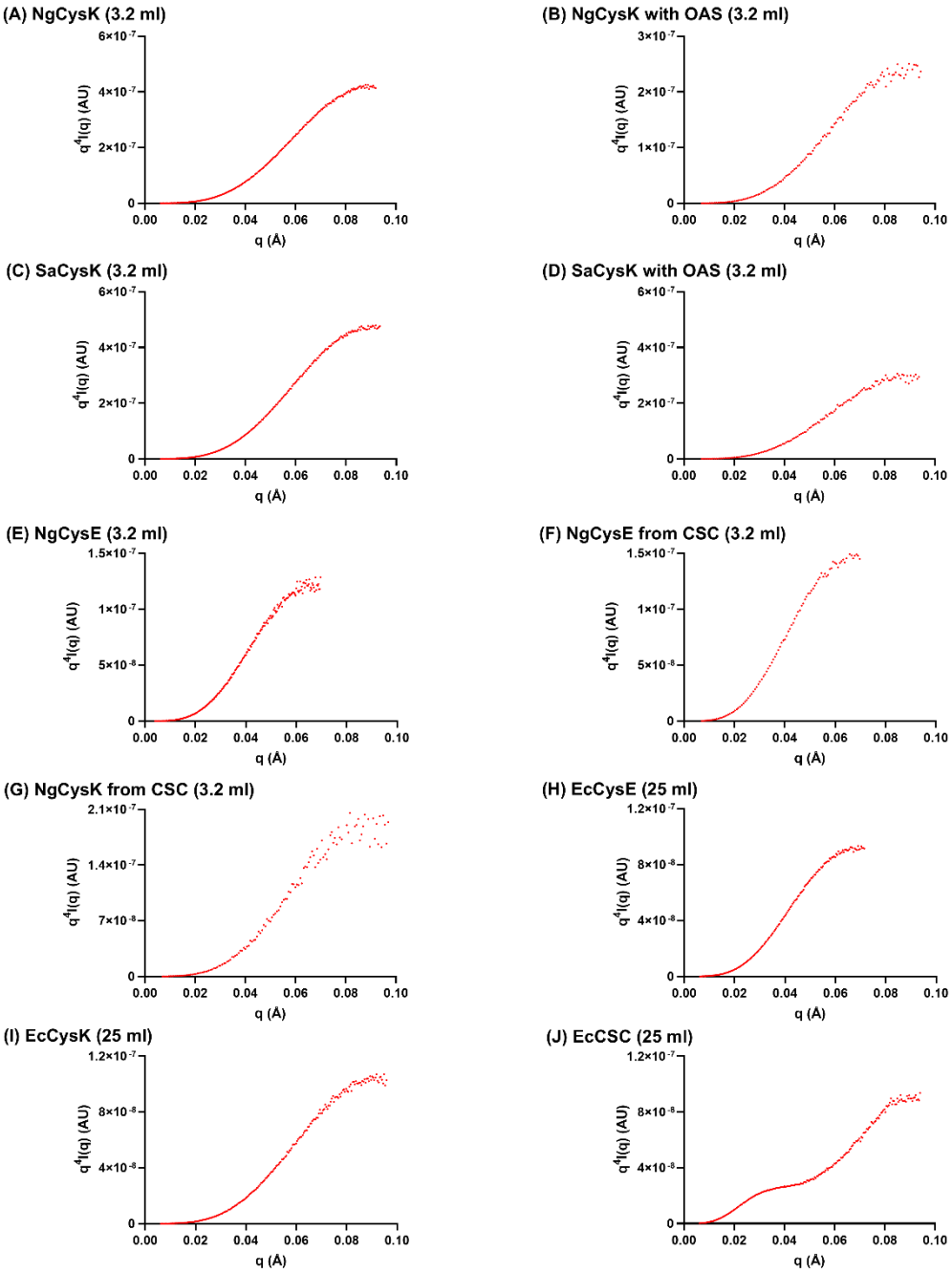


**Figure B.4:** Porod-debye plots defining the q range used for determining the Porod volume ($V_P$)

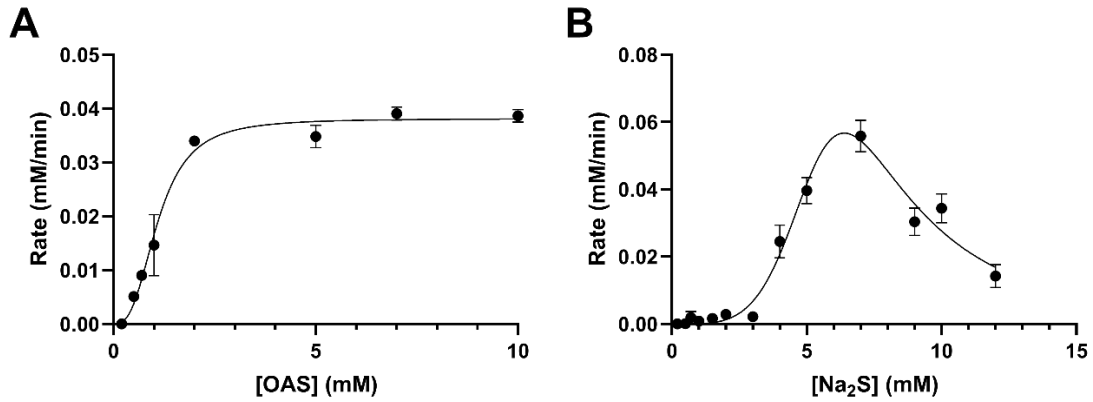


**Figure B.5:** Kinetic analysis of NgCysK substrates OAS and $Na_2S$ in the presence of glycerol. (**A**) Allosteric sigmoidal fit (occurs when the enzyme has cooperative subunits) for OAS. (B) Constrained allosteric sigmoidal substrate inhibition fit (occurs when the enzyme has cooperative subunits and exhibits cooperativity at low substrate concentrations and inhibition at high substrate concentrations) for $Na_2S$. OAS and $Na_2S$ assays in the presence of glycerol were collected at saturating concentrations of 10 mM OAS and 7 mM $Na_2S$, respectively. Plotted data points represent mean alongside SEM of three replicates.

**Table B.1:**Kinetic parameters of NgCysK in the presence of glycerol

| Parameter | *O*-acetylserine (OAS)[a] | Sodium sulfide ($Na_2S$)[a] |
|---|---|---|
| $v_{max}$ ($mM.min^{-1}$) | 0.038 ± 0.002 | 2.530 ± 4.601 |
| $K_M$ (mM) | - | 12.43 ± 8.133 |
| $K_{half}$ (mM) | 1.101 ± 0.138 | - |
| $k_{cat}$ ($s^{-1}$) [b] | 16.04 ± 0.84 | (1.07 ± 1.95) x $10^3$ |
| $k_{cat}/K_M$ ($M.s^{-1}$) | (14.57 ± 1.98) x $10^3$ | (8.60 ± 16.6) x $10^4$ |
| $K_i$ (mM) | - | 5.146 ± 5.012 |
| h | 2.810 ± 0.899 | 4.159 ± 1.549 |
| $R^2$ | 0.9795 | 0.9573 |

[a] Error is SEM of three replicates
[b] $k_{cat}$ calculated by dividing the rate ($M.s^{-1}$) by enzyme concentration using the concentration of the NgCysK dimer (67.582 kDa)

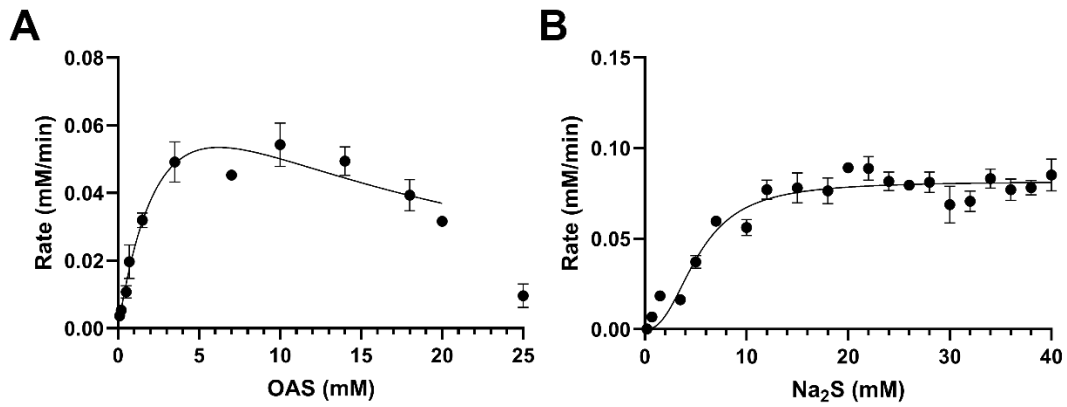


**Figure B.6:** Kinetic analysis of SaCysK substrates OAS and $Na_2S$ in the presence of glycerol. (**A**) Substrate inhibition fit (occurs when the enzyme exhibits inhibition at high substrate concentrations) for OAS. (**B**) Allosteric sigmoidal fit (occurs when the enzyme has cooperative subunits) for $Na_2S$. OAS and $Na_2S$ assays in the presence of glycerol were collected at saturating concentrations of 10 mM OAS and 15 mM $Na_2S$, respectively. Plotted data points represent mean alongside SEM of three replicates.

**Table B.2:** Kinetic parameters of SaCysK in the presence of glycerol

| Parameter | *O*-acetylserine (OAS)[a] | Sodium sulfide ($Na_2S$)[a] |
|---|---|---|
| $v_{max}$ ($mM.min^{-1}$) | 0.129 ± 0.087 | 0.082 ± 0.004 |
| $K_M$ (mM) | 4.387 ± 4.404 | - |
| $K_{half}$ (mM) | - | 5.266 ± 0.679 |
| $k_{cat}$ ($s^{-1}$) [b] | 54.85 ± 36.96 | 34.87 ± 1.70 |
| $k_{cat}/K_M$ ($M.s^{-1}$) | (1.25 ± 1.51) x $10^4$ | (6.62 ± 0.91) x $10^3$ |
| $K_i$ (mM) | 8.810 ± 7.348 | - |
| h | - | 2.397 ± 0.906 |
| $R^2$ | 0.9347 | 0.9184 |

[a] Error is SEM of three replicates
[b] $k_{cat}$ calculated by dividing the rate ($M.s^{-1}$) by enzyme concentration using the concentration of the SaCysK dimer (68.022 kDa)

**Table B.3:** Crysol results and parameters. 3.2 and 24 refer to the column volume used during SEC-SAXS run.

| | ***Ng*CysK (3.2)** | ***Ec*CysK (24)** | ***Sa*CysK (3.2)** | ***Ec*CysE (24)** | ***Ng*CysE (3.2)** | ***Ng*CysK + OAS (3.2)** | ***Sa*CysK + OAS (3.2)** |
|---|---|---|---|---|---|---|---|
| **Symmetry, anisotropy assumptions** | P2 | P2 | P2 | P6 | P6 | P2 | P2 |
| **Red. $\chi^2$, CorMap, Anderson-darling, Probability of fit** | 0.542, 75, 24.986, 1.000 | 0.373, 22, 52.319, 1.000 | 0.616, 89, 14.997, 1.000 | 2.513, 124, 45.384, 0.0 | 0.542, 99, 37.826, 1.0 | 0.977, 15, 0.918, 0.654 | 1.083, 20, 3.126, 0.046 |
| **Optimal hydration shell contrast (Dro, e Å$^{-3}$)** | 0.018 | 0.014 | 0.021 | 0.100 | 0.065 | 0.022 | 0.025 |
| **Predicted $R_g$ (Å)** | 24.65 | 24.65 | 24.65 | 34.43 | 34.71 | 24.65 | 24.65 |
| **Optimal Excluded volume (Vol, Å$^3$)** | 70813 | 70813 | 70813 | 211505 | 195566 | 70813 | 70813 |
| **Crysol (default parameters used)** | | | | | | | |
| **Maximum angle** | 0.5 Å$^{-1}$ | 0.5 Å$^{-1}$ | 0.5 Å$^{-1}$ | 0.5 Å$^{-1}$ | 0.5 Å$^{-1}$ | 0.5 Å$^{-1}$ | 0.5 Å$^{-1}$ |
| **Number of points** | 501 | 501 | 501 | 501 | 501 | 501 | 501 |
| **Solvent density** | 0.334 e/Å$^3$ | 0.334 e/Å$^3$ | 0.334 e/Å$^3$ | 0.334 e/Å$^3$ | 0.334 e/Å$^3$ | 0.334 e/Å$^3$ | 0.334 e/Å$^3$ |
| **Hydration shell constant** | 0.03 e/Å$^3$ | 0.03 e/Å$^3$ | 0.03 e/Å$^3$ | 0.03 e/Å$^3$ | 0.03 e/Å$^3$ | 0.03 e/Å$^3$ | 0.03 e/Å$^3$ |
| **Maximum order of harmonics** | 70 | 70 | 70 | 70 | 70 | 70 | 70 |
| **Order of Fibonacci grid** | 17 | 17 | 17 | 17 | 17 | 17 | 17 |
| **Shell type** | Directional | Directional | Directional | Directional | Directional | Directional | Directional |

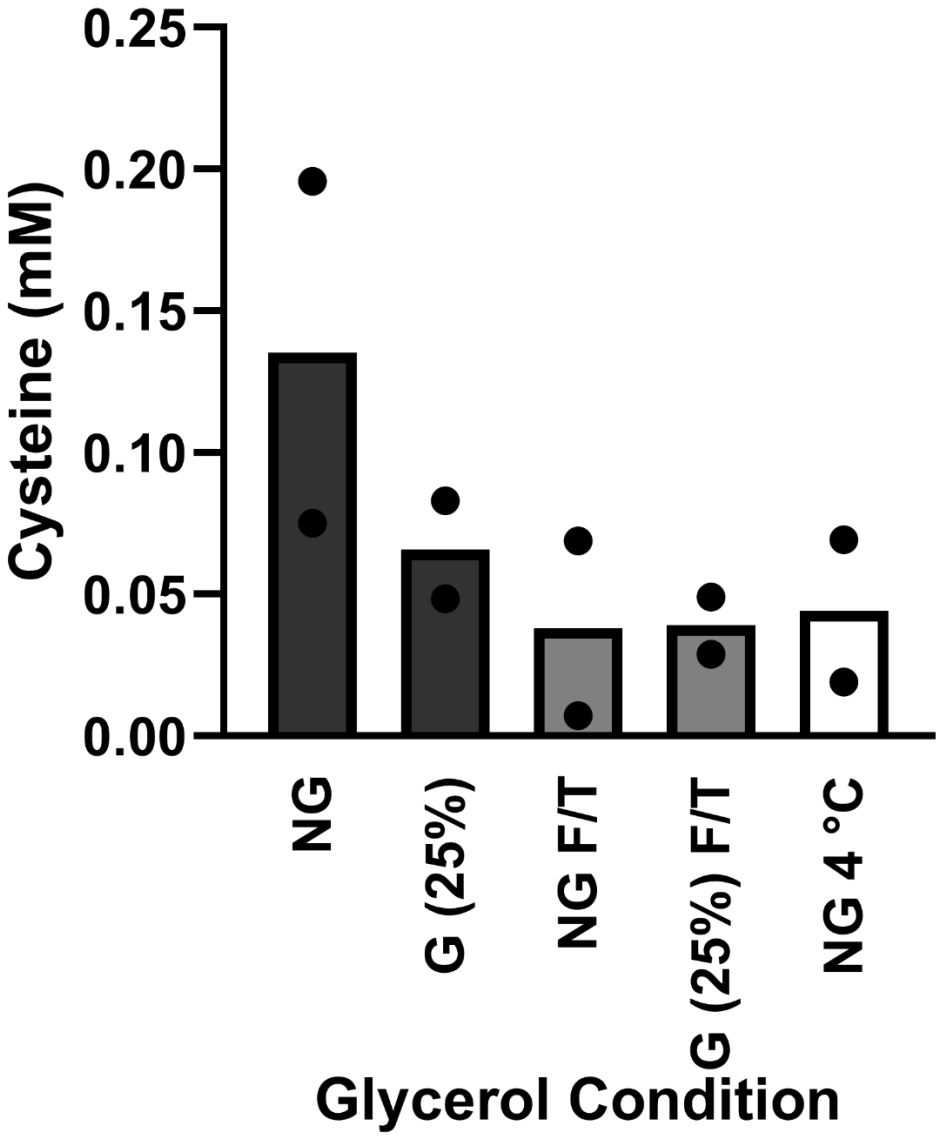


**Figure B.7:** Column graph displaying the effect of glycerol on enzyme activity under varying conditions at 0.704 and 1.408 ug. NG: fresh NgCysK without glycerol. G (25%): fresh NgCysK with 25% (v/v) glycerol. NG F/T: freeze/thawed NgCysK without glycerol. G (25%) F/T: freeze/thawed NgCysK with 25% (v/v) glycerol. NG 4 ºC:NgCysK without glycerol refrigerated for 3 days. Each concentration was collected in duplicate under each condition. Points shown under each condition are the mean of each enzyme concentration. Columns shown are the mean of both concentrations in that condition.

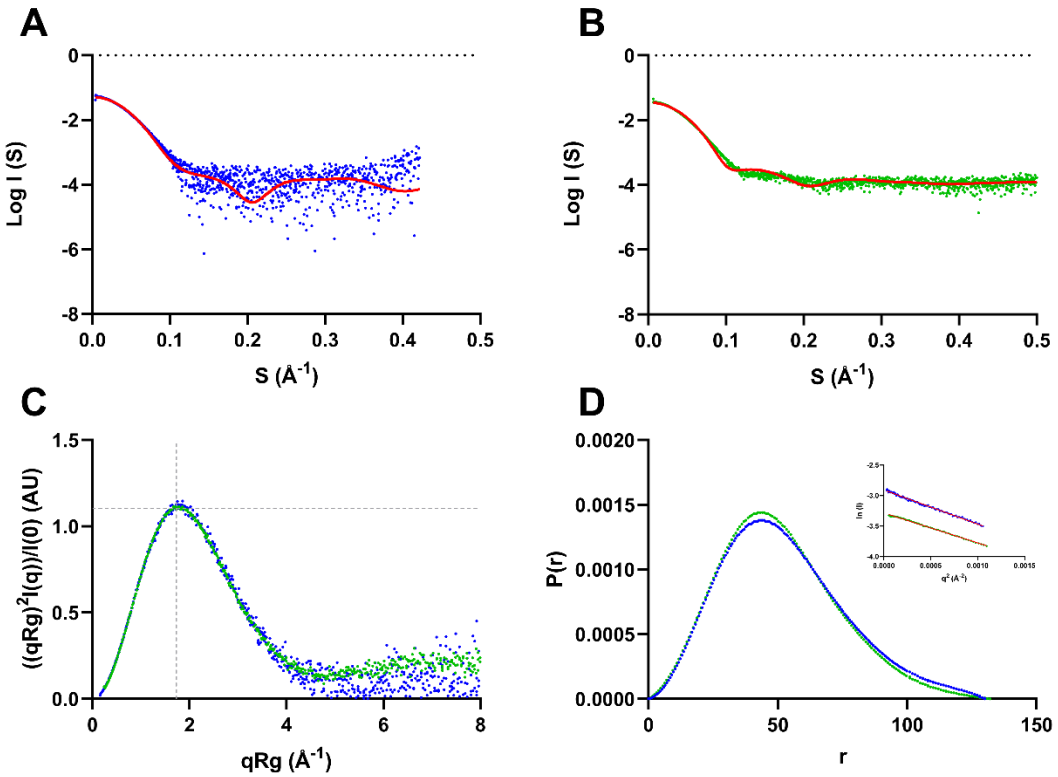


**Figure B.8:** SAXS profiles of NgCysE (all blue curves) and EcCysE (all green curves). (**A**) Scattering plot of NgCysE with theoretical scattering fit of NgCysE (6WYE) shown in red. (**B**) Scattering plot of EcCysE with theoretical scattering fit of EcCysE (1T3D) shown in red. (**C**) Kratky plots of NgCysE (blue) and EcCysE (green). The grey dashed lines represent the expected peak maxima for folded, globular proteins, where $(qRg)^2I(q)/I(0) = 1.104$ in a q range of 0.05 – 0.1 $Å^{-1}$ (Makowski, Berkowitz, & Houde, 2020; Receveur-Brechot & Durand, 2012). (**D**) Pair distance distribution function (P(r)) analysis of NgCysE (blue) and EcCysE (green) with inlaid Guinier plots. A red trend line is present in both Guinier plots. The P(r) values are normalised by relative intensity for comparison of both enzymes on the same scale.

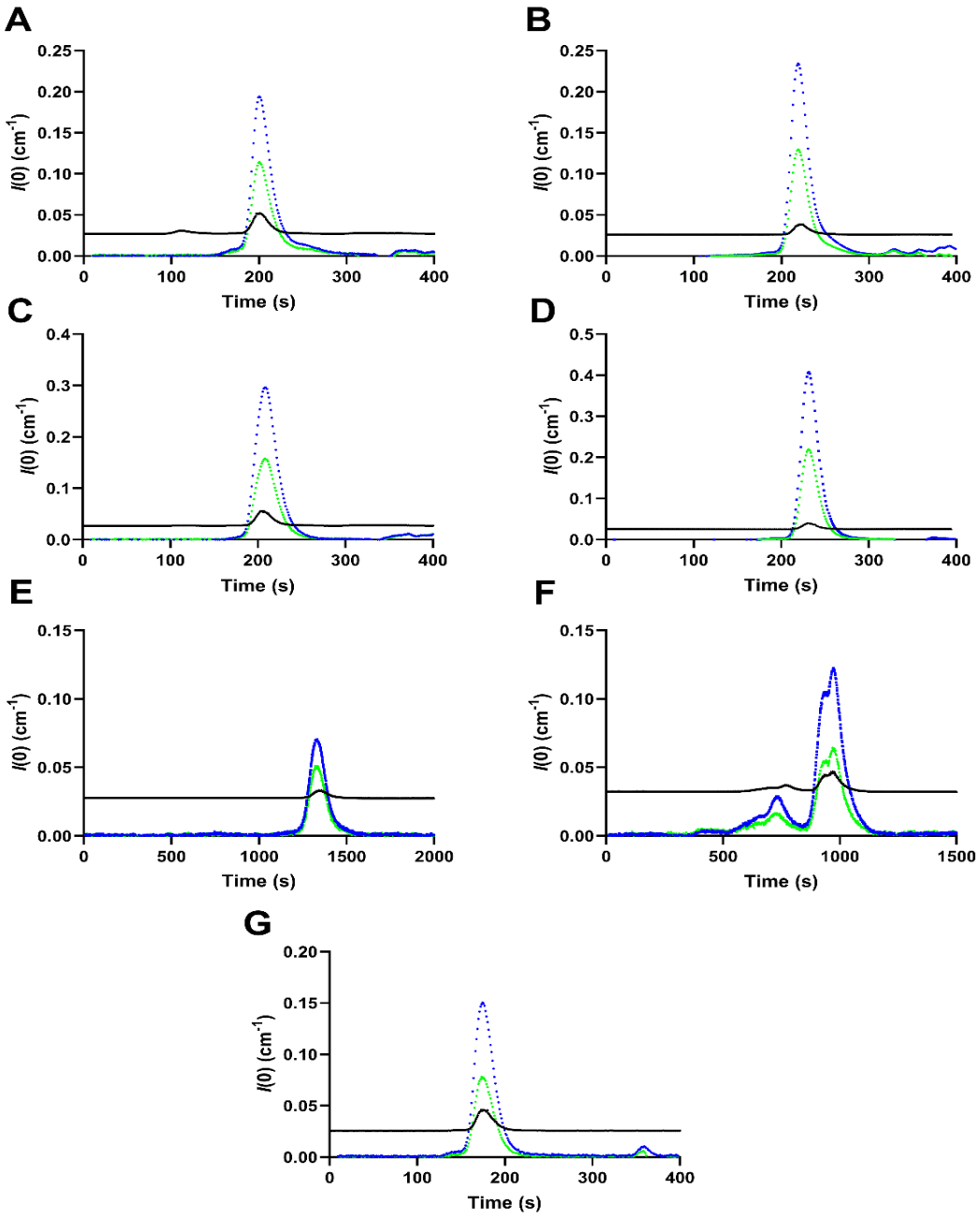


**Figure B.9:** UV traces and CHROMIXS scattering of all individual enzymes tested, excluding those involved in CSC formation. (A) NgCysK. (B) NgCysK + OAS. (C) SaCysK. (D) SaCysK + OAS. (E) EcCysK. (F) EcCysE. (G) NgCysE. For all curves, UV $A_{280}$ trace is shown in blue, UV $A_{260}$ is shown in green, and CHROMIXS scattering is shown in black.

**Required reagents and kinetic assay reagent compositions:**

**PLP (Pyridoxal 5'-phopshate, 2mM)**

4.94 mg PLP

10 ml $MQH_2O$

***O*-acetylserine (50 mM)**

45.9 mg *O*-acetyl-L-serine hydrochloride

5 ml $MQH_2O$

***O*-acetylserine (5 mM)**

1 ml *O*-acetylserine (50 mM)

9 ml $MQH_2O$

**Sodium sulfide (90 mM)**

35.12 mg Sodium sulfide

5 ml $MQH_2O$

**Sodium sulfide (75 mM)**

29.27 mg Sodium sulfide

10 ml $MQH_2O$

**Sodium sulfide (50 mM)**

19.51 mg Sodium sulfide

5 ml $MQH_2O$

**Sodium sulfide (5 mM)**

1 ml Sodium sulfide (50 mM)

9 ml $MQH_2O$

**Sodium thiosulfate (100 mM)**

158.11 mg Sodium thiosulfate

10 ml MQ$H_2O$

Appropriate dilutions were made

**Acid Ninhydrin Reagent**

250 mg Ninhydrin

6 ml Glacial acetic acid

4 ml Concentrated hydrochloric acid (10 M)

**Trichloroacetic acid (25% v/v)**

1.25 g Trichloroacetic acid

5 ml MQ$H_2O$

**MOPs buffer (100mM, pH 7)**

2.093 g MOPs

Make up to 10 ml MQ$H_2O$

**DTT (Dithiothreitol, 481.5mM)**

371.379 mg DTT

Make up to 5 ml with MOPs buffer

pH to 7 with NaOH

**L-cysteine (50mM)**

60.58 mg L-cysteine

10 ml MQ $H_2O$

pH to 2.0

**L-cysteine (5 mM)**

1 ml of 50mM L-cysteine

9 ml MQ $H_2O$

# Appendix D: Co-Authorship forms

## D.1 Co-authorship form for Chapter Two: Literature Review

THE UNIVERSITY OF WAIKATO
Te Whare Wānanga o Waikato

**Co-Authorship Form**

**School of Graduate Research**
The University of Waikato
Private Bag 3105
Hamilton 3240, New Zealand
Phone +64 7 838 5096
Email: SGR@waikato.ac.nz
Website: http://www.waikato.ac.nz/students/research-degree

This form is to accompany the submission of any PhD that contains research reported in published or unpublished co-authored work. **Please include one copy of this form for each co-authored work.** Completed forms should be included in your appendices for all the copies of your thesis submitted for examination and library deposit (including digital deposit).

Please indicate the chapter/section/pages of this thesis that are extracted from a co-authored work and give the title and publication details or details of submission of the co-authored work.

Chapter 2: Literature review

Hicks, J. L., Oldham, K. E. A., McGarvie, J., & Walker, E. J. (2022). Combatting antimicrobial resistance via the cysteine biosynthesis pathway in bacterial pathogens. Bioscience reports, 42(10), BSR20220368. 10.1042/BSR20220368.

| | |
|---|---|
| Nature of contribution by PhD candidate | Analysis of literature, figure creation, drafting and editing of manuscript |
| Extent of contribution by PhD candidate (%) | 40 |

**CO-AUTHORS**

| Name | Nature of Contribution |
|---|---|
| Joanna Hicks | Drafting and editing of manuscript, project administration and funding acquisition |
| Keely Oldham | Analysis of literature, figure creation, drafting and editing of manuscript |
| Emma Walker | Analysis of literature, figure creation, drafting and editing of manuscript |
| | |
| | |
| | |

**Certification by Co-Authors**

The undersigned hereby certify that:

- the above statement correctly reflects the nature and extent of the PhD candidate's contribution to this work, and the nature of the contribution of each of the co-authors; and
- that the candidate wrote all or the majority of the text.

| Name | Signature | Date |
|---|---|---|
| Joanna Hicks | 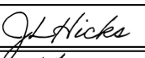 | 25 March 2025 |
| Keely Oldham | 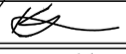 | 24 March 2025 |
| Emma Walker |  | 25 March 2025 |
| | | |
| | | |
| | | |

July 2015

## D.2 Co-authorship form for Chapter Three: Identification of inhibitors of *O*-acetylserine sulfhydrylase A from *Neisseria gonorrhoeae*

THE UNIVERSITY OF WAIKATO
Te Whare Wānanga o Waikato

**Co-Authorship Form**

**School of Graduate Research**
The University of Waikato
Private Bag 3105
Hamilton 3240, New Zealand
Phone +64 7 838 5096
Email: SGR@waikato.ac.nz
Website: http://www.waikato.ac.nz/students/research-degree

This form is to accompany the submission of any PhD that contains research reported in published or unpublished co-authored work. **Please include one copy of this form for each co-authored work**. Completed forms should be included in your appendices for all the copies of your thesis submitted for examination and library deposit (including digital deposit).

| |
|---|
| Please indicate the chapter/section/pages of this thesis that are extracted from a co-authored work and give the title and publication details or details of submission of the co-authored work.<br>Chapter Three:<br>McGarvie, J., Warrender, A. K., Oldham, K. E. A., Jiao, W., & Hicks, J. L. (2025). Identification of inhibitors of O-acetylserinesulfhydrylase A from Neisseria gonorrhoeae (ready for submission) |

| | |
|---|---|
| Nature of contribution by PhD candidate | data analysis, processing and analysis, method optimisation, drafting and editing of manuscript, figure creation |
| Extent of contribution by PhD candidate (%) | 80 |

**CO-AUTHORS**

| Name | Nature of Contribution |
|---|---|
| Joanna Hicks | Drafting and editing of manuscript, project administration and funding acquisition |
| Wanting Jiao | Data collection and analysis, figure creation, drafting and editing of manuscript |
| Annmaree Warrender | Crystallisation of protein |
| Keely Oldham | Data collection and scaling |
| Erica Prentice | Data interpretation |
| | |

**Certification by Co-Authors**

The undersigned hereby certify that:

- the above statement correctly reflects the nature and extent of the PhD candidate's contribution to this work, and the nature of the contribution of each of the co-authors; and
- that the candidate wrote all or the majority of the text.

| Name | Signature | Date |
|---|---|---|
| Joanna Hicks | J Hicks | 24 Mar 2025 |
| Wanting Jiao | Wanting Jiao | 25/03/2025 |
| Annmaree Warrender | | 24 Mar 2025 |
| Keely Oldham | | 24 Mar 2025 |
| Erica Prentice | E Prentice | 25/03/2025 |
| | | |

July 2015

## D.3 Co-authorship form for Chapter Four: Characterisation of *O*-acetylserine sulfhydrylase (CysK) from bacteria lacking a sulfate reduction pathway

THE UNIVERSITY OF WAIKATO
Te Whare Wānanga o Waikato

# Co-Authorship Form

School of Graduate Research
The University of Waikato
Private Bag 3105
Hamilton 3240, New Zealand
Phone +64 7 838 5096
Email: SGR@waikato.ac.nz
Website: http://www.waikato.ac.nz/students/research-degree

This form is to accompany the submission of any PhD that contains research reported in published or unpublished co-authored work. **Please include one copy of this form for each co-authored work**. Completed forms should be included in your appendices for all the copies of your thesis submitted for examination and library deposit (including digital deposit).

Please indicate the chapter/section/pages of this thesis that are extracted from a co-authored work and give the title and publication details or details of submission of the co-authored work.

Chapter 4:
McGarvie, J., Oldham, K. E. A., Warrender, A. K., Prentice, E., Hicks, J. L. (2025). Characterisation of O-acetylserine sulfhyrdrylase (CysK) enzymes from bacteria lacking a sulfate reduction pathway (submitted)

| | |
|---|---|
| Nature of contribution by PhD candidate | data collection, processing and analysis, method optimisation, figure creation, drafting and editing of manuscript |
| Extent of contribution by PhD candidate (%) | 90 |

## CO-AUTHORS

| Name | Nature of Contribution |
|---|---|
| Keely Oldham | Purification of CysE |
| Annmaree Warrender | Initial expression trials of NgCysK |
| Erica Prentice | Analysis and interpretation of kinetic data |
| Joanna Hicks | Data collection, project supervision, drafting and editing of manuscript |
| | |
| | |

## Certification by Co-Authors

The undersigned hereby certify that:

- the above statement correctly reflects the nature and extent of the PhD candidate's contribution to this work, and the nature of the contribution of each of the co-authors; and
- that the candidate wrote all or the majority of the text.

| Name | Signature | Date |
|---|---|---|
| Keely Oldham |  | 24 Mar 2025 |
| Annmaree Warrender | 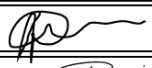 | 24 Mar 2025 |
| Erica Prentice |  | 25/03/2025 |
| Joanna Hicks |  | 24 Mar 2025 |
| | | |
| | | |